

University of Southern Queensland
Faculty of Engineering & Surveying

**Universal Design Framework for optimal application of
chemical monolayer to open water surfaces**

A thesis submitted by

Gavin Neil Brink

in fulfilment of the requirements of

Doctor of Philosophy

Submitted: June, 2011

Abstract

Annual evaporation losses from farm water storages in Australia typically exceed 40% of their storage volume. Potentially chemical films such as monolayers are an economical low-impact means of reducing evaporative loss, however, their performance has been shown to be highly variable. They are affected by a number of climatic and environmental factors, principally wind-induced drift, deposition on the lee shore, submergence by waves, volatilisation and bio-degradation. Although these limitations must be accommodated for in the management of the applied monolayer by means of appropriate and timely autonomous application, these limitation will vary for every location. Every given site will have its own unique characteristic climatic and environmental factors. It is this variability that presents major difficulties to the general one-size-fits-all design approach. Hence, to achieve optimal evaporation mitigation performance the development of a methodology to inform the design, installation and operation of a tailored monolayer application system for any given site was seen as essential.

This thesis reports the conception, development and desktop evaluation of a Universal Design Framework (UDF) to optimise the use of monolayer materials for evaporation mitigation. The UDF is designed to inform: (i) the most appropriate choice of monolayer material; (ii) the optimal type of application system and the site-specific configuration required; (iii) the amount and re-application rate of monolayer to be applied; and hence (iv) the expected performance of the application system. The UDF incorporates all the necessary information with respect to water storage geometry, monthly climate data (in particular, detailed wind statistics), water quality and biological factors plus user performance criteria (the desired extent and duration of coverage). This information is then used in four key analysis stages:

1. Monolayer material is selected via a decision table, which allows the user to make comparisons between three previously benchmarked South East Queensland (SEQ) reservoirs and their own, to determine a best match monolayer material.
2. Application system design is determined using a simulation platform, which allows the user to predict surface coverage and application rate according to wind conditions via an iterative process in which the number and/or location of applicators may be varied until user performance criteria are met.
3. Likewise application strategies, namely which applicators to apply from and their respective application rate for each wind condition, are also determined with the simulation platform for detailed wind conditions (both strength and direction) to create a decision table. This table forms the basis for real-time (hour-by-hour) decision and control when the system is installed on-site, and
4. system performance is calculated for monthly site-specific wind statistical data (using the simulation platform), and compared with user performance criteria to determine which months are suitable for application and monthly monolayer cost.

The simulation platform and the algorithms used to calculate firstly, the spreading rate and spreading pattern of monolayer (without wind stress), and secondly the drift rate, spreading rate and spreading pattern of monolayer (with wind stress), are described. In order to calibrate the algorithms, and to research the requirements for (both current and future) monolayer material characterisation, an empirical study for the commonly used evaporation-retarding monolayer stearyl alcohol ('C18OH' as a water-emulsion) was undertaken. This involved the analysis of its observed spreading performance under different application and windspeed conditions on an indoor 6 m diameter tank with controlled airflow.

Finally the scope of the UDF is discussed with regard to design, planning, installation and also daily, hour-by-hour management of monolayer application. This was informed by a demonstration of the UDF for a theoretical installation on a typical SEQ storage dam.

Publications

The following journal and conference papers, patent and research report have been published or are in preparation for submission about the research contained within this dissertation.

Journal

Brink, G., Symes, T. and Hancock, N. (2011), 'Development of a 'smart' monolayer application system for reducing evaporation from farm dams introductory paper', *Australian Journal of Multidisciplinary Engineering*. [*In press*]

Brink, G., Wandel, A., Hancock, N., Herzig, M. and Pather, S. (2011), 'Spreading rate and dispersion behaviour of evaporation-suppressant monolayer. Part 1 zero wind stress', *Water Resources Research*. [*Prepared: to be submitted with Part 2 following*]

Brink, G., Wandel, A., Hancock, N. and Pather, S. (2011), 'Spreading rate and dispersion behaviour of evaporation-suppressant monolayer. Part 2 wind stress', *Water Resources Research*. [*In preparation*]

Brink, G., Hancock, N. and Pather, S. (2011), 'Universal Design Framework for optimal application of chemical monolayer to open water surfaces', *Agricultural Water Management*. [*In preparation*]

Conference

Brink, G., Wandel, A., Pittaway, P., Hancock, N. and Schmidt, E. (2011), Optimising the design, installation and operation of a monolayer application system on a farm dam via a ‘Universal Design Framework’. *Australian Irrigation Conference and Exhibition 2011*, 22-25 August, Launceston, Australia. [*Accepted for presentation*]

Schmidt, E., Brink, G. and O’Shannassy, G. (2011), Application systems for optimal management of monolayer. *Urban Water Security Alliance Science Forum*, 14-15 September, Brisbane, Australia. [*Accepted for presentation*]

Brink, G. (2011), Optimising monolayer application system design, installation and operation on agricultural reservoirs through the use of a ‘Universal Design Framework’. *Water Panel’s Post-Graduate Presentation Evening*, 18 May, Brisbane, Australia.

Brink, G., Wandel, A., Pittaway, P., Hancock, N. and Pather, S. (2010), A ‘Universal Design Framework’ for installation planning and operational management of evaporation-suppressing films on agricultural reservoirs. *International Conference on Agricultural Engineering*, 6-8 September, Clermont-Ferrand, France.

Brink, G., Wandel, A., Pittaway, P., Hancock, N. and Pather, S. (2010), Determining operational requirements to optimise monolayer performance on a farm dam via a ‘Universal Design Framework’. *Australian Irrigation Conference and Exhibition 2010*, 8-10 June, Sydney, Australia.

Symes, T. and Brink, G. (2010), A scalable distribution system for the optimal application of evaporation suppressant film to farm dams. *Australian Irrigation Conference and Exhibition 2010*, 8-10 June, Sydney, Australia.

Brink, G., Wandel, A., Hancock, N. and Pather, S. (2009), Towards adaptive operational requirements for optimal application of evaporation-suppressing monolayer to reservoirs via a ‘Universal Design Framework’. *International Workshop on Evaporation from Reservoirs (IWER 2009)*, 9-11 December, Gold Coast, Australia.

Brink, G., Symes, T. and Hancock, N. (2009), Development of a ‘smart’ monolayer application system for reducing evaporation from farm dams introductory paper. *CIGR International Symposium of the Australian Society for Engineering in Agriculture*, 13-16 September, Brisbane, Australia.

Brink, G., Hancock, N. and Pather, S. (2009), ‘Smart’ monolayer application and management to reduce evaporation on farm dams - formulation of a universal design framework. *WaterTAPs Presentation*, 1 June, Toowoomba, Australia.

Brink, G., Symes, T., Pittaway, P., Hancock, N., Pather, S. and Schmidt, E. (2009), Smart monolayer application and management to reduce evaporation on farm dams - formulation of a universal design framework. *Environmental Research Conference*, 10-13 May, Noosa, Australia.

Patent

Brink, G. N. and Symes, T. W. (inventors) (2010), Evaporation inhibitor application. [*lodged April 2010*]

Research Report

Brink, G., Symes, T. (2010), Monolayer application systems: design, control and application strategies, Technical report, National Centre for Engineering in Agriculture, Toowoomba, QLD, 4350, Australia. [*unpublished*]

Certification of Dissertation

I certify that the ideas, designs and experimental work, results, analyses and conclusions set out in this dissertation are entirely my own effort, except where otherwise indicated and acknowledged. I also certify that the work is original and has not been previously submitted for assessment in any other course or institution, except where otherwise stated.

GAVIN NEIL BRINK

0050083224

Signature of Candidate

Date

ENDORSEMENT

Signature of Supervisors

Date

Acknowledgments

Firstly I want to thank my family. Without their education, guidance, sacrifice, love and support I would not have had the opportunities I have been so lucky to have. I can't thank them enough. I would also like to thank my beautiful, strong and loving girlfriend who has stuck with me throughout all of the highs and lows.

A big thank you to Erik Schmidt at the NCEA, who I first spoke with back in 2006 about monolayers, and since then has provided and created for me many opportunities over the years. Thanks you to my supervisors Associate Professor Nigel Hancock and Dr Selvan Pather for their invaluable guidance, patience, belief and assistance. Also a big thanks to Dr Andrew Wandel from FoES for his help, guidance and assistance with the development of the simulation and in finalising journal papers.

I appreciate the advice and support from FoES and NCEA staff, particularly Dr Pam Pittaway, my neighbour for a while there, has always helped to put things into perspective for me. Thank you for convincing me to stick with it. Also, thank you to Geoff O'Shannassay for all of his help with the monolayer work. Unfortunately, I can't thank Troy Symes in person today as he passed away last year, but I appreciate all he did for me.

Thank you to Michael Herzig for all of his effort in the development and formulation of a suitable monolayer material for testing and for his invaluable discussions on the finer points of physical chemistry. On this point, I would also like to thank the ever so wise Emeritus Professor Geoffrey Barnes for his insightful discussions and his unwavering devotion to monolayer work. Thanks also to Paul Coop for the many hours he spent with me on technical discussions relating to all things 'monolayer'.

During my time at USQ I have made many friends both professionally and socially from all over the world of whom I wish to thank for their support, specifically, Nicholas Stuckey, Dr Xavier Burgos, Dr Belen Gallego, Professor Victoriano Martinez, Nicholas Roberts, Nishant Pradhan, Adrian Blockland, Mohan Trada and Terry Byrne.

Finally I acknowledge the Australian Postgraduate Award scholarship funding provided to me by the Australian Government. Also the Cooperative Research Centre for Irrigation Futures for their invaluable project funding, conference and travel support and post-graduate events.

GAVIN NEIL BRINK

University of Southern Queensland

June 2011

Contents

Abstract	i
Publications	iii
Acknowledgments	vii
List of Figures	xix
List of Tables	xxxvii
Acronyms & Abbreviations	xliv
Chapter 1 Introduction	1
1.1 Background	1
1.1.1 Context	1
1.1.2 Using a chemical monolayer to protect open water surfaces . . .	3
1.2 Hypothesis and research aim and objectives	5
1.2.1 Hypothesis	5

1.2.2	Research aim and objectives	5
1.3	Overview of dissertation	7
Chapter 2 Summary Literature and Science Review		11
2.1	Introduction and overview	11
2.2	Surface chemistry of monolayer materials	13
2.3	Physics of evaporation (free-water surface)	15
2.4	Monolayer mechanisms for evaporation mitigation	17
2.5	Factors affecting monolayer performance	19
2.5.1	Temperature differentials and gaseous exchange	19
2.5.2	Wind-induced effects	20
2.5.3	Volatilisation	22
2.5.4	Biodegradation	24
2.5.5	Rainfall	26
2.6	Monolayer application	26
2.6.1	Application strategies	26
2.6.2	Application systems design	32
2.7	Monolayer detection	35
2.8	Water surface management	35
2.9	Conclusions	37

Chapter 3	Conception of the ‘Universal Design Framework’	39
3.1	Introduction and scope	39
3.2	Development of the ‘Universal Design Framework’	40
3.2.1	Monolayer material selection	40
3.2.2	Application system design	43
3.2.3	Application strategies	44
3.3	Illustration and overview of the UDF	45
3.4	UDF research tasks	49
Chapter 4	Development of a Monolayer Material Formulation	52
4.1	Introduction	52
4.2	Experimental objectives	54
4.3	Materials and methods	55
4.4	Results and discussion	56
4.5	Conclusions	58
Chapter 5	Monolayer Spreading (without wind stress)	60
5.1	Introduction	60
5.2	Background	61
5.3	Experimental objectives	64
5.4	Materials and methods	64

5.4.1	Monolayer material and application amounts	64
5.4.2	Measurement of initial spreading force	65
5.4.3	Experimentation with 0.3 m diameter tank	66
5.4.4	Experimentation with 2 m diameter tank	71
5.4.5	Experimentation with 6 m diameter tank	72
5.5	Results	74
5.6	Analysis and discussion	78
5.6.1	Comparison with theoretical parameters	78
5.6.2	Comparison and reconciliation across different experimental scales	79
5.7	Conclusions	83
Chapter 6 Monolayer Spreading and Drift (with wind stress)		85
6.1	Introduction and Background	85
6.2	Experimental objectives	88
6.3	Materials and methods	90
6.3.1	Water tank and wind apparatus	90
6.3.2	Monolayer material and application	92
6.3.3	Water surface cleaning process	93
6.3.4	Wind velocities and velocity profiles	94
6.3.5	Drift velocity tests	96
6.3.6	Spreading angle tests	99

6.4	Results	101
6.4.1	Drift velocity	101
6.4.2	Spreading angle	107
6.5	Analysis	111
6.5.1	Relationship between drift velocity and wind velocity	111
6.5.2	Spreading angle and empirical relationship	112
6.6	Discussion	114
6.7	Conclusions	116
Chapter 7 Monolayer Simulation Platform		117
7.1	Introduction	117
7.1.1	Spreading rate	118
7.1.2	Wind-driven transport	118
7.1.3	Coverage area and coverage pattern	119
7.1.4	Application rate calculation	120
7.2	Rationale, formulation and overview	120
7.3	Simulation platform structure	123
7.3.1	Assumptions	124
7.3.2	Inputs	125
7.3.3	Simulation platform processes	126
7.3.4	Distribution calculation for quiescent conditions	127

7.3.5	Distribution calculation for wind conditions	128
7.3.6	Application calculations	130
7.3.7	Outputs	131
7.4	Discussion	134
7.5	Conclusion	136
Chapter 8 Indicative Modelling of Monolayer Distribution		137
8.1	Introduction, rationale and overview	137
8.2	Materials and methods	139
8.2.1	Study (1)	139
8.2.2	Post-Process 1	140
8.2.3	Storage size and wind site selection	140
8.2.4	Applicator arrangements	146
8.2.5	Study (2)	149
8.3	Results	150
8.3.1	50 x 50 m storage	151
8.3.2	500 x 500 m storage	154
8.3.3	5000 x 5000 m storage	157
8.3.4	Optimised applicator arrangements	160
8.4	Discussion	160
8.4.1	50 x 50 m storage	160

8.4.2	500 x 500 m storage	162
8.4.3	5000 x 5000 m storage	162
8.4.4	Optimised applicator arrangements	163
8.5	Conclusion	164
Chapter 9 Scope of the ‘Universal Design Framework’		166
9.1	Introduction	166
9.2	Overview of analyses	168
9.3	Monolayer product decision table	169
9.4	Iterative modelling and Post-Process 1	171
9.5	Detailed wind condition modelling	172
9.6	Post-Process 2	173
9.7	Demonstration of the UDF	175
9.7.1	Site selection	175
9.7.2	Gathering necessary information	175
9.7.3	Determination of suitable monolayer product/s	178
9.7.4	Determination of optimal application system	178
9.7.5	Decision tables for real-time application	180
9.7.6	Expected performance of application system	183
9.8	Summary and conclusion	187

Chapter 10 Conclusions and recommendations	189
10.1 Achievement of objectives	190
10.2 Recommended further work	191
10.2.1 Expand monolayer product decision table	191
10.2.2 Laboratory characterisation of more monolayer products	192
10.2.3 Monolayer simulation platform development	192
10.2.4 Validation of the UDF	193
References	194
Appendix A Literature Reviewed	208
A.1 Introduction	208
A.2 Methods for estimating evaporation	208
A.3 Monolayer materials	217
A.3.1 Monolayer spreading properties	218
A.3.2 Monolayer forms	218
A.3.3 Evaporative resistance of monolayers	219
A.3.4 Existing product performance	220
A.4 Monolayer application technologies	225
A.4.1 Solution application (liquid)	226
A.4.2 Oil application (liquid)	230

A.4.3	Emulsion application (liquid)	233
A.4.4	Molten application (liquid)	238
A.4.5	Aerial application (liquid & solid)	240
A.4.6	Powder application (solid)	240
A.5	Systems for monolayer detection	246
A.6	Water surface management technologies	249
A.6.1	How wind generates water waves	249
A.6.2	Basic water wave theory	252
A.6.3	Wind speed reducing technologies	252
A.6.4	Wave suppression technologies	263
A.6.5	Film containment technologies	278
Appendix B Simulation Platform Source Code		288
B.1	The latest_mono.m main program	288
B.2	The calcdistrib.m function	290
B.3	The spreadangle.m function	293
B.4	The drift_speed.m function	293
B.5	The output.m function	294
Appendix C Wind Frequency Data Used For Modelling		295
C.1	Wind frequency data for Amberley, QLD	295

C.2	Wind frequency data for Moree, NSW	301
Appendix D Illustrative UDF Decision Tables		308
D.1	‘Table A’	308
D.2	‘Table B’	327
Appendix E Monolayer Application System Design		347
E.1	Application system options	347
E.1.1	Centralised system	348
E.1.2	De-centralised system	349
E.1.3	Hybrid (centralised and de-centralised) system	350
E.2	Design of methods for monolayer application	350
E.2.1	Solid-cast application	352
E.2.2	Tape application	355
E.2.3	Molten application	357
E.2.4	Effervescent application	359
E.3	De-centralised applicator design	362
E.3.1	Floating applicator conceptual design	362
E.3.2	Shore-based applicator conceptual design	364
E.3.3	Prototype floating applicator	367

List of Figures

1.1	Block diagram of dissertation overview.	8
2.1	The relationship between the area occupied (\AA^2) per molecule and the surface pressure (π) exerted by the film. (a) refers to the gaseous film phase, (b) the liquid-expanded phase, and (c) the solid phase. Although the liquid-condensed phase is not shown here, this phase is similar to the solid, however, the molecules are oriented diagonally instead of vertically. Reproduced from Gladyshev (2002).	14
2.2	Diagrammatic illustration of the physics of thermal transport processes: (a) details the atmospheric and liquid layers; (b) details the gaseous boundary layer and liquid diffusion sublayer near the interface. Reproduced from Hancock, Pittaway & Symes (2011).	20
2.3	Degradation of three monolayer compounds supplied as the sole carbon source for the common freshwater bacterium <i>Acinetobacter</i> in a mineral salts medium. The resilience of two fatty alcohols (C16OH, C18OH) and a ethylene glycol monooctadecyl ether (C18E1) monolayer were compared. Chloroform was used to extract the monolayer in the medium after two, three and four days of incubation prior to analysis using a gas chromatograph. Reproduced from Brink, Wandel, Pittaway, Hancock & Pather (2010).	25

2.4	Reiser demonstrating suppression of surface waves with a monolayer film. (a) Waves in water-wind tunnel with 25 mph wind with no monolayer. (b) Smooth surface at 25 mph after the application of a surface film. Reproduced from Reiser (1969).	28
2.5	Comparison of application rates as a function of wind speed calculated using three different application rate equations. This is the application rate (grams of monolayer per hour) required to cover a 1 ha surface area with C18OH at various wind speeds ranging from 4-26 km/h.	30
3.1	Laboratory (Langmuir trough) measurements of surface pressure and evaporative resistance of the same three monolayer compounds applied to clean water. Reproduced from Brink et al. (2010).	42
3.2	Laboratory (Langmuir trough) measurements of surface pressure and evaporative resistance of the same three monolayer compounds applied to brown, Narda Lagoon water. Reproduced from Brink et al. (2010).	42
3.3	Illustration of the necessary water quality and biology information required for the UDF.	47
3.4	Illustration of the necessary topographical information required for the UDF.	48
3.5	Illustration of the necessary historical climate information required for the UDF. Sample data is from the BOM weather station located at the University of Queensland, Gatton Campus, Queensland, Australia.	50
3.6	Illustration of the necessary water value information required for the UDF. Sample data in this illustration is purely illustrative.	51
4.1	Spreading of the alcohol emulsions made with Brij78 compared to powdered alcohols using a 6x application. Reproduced from Herzig, Barnes & Gentle (2011).	57

-
- 4.2 A comparison of evaporation resistances of monolayers spread from powder and emulsion using a 6x application amount. These emulsions were made with Brij emulsifiers. Reproduced from Herzig et al. (2011). . . . 58
- 5.1 (a) Polypropylene plastic bin, diameter 0.3 m; and (b) polyethylene cattle trough, used for spreading rate tests. The trough is shown with a measuring tape suspended across the top for calibrating the digital rulers used during video analysis. 67
- 5.2 (a) Talcum powder application (prior to monolayer application) to visualise the spreading characteristics of the monolayer on the water surface; and (b) monolayer spreading in a circular pattern as is identified by the talcum powder collecting around the edges of the spreading front (both shown here for the 6 m diameter tank). 69
- 5.3 Screen shots of video analysis using Adobe Flash (2 m diameter tank shown): (a) First point of contact at $t = 0$ seconds (no monolayer has been applied yet); (b) Radius of the monolayer 5 seconds after application; (c) Radius of monolayer 10 seconds after application; (d) Radius of monolayer 15 seconds after application. 70
- 5.4 6 m diameter water tank (lined with a black polyethylene liner) used for spreading rate tests. Monolayer is being then applied (by the author) with a calibrated medical syringe fixed to the end of a 3 m long aluminium tube for reach. Another aluminium tube, inside the larger diameter aluminium tube, is used to push down on the syringe plunger to apply monolayer. 73
- 5.5 Radius increase versus time for monolayer spreading on the 2 m and 6 m diameter tank. As is visible in both tanks, the monolayer spreads until nearing the edge of the tank where the spreading rate drops to zero. . . 74

5.6 The leading edge radius versus time for a 6x application of monolayer placed at the centre of the 0.3 m diameter tank (at time = 0). At each timestep the error bars represent the mean and standard deviation of five replicate experiments. The average standard deviation is 0.0045 m. 75

5.7 The leading edge radius versus time for three different application amounts of monolayer (1x, 3x and 6x) placed on the 2 m diameter tank (at time = 0). At each timestep the mean and standard error resulting from replicate experiments is shown. 76

5.8 The leading edge radius versus time for three different application amounts of monolayer (1x, 3x and 6x) spread on the 6 m diameter tank (at time = 0). At each timestep the mean and standard error resulting from replicate experiments is shown. 76

5.9 Comparison of radius increase over the first 10 seconds for 7 mg of emulsion spread on the 2 m and 6 m diameter tanks. Each line represents the average of three replicates. The error bars represent the standard deviation for the three replicates. The standard deviations are 0.024 and 0.027 for the 2 m and 6 m tanks respectively. The influence of surface area on spreading rate is clearly evident. (The data for the 6m tank at t=3.5 s is anomalous and attributed to an erroneous measurement rather than a physical effect.) 78

5.10 Comparison of measured spreading front radius versus time for the 0.3 m diameter tank, (i) measured data, (ii) equation (5.1) with $K = 1.15$ and $n = 0.75$ (Berg and Chebbi values), and (iii) equation (5.1) with K and n values from Table 5.2. 79

5.11 Comparison of measured spreading front radius versus time for the 2 m diameter tank at a 6x monolayer application, (i) measured data, (ii) equation (5.1) with $K = 1.15$ and $n = 0.75$ (Berg and Chebbi values), and (iii) equation (5.1) with K and n values from Table 5.2. 80

5.12	Comparison of measured spreading front radius versus time for the 6 m diameter tank at a 6x monolayer application, (i) measured data, (ii) equation (5.1) with $K = 1.15$ and $n = 0.75$ (Berg and Chebbi values), and (iii) equation (5.1) with K and n values from Table 5.2.	81
5.13	Comparison of the predicted spreading front radius versus time derived from the three different tanks scales by extrapolation to 100 s duration via equation (5.1). Each extrapolation used the empirically-derived K and n values (Table 5.2) for the 6x application.	81
5.14	Comparison of the predicted spreading front radius versus time derived from the three different tanks scales by extrapolation to 100 s duration via equation (5.1) using scale-dependant K values (Table 5.2) with the global mean empirical scaling exponent $n = 0.78$	82
6.1	Monolayer coverage maps based on hourly observations made by an observer using a plane table and alidade from a vantage point atop a 27.4 m tower. The above map shows coverage achieved under a 12.4 km/h wind speed and the map below shows coverage during a 17.7 km/h wind speed. Reproduced from Crow & Mitchell (1975).	89
6.2	Diagrammatic overview of experimental set-up, shown in plan view, comprising axial-flow fan, air duct, adjustable wind vanes, expansion chamber, air straighteners and water tank.	91
6.3	Experimental set-up in the laboratory.	92
6.4	Adjustable wind vane apparatus allowing control over the direction of air flow to evenly fill the volume of the expansion chamber. This apparatus was necessary in producing a uniform wind velocity profile at the outlet.	93

- 6.5 Vertical velocity profiles measured at 20 mm intervals above the water surface for 1 m and 3m distances from the middle of the outlet of the duct: (a) velocity profile for 3.8 m/s wind velocity; (b) velocity profile for 4.5 m/s wind velocity; (c) velocity profile for 5.2 m/s wind velocity; (d) velocity profile for 8.3 m/s wind velocity. 95
- 6.6 The average of the horizontal wind velocity profiles (i.e. the average of all 88 individual wind velocities measured in the x and y direction) for the four test wind velocities of: 3.7, 4.5, 5.2 and 8.3 m/s. Error bars represent the standard deviation of 7 individual measurements for each point. 96
- 6.7 The float depth of a 7 mm diameter polyethylene sphere, which were used as an indicator for the drift velocity of the water surface. The centroid of the submerged portion of the sphere was estimated to be 1.75 mm below the water surface. 97
- 6.8 Snap shots from video showing the evolution of the spreading of monolayer continuously applied under a uniform imposed wind velocity of 4.5 m/s: (a) predetermined wind velocity has been reached and monolayer application has just begun at A; (b) monolayer is now spreading laterally and drifting down wind; (c) spreading angles have now equilibrated and measurement of the angle can begin; (d) the equilibrium spreading angle is maintained, even after almost 60 seconds. 100
- 6.9 Video analysis process for determining the spreading angles of monolayer (Part 1): (a) a box representing the boundaries of the designated workable wind area is overlaid over the video; (b) a line of best fit is manually fitted to each defined edge between calm and wavy water surface by eye. 102
- 6.10 Video analysis process for determining the spreading angles of monolayer (Part 2): (c) the fit of the line is manually checked for at least 60 seconds of video; (d) an angle template is then fitted over the lines of best fit, by eye, to determine the spreading angle. 103

6.11 Comparison of the drift velocities at three difference reference wind velocities plotted as a function of application rate. Each point on the graph represents the average of four replicates. Error bars represent the standard deviation of the four replicates for each point.	104
6.12 Comparison of measured sphere velocity with continuous application of monolayer, and without the presence or application of monolayer, plotted as a function of the reference wind velocity.	106
6.13 Series of still images depicting the growth stages of the monolayer spreading pattern under wind stress: (a) spread pattern about 1 second after application was initiated; (b) after 4 seconds; (c) after 7 seconds; (d) after 9 seconds; (e) after 13 seconds; (f) after 14 seconds; (g) after 17 seconds; (h) after 20 seconds.	109
6.14 Relationship between spreading angle and application rate at the four reference wind velocities. Error bars represent the standard deviation of the angle measurement for each test.	110
6.15 Relationship between spreading angle and reference wind velocity. . . .	110
6.16 Comparison of measured sphere velocity with continuous application of monolayer and without the presence or application of monolayer plotted as a function of the reference wind velocity.	112
6.17 Diagram of the wedge (i.e. circular segment) shaped spread pattern of monolayer under wind stress. The length of the edge of the wedge is calculated from the drift rate measured in Section 6.4.1, and denoted as, $d_{ex}(t)$. Also shown is the resultant or net force, F_{net} , of the wind shear force, τ_u , and the net spreading force, S_{net} , acting on the edge of the wedge, thereby creating the internal angle of the half-wedge ($\theta/2$). . . .	113
7.1 Illustrative overview of the basic model inputs, outputs and simulation requirements.	122

- 7.2 Illustration of the wedge on-water (green) and off-water (red) surface areas for each applicator at a user-specified wind speed and wind direction. Only applicators 2 and 3 have an on-water coverage area of $\geq 50\%$. Whereas applicators 1 and 8 have an on-water coverage area of $< 50\%$. Therefore, under this scenario, applicators 2 and 3 will be used for dosing. 129
- 7.3 Illustration of the effective water surface area that each applicator will cover with monolayer at a user-specified wind speed and wind direction. The coverage area overlap between applicators 2 and 3 has been divided up by the proportion each contributes to the overlap so that there is no double-up when calculating the application rate. 130
- 7.4 Graph of the percentage of surface coverage over time as output from the MATLAB simulation platform. 132
- 7.5 The distribution of monolayer coverage at the end of the simulation period as output from the MATLAB simulation platform. Although there are actually 8 applicators here, only 3 are shown to be applying monolayer for this wind speed and wind direction (green = applicators on; red = applicators off). 133
- 7.6 (a) Illustration of ‘pre’ steady-state conditions, the applicator within the waterbody is providing added coverage. (b) Illustration of ‘post’ steady-state, the applicator within is now not providing any additional coverage to that already being provided by the applicator near the shore. 135
- 8.1 Amberley, QLD (low-wind site) is located 51 km West of Brisbane, 53 km East of Gatton, 89 km East of Toowoomba and 433 km North East of Moree. 142
- 8.2 BOM annual wind roses for Amberley, QLD (low-wind site): (a) 9 am wind rose; and (b) 3 pm wind rose. 143
- 8.3 Moree, NSW (high-wind site) is located 473 km South West of Brisbane, 381 km North East of Dubbo and 639 km North West of Sydney. 144

8.4	BOM annual wind roses for Moree, NSW (high-wind site): (a) 9 am wind rose; and (b) 3 pm wind rose.	145
8.5	50 x 50 m storage applicator arrangements: (a) 4 + 1, an applicator in each corner plus 1 in the centre of the storage; (b) 4 applicators placed in each corner; and (c) 1 applicator placed in the centre of the storage. .	146
8.6	500 x 500 m storage applicator arrangements: (a) 6 x 6 applicator grid, with 100 m spacing between applicators; (b) 12 + 1, four applicators on each side plus 1 in the centre of the storage; (c) 4 + 1, an applicator in each corner plus 1 in the centre of the storage.	147
8.7	5000 x 5000 m storage applicator arrangements: (a) 21 x 21 applicator grid (441 applicators), with 250 m spacing between applicators; (b) 11 x 11 applicator grid (121 applicators), with 500 m spacing between applicators; and (c) 6 x 6 applicator grid (36 applicators), 1000 m between applicators.	148
8.8	Wind rose of the BOM annual wind speed and direction frequencies for Moree, NSW.	149
8.9	500 x 500 m storage asymmetrical applicator arrangements: (a) 15 + 1, 15 strategically located applicators on the shore and 1 floating applicator in the middle; (b) 18 + 12, 18 strategically located applicators on the shore and 12 evenly spaced apart floating applicators.	150
8.10	Percentage of time a minimum area is covered for the 50 x 50 m storage after 1 hour of application. Results are shown for all three application arrangements, 4 + 1, 4 and 1, for both Amberley and Moree wind conditions.	152
8.11	Percentage of time a minimum area is covered for the 500 x 500 m storage after 3 hours of application. Results are shown for all three application arrangements, 6 x 6, 12 + 1 and 4 + 1, for both Amberley and Moree wind conditions.	155

8.12	Percentage of time a minimum area is covered for the 5000 x 5000 m storage after 5 hours of application. Results are shown for all three application arrangements, 21 x 21, 11 x 11 and 6 x 6, for both Amberley and Moree wind conditions.	158
9.1	Overview of the UDF processes, which involves input of necessary information, analysis of the information to inform design, planning, installation and operation/management of a monolayer application system. Green boxes represent inputs, orange boxes represent analysis, blue boxes represent user performance criteria and purple boxes represent outputs. The grey box represents the iterative modelling process. .	167
9.2	‘Google Earth’ satellite image of the rectangular ring tank storage used in this demonstration. The storage is located at Amberley in Queensland and has a width of 300 meters and a length of 460 meters, which is a surface area of 13.8 ha.	176
9.3	Wind rose of the annual wind speed and direction frequencies for Amberley, QLD.	179
9.4	Asymmetrical applicator arrangement that satisfied the user-specified performance criteria by providing at least 60% cover at least 90% of the time within a 3 hour response time for the Amberley dam of Figure 9.2. As shown, a greater density of applicators are required on the East and South shores. (There is no applicator at the origin (0,0).)	180
9.5	Volume of water saved by the monolayer for each month of the year and the quantity of monolayer product used to achieve these savings.	186
A.1	Factors that effect a change in water volume (Craig et al. 2005b)	215
A.2	Druck 4030 pressure sensitive transducer (Craig et al. 2005b)	216

A.3	Schematic diagram showing the structures of the liquid-condensed and solid monolayer phases. The hydrophilic groups are shown as open circles, and the hydrocarbon (alkyl) chains as grey lines (Barnes 2008) . . .	217
A.4	The evaporative reduction performance of three monolayer products during trough Trial 6, T1=C18E1; T2=Silicone oil (Aquatain); T3=C16 (WaterSavr at the recommended application rate); T3b=C16 (WaterSavr at 2x recommended); T4=Control (no monolayer), are presented as the depth deviation from the control. The blue arrow indicate when product was applied, and the bolder red arrows represent missed applications for C18E1 (Morrison, Gill, Symes, Misra, Craig, Schmidt & Hancock 2008)	223
A.5	Microbial degradation rates of C16OH, C18OH and C18E1 (Pittaway 2008)	224
A.6	Surface Pressure vs. Time for Δ - C16OH and <i>O</i> - C18E1. It is significant that C18E1 reaches a higher surface pressure in a much shorter time than C16OH, which indicates that C18E1 spreads more rapidly. Graph reproduced from Deo, Kulkarni, Gharpurey & Biswas (1962)	225
A.7	Floating application units for application of monolayer in a solvent form. (a) Floating solvent application unit. (b) Detailed section of wind valve for application unit. (c) Floating gear driven water-wheel pump for solvent application. (Treloar 1959)	227
A.8	Underwater gravity-type monolayer film dispenser (Koberg 1969)	228
A.9	Film pump for producing and spreading a monolayer (Pauken, Jeter & Abdel-Khalik 1996)	230
A.10	Aquatain Dosing Units. (a) DS-1 gravity feed tap-timer system (b) DS-2 peristaltic pumping system	231
A.11	Apparatus for applying oil to the surface of a solar pond (Lahav & Alto 1984)	232

A.12 Oil application, collecting, purifying, controlling and recirculating system (Lahav & Alto 1984)	233
A.13 Venturi style emulsion application of molten cetyl alcohol (Reiser 1970)	234
A.14 Wind controlled apparatus for the application of emulsified cetyl alcohol (Reiser 1970)	234
A.15 Detail of wind controlled valve on the spray heads (Reiser 1970)	235
A.16 JV-225 boat mounted WaterSavr mixing system (FSI 2007)	236
A.17 WaterSavr mixing system designed and built by Bio-Systems Engineering (FSI 2007)	237
A.18 Diagram of a Hot-Spray Application System (Florey 1965)	239
A.19 Diagrams of a Robertson grinder-duster. (a) Detailed internal view (b) Section along 2-2 (Robertson 1966)	242
A.20 Diagrammatic sketch of the wind operated powder dispensing system. Reproduced from: (Nicholaichuk & Pohjakas 1967)	243
A.21 Nylex pneumatic spreader (Craig 2006)	244
A.22 WaterSavr powder being pneumatically spread from just below the water surface (Brink & Symes 2010)	245
A.23 M-60 Automatic Spreader (FSI 2007)	245
A.24 Prototype temperature differential detection unit (Coop et al. 2008)	248
A.25 Comparison of temperature difference between water inside the Y-tube and bulk water outside the tube. Water temperature inside the Y-tube is the thick line. Bulk water temperature outside is the thin line. Humidity at 32% and wind speed at fan is 5.3 m/s. (Coop et al. 2008)	249

- A.26 Water particles at the surface move clockwise on nearly circular paths as the wave moves from left to right (Cutnell & Johnson 2001) 252
- A.27 Relative evaporation and wind speed at various distances from 60% porous slat-fence barrier. Plotted data are averaged from five observation periods with open-field wind speeds from 6.2 to 7.1m/sec at an elevation of 1.42m above soil surface. Reproduced from (Skidmore & Hagen 1970) 253
- A.28 Relative evaporation and wind speed at indicated distances from 40% porous slat-fence barrier. Plotted data are averaged from five observation periods with open-field wind speeds from 5.6 to 6.2m/sec at an elevation of 1.42m. Reproduced from (Skidmore & Hagen 1970) 254
- A.29 Relative evaporation and wind speed at various distances from 60% porous slat-fence barrier. Plotted data are averaged from five observation periods with open-field wind speeds from 6.2 to 7.1m/sec at an elevation of 1.42m above soil surface. Reproduced from (Skidmore & Hagen 1970) 254
- A.30 Crow's experimental pond showing 'Type B' closed wind/film barriers for reducing wind speed and confining monolayer within each bay. Reproduced from (Crow 1963) 256
- A.31 Crow's evaporation reduction tests of wind barriers and baffles with and without monolayer. (a) The effectiveness of closed wind barriers of different spacing/height (L/H) ratios for reducing evaporation. These tests were made without monolayer. (b) Relative evaporation reduction resulting from confinement of C16OH and C18OH fatty alcohol monolayer confined within closed wind/film barriers of different L/H ratios. Reproduced from (Crow 1963) 257

- A.32 The effect of a snow-fence windbreak and a monolayer film on cumulative evaporation. The vertical axis is cumulative evaporation ranging from 0 to 110 cm and the horizontal axis is time ranging from 0 to 170 days. Reproduced from Nicholaichuk (1978). 259
- A.33 The effect of a snow-fence windbreak, monolayer film and floating grids on cumulative evaporation. The vertical axis is cumulative evaporation ranging from 0 to 110 cm and the horizontal axis is time ranging from 0 to 170 days. Reproduced from Nicholaichuk (1978). 260
- A.34 The wind speed reduction by different shelterbelts. Reproduced from (Naegeli 1953) 261
- A.35 Perspective view of Magill's preferred embodiment of his baffle plate breakwater (Magill 1953) 264
- A.36 Mito's floating breakwater design. (a) Longitudinal side sectional view of the elongated floating housing bodies. (b) A plurality of elongated floating housing bodies arranged in parallel to each other. (Mito 1974) . 265
- A.37 John O. Olsen's floating breakwater consisting of a large number of plastic interlocking pontoon modules arrangement (Olsen 1975) 266
- A.38 Kodairo and Kunitachi's floating breakwater design. (a) Plan view of the floating breakwater. (b) Side view showing a partial cross-section of the floating breakwater (Kodairo & Kunitachi 1976) 267
- A.39 Wallace W. Bowley's floating wave barrier arrangement comprising a plurality of submerged vessels (Magill 1953) 268
- A.40 Perspective view of Angioletti's floating breakwater and the association of thei device with water waves (Angioletti 1980) 269
- A.41 Side view of Kann's wave suppression system including a plurality of wave suppression members coupled together along a water surface (Kann 1998) 269

- A.42 Side view, on a greatly enlarged scale, of one end of the devices and a cross-section of the device showing the internal construction. (Kiefer 1967) 270
- A.43 End view in cutaway cross-section of Stanwood's pool lane float (Stanwood 1970) 270
- A.44 Side view of a section of one of the racing lane markers and a side view of the racing lane markers arranged with the float means (Walket 1973) 270
- A.45 Perspective view of one of the baffle elements and side view of a portion of the assembly, on an enlarged scale (Walket 1974) 271
- A.46 Side view of a cross-section of Lowe's wave suppression device and a partial side view of a length of the wave suppression device with portions thereof broken away to show detail (Lowe 1974) 272
- A.47 Baker's wave suppression float member. (a) Cross-sectional view through the float member. (b) Logitudinal section and a cross-section through a float member (Baker 1977) 273
- A.48 Perspective view of a pair of the devices in place on a section of cable and a typical end elevation of one of the units (Kajlich 1977) 273
- A.49 Exploded side view of a fragmentary portion of Rademacher's lane marker (Rademacher 1986) 274
- A.50 Perspective view of the Kiefer wave suppression element (Kiefer 1990) . 275
- A.51 Graphical representation of the energy dissipation efficiency of the present invention compared to a prior art wave suppression means (Kiefer 1990) 276
- A.52 Eddy's wave suppressor design. (a) Side view of a pair of wave suppressors shown as wound around a storage reel. (b) Side view of the wave suppressor and floatation means prior to insertion. (Eddy 1996) 276

-
- A.53 A plurality of flexible wave inhibiting devices for a pool lane divider arranged on a cable (Kajlich 2006) 277
- A.54 Diagrammatic view of Ruhlman's water barrier curtain installed in a body of water. Reproduced from: (Ruhlman 1972) 279
- A.55 Thurman's floating oil containment boom. (a) Side view of a portion of the floating oil containment boom. (b) Front sectional view through the floating oil containment boom. Reproduced from: Thurman (1973) . . . 280
- A.56 Cerasari's floating oil containment boom. (a) Side elevational view illustrating the buoyant support member. (b) Front elevational view of several buoyant support members. Reproduced from: (Cerasari 1974) . 281
- A.57 Fragmental perspective view of the oil fence in a patent by Kinase et al. (1976) 282
- A.58 Isometric view of one individual outrigger-float and frame of the floating barrier. Reproduced from: (Casey 1976) 283
- A.59 Geist's articulated floating oil barrier. (a) Perspective view of an assembled preferred embodiment of the barrier. (b) Plan view in section of a portion of two assembled sections of the barrier. Reproduced from: Geist (1977) 284
- A.60 Illustration of a transverse cross-section of this boom at the location of a stiffener. Reproduced from: Jaffrennou & Cessou (1984) 284
- A.61 Smith's oil containment system for emergency use. (a) Partial cross-sectional view of the oil containment system in its stored position. (b) Side elevational view of the containment system in the deployed position. Reproduced from: Smith (1992) 285

A.62 Vidal's liquid film maintenance apparatus: (a) Enlarged plan view of an assembled float member. (b) Perspective view of the various disassembled parts of one of the float members. Reproduced from: Vidal (1967)	286
A.63 Plan view of a typical installation for Vidal's apparatus. Reproduced from: Vidal (1967)	286
A.64 Plan view of Neilsen's oil boom fending device. Reproduced from: Nielsen (1977)	287
A.65 Plan view illustrating a mode of use of the fending devices. Reproduced from: Nielsen (1977)	287
E.1 The design for a centralised monolayer application system.	348
E.2 The design for a de-centralised monolayer application system.	349
E.3 The design for a hybrid application system, which is a combination of the centralised and de-centralised systems.	351
E.4 A concept of a method for applying monolayer as a fine powder ground from a solid-cast rod using a wire-brush.	353
E.5 A variety of other concepts for grinding solid-cast monolayer into a fine powder for application.	354
E.6 This is a concept for the application of monolayer from a wax tape. The general idea is that monolayer would be applied to one side of a long length of wax tape and then the wax tape would be rolled onto a spool ready for application.	356

-
- E.7 Concept for the spray application of molten monolayer. When the molten monolayer is sprayed into the air just above the water surface it would solidify into fine particles, which would fall onto the water surface. It is believed that this form of application would improve the spreading properties of the monolayer. 358
- E.8 Concept for the application of monolayer as an effervescent tablet. . . . 360
- E.9 Concept for the application of monolayer as an effervescent ball/sphere. A sphere shaped tablet would increase surface area over the traditional disk shaped tablet, thereby enhancing the effervescent reaction upon contact with water. 361
- E.10 Concept floating monolayer applicator design. 363
- E.11 Concept design for a low cost adaptation of the current (or similar) CRCIF Floating Applicator for shore-based delivery of monolayer product. 365
- E.12 A pseudo-sectional view of the simple cantilever anchoring system for the shore-based monolayer applicator. 366
- E.13 Pre-prototype floating applicator; (a) three-quarter view of the applicator; (b) view underneath the applicator; (c) view inside the metal housing; and (d) schematic of the anchor and self-adjusting mooring set-up for the applicator on a farm dam (the rope is free to slip through the eye in the anchor). Reproduced from Brink et al. (2011). 368

List of Tables

1.1	Summary table of three commercially available evaporation mitigation products evaluated by the NCEA to determine a range (from low to high) for their evaporative reduction performance (%), installation cost (\$/m ²), operating and maintenance cost (\$/ha/yr) and breakeven cost (\$/ML saved). Reproduced from Craig et al. (2005b).	3
2.1	Comparison of various laboratory studies investigating the relationship between monolayer surface drift speed (U_m) and wind speed (U_w). Adapted from Lange & Huhnerfuss (1978) and Hale & Mitchell (1997).	21
2.2	Comparison of the various U_{MAX} values (wind speed cut-off point for monolayer application) adopted by researchers during field trials.	22
2.3	Fractional loss of monolayer material from a monolayer film at a surface pressure of 35mN/m. Adapted from Brooks & Alexander (1960).	23
2.4	Summary of relevant information from field studies employing distributed application systems for monolayer in a liquid form.	34
5.1	Surface pressures measured for C18OH and Brij78 in water-emulsion at different application amounts.	65

5.2	Summary of monolayer quantities applied and water temperatures during testing, including the constants and exponents derived from the 0.3, 2 and 6 m diameter tank results.	77
6.1	Comparison of various laboratory studies investigating the relationship between clean water surface drift speed (u_s) and wind speed (u_w). Field studies in lakes and open oceans have been omitted from this table as u_s is generally greater, most likely due to an increase in Stokes mass transport by developed deep-water waves (Lange & Huhnerfuss 1978). Adapted from (Lange & Huhnerfuss 1978) and (Hale & Mitchell 1997). . .	86
6.2	Summary of the drift velocity test application rates used for each reference wind velocity.	101
6.3	Summary of the spread angle test application rates used for each reference wind velocity.	107
7.1	Table as output from the MATLAB simulation platform showing the Cartesian coordinates (x and y location) of each applicator and the corresponding total amount of monolayer applied for that applicator. Applicator locations are listed anti-clockwise, starting from the bottom left-hand corner of the distribution graph (Figure 7.5).	134
8.1	BOM wind rose speed ranges and the corresponding wind speeds used in modelling.	141
8.2	Percentage of time a minimum area is covered for the 50 x 50 m storage after 1 hour of application. Including the average of the percentages of time, the aggregate application rate over that period and the total amount of monolayer applied for each arrangement. Results calculated using BOM average annual wind speeds and directions for both Amberley and Moree.	153

8.3	Percentage of time a minimum area is covered for the 500 x 500 m storage after 3 hours of application. Including the average of the percentages of time, the aggregate application rate over that period and the total amount of monolayer applied for each arrangement. Results calculated using BOM average annual wind speeds and directions for both Amberley and Moree.	156
8.4	Percentage of time a minimum area is covered for the 5000 x 5000 m storage after 5 hours of application. Including the average of the percentages of time, the aggregate application rate over that period and the total amount of monolayer applied for each arrangement. Results calculated using BOM average annual wind speeds and directions for both Amberley and Moree.	159
8.5	Percentage of time a minimum area is covered for the 500 x 500 m storage after 3 and 6 hours, the average of the percentages of time, the aggregate application rate over that period and the total amount of monolayer applied for each arrangement. Results calculated for Moree only.	161
9.1	Decision table capturing the water quality attributes of three water storages in south-east Queensland (Pittaway & van den Ancker 2010) were matched with the performance specifications of three monolayer compounds to predict which product will best perform on a given storage.	170
9.2	Data output from the simulation platform, which details the percentage of cover achieved, the aggregate application rate and the time to steady-state for each wind condition.	181
9.3	Data output from Post-Process 1 using the percentages of cover for each wind condition, as output from the simulation platform (Table 9.2), and applying a weighting for the frequency of that wind condition occurring. The frequency weightings were derived from BOM wind speed and direction frequency data for Amberley, Qld.	182

9.4	Data required for Post-Process 2. These data were determined via the simulation platform and Post-Process 1 using monthly wind speed and direction frequency data from the BOM for Amberley, Qld. Simulations were run firstly for all applicators, and secondly for the shore-based applicators only.	185
9.5	Data output from Post-Process 2 detailing the monthly quantity of mono-layer product used and the volume of water saved.	187
A.1	Summary of the advantages and disadvantages of various methods for measuring evaporation from farm water storages (Part 1). Overview based on Craig and (Hancock 2008)	210
A.2	Summary of the advantages and disadvantages of various methods for measuring evaporation from farm water storages (Part 2). Overview based on Craig and (Hancock 2008)	211
A.3	Summary of the advantages and disadvantages of various methods for measuring evaporation from farm water storages (Part 3). Overview based on Craig and (Hancock 2008)	212
A.4	Summary of the advantages and disadvantages of various methods for measuring evaporation from farm water storages continued (Part 4). Overview based on Craig and (Hancock 2008)	213
A.5	Summary of the advantages and disadvantages of various methods for measuring evaporation from farm water storages continued (Part 5). Overview based on Craig and (Hancock 2008)	214
A.6	Commercially produced chemical film products currently available in Australia (CSIRO 2008)	221

A.7	Mean wind speed reduction in the lee of four different density shelterbelts over distances of 10H, 20H and 30H. H is the distance (down wind) from the shelterbelt where the wind speed measurement was taken. Reproduced from (Naegeli 1953)	262
C.1	Amberley average annual (9am and 3pm) wind frequency table used in modelling (Part 1).	300
C.2	Amberley average annual (9am and 3pm) wind frequency table used in modelling, continued (Part 2).	301
C.3	Moree average annual (9am and 3pm) wind frequency table used in modelling (Part 1).	306
C.4	Moree average annual (9am and 3pm) wind frequency table used in modelling, continued (Part 2).	307
D.1	Decision table A (Part 1).	309
D.2	Decision table A (Part 2).	310
D.3	Decision table A (Part 3).	311
D.4	Decision table A (Part 4).	312
D.5	Decision table A (Part 5).	313
D.6	Decision table A (Part 6).	314
D.7	Decision table A (Part 7).	315
D.8	Decision table A (Part 8).	316
D.9	Decision table A (Part 9).	317
D.10	Decision table A (Part 10).	318

D.11 Decision table A (Part 11).	319
D.12 Decision table A (Part 12).	320
D.13 Decision table A (Part 13).	321
D.14 Decision table A (Part 14).	322
D.15 Decision table A (Part 15).	323
D.16 Decision table A (Part 16).	324
D.17 Decision table A (Part 17).	325
D.18 Decision table A (Part 18).	326
D.19 Decision table A (Part 19).	327
D.20 Decision table B (Part 1).	328
D.21 Decision table B (Part 2).	329
D.22 Decision table B (Part 3).	330
D.23 Decision table B (Part 4).	331
D.24 Decision table B (Part 5).	332
D.25 Decision table B (Part 6).	333
D.26 Decision table B (Part 7).	334
D.27 Decision table B (Part 8).	335
D.28 Decision table B (Part 9).	336
D.29 Decision table B (Part 10).	337
D.30 Decision table B (Part 11).	338

D.31 Decision table B (Part 12).	339
D.32 Decision table B (Part 13).	340
D.33 Decision table B (Part 14).	341
D.34 Decision table B (Part 15).	342
D.35 Decision table B (Part 16).	343
D.36 Decision table B (Part 17).	344
D.37 Decision table B (Part 18).	345
D.38 Decision table B (Part 19).	346

Acronyms & Abbreviations

\AA	Angstrom ($=10^{-10}\text{m}$)
\AA^2	Square angstrom ($=10^{-20}\text{m}^2$)
ABS	Australian Bureau of Statistics
BOM	Bureau of Meteorology (Australia)
C12OH	Dodecyl or lauryl alcohol or dodecanol ($\text{C}_{12}\text{H}_{26}\text{O}$)
C14OH	Myristyl alcohol or tetradecanol ($\text{C}_{14}\text{H}_{30}\text{O}$)
C16OH	Cetyl alcohol or hexadecanol ($\text{C}_{16}\text{H}_{34}\text{O}$)
C18OH	Stearyl alcohol or octadecanol ($\text{C}_{18}\text{H}_{38}\text{O}$)
C20OH	Arachidyl alcohol or icosanol ($\text{C}_{20}\text{H}_{42}\text{O}$)
C18E1	Ethylene glycol mono-octadecyl ether ($\text{C}_{20}\text{H}_{42}\text{O}_2$)
CRC-IF	Cooperative Centre for Irrigation Futures
CSIRO	Commonwealth Scientific and Industrial Research Organisation
ERF	Evaporation reduction factor
GL	Gigalitre ($=10^9\text{L}$)
ML	Megalitre ($=10^6\text{L}$)
NCEA	National Centre for Engineering in Agriculture
SEQ	South East Queensland
SGS	Société Gènèrale de Surveillance
UDF	Universal Design Framework
U_m/U_w	Ratio of monolayer surface drift speed and wind speed
U_{MIN}	Minimum wind speed threshold
U_{MAX}	Maximum wind speed threshold
UNE	University of New England
USQ	University of Southern Queensland
UV	Ultra-violet

Chapter 1

Introduction

1.1 Background

The following section provides an introduction to the Australian agricultural context, estimates of water loss from farm water storages due to evaporation and available technologies to farmers to mitigate these losses. Further detail with respect to using a chemical monolayer¹ to protect open water surfaces is also provided.

1.1.1 Context

Australia is the driest inhabited continent on the Earth. It is a continent of climatic extremes, experiencing great variations in rainfall and evaporation, according to region and season. Rainfall is generally confined to a narrow strip along the north and east coast of the continent, including Tasmania (BOM 2007). Australia's often hot temperatures, dry air and strong winds means that water evaporates into the atmosphere at high rates. On average 92% of rainfall is re-evaporated, 7% reaches the sea and 1% recharges aquifers (ABS 2004). Seventy per cent of the country experiences mean monthly potential evaporation greater than its mean monthly rainfall, and for nearly half of Australia mean annual evaporation is more than twice the mean annual rainfall

¹Throughout this thesis, the word 'monolayer' refers to a monolayer film-forming material being applied, and does not imply that an effective monolayer actually forms on the surface.

(Fietz 1970).

Annual evaporation losses from farm water storages in Australia can potentially exceed 40% of storage volume (Craig et al. 2005a). While the extent and distribution of farm water storages is not accurately known, it is conservatively estimated that nationally there is in excess of 12,500 GL of water stored on an estimated 22,000 agricultural enterprises. There are also approximately 500 registered large dams across Australia representing a further 85,000 GL of water. In addition, considerable water distribution losses are present in irrigation channels due to evaporation and seepage.

Although it is hard to accurately estimate Australia's total evaporative water loss, it is probable that thousands of GLs of water are lost each year from water storages. As a consequence, production opportunities worth tens of millions of dollars evaporate with the water. The outlook for the future is no better with the effects of climate change predicted to increase average temperatures across Australia, which will seriously affect evaporation and the viability of our current land use. It is predicted that by 2030 most of Australia will experience an annual warming of between 0.4°C and 2°C relative to 1990, and by 2070, temperatures are estimated to rise between 1°C and 6°C (CSIRO 2008).

Evaporation losses from storages can be minimised to some extent during design and construction through deep, small surface area storages or construction of storages with cells. Also the use of wind barriers, shelter belts and even dam destratification can help to reduce evaporative loss. Beyond this there are commercially available products such as floating covers (E-VapCap), suspended shade structures (NetPro) and chemical additives (WaterSavr).

The National Centre for Engineering in Agriculture (NCEA), which has been working actively in the field of evaporation mitigation for a number of years, conducted large scale engineering assessments of the three evaporation mitigation technologies noted above (Craig et al. 2005b). Table 1.1 summarises the product performance and breakeven costs of these products.

Chemical monolayers, (e.g. WaterSavr in Table 1.1), can provide the lowest potential

cost of water saved (\$130/ML at 30% efficiency). In addition, chemical monolayers need only be applied when water is in storage or when evaporation rates are high. This can reduce cost (\$/ML) to 75% of that shown in Table 1.1 when for example water is only held in storage between October and March (expected period of high evaporation). Further savings can also be achieved by more judicious monolayer application strategies.

1.1.2 Using a chemical monolayer to protect open water surfaces

Monolayers are not a new technology; in 1925 it was shown that the application of monomolecular films of certain organic compounds to a water surface can decrease the rate of evaporation (Frenkiel 1965). Following this discovery there were intensive laboratory studies, but it was not until 1952, in Australia, that the first attempts were made to apply monolayer under natural conditions to open water surfaces to reduce evaporation (Mansfield 1955). Subsequently many investigations have followed in Australia: Treloar (1959), Vines (1960*a*), Robertson (1966); in United States of America: Dressler & Guinat (1973), Crow (1963), Florey (1965), Reiser (1969), Koberg (1969); in Canada: Nicholaichuk (1978); in India: Walter (1963) and in Israel: Lahav

Table 1.1: Summary table of three commercially available evaporation mitigation products evaluated by the NCEA to determine a range (from low to high) for their evaporative reduction performance (%), installation cost (\$/m²), operating and maintenance cost (\$/ha/yr) and breakeven cost (\$/ML saved). Reproduced from Craig et al. (2005b).

Product	Evaporation Reduction (%)		Installation Cost (\$/m ²)	Operating Cost (\$/ha/yr)	Breakeven Cost (\$/ML saved)
	Small Tank (measured)	Farm Dam (estimate)			
E-VapCap	94%-100%	85%-95%	\$5.50-\$8.50	\$112-\$572	\$302-\$338
NetPro	69%-71%	60%-80%	\$7.00-\$10.00	\$112-\$537	\$296-\$395
WaterSavr	10%-40%	5%-30%	\$0.00-\$0.38	\$826-\$4,050	\$130-\$1,191

& Alto (1984). A full review of these studies is provided in Appendix A.

Although chemical monolayers offer great potential, their evaporation reduction performance has been shown to be highly variable and is affected by a number of influencing factors; in particular wind and wave action. In field studies at Lake Hefner, U.S. Bureau of Reclamation researchers found wind to be the single most important factor in the application and maintenance of monolayer film (Fietz 1959). Subsequently several strategic approaches were employed to reduce or eliminate the adverse effects of wind. They include: (1) continuous replenishment of monolayer at the up-wind shore, (2) reduction of wind speed near the water surface by wind-breaks along the shore or floating on the surface, and (3) restriction of air and film movement by confinement within a network of floating compartments.

The three strategies noted above were trialled at the Oklahoma Agricultural Experimental station (Crow 1963). At the conclusion of the trial, Crow noted that the method of continuous application of monolayer is the only feasible approach to the wind problem on large reservoirs. Alternatively, approaches 2 and 3 only offer an economical means of reducing evaporation losses from small farm storages.

Currently the bulk of research and development into evaporation mitigation by monolayers is being undertaken by the NCEA within their ‘Dam Evaporation Mitigation’ project, which was funded by the Cooperative Research Centre for Irrigation Futures (CRC-IF)². Also collaborating with the NCEA through the CRC-IF is a group at the University of New England (UNE) who are developing sensing technologies for detecting the presence of a monolayer film on the water surface. These sensing technologies are particularly relevant to this project and are fundamental in determining monolayer spatial distribution, breakdown and overall performance.

²Although the CRC-IF ended its 7 year term on June 30, 2010 this following link serves as an archive for all its research, education and training outputs: <http://www.irrigationfutures.org.au>

1.2 Hypothesis and research aim and objectives

1.2.1 Hypothesis

The central hypothesis of this research is:

- i. that present application systems and application strategies for applying chemical monolayer materials to open water surfaces are sub-optimal which has a deleterious effect on the spread and formation of an effective cover, which in turn results in an inconsistent and usually poor evaporation reduction performance; and
- ii. that significant improvements in monolayer performance maybe achieved through:
 - developing a better understanding of factors that influence monolayer performance and the environmental range/boundaries for the effective use of monolayer, then
 - utilise this information for the design, installation and operation of an automated monolayer application system, which is tailored to site-specific environmental conditions and user requirements.

1.2.2 Research aim and objectives

The aim of this research is to formulate and develop a universal framework to inform the selection of suitable monolayer material/s, the design of the application system and the application strategies to be used for a specific site. As every user and site is likely to be different, the framework developed will need to be robust enough to handle the differing site conditions and user requirements. It is anticipated that this universal framework will help to optimise the evaporation suppressing performance of the selected monolayer.

The aim to develop a Universal Design Framework (UDF) has led to the following research objectives and associated tasks:

Objective 1 - Formulation of the UDF:

- Identify environmental conditions that effectively nullify monolayer performance. These conditions will form the working environmental range/boundaries for monolayer use as well as the UDF.
- Identify influencing factors that will need to be taken into consideration for the design, planning, installation and operation/management of the application system.
- Identify the UDF information and processing requirements needed in order to determine suitable monolayer material/s, application system design and application strategies for a particular storage and user requirements.
- Formulate a UDF that incorporates all of the important influencing factors, environmental boundaries and processing requirements identified.

Objective 2 - Large-scale laboratory study of monolayer dispersion characteristics:

- Identify an existing evaporation suppressing monolayer material and develop a form in which the material can easily be used for all empirical work and for possible future field trials.
- Characterise the spreading rate and spreading pattern of monolayer for calm wind conditions when non-continuous application would be required.
- Characterise drift rate, spreading rate and spreading pattern for a range of wind conditions when continuous application would be required.
- Derive algorithms from the above empirical work for calibration of the simulation platform.

Objective 3 - Simulation platform development and demonstration:

- Develop a basic simulation platform capable of estimating/predicting monolayer surface coverage for different applicator arrangements, wind conditions and spatial scales.

- Calibrate the model with the algorithms derived from the laboratory study of monolayer dispersion characteristics.
- Demonstrate the ability and robustness of the simulation platform in modelling the distribution of monolayer for different wind conditions, storage sizes and application periods.

Objective 4 - Scope and demonstration of the UDF:

- Create a decision table that will allow the user to make numerical comparisons between the South East Queensland (SEQ) benchmark reservoirs and their own to determine the most suitable monolayer compound/s for their storage.
- Develop a process for using the UDF to determine a customised applicator arrangement with the simulation platform.
- Demonstrate the ability of the UDF for determining suitable monolayer product/s, optimal application system, decision tables for real-time application and the expected performance of the application system.

1.3 Overview of dissertation

This dissertation consists of ten chapters and five appendices. The relationship between the chapters is shown in Figure 1.1.

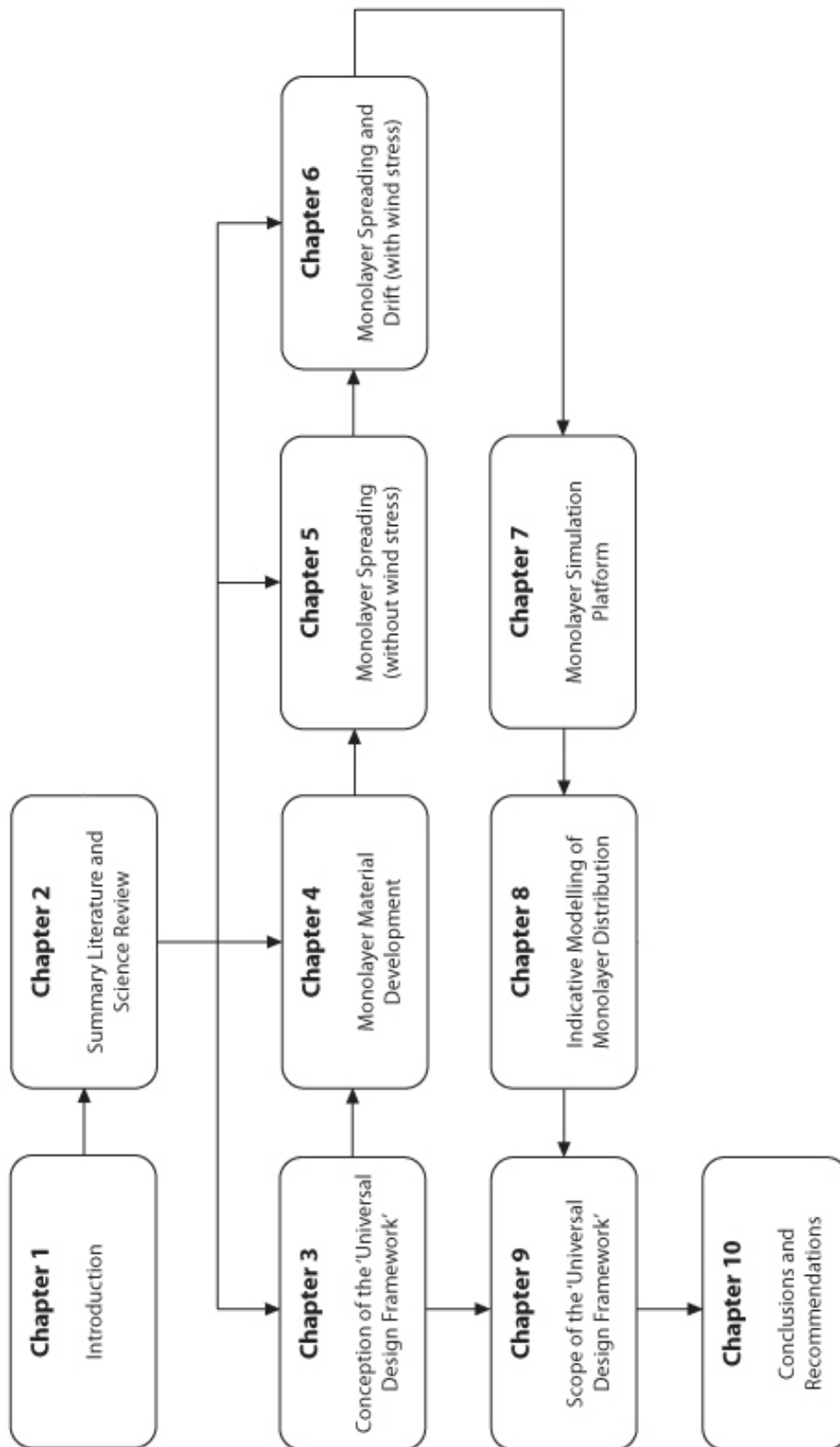


Figure 1.1: Block diagram of dissertation overview.

- **Chapter 2** provides a literature and scientific review of many different specialty areas within chemistry, physics and biology relating to the use of a monolayer for evaporation mitigation on agricultural water storages. Much of this information is largely summarised from Appendix A. Through the literature review the fundamental gaps in knowledge were identified, which also helped provide the necessary background information for Chapter 3 and the empirical studies conducted in Chapters 4, 5 and 6.
- Due to the complexity and quantity of the interactions occurring at the triple interface when using a monolayer, both at a macro and micro scale, and the fact that these conditions will likely differ for every situation, the Universal Design Framework was conceived. **Chapter 3** details the UDF introduction and scope, the initial development, an overview and sets out the research requirements that were handled in subsequent chapters.
- As monolayer-based evaporation mitigation is fundamentally reliant on the maintenance of the monolayer film over the great majority of the water surface, and the fact that wind is the number one determining factor of this, a study of the surface transport characteristics of monolayer under differing wind conditions was seen as a requirement. However, as a suitable monolayer material in a liquid form for ease of application was unavailable at the time, a suitable monolayer material was developed for all empirical work for this PhD. The development of this monolayer material is detailed in **Chapter 4**.
- Once a suitable monolayer material was developed, an empirical study, **Chapter 5**, was conducted to characterise the spreading rate and spreading pattern of monolayer without wind stress.
- A second empirical study, **Chapter 6**, was conducted to characterise spreading rate, spreading pattern and drift rate of monolayer with wind stress.
- A simulation platform was then developed for use as part of the UDF process in order to allow prediction of the expected water surface coverage with monolayer for different user scenarios (i.e. different size reservoirs, wind conditions and applicator arrangements). The simulation platform was calibrated with algorithms derived from the empirical work conducted in chapters 5 and 6. **Chapter 7**

details the rationale, formulation, development and overview of the simulation platform. Appendix B details the source code for the simulation platform.

- A demonstration of the simulation platform's capabilities and the post-processing of the simulated output data is provided in **Chapter 8**. The wind frequency tables used in post-processing and the Bureau of Meteorology (BOM) historical site-specific wind frequency data used to generate the tables are set out in Appendix C.
- The current scope (i.e. inputs, analyses and outputs) of the UDF methodology is detailed in **Chapter 9**, including a complete step-by-step theoretical demonstration of the UDF process. The decision tables, A and B, as output from the UDF for the on-site application strategies for the first 37 wind conditions are set out in Appendix D. Following the conclusions from the UDF outputs a number of monolayer applicator and system conceptual designs are presented in Appendix E.
- **Chapter 10** concludes with a summary of the achievement of objectives and recommendations for further work.

Chapter 2

Summary Literature and Science Review

2.1 Introduction and overview

In the pursuit of developing a strategic approach to the use of monolayer on a farm dam for evaporation mitigation, a wide-ranging cross-disciplinary literature review was conducted. It was initially proposed that an autonomous application system could simply be designed and deployed on a farm dam to reapply monolayer in response to wind speed and direction measured on-site. However, it became apparent that many unanswered questions remain from research from the 1950s, 1960s and 1970s, which must be addressed if we are to have any greater success than they had. Although, technologically we have advanced significantly and are able to design and manufacture far superior application systems for less with improved accuracy and reliability, it is the application strategies that require development. The application strategies, i.e. knowing how much monolayer to apply, where spatially to apply it and when to apply it, need to be improved as it is this knowledge that makes the application system 'smart'.

Application of monolayer appears, at first, a simple proposition. However, when dealing with a monomolecular film tens of nanometers thick on a farm dam exposed to the

elements, it is anything but simple. Many interactions occur at the triple interface, i.e. water/monolayer/air, both at a macro and micro scale. Therefore, literature in many different specialty areas within chemistry, physics and biology were consulted. As a first step in reviewing relevant literature, an understanding of exactly what a monolayer is and how it attaches and orientates itself into an orderly close packing monomolecular film on the water surface was required. In addition, the basics of evaporation and the effects that drive evaporation were determined, including an investigation into the mechanisms by which a monolayer film employs to suppress evaporation.

Upon reviewing literature reporting the in-field performance of monolayers, it quickly and clearly becomes apparent that the evaporation suppressing performance of a monolayer film is highly variable. Therefore, much research was conducted into the reasons for this variable performance and the main environmental factors responsible for this variability. Although many of these environmental factors are out of our control, the approach should be to manage the impact through strategic and timely application when conditions are 'right'. In the past, this has been the general approach when it comes to wind, as wind causes drift, sublimation, beaching and submergence (through wave action). Thus, a thorough review was conducted into the application strategies employed by researchers during field trials to manage the impact of wind on monolayer performance.

As noted, application system hardware used back in the 1950s, 1960s and 1970s are now very much out of date, however, it still seemed pertinent to review what had been done in the past and to identify the more promising methods of application. In reviewing this literature, particular attention was paid to the thinking behind the design of these systems, their on-site layout (specifically spacing between applicators), the form of monolayer used (i.e. powder, emulsion, etc.) and their general performance and reliability. Following this literature review a summary conclusion is provided, which highlights the knowledge gaps and makes some recommendations for future research.

The findings of the literature review are summarised in this chapter but is only a fraction of the literature reviewed over the life time of this PhD. Appendix A provides the details of the further literature reviews undertaken which covered the following topics: evaporation measurement, monolayer compounds, monolayer application and

control, monolayer detection and water surface management.

2.2 Surface chemistry of monolayer materials

Monolayer molecules, also known as amphiphiles, are characterised as having a hydrophilic head (attracted to water) and a hydrophobic tail (repels water), rendering them immiscible in water. The hydrophilic head (hydroxyl group) attaches to the water molecules within the very top layer of water, which changes the surface properties and causes a decrease in surface tension. The hydrophobic tail (alkyl chain), on the other hand, orients itself in the opposite direction of water. The amphiphiles are also attracted to each other through an intermolecular van der Waals force (Barnes & Gentle 2005). Amphiphiles consisting of saturated non-ionic carbon chains, such as stearyl alcohol, are more likely to have greater interaction between their alkyl chains (van der Waals) and hydroxyl groups (H-bonding) thereby increasing surface density, which leads to increased order and packing within the monolayer film (Henry et al. 2010). The relationship between area occupied per molecule and surface pressure indicates that monolayers suitable for evaporation mitigation have a small area occupied per molecule and a correspondingly high surface pressure (i.e. tight orderly packed monolayer molecules).

Spreading of crystalline solids such as cetyl and stearyl alcohols has been a technique of choice for many years. Solid amphiphiles when placed on a water surface will spread spontaneously as a monolayer until an equilibrium is reached between crystalline solid and monolayer or until the supply of bulk material is exhausted (Barnes 2008). The surface pressure at this point is called the equilibrium spreading pressure. It is desirable to have a high surface pressure (i.e. >30 mN/m) as this usually indicates a high evaporation resistance, spreading and re-spreading rate. The equilibrium spreading pressure is therefore an important monolayer performance indicator.

A monolayer spread on the water surface may exist in four phases; solid, liquid-condensed, liquid-expanded and gaseous (Figure 2.1). Monolayers in the liquid-condensed and solid phases consist of molecules that are parallel, fully extended and closely packed

(Barnes 2008). Whereas in the liquid-expanded phase the molecules lack the regularity to pack, thereby occupying approximately twice the molecular area. In the gaseous phase, the molecules are widely separated, occupying up to forty times the molecular area of a condensed monolayer (Gladyshev 2002).

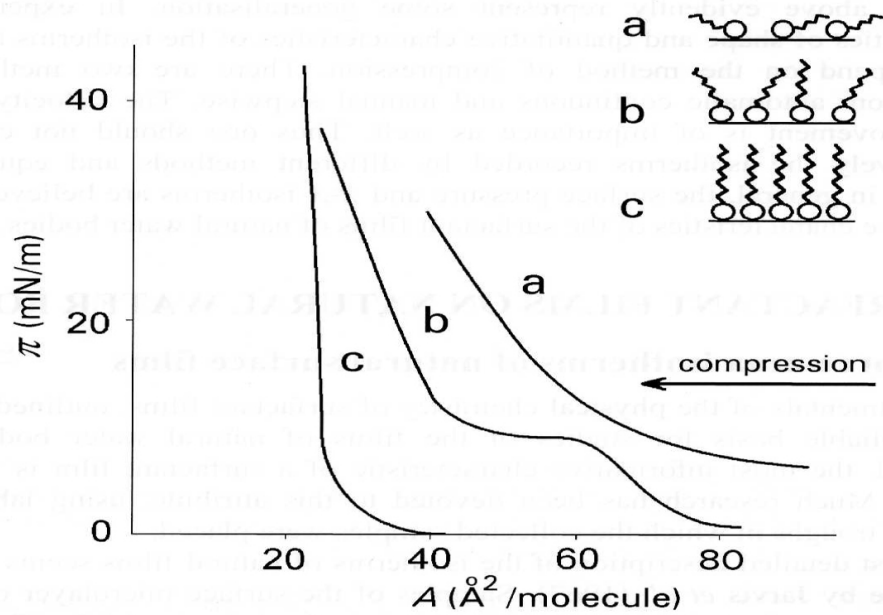


Figure 2.1: The relationship between the area occupied (\AA^2) per molecule and the surface pressure (π) exerted by the film. (a) refers to the gaseous film phase, (b) the liquid-expanded phase, and (c) the solid phase. Although the liquid-condensed phase is not shown here, this phase is similar to the solid, however, the molecules are oriented diagonally instead of vertically. Reproduced from Gladyshev (2002).

The surface tension gradient created between the clean water surface (γ_w) and the monolayer covered water surface (γ_m) is what causes monolayer to rapidly spread. This phenomenon of fluid flow caused by surface tension gradients is known as Marangoni flow (Jensen 1995, Dussaud & Troian 1997, Tarasov et al. 2006, Berg 2009). Marangoni flow is typically a very rapid transport process whose speed is controlled by the initial spreading coefficient (S), which is defined as:

$$S = \gamma_{w/a} - (\gamma_{m/a} + \gamma_{m/w}) \quad (2.1)$$

If $S < 0$ monolayer will sit static on the water surface and not spread, however when $S \geq$

where:

S	=	spreading coefficient	[mN/m]
$\gamma_{w/a}$	=	surface tension of water/air interface	[mN/m]
$\gamma_{m/a}$	=	surface tension of monolayer/air interface	[mN/m]
$\gamma_{m/w}$	=	surface tension of monolayer/water interface	[mN/m].

A monolayer will spread outwards towards areas of greater surface tension. Therefore, a monolayer that exerts a high surface pressure is highly desirable as it will spread rapidly and provide greater resistance to evaporation by virtue of its tightly packing molecules.

2.3 Physics of evaporation (free-water surface)

Evaporation is essentially the mass transfer of water molecules across the gas-liquid interface into the air (Davies & Rideal 1963). At the air-water interface there is a net attraction between water molecules. This attraction is greatest in the bulk water and weakest at the surface, which causes the interface to contract due to the greater pull from the bulk (Davies & Rideal 1963). This phenomena is known as surface tension. To evaporate from the bulk liquid phase, a molecule must overcome a series of resistances:

- the liquid phase resistance
- the interfacial resistance
- the gas phase resistance

In the liquid phase, a molecule must overcome the resistance of the bulk phase, to adsorb to the surface (MacRitchie 1969). Once adsorbed, the molecule must overcome interfacial resistance (including surface tension), vaporising from molecules at the surface into the gaseous phase. From the kinetic theory of materials (above absolute zero), all liquids and solids have a tendency to evaporate into the gaseous phase, and all gases have a tendency to condense back into the liquid phase. However, no net evaporation will occur if the gas pressure is equal to the vapour pressure at the temperature of the

liquid surface (Jones 1992). If the vapour pressure is reduced (for example by the continuous transport of vapour molecules away from the surface by wind), the gas phase resistance is less, resulting in higher rates of evaporation.

Using thermodynamic principles, the maximum evaporation rate for an open water surface at atmospheric pressure exposed to dry air at high wind speed can be calculated using the Hertz-Knudsen equation (Jones 1992). To achieve this maximum rate, the temperature of the water must be constant, and the vapour pressure must be minimal. de Boer (1953) defines such an experiment, where the temperature of water is maintained at 20°C and all the water vapour is removed and continually removed (i.e. preventing any molecules from returning to the liquid), the maximum theoretical evaporation rate is 9 m/hr. This implies that many lakes and seas should evaporate completely within a matter of hours. However, maximum rates of evaporative loss recorded for terrestrial and marine water bodies are 5 to 6 orders of magnitude less (e.g. for a temperate lake 0.5 m/yr, and a tropical sea 2 m/yr). The theoretical evaporation rate only reduces by about two orders of magnitude, if the vapour pressure is increased and the air is very humid, conditions that increase the gas phase transport resistance. This discrepancy between theoretical and observed evaporation rates indicates that at or near the surface, other phenomena must affect the transport resistance of water molecules moving from the bulk phase to the gas phase.

One phenomenon is the molecular diffusion sublayer (recognised in boundary layer fluid mechanics), adjacent to any static boundary in an airflow. The thickness of this layer is dependent on the friction properties of the static surface as well as the velocity of the bulk air, operating at a micrometer scale. At this scale, the highly efficient (and therefore low resistance) process of fully forced turbulent transport cannot develop. In this sublayer, water vapour pressure will be close to saturation, and the transport of water molecules will be governed by the physics of diffusion. Unless this layer is mechanically disturbed, the transport resistance (the concentration gradient normal to the surface) is very high, despite the relative thinness of the sublayer.

A boundary or diffusion sublayer also exists in the liquid phase. The thickness of the layer immediately below the interface is determined by the temperature difference between the surface and the bulk water, the upward heat flux, the kinematic viscosity,

density and thermal conductivity of water, and the shearing stress in the air above the water (Jones 1992). In the ocean, the estimated thickness of the cooler boundary (thermal) layer is between 4 and 0.25 mm with light winds, reducing to 0.25 to 0.1 mm for strong winds (Wu 1971*a*). The thermal layer may be mechanically disrupted by wave-breaking, but is rapidly restored by the undulating motion of turbulent flow.

In summary, water molecules in the bulk phase must adsorb into the liquid phase. Water molecules must then diffuse across the liquid sublayer, to vaporize into the gas sublayer. Molecules must diffuse across the gas sublayer, into the gas phase. In the gas phase, molecules are transported via convection to the edge of the gas boundary layer (MacRitchie 1969). Despite the relative thinness of both diffusion sublayers, the resistance imposed on the transport of water molecules across the air/water interface is sufficient to explain the discrepancy between theoretical and observed maximum evaporation rates (Jones 1992). Beyond the gas boundary layer, air turbulence (wind) is the key driver of evaporative loss.

A full review of methods for estimating evaporation can be found in Appendix A.2.

2.4 Monolayer mechanisms for evaporation mitigation

The rate of evaporative loss is highest, when the transportation of water molecules from the bulk phase into the liquid boundary layer, from the liquid boundary layer into the vapour layer, and from the vapour layer into the air flow is rapid. Transport from the vapour layer into the air flow is determined by the wind shear (Wu 1971*b*). In the presence of capillary waves, the surface roughness of the water increases, increasing the wind shear. If the formation of capillary waves is suppressed, the wind shear will decrease allowing the vapour pressure at the water surface to increase. As the vapour pressure increases, the rate of condensation will also increase, reducing evaporative loss. Capillary waves can be suppressed by reducing the surface tension of water, and by reducing convective circulation.

A reduction in surface tension can easily be achieved by the application of a surface active material (i.e. amphiphilic monolayer molecules). Huhnerfuss et al. (1983) showed

that a monomolecular surface film consisting of oleyl alcohol was not only capable of reducing capillary waves, but also long surface waves in the ocean. He found that waves with wavelengths of 3.2 m were significantly damped when they passed through a 1.5 km long monomolecular surface film. Attenuation of waves by a surface film can be explained by the Marangoni effect (a surface tension driven effect), causing a resonance-type damping due to the viscoelastic properties of the film (Levich 1940). This indicates that a monolayer film with viscoelastic properties is highly desirable.

A compound of specific interest for studying a monolayer's affect on capillary waves, without reducing evaporative loss, is oleyl alcohol. Oleyl alcohol has been found to inhibited natural convection in the water, thereby increasing the thickness of the thermal boundary layer (Saylor et al. 2000). The increased thickness of the thermal boundary layer was sufficient to reduce gaseous exchange in the water (Saylor & Handler 1999), but evaporative convection at the air interface was relatively unaffected. These results suggest that at the molecular level, damping capillary waves alone is insufficient to substantially retard evaporative loss.

As oleyl alcohol is a bulky molecule due to its permanently bent structure (a consequence of the 'cis' double bond), the carbon chains are less likely to pack together tightly to form an ordered, tightly packing film immediately above the air/water interface (Davies & Rideal 1963). Whereas, stearyl alcohol (C18OH), which is a saturated fatty alcohol, does form an ordered tightly packing film at the water-air interface. It is a surface film of this form that provides increased resistance to the movement of water molecules from the liquid boundary layer into the vapour layer. Therefore, in combination with the damping of capillary waves, the presence of an ordered, closely packed long-chain molecular barrier may increase the thickness of both the vapour and liquid boundary layers, thereby reducing evaporation.

As both energy (heat) and mass are transferred when water molecules evaporate, this lowers the water temperature. However, when a closely packed long-chain monomolecular barrier is present, this heat transfer process is markedly altered, which increases the water temperature. Modelling by McJannet et al. (2008), for the use of monolayer over a three year period, indicated an average water temperature increase of 2.2°C. During summer, the average water temperature increase was 3.0°C while in winter it was only

1.0°C. Similar changes in water temperature have also been observed by Wolbeer (1963) and Harbeck & Koberg (1959). Over a 21 day study Harbeck & Koberg (1959) noted a 1.9°C increase in water temperature. This highlights that the evaporation suppressing ability of monolayer is likely to be reduced by increasing water temperature (McJannet et al. 2008).

For further background, a full review of monolayer materials, spreading properties, forms, evaporative resistance and existing product performance can be found in the Appendix A.3.

2.5 Factors affecting monolayer performance

2.5.1 Temperature differentials and gaseous exchange

The difference between the air and water temperatures and the wind speed affect the dynamics of the natural convective circulation, by changing the temperature of the surface film (Gladyshev 2002). Cold surface films produce downward cellular convection, whereas, warm surface films are gravitationally stable. The mass transfer of heat through a cold surface film is much greater than that of a warm surface film, due to the descent of convective thermals and the formation of capillary waves reducing the thickness of the liquid thermal boundary layer. Whereas, the liquid boundary layer under a warm surface film is an order of magnitude greater than that of a cold film, with warm film boundaries extending 60 to 80 mm immediately below the surface (Gladyshev 2002).

All surfactants reduce the surface tension to some degree and this has the effect of increasing the stability and thickness of the liquid diffusion sublayer near the interface where molecular transfer of heat dominates. The surfactant binds this layer to the interface tending to make it less mobile, thereby increasing the thickness of both the gaseous boundary and the liquid thermal boundary layers (Figure 2.2). As a consequence, total heat flux and stress transfer is reduced. However, under certain conditions, such as high relative humidity in the absence of wind (when a warm surface film is pro-

duced), evaporation will be inhibited even in the absence of a liquid-condensed film (Gladyshev 2002).

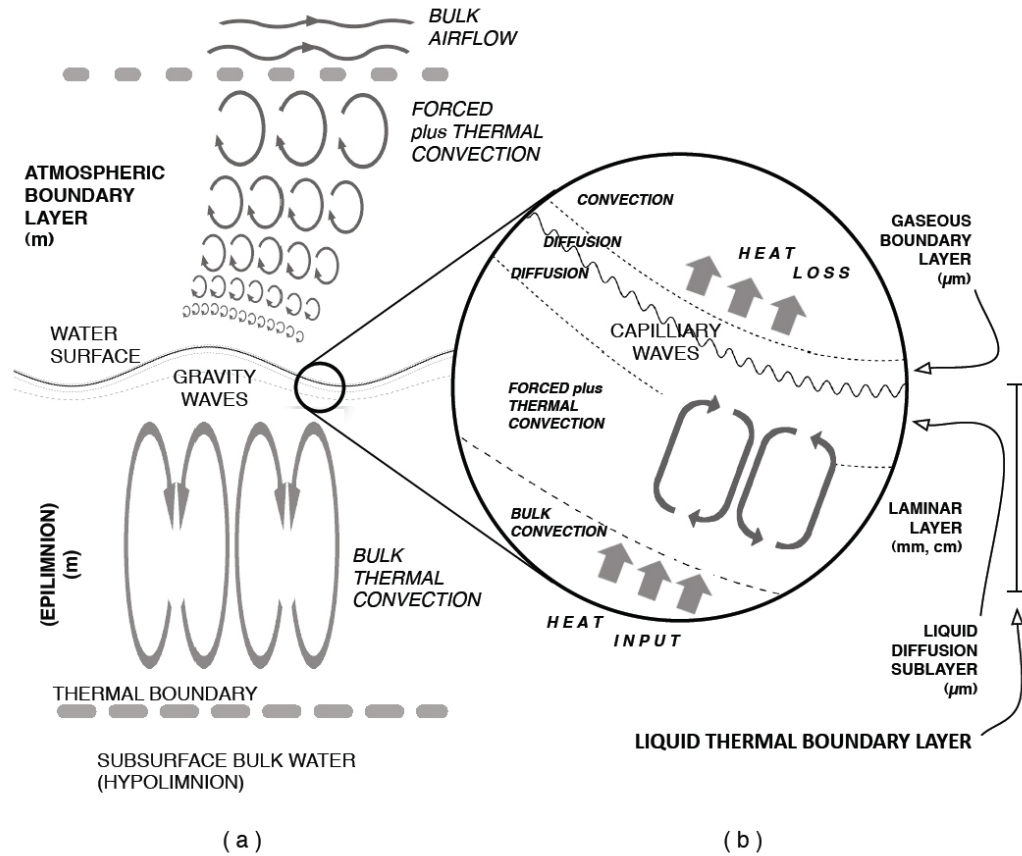


Figure 2.2: Diagrammatic illustration of the physics of thermal transport processes: (a) details the atmospheric and liquid layers; (b) details the gaseous boundary layer and liquid diffusion sublayer near the interface. Reproduced from Hancock et al. (2011).

2.5.2 Wind-induced effects

Many researchers have reported that wind is the single most important influencing factor in terms of monolayer performance. Deleterious effects induced by wind include: surface drift, submergence by waves and beaching on the lee shore. All of these wind-induced effects effectively reduce surface coverage allowing water to freely evaporate thereby reducing monolayer efficiency.

As a monolayer film is only 2 nm thick, coupled to the top layer of the water surface

by its hydrophilic head (Barnes 2008), it is subject to transport by the wind (Crow 1963, Fitzgerald & Vines 1963, Frenkiel 1965, Reiser 1969). The cause of this surface transport/drift is a consequence of two main components; the wind induced shear stress and Stokes mass transport related to wave characteristics (Lange & Huhnerfuss 1978, Dobroklonskiy & Lesnikov 1972). Vines (1962) reported that wind induced drift of a monolayer film across the water surface starts to occur at wind speeds of around 3.2 km/h. McArthur (1962) and Crow & Mitchell (1975) have reported similar values. Above this minimum wind speed threshold (U_{MIN}), the ratio of monolayer surface drift speed (U_m) to wind speed (U_w) has been reported by many researchers (Table 2.1). The average of the measurements for this ratio from laboratory studies is $0.035(\pm 0.006)$.

Table 2.1: Comparison of various laboratory studies investigating the relationship between monolayer surface drift speed (U_m) and wind speed (U_w). Adapted from Lange & Huhnerfuss (1978) and Hale & Mitchell (1997).

Source:	Length (m):	Depth (m):	Detection Method:	Wind Speed Range (km/h):	Ratio of U_m/U_w :
Fitzgerald (1964)	1.83	0.15	Talcum powder	13-27	0.03-0.045
Reiser (1969 <i>b</i>)	65	1.2	Sulfur powder	5-39	0.031
Lange & Huhnerfuss (1978)	18	0.5	Talcum powder	9-31	0.03-0.043
Hale & Mitchell (1997)	2.5	0.1	Talcum powder	7-18	0.03-0.041

Many researchers also indicate that the application of monolayer becomes impractical at a certain maximum wind speed threshold (U_{MAX}), suggesting that monolayer application should be stopped once that threshold wind speed is reached. Wu (1971*b*) reports that a monolayer is able to calm the water surface up to wind speeds in the range of 18-25 km/h. For wind speeds above this range surface roughness is comparable to that for clean water (i.e. little to no waves damping effect), which indicates that monolayer is overcome by waves. In light of this, Wu (1971*b*) suggested that an upper limit of wind speed could be imposed on the application of monolayers for the

retardation of evaporation. Other researchers have reported this U_{MAX} to be as low as 16 km/h (Walter 1963) and as high as 40 km/h (Reiser 1969). The average of all the U_{MAX} values sighted in literature to date is $26.4(\pm 5)$ km/h (Table 2.2).

Table 2.2: Comparison of the various U_{MAX} values (wind speed cut-off point for monolayer application) adopted by researchers during field trials.

Source:	Monolayer Compound/s:	Formulation/s:	Storage Size (ha):	U_{MAX} (km/h):
U.S. Bureau of Reclamation (1957)	C16OH	Pellets, solid blocks and fine powder	40.5	24
U.S. Bureau of Reclamation (1959)	C16OH	Water slurry	1012	28
Grundy (1962)	C16OH and C18OH	Pellets, flakes, solution and emulsion	0.4-53	28
U.S. Bureau of Reclamation (1960)	C16OH and C18OH	Molten application	405	32
Fitzgerald & Vines (1963)	C16OH and C18OH	Fine powder	405	24
Crow (1963)	C16OH	Water slurry	0.112	20
Walter (1963)	C16OH and C18OH	Solvent and emulsion	11.4	16
Reiser (1969)	C16OH	Emulsion	0.017	40
Nicholaichuk & Pohjakas (1967)	C16OH	Powder	0.17	25

2.5.3 Volatilisation

Volatilisation from a monolayer film (i.e. evaporation of the monolayer molecules) is considered to be one of the most significant factors of loss (Mansfield 1962). However, volatilisation of a monolayer from a water surface has received very limited attention,

and only on a very small scale and under limited laboratory conditions by Mansfield (1959) and Brooks & Alexander (1960). Brooks and Alexander showed that saturated fatty alcohols, particularly those with shorter chain lengths such as myristyl alcohol (C14OH) and cetyl alcohol (C16OH), lose significant amounts of material to volatilisation. Brooks & Alexander (1960) calculated rate of loss by maintaining the monolayer film at a constant surface pressure. As monolayer material was lost from the film over time, the film covered surface area was reduced to compensate for these losses and maintain the film at a surface pressure of 35 mN/m. Changes in the film covered surface area were then used to calculate the fraction lost (of monolayer material) in unit time (Table 2.3).

Table 2.3: Fractional loss of monolayer material from a monolayer film at a surface pressure of 35mN/m. Adapted from Brooks & Alexander (1960).

Monolayer compound:	Fractional loss ($\times 10^{-6} \text{ sec}^{-1}$) at:		
	5°C	20°C	40°C
Myristyl (C14OH)	20	58	1900
Cetyl (C16OH)	1	4	150
Stearyl (C18OH)	0	0	20

It can be observed that carbon chain length of the monolayer molecule, in the case of long-chain fatty alcohols, has a significant affect on volatilisation. The less carbon atoms, the greater the volatilisation rate. In addition, as water temperature increases so does volatilisation. For C14OH and C16OH, a water temperature increase from 5 to 20°C the fractional loss of monolayer material more than doubles, whereas, from 20 to 40°C the fractional losses increase by a factor of more than 30.

Mansfield (1959) noted, that when a complete monolayer is spread upon an open water surface, the fractional loss by volatilisation may be estimated approximately from:

$$dF_e = \frac{D_a \times c_a \times v_2}{40 \times c_s} \quad (2.2)$$

Mansfield went on to provide an estimate of the parameters required in Equation 2.2

where:

dF_e	=	fractional loss by volatilisation	[second]
D_a	=	coefficient of diffusion of monolayer vapour in air	[cm ² /sec ⁻¹]
c_a	=	concentration of vapour in equilibrium with the monolayer	[g/cm ⁻³]
v_2	=	wind velocity	[cm/sec ⁻¹]
c_s	=	surface concentration of monolayer	[g/cm ⁻²].

for the fatty alcohol C16OH at a temperature of 25°C. However Mansfield did note that this equation, due to being linearly related to wind, did not apply accurately to low wind velocities. Fractional losses into still air best correspond with wind velocities between 0.5 and 0.7 m/s with this equation, as related by a similar study. After their introduction, the fractional rate of loss from a cetyl alcohol monolayer film at an equilibrium surface pressure of 40 mN/m is:

$$dF_e = 6.8 \times 10^{-7} \times v_2 \quad (2.3)$$

In summary, an increase in wind velocity and/or water temperature will enhance the fractional loss due to volatilisation. Therefore, monolayer materials with shorter carbon chains, such as C14OH and C16OH, should be avoided.

2.5.4 Biodegradation

If wind conditions remain consistently still (i.e. <3.2 km/h), where little if any monolayer drift would be experienced (Vines 1962), biodegradation could start to become a significant issue. However, the rate of monolayer biodegradation (expected half-life) is a complex factor to determine. Recent studies have indicated the potential for surface films that naturally occur on fresh water bodies (a microlayer), to interact with and adversely affect artificial monolayers (Pittaway & van den Ancker 2010). Natural microlayers are produced by hydrophobic plant waxes, phenolic compounds and other humified material, which concentrates microbial populations capable of utilising these materials as organic substrates. Hydrophobic fatty alcohols with carbon chain

lengths of 16 are readily converted to lipid storage compounds by aquatic microbes, explaining why monolayer compounds such as the C16OH are highly susceptible to microbial degradation. Figure 2.3 shows the performance of three monolayer compounds (including C16OH), which were assessed in the laboratory with respect to microbial degradation (Pittaway & van den Ancker 2010).

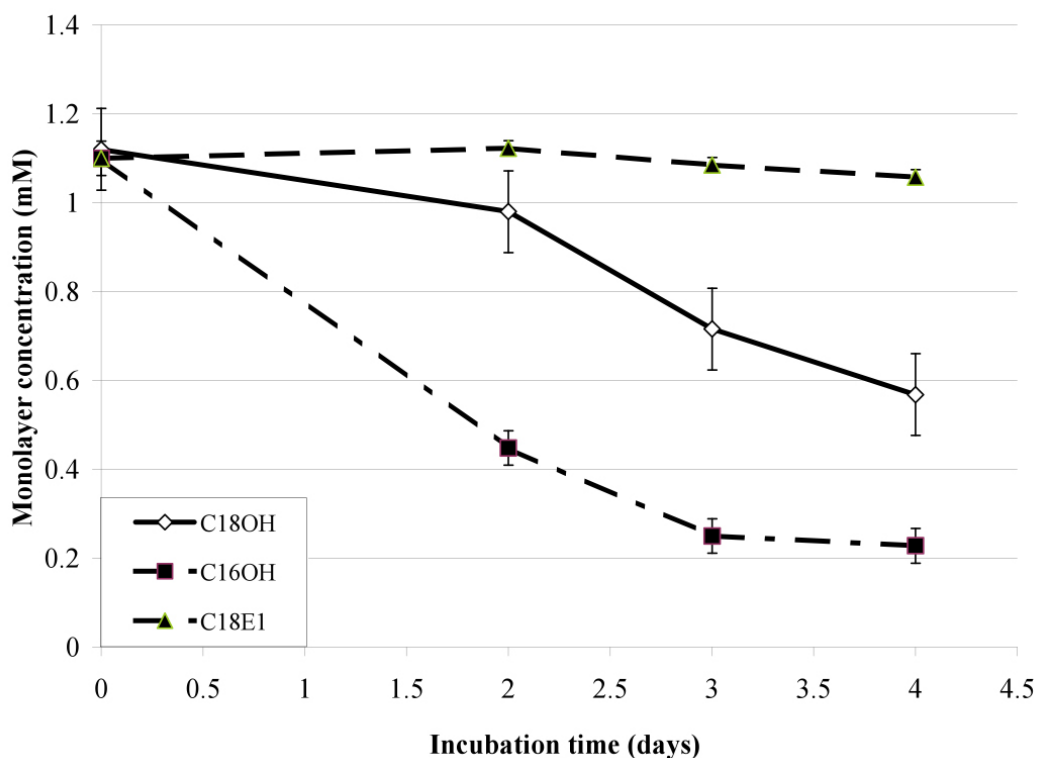


Figure 2.3: Degradation of three monolayer compounds supplied as the sole carbon source for the common freshwater bacterium *Acinetobacter* in a mineral salts medium. The resilience of two fatty alcohols (C16OH, C18OH) and a ethylene glycol mono-octadecyl ether (C18E1) monolayer were compared. Chloroform was used to extract the monolayer in the medium after two, three and four days of incubation prior to analysis using a gas chromatograph. Reproduced from Brink et al. (2010).

In summary, microlayer compounds have the potential to disrupt monolayers in at least the following three ways: as substrates for microbes capable of degrading monolayer compounds, as chromophores accelerating photodegradation, and as impurities disrupting the molecular packing required to reduce evaporative loss (Pittaway & van den Ancker 2010).

2.5.5 Rainfall

To the author's knowledge, there have only been two research studies into the effect of rain on monolayer. The findings from both of these studies are however in disagreement with each other. A study conducted in the laboratory by Green & Houk (1979), concluded that the rate of removal of monolayer by rain to be significant and increases markedly with increasing drop size and rainfall intensity. Green and Houk report that monolayer is removed from the surface by Rayleigh jet drops and spray droplets, stemming from raindrop impact (Hobbs & Kezweeny 1967), and by jet drops associated with breaking bubbles (Blanchard & Woodcock 1975), all of which have a high concentration of monolayer and are swept away by air movements.

In contrast, a field study by Baier (1972) found that natural surface films are maintained during periods of rain. This result may reflect that a higher concentration of monolayer material was used in comparison to Green and Houk, who used a very low concentration of C16OH monolayer (only 1 mg/m²). In addition, significant amounts of monolayer material may have been deposited on the polystyrene tank walls of Green and Houk's experimental set-up due to droplet impact. Therefore, more thorough studies are required to fully quantify the removal phenomena and to clarify the discrepancy between laboratory and field results.

2.6 Monolayer application

This section provides a review and analysis of the monolayer application strategies employed and developed by researchers during field trials. A summary review of the design of the monolayer application systems employed by these researchers is also provided.

2.6.1 Application strategies

Strategies to date appear to be based on the monolayer requirement to maintain an unbroken film. As monolayer films are so readily transported by wind, the general approach has been to continually apply monolayer in accordance with the wind speed

measured on-site (Frenkiel 1965, Crow 1963, Reiser 1969). To the author's knowledge, the only equations for monolayer application rate presented in published literature are by Crow (1963), Reiser (1969) and Crow & Mitchell (1975). Only three monolayer application rate equations presented in literature to date seems a small number as there have been more than twenty individual field studies conducted since the 1950s (Frenkiel 1965, McJannet et al. 2008).

Crow's application rate equations were derived through testing on two identical adjacent ponds (30.5 m x 36.6 m and 2.1 m deep). Wind speeds were measured by a standard cup type anemometer located on the centre dike between the two ponds at a height of 2 m above the water surface. A mixture of powdered fatty alcohols, including 5% C14OH, 44% C16OH, 46% C18OH, and 5% C20OH, was continually applied as a slurry with automatic controls regulating the rate and point of application of the monolayer in response to wind speed and direction. A mixture of alcohols was used as the shorter carbon chain alcohols, C14OH and C16OH, increase spreading rate while the longer chain alcohols, C18OH and C20OH, improve evaporative resistance (Frenkiel 1965). Application rate was determined by the minimum amount of monolayer required to maintain a film on the pond surface for various wind speeds. The presence of the film on the water surface was determined by eye due to the smoothing effect of the monolayer on small waves. Throughout each test the application rate was controlled in such a manner that the rate of film application did not exceed the rate of removal by wind. Crow's empirical application rate equation is:

$$R = 9.3U^{2.02} \times 10^{-6} \quad (2.4)$$

where:

$$\begin{aligned} R &= \text{application rate} \quad [\text{pounds of chemical per hour} \\ &\quad \text{per foot normal to the wind}] \\ U &= \text{wind speed} \quad [\text{miles per hour}]. \end{aligned}$$

Reiser's equations were derived through testing on a water-wind tunnel which has an 2.4 m square air passage above the water tunnel which is 1.8 m deep and 68 m in length. Wind speed was measured at the entrance of the wind tunnel at a height of 1.2 m

and half the width. Monolayer applied continuously as a water-emulsion of C16OH and C18OH alcohols with and without ethoxylate adduct (to stabilise the emulsion). Equations for re-application rate were determined according to the alcohol required to maintain a smooth surface (Figure 2.4b). As Reiser notes, "... a more important factor which generally has been neglected is the loss by wave action and submergence. Since the film can only be effective if it exists at the surface layer on top of the water, it is necessary to add sufficient material to dampen the waves and prevent 'drowning' of the alcohol by wave action".

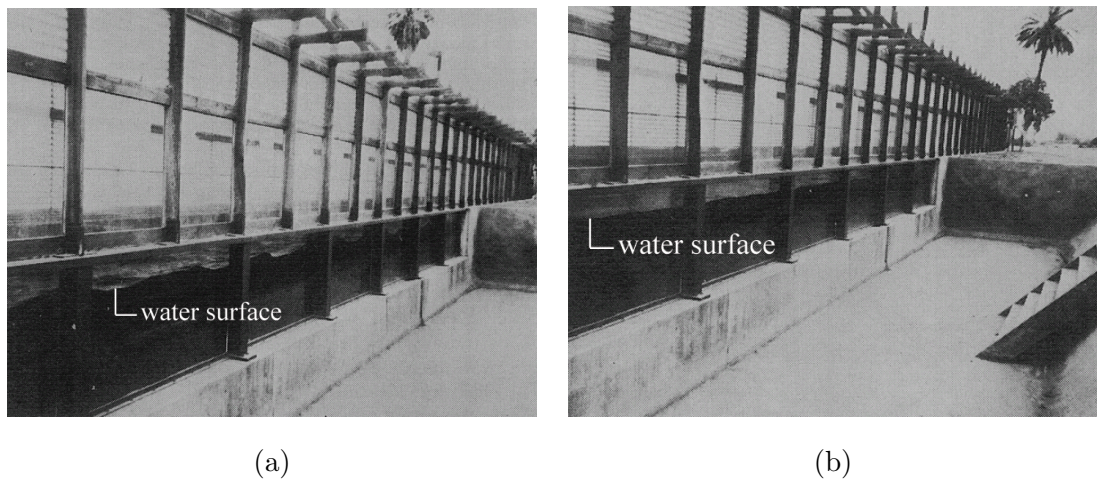


Figure 2.4: Reiser demonstrating suppression of surface waves with a monolayer film. (a) Waves in water-wind tunnel with 25 mph wind with no monolayer. (b) Smooth surface at 25 mph after the application of a surface film. Reproduced from Reiser (1969).

Using this premise of alcohol required to maintain a smooth surface, Reiser found that it was possible to maintain a smooth surface up to a critical wind speed of 27 mph (43.5 km/h) if sufficient alcohol was applied (Figure 2.4). However, as the wind speed exceeds 9 mph (14.5 km/h), the suppression of waves which tend to submerge a film becomes the controlling factor for the addition rate. Therefore, Reiser determined two application rate equations are needed, one for wind speeds below 9 mph:

$$\frac{Lb./Hr.}{100ft.of\ shore} = 2.9 \times 10^{-5} VM \quad (2.5)$$

and one for wind speeds above 9 mph:

$$\frac{Lb./Hr.}{100ft.of\ shore} = 3.2 \times 10^{-5} V^2 M \quad (2.6)$$

where:

$$\begin{aligned} V &= \text{wind velocity} && \text{[miles per hour]} \\ M &= \text{molecular weight of film-forming material} \\ &\quad \text{per hydrophilic group} && \text{[atomic mass].} \end{aligned}$$

Crow, in partnership with Mitchell, presented another equation this time for Lake Hefner, which is a very large off-stream impoundment with a 1,012 ha surface area. Lake Hefner had good exposure to prevailing southerly winds with a South to North fetch distance of about 3,505 m. Wind speeds were measured in the centre of the lake at a height of 2 m. Monolayer was applied as a water-based slurry through rotary irrigation sprinklers spaced 150 ft (45.7m) apart. The application system was located near the south shore for maximum film cover during southerly winds. The film forming chemical used was 29% C16OH, 61% C18OH, 7% other alcohols, and 3% non-alcohols. To determine the application rate required to replace film removed by the wind, film cover maps were made at one hour intervals by an observer using a plane table and alidade from a vantage point (atop a 27.4 m tower). The observer was in radio communication with the batch plant to recommended changes in the application rate based on his evaluation of wind speed and direction and its effect on the film cover. Crow and Mitchell's application rate equation is:

$$R = 1.18U^{1.81} \times 10^{-4} \quad (2.7)$$

where:

$$\begin{aligned} R &= \text{monolayer material requirement} && \text{[pound per hour per foot} \\ &&& \text{of distribution line]} \\ U &= \text{wind velocity} && \text{[miles per hour].} \end{aligned}$$

To look more critically at the three application rate equations presented above, an

analysis of the monolayer requirement (grams per hour) is made for each. In addition to the three application rate equations analysed, a fourth application rate equation is included in the analysis. This fourth application rate equation is purely based on the monolayer drift rate according to Fitzgerald (1964). Fitzgerald found that the ratio of surface velocity to wind velocity rose linearly from 0.03 for low wind speeds to a constant value of 0.045 for wind speeds greater than 19.8 km/h. The Fitzgerald equation is included in this analysis to show the similarity with Crow's and Riser's application rate equations.

The analysis is based on a 100 x 100 m square water storage (1 ha in surface area). The application requirement is calculated for a range of wind speeds blowing continuously over a 1 hour duration. The results are presented in Figure 2.5.

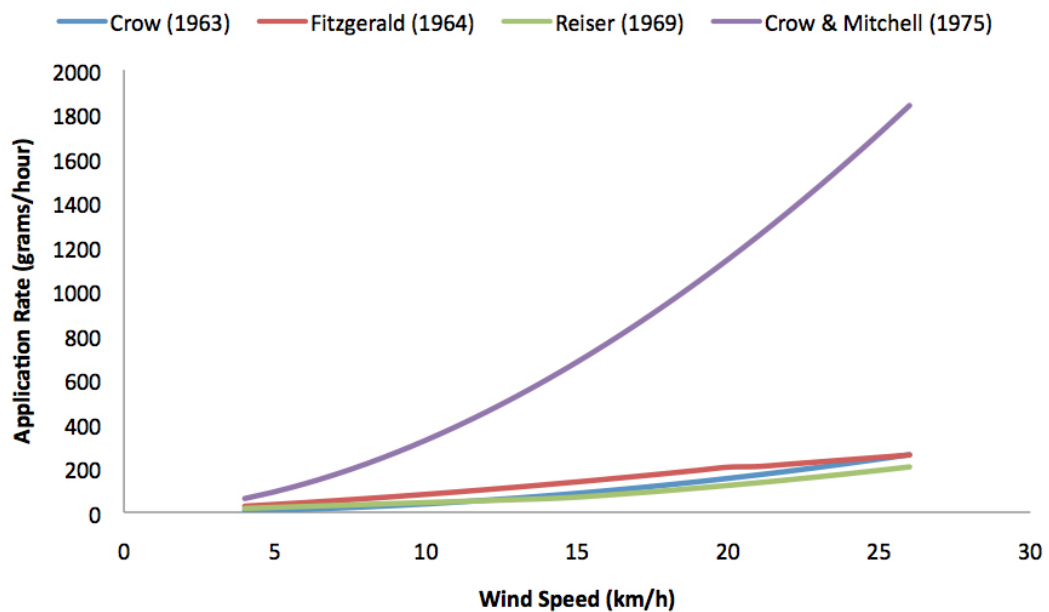


Figure 2.5: Comparison of application rates as a function of wind speed calculated using three different application rate equations. This is the application rate (grams of monolayer per hour) required to cover a 1 ha surface area with C18OH at various wind speeds ranging from 4-26 km/h.

It can be seen that the Crow, Fitzgerald and Reiser equation's are in general agreement with one another. As the monolayer requirement determined using Crow's and Reiser's equations are quite similar to that for Fitzgerald's, it can safely be assumed that their application rate equations are largely based on the monolayer drift rate. Therefore, they

believe that the primary cause of monolayer removal is surface induced drift by wind and beaching on the lee shore. Having said that, Reiser did note that the application rate equation he published did not take into account the other monolayer removal processes, primarily, biological attrition, solution or volatilisation. The most significant removal process next to surface induced drift, and not accounted for by Crow, Fitzgerald or Reiser, is believed to be volatilisation (Shukla & Kulkarni 1962).

Also, when looking at the monolayer requirement determined using Crow and Mitchell's equation for Lake Hefner (1,012 ha surface area) in comparison with the monolayer requirement determined using Crow's and Reiser's equations, which were developed using surface areas of 0.11 ha and 0.016 ha respectively, there appears to be a significant increase with large surface area and/or fetch distances. Crow and Mitchell provided three possible influencing factors to explain the greater monolayer requirement at Lake Hefner than for the experimental pond:

- Fetch length may be a factor, noting that the average increase in the wind speed measured at the 2 m height above the water surface was 28%. Crow and Mitchell noted that, "The longer fetch (north to south) undoubtedly contributed to greater film requirement".
- The off-shore distance of 243.4 m to the actual point of application may be another factor, noting that some capillary wave action occurred between the shore and the application point and required greater application rates to suppress the waves.
- Spacing between the application points may be a factor, noting that lateral spreading of the monolayer between the application points took place slowly and only under moderate wind speeds would the monolayer plumes actually merge into a continuous film about 304.8 m downwind. Monolayer was applied with rotating irrigation sprinklers spaced 45.7 m apart with an effective spray/coverage pattern of 15.2 m each. Failure to merge was also observed by Reiser, who reported that he could not obtain a continuous film with application points spaced 15.2 m apart if the wind speed exceeded 20 km/h.

2.6.2 Application systems design

Most application systems appear to be rather prototypical designed for research and evaluation purposes. Very few were reliably automated to dynamically dose monolayer in accordance with on-site wind speed, most likely a consequence of the vintage of many of these systems. As monolayer is so readily transported by wind, automated application is a desirable characteristic, especially with the amount of cheap and reliable off-the-shelf automation control technologies available today. Of the systems reviewed, large broadcasting techniques such as the ‘Robertson Grinder/Duster’ and aerial application are generally incapable of satisfying the highly dynamic application demand imposed by the wind. In addition, application systems designed for film-forming material in a solid form (i.e. powder, solid casting, pellets) tended to require high levels of maintenance and/or manual operation and control.

Systems designed for dosing monolayer in a liquid form (i.e. slurry, emulsion, solution, molten) incorporated many application points around and within the water storage, which appeared to be the better strategic approach in maintaining monolayer coverage during wind conditions (Frenkiel 1965). However, there did not seem to be a large amount of science involved in determining number and spacing between applicators and their locations on-site. Most systems consisted of a single pump and/or mixing system from which monolayer is distributed through a series of pipes to application points (Reiser 1969, Crow 1963, Crow & Mitchell 1975). The major drawbacks of a system like this is: accurate metering at outlets is difficult; the pipe network needs to be regularly flushed; pump size and power requirements can be onerous (depending on monolayer viscosity, pipe size and pressure requirements at the outlets) and strong connections between piping and anchoring is required. Hence, multiple self-contained applicators with their own pump, reservoir of monolayer and electronic controls would be a better option. Some conceptual designs for monolayer applicators of this nature are presented in Appendix E.

Although methods of applying monolayer in a liquid form appeared favourable, monolayer in a volatile solution is not considered suitable for use on many water storages because of cost and environmental concerns associated with the volatile solvents used

(Barnes 2008). Monolayer mixed as a slurry with water, especially C16OH containing significant amounts of C18OH is problematic, as prolonged contact with water means that the monolayer is predominantly in the slow-spreading α phase when used (Vines 1960*b*, Barnes 2008). In contrast, Dressler & Guinat (1973) and Reiser (1969) developed a suspension process which used an emulsifying material to create emulsions that were stable (i.e. no separation of the monolayer from the water) for long periods of time and displayed improved spreading ability. The emulsifying material used by Reiser was Conoco 1812-6 ethoxylate consisting of a mixture of alcohols with 12-18 length carbon chains and an ethylene oxide (amounting to 60% of the combined weight). Another method that showed potential was molten application of monolayer (Florey 1965).

One critical aspect in the design of a distributed application system, whether a single pump and pipe network or multiple self-contained units are used, is the on-site arrangement of applicators. This is an important consideration in order to achieve optimal coverage under a range of wind speeds and directions. The lateral spreading ability of monolayer would dictate spacing between applicators/application points, which in turn influences their arrangement on-site. Although the lateral spreading ability of monolayer is influenced by wind speed (i.e. lateral spreading is decreased by increasing wind speed) (McArthur 1962), no researcher (to the author's knowledge) has studied this effect in detail.

Some researchers have reported spacing between applicators/application points (Table 2.4). However, there is no general consensus, as optimal spacing would differ according to local prevailing wind conditions, storage size and monolayer material used. In summary, Mansfield (1962) stated:

“It is clear that no one method of applying/spreading (monolayer) material is suitable for all locations. Factors such as storage size and shape, wind pattern, and the costs of material and labour affect both the feasibility of each technique and the details of its use.”

Table 2.4: Summary of relevant information from field studies employing distributed application systems for monolayer in a liquid form.

Source:	Monolayer: Compound/s:	Formulation:	Storage Size (ha):	Max. Working Wind Speed (km/h):	Spacing Between Applicators (m):
McArthur (1962)	Blend of C16OH and C18OH	Volatile solution	769	25	Unknown
Crow (1963)	C16OH	Water-based slurry	0.11	24	3
Reiser (1969 <i>a</i>)	Blend of C16OH, C18OH and C20OH	Water emulsion	113	20	6
Crow & Mitchell (1975)	Blend of C16OH and C18OH	Water-based slurry	1052	20.8	45.7

All of the application systems reviewed for applying monolayer and oil materials to water surfaces can be found in Appendix A.4.

2.7 Monolayer detection

Despite the various methods that have been devised for determining the presence and spatial distribution of a monolayer film on a water surface (see Appendix A.5), the fact still remains that a monolayer film is only 2 nm thick and is therefore very difficult to detect, let alone develop an autonomous system for real-time monolayer detection. Coop (2011) has been working towards this objective and his work in this area remains of particular interest as a potential method for estimating evaporation rate, percentage of monolayer coverage and spatial distribution of the monolayer film on a water surface.

Coop's current temperature differentials measurement system employs an insulated Y-tube sealed at the bottom, which sits in the water, creating a trough. The tube has a slot cut in its side at the water surface to allow water to fill the trough. One branch of the Y is open and the other has an electric fan, which is used to cool the water surface in the trough. Temperature measurements are then taken inside at the bottom of the trough and of the outside bulk water temperature using thermocouples. If an effective monolayer is present on the water surface there will be a cooling effect inside the tube. The accumulation of this cold water inside the tube is then compared with the bulk water. The greater the temperature difference the greater the evaporative resistance provided by the monolayer (Coop 2011). An illustration detailing Coop's monolayer detection device can be found in Appendix A.5.

2.8 Water surface management

It has been identified by Crow (1963) and Nicholaichuk (1978) that the negative effects of wind on monolayer film coverage and thus performance could be reduced to some extent by limiting the wind speed across the water surface, or confining the surface film between an arrangement of floating compartments. Another option may be to calm

the water surface by dissipating wave action. For each of these strategies a number of technologies have been identified as potential options to reduce wind speed or film drift across the water surface, and or dissipate wave action (A full review of these technologies is provided in Appendix A.6).

Two options for reducing the wind speed across the water surface are man made wind breaks and/or natural shelterbelts (eg. trees). Either option principally requires the same desired characteristics in order to provide a meaningful reduction in wind speed and evaporation in the lee of the barrier/shelterbelt. According to Naegeli (1953) when wind reduction extending far behind the wind barrier or shelterbelt is required, high belts or barriers of medium density/porosity are best. It is also worth noting that natural shelterbelts not only improve soil-climate and microclimate, they are also used to recover a landscape and improve its whole natural economy. Further information in regards to wind barriers and shelterbelts can be found in Sections A.6.3 and A.6.3 of Appendix A respectively.

Containment of the monolayer film within a pre-defined area appears to be a feasible option to help improve the efficiency and economy of a monolayer product. Crow (1963) notes that one of the expected benefits of a floating grid network of barriers is preventing film loss by wind action. Crow also reported a 9.1% reduction in evaporation with a floating grid network of barriers and a 31.3% reduction in evaporation when used in combination with a monolayer. Nicholaichuk (1978) has reported similar results from experiments with monolayer in combination with wind baffles and floating grids (Appendix A.6.3).

The wave suppression technologies reviewed indicates that most of these devices may have a deleterious effect on a monolayer surface film. Many of these devices consist of a multiple of finned or perforated elements to aerate and create localised turbulence to dampen the energy of waves washing through (Appendix A.6.4). The localised turbulence created by these devices during wave conditions will most likely break-up the monolayer film causing a reduction in coverage, which is highly undesirable as this would increase evaporation. Although a monolayer film may have the ability to reform after passing through the turbulence created by a wave suppressing device, the extent to which the surface film may be permanently damaged is unknown.

2.9 Conclusions

There are many different factors that can affect monolayer performance, most of which are highly dynamic and some are constantly changing. It is a tough proposition to design a system capable of optimally applying chemical monolayer under all of these dynamic conditions. Considering the information available, it is possible to identify a range of environmental conditions under which the application of monolayer appears potentially useful for evaporation mitigation. These are as follows:

- When wind speed is below the maximum wind speed threshold (U_{MAX}). The average of all of the U_{MAX} values cited in literature to date is $26.4(\pm 5)$ km/h.
- When it is not raining.
- When the evaporation demand is high enough to justify the application of monolayer (both practically and economically).
- When the temperature differential between surface and sub-surface water is low (i.e. downward cellular convection) so that the thermal boundary layer of the water is very thin.
- When microbial activity or concentration in the surface and sub-surface water is medium to low.

Within the above monolayer environmental limits there are still a number of key requirements that need to be satisfied in order to reduce evaporation from large water storages. They are as follows:

- A suitable monolayer material that is capable of rapidly spreading between application points to form a homogeneous tightly packed surface film (i.e. low area per molecule) on the water surface is needed. A monolayer with these characteristics should have a high equilibrium surface/spreading pressure which will reduce surface tension and calm some wave action. In addition, the monolayer must provide a surface resistance to the evaporation of water molecules. The monolayer must

also be non-toxic and environmentally benign, i.e. biodegradable so it does not build up in the environment, nor result in unacceptable residual compounds.

- Once a monolayer with the above characteristics has been selected for use, the monolayer must be produced in a formulation that is conducive to application while retaining the above characteristics. According to literature, a liquid (as opposed to solid) monolayer formulation appears to show the most promise, specifically, as an emulsion, or molten (i.e. in pure liquid form).
- Then an automated application system capable of continuous and intermittent dosing of the monolayer formulation at different rates is required. The more successful application systems appear to be made up of a series of applicators or application points strategically placed around and within a given waterbody. Each application system reviewed appears to be custom designed (i.e. for a specific waterbody and/or set of wind conditions). Therefore, a system designed for modularity would be desirable so as to allow each system to be tailored to a specific site.
- The monolayer formulation then needs to be dosed at a rate matching that at which it is lost from the water surface. The factors that cause removal of monolayer from the water surface are likely to be: downwind drift, beaching on the shore, volatilisation, submergence and/or biodegradation. Considering that the factors that remove monolayer are going to be highly variable, the application rate in-turn, will also need to be highly variable.

It is only once all of the above criteria have been satisfied that a monolayer application system can be considered ‘smart’ or ‘optimal’.

Chapter 3

Conception of the ‘Universal Design Framework’

3.1 Introduction and scope

Despite some advances in monolayer application technology (Brink et al. 2010) and improved monolayer compounds (Gill et al. 2010), there are still some fundamental questions on the practicalities of deployment and operation that remain unanswered. These are principally:

1. criteria for selecting the most appropriate monolayer material,
2. the type of application system and the site-specific configuration required, and
3. the amount and re-application rate of monolayer to be applied?

When a surface film in the tens of nanometers thick scale is used on a farm dam it will be subject to transport and/or removal by wind, submergence by waves, damage by rain and biological degradation. Due to the nature and complexity of these interactions and the fact that these conditions will vary for time to time and from location to location, a general design framework has been formulated. The framework recognises that every reservoir will have a specific set of user and environmental considerations, which

will need to be effectively captured, in order to determine a unique set of operational requirements.

The framework is used to inform both planning and operation of a unique monolayer application system design for any given site. In **planning mode**, the framework will need to inform monolayer product selection, monolayer application equipment, including number of applicators and their arrangement on-site. In **operational mode**, the framework will need to inform the application strategies to be implemented for the site on a time-step (i.e. 15 minute, 30 minute, hourly, or even daily) basis according to on-site weather conditions. Hence, the framework has been dubbed the Universal Design Framework (UDF).

3.2 Development of the ‘Universal Design Framework’

To develop a framework that will adequately address factors 1, 2 and 3, as outlined in Section 3.1, a number of key influencing factors have been selected. The importance and proposed use of these key influencing factors have been documented and are detailed in Sections 3.2.1, 3.2.2 and 3.2.3 below.

3.2.1 Monolayer material selection

Pittaway & van den Ancker (2010) benchmarked three reservoirs within South East Queensland (SEQ) with respect to water quality and biological characteristics. Qualitative assessments were made of water source/s, water colour, turbidity, catchment vegetation type and storage size. Water chemistry was also characterised using pH, electrical conductivity (EC), dissolved oxygen, biochemical oxygen demand and ultra-violet (UV) absorbance. Then the performance of three different monolayer compounds, C16OH, C18OH and C18E1¹, was assessed in the laboratory with respect to microbial degradation (Figure 2.3 can be found in Section 2.5.4). In addition, the evaporative resistance and surface pressure of these three monolayer compounds on clean water (Figure 3.1) and brown water (Figure 3.2) from a storage with a very high microbial

¹Refer to the list of Acronyms and Abbreviations.

concentration were compared.

The laboratory performance of the three monolayer compounds has been matched to the biological conditions recorded for each of the three SEQ benchmark reservoirs. Field-derived information on the potential for microlayer compounds to interfere with monolayer performance, and on the population density and activity of monolayer-degrading bacteria, was used to predict the likely performance of the three monolayer compounds in reducing evaporative loss when applied to the three benchmark reservoirs. Key water quality criteria that best predicted the performance of a specific monolayer product applied to a reservoir has been selected. The key indicators that appear to be influencing monolayer performance are history and frequency of algal blooms, measured UV absorbance of a water sample, water colour and storage size. The significance of each of these indicators is detailed at length in Section 9.3.

Such information would be captured as part of a decision table which would allow the user to make comparisons between the SEQ benchmark reservoirs and their own (once characterised with respect to the key indicators) to determine a best match (Section 9.3).

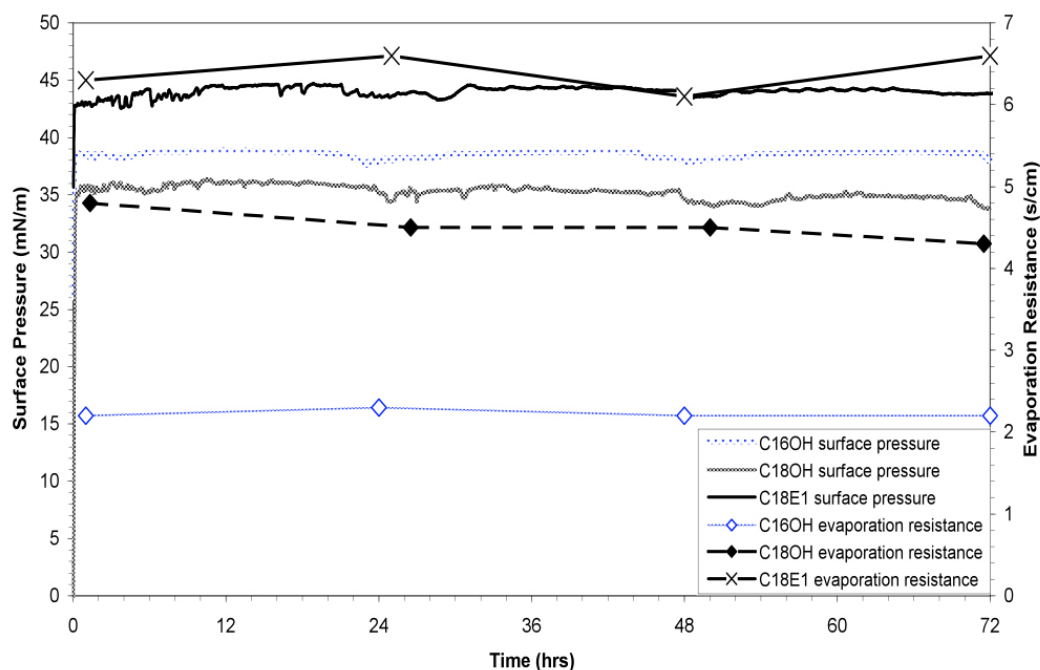


Figure 3.1: Laboratory (Langmuir trough) measurements of surface pressure and evaporative resistance of the same three monolayer compounds applied to clean water. Reproduced from Brink et al. (2010).

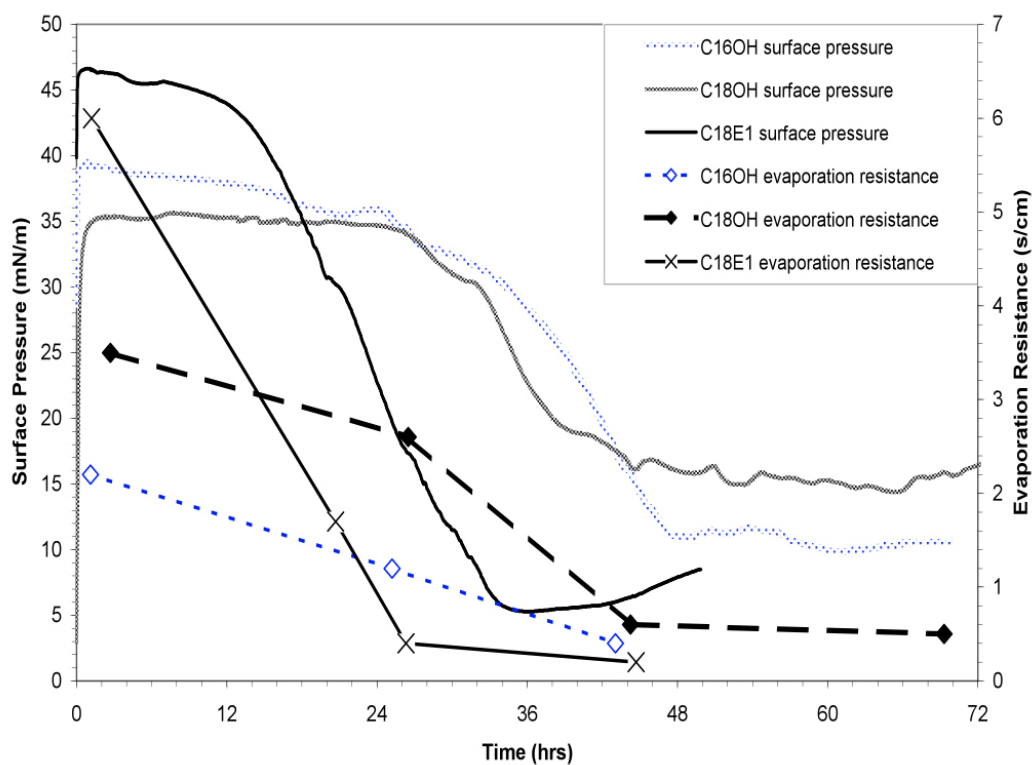


Figure 3.2: Laboratory (Langmuir trough) measurements of surface pressure and evaporative resistance of the same three monolayer compounds applied to brown, Narda Lagoon water. Reproduced from Brink et al. (2010).

3.2.2 Application system design

If the design principle of employing a series of applicators or application points strategically placed around and within a given waterbody is adopted, three questions immediately arise:

1. How many applicators are needed?
2. How far are they to be spaced apart?
3. How are they to be arranged on-site?

The literature available to date, as summarised in Section 2.6.2, only provides rough estimates for spacing between applicators or application points, there is no general theory or design formula provided to work this out. Ultimately, the spacing between applicators needs to be based on the monolayers ability to spread laterally between applicators. However, this will change whenever the wind speed changes. As McArthur (1962) noted, the lateral spreading width of monolayer decreases with increasing wind speed. Other than this in-field observation there is no other information available to help answer these questions. If a formula could be developed for calculating the spreading angle of monolayer under different wind speeds, question 2 could be answered with relative ease. Question 1 could also be answered by the same formula, if the size of a given waterbody was known as well.

Question 3 is somewhat answered by the design strategy that some applicators are placed around and within the waterbody. It may be that applicators around the perimeter of the waterbody are more effective than those within, for the simple reason that more surface area could be covered by monolayer spreading all the way from the up-wind shore to the down-wind shore as compared to an applicator placed halfway along this length. Another unanswered question is whether having applicators symmetrically laid out as opposed to strategically arranged according to the on-site prevailing wind direction is better or worse. This may not always be the same answer as the size, shape and on-site wind conditions for every waterbody is likely to be different.

To determine the effect of different application system arrangements (i.e. number of applicators, applicator types and location of applicators) under different wind speeds, wind directions and storage sizes, shapes and orientations on the spatial distribution of monolayer coverage, a monolayer dispersion model/simulation needs to be developed. This would allow quick and easy iterative simulations to be conducted to determine an optimal application system arrangement (as determined by the user) for a specified storage size and wind condition. Therefore key factors that are likely to affect the type of application system and its site-specific configuration are size, shape and orientation of the water storage and historical wind speed and direction frequencies for the site.

3.2.3 Application strategies

In determining application strategies for monolayer a simple robust method of detecting a monolayer on the water surface is desirable. As noted in Section 2.7, Coop (2011) has developed a prototype detection method, which is a spot measurement device, requiring a number of these units on the water surface to give an indication of spatial distribution. However, due to the timelines of this work and that of Coop’s, it was not possible to use his detection device. Beyond this, to the best of the authors’ knowledge, there are no other simple robust options readily available for in-field use.

Although a ready-to-go detection method was not available for in-field use during this PhD, it was hypothesised that a monolayer dispersion model/simulation, as suggested above in Section 3.2.2, could also be used to determine which applicators to apply from for a specific wind direction and the amount of monolayer each needs to apply for a specific wind speed. The simulation could be run to determine all possible wind condition combinations (wind speed and direction) to be expected on-site. This information could then be used to produce a decision chart to enable variable dosing strategies to be implemented by the application system for real-time wind conditions on-site.

3.3 Illustration and overview of the UDF

The UDF seeks to force the consideration of all of the key factors that affect monolayer performance. These key factors are all interconnected and can be grouped into four main categories: water quality and biology, topography, climate and water value. They should also be considered to be site-specific and will therefore need to be determined for each water storage.

According to the literature reviewed in Section 2, there are certain environmental conditions that when encountered reduce monolayer performance by such a large extent that the use of monolayer should be temporarily or even permanently stopped. These environmental conditions also establish the working environmental range/boundaries for the UDF. The environmental boundaries for the UDF are summarised as follows:

- The most important limit to be placed on monolayer application should be that of high wind speed. As reported by many researchers, once wind speeds in the range of $26.4(\pm 5)$ km/h are reached the application of monolayer becomes impractical.
- Rainfall is another factor that negatively affects monolayer performance by breaking up the surface film and causing submergence and increased volatilisation of the monolayer material.
- Certain water bodies with the following characteristics would indicate high levels of biological activity and a less than ideal environment for monolayer use:
 - regular algal blooms,
 - high UV absorbance,
 - dark brown water colour, and
 - relatively small area (i.e. <1 ha).

- During periods of very little to no wind together with high relative humidity, such that a warm surface film is established, there would be no added benefit in using a monolayer for evaporative suppression (Gladyshev 2002)².

As the key factors that influence monolayer performance are likely to be different for every situation, the first objective would be to characterise one's storage with respect to water quality and biology, topography, climate and water value. It is envisaged that the minimum required information under each of these four category headings would be as follows:

1. Water quality and biology: It is envisaged that an on-site analysis would need to be conducted to determine the key water quality and biological indicators. Water colour, although subjective, would need to be done by eye to determine a best match with the colour swatches provided (Figure 3.3). Electrical conductivity on the other hand can be measured with a probe on-site, or a water sample can be sent to any commercial laboratory, such as Société Générale de Surveillance (SGS)³, for analysis. Storage size only needs to be a simple estimation of the average volume of water stored, normally by the farm owner/manager. The frequency of algal blooms also needs to be provided by the farm owner/manager.

2. Topography: The topographical features of a site could be determined remotely via 'Google Earth' or on-site while conducting the water quality and biology analysis. Key features to be determined are dam type, shape, size and orientation (Figure 3.4). This information would be necessary for modelling the spatial distribution of monolayer for a particular site.

3. Climate: Historical climate information can be collected via internet sources,

²It is noted that even at 100% relative humidity, finite evaporation can still exist when there is a temperature gradient in the air (since there will still be a gradient in water vapour concentration). But because the monolayer does not act as an impervious film 'sealing off' the surface, it will not significantly impede the (very minor) evaporation occurring in this situation.

³SGS has a number of regional laboratories that provide water quality test services to the agricultural industries in Western Australia, South Australia, Victoria, New South Wales and Queensland. A list of SGS regional laboratories can be found via the following link: http://www.au.sgs.com/home_au_v2/contact_us_australasia.htm?lob=1&x=14&y=11

1. Water quality and biology
Water colour (select best match):

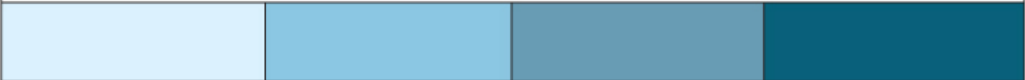


UV absorbance:
Storage size (surface area and water volume):
Algal bloom frequency:

Figure 3.3: Illustration of the necessary water quality and biology information required for the UDF.

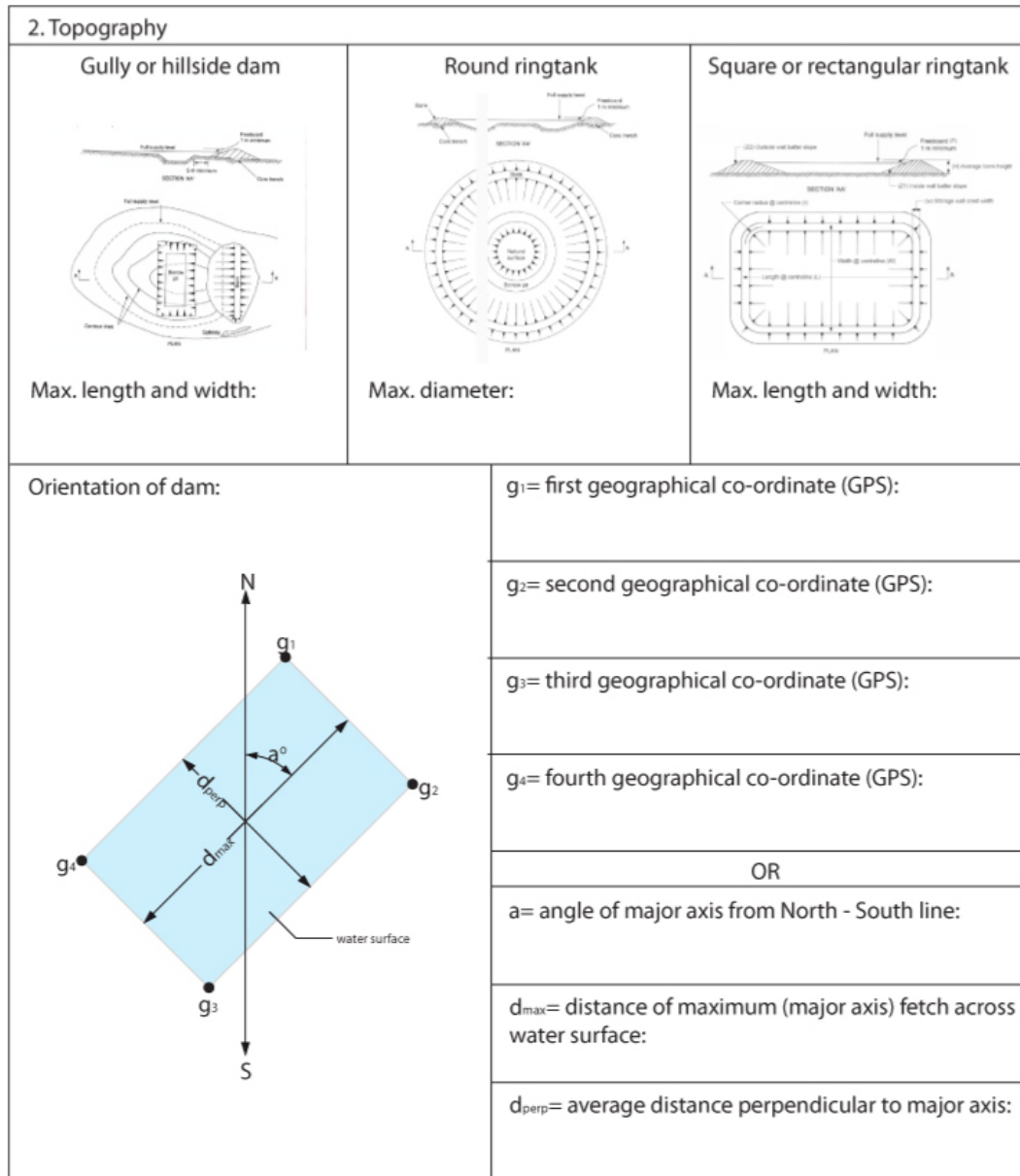


Figure 3.4: Illustration of the necessary topographical information required for the UDF.

such as the Bureau of Meteorology (BOM) and/or SILO. Wind speed and direction frequencies are available from the BOM in the form of a windrose for 9 am and 3 pm data. This would be fundamental to modelling the spatial distribution of monolayer and provides a necessary insight into the wind conditions to be expected on-site. The monthly potential evaporation rate is necessary in determining which months may be more economically feasible for applying monolayer. Monthly number of rainfall days indicates the days on which applying monolayer would not be practical. It would also be expected that evaporation rates on rainfall days would be rather low. Figure 3.5 illustrates the necessary information to be collected.

4. Water value: The average cost of water would need to be provided by the user including an estimation of the value of water to the user for every month of the year. The water value may change depending on water availability, crop type, cropping cycles, crop value, nearness to harvesting, etc. This information would also be helpful in determining which months may be more economically feasible for applying monolayer (Figure 3.6).

3.4 UDF research tasks

A number of research tasks have been undertaken in order to develop the UDF to a point where it can be used to determine the most suitable monolayer material, application system design and application strategies for a particular storage. These are as follows:

- A decision table has been developed to allow the user to make comparisons between the SEQ benchmark reservoirs and their own (once characterised with respect to the key indicators) to determine a best match monolayer material. The final table and a demonstration of usage is set out in Chapter 9.
- A suitable monolayer material for all empirical work has been developed (Chapter 4).
- The dispersion characteristics of a monolayer on a water surface have been studied in the laboratory for different wind conditions to determine the following:

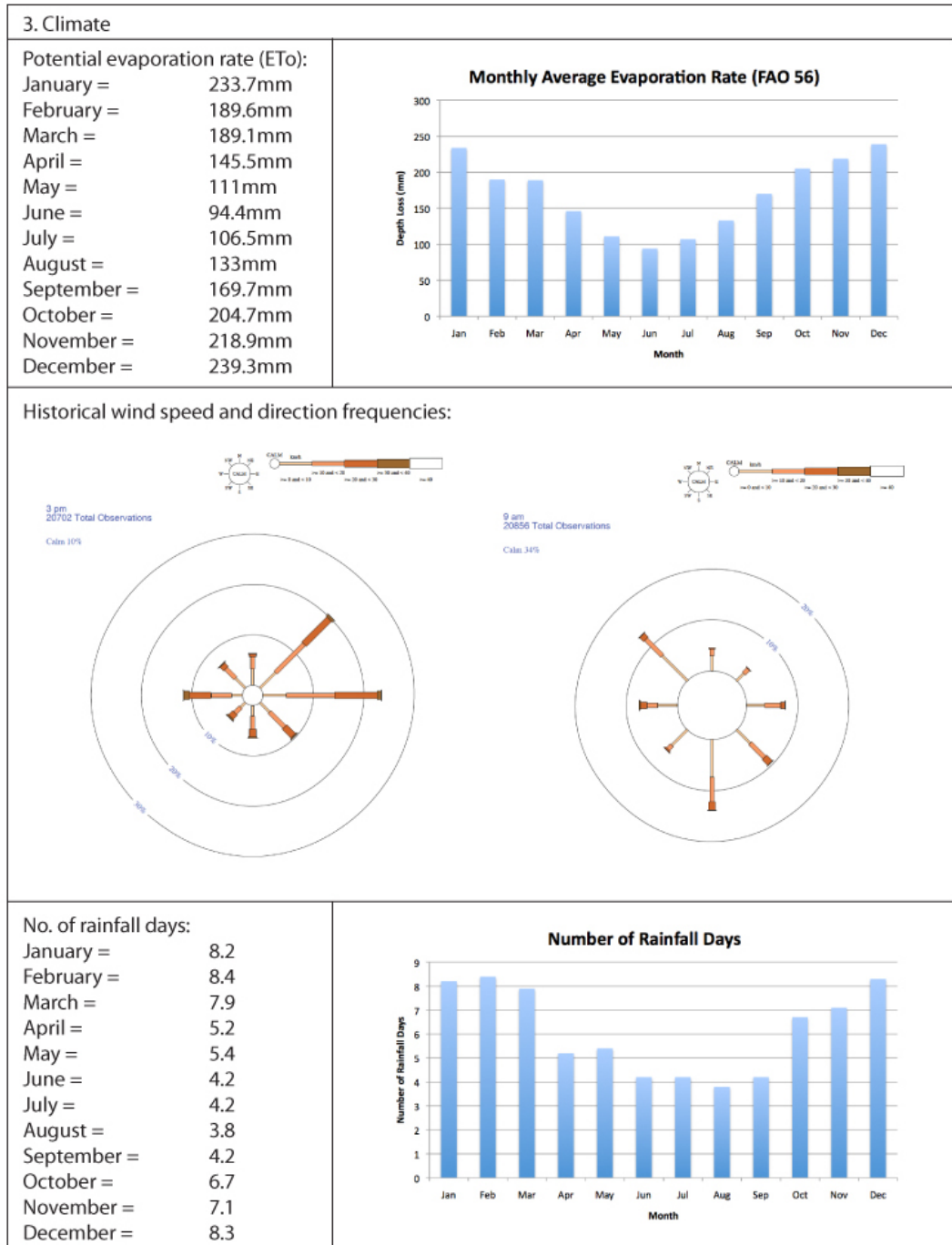


Figure 3.5: Illustration of the necessary historical climate information required for the UDF. Sample data is from the BOM weather station located at the University of Queensland, Gatton Campus, Queensland, Australia.

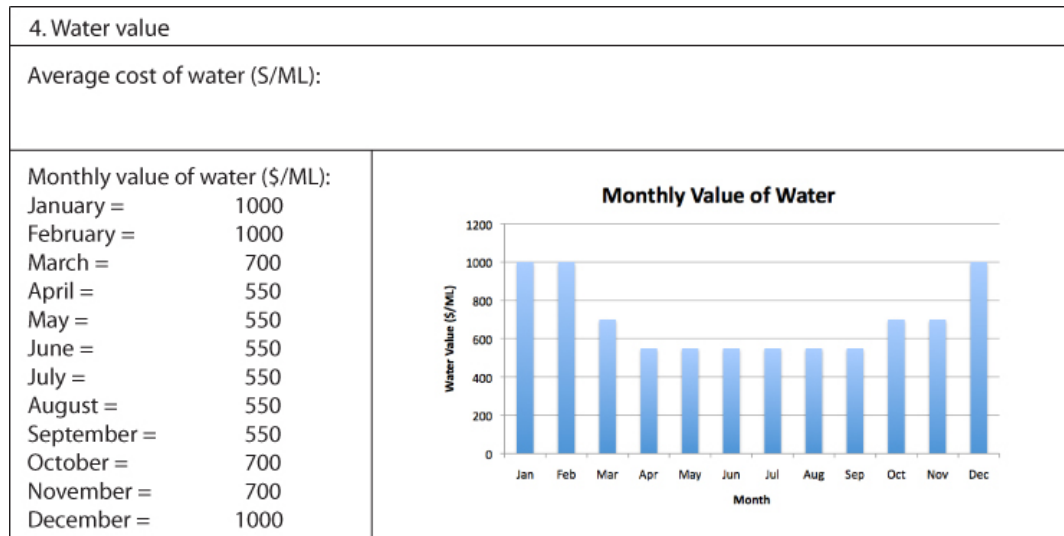


Figure 3.6: Illustration of the necessary water value information required for the UDF. Sample data in this illustration is purely illustrative.

- spreading rate and spreading pattern of monolayer for calm wind conditions when non-continuous application is required (Chapter 5).
- spreading rate and spreading pattern for a range of wind conditions when continuous application is required (Chapter 6).
- drift rate for monolayer while being continuously applied under a range of wind conditions (Chapter 6).

This research also demonstrates how the characterisation will need to be repeated for different monolayer materials.

- A basic model has been developed for simulating a number of different arrangements of applicators under the influence of different wind conditions to estimate/predict surface coverage at a nominated spatial scale (Chapter 7). The model is calibrated with the algorithms derived from the laboratory characterisation of monolayer dispersion.

Chapter 4

Development of a Monolayer Material Formulation

4.1 Introduction

It has long been known that increasing the alkyl chain length of a monolayer material will improve evaporation resistance but also reduce spreading rate. While stearyl alcohol (C18OH) has a much higher evaporation resistance than cetyl alcohol (C16OH), its rate of spreading is not adequate and most trials have been limited to using C16OH. In addition, many performance and operational difficulties have been experienced with autonomous application of solid or powdered monolayer (Frenkiel 1965).

An alternative is to improve the spreading of long-chain alcohols by creating a liquid suspension of the monolayer material in water. This is generally considered to make application easier, in comparison to powders, as liquids are easier to store, handle, distribute and apply. Furthermore, the highest evaporative reduction efficiencies have been obtained from the application of alcohol suspensions (Cluff 1966). As the rate of spreading is proportional to the line of contact between solid particles and the water surface, it is advantageous to have small particles. Considering the requirement of a stable suspension is to have the solid particles small enough to remain suspended, there is a large improvement in spreading compared to solid powder (Smith 1962).

From a practical application point of view, a suitable monolayer suspension with the following properties would be desirable:

- Non-toxic and environmentally benign for use on agricultural water bodies.
- High spreading rate for the initial formation of the monolayer film and for the spontaneous repair of any damage.
- Good stability of the suspension with no separation of the materials over long storage periods.
- Low viscosity so as to be fluid enough to pump through distribution hoses for application.

In the production of alcohol in water suspensions, many issues have been experienced such as, settling out of the alcohol (fatty alcohols are hydrophobic) and slow spreading due to prolonged contact with water (especially with C16OH) (Barnes 2008). In contrast however, Dressler & Johanson (1958); Dressler & Guinat (1973) and Reiser (1969) have all developed and used the suspension process to achieve substantial reductions in evaporation during field trials.

According to research by Dressler, Reiser, and Cruse the key to overcoming the aforementioned issues is by adding an emulsifying material which helps to produce suspensions of finely divided alcohol particles in water. Suspensions produced with the addition of an emulsifying material are reported as being stable for months at a time while displaying excellent spreading properties (Dressler & Johanson 1958, Reiser 1969, Smith 1962). In light of this information the development of a suitable monolayer-water emulsion was undertaken. In producing a suitable monolayer-water emulsion, different emulsifiers were evaluated with respect to spreading rate and evaporation resistance, and were compared to that of pure powders.

It should be highlighted here that surface chemists measure spreading rate as the surface pressure increase of a monolayer film over time. Whereas, engineers typically measure spreading rate as the distance the monolayer film moves on the water surface over time. Although, as Hale & Mitchell (1997) note, surface pressure increase over time does not

provide a direct measurement of the spreading rate on the water surface, it can be used to predict whether spreading will occur and the rate at which spreading will occur. The reason surface pressure over time can be used to predict the rate at which monolayer spreads on the water surface is because monolayer spreading is surface tension driven (see Section 2.2 for more detail). A monolayer film-forming material that achieves a high surface pressure (i.e. >30 mN/m) in a couple of minutes is a good indication that it will spread rapidly upon the water surface. Hence, surface pressure increase over time, as measured in this Chapter, is sometimes referred to as spreading rate.

4.2 Experimental objectives

After reviewing the literature it became apparent that only two monolayer products were commercially available, WaterSavr and HeatSavr. Both products are produced and sold by Flexible Solutions International (FSI)¹. WaterSavr is a solid form monolayer product consisting of a blend of C16OH, C18OH and hydrated lime. HeatSavr is a liquid form product consisting of C18OH in solution with isopropanol. As WaterSavr is in a powder form, application is more difficult than for HeatSavr. WaterSavr is also approximately 95% hydrated lime which makes accurate dosing of small amounts of the monolayer almost impossible (Hancock et al. 2011) and is ultimately dependent on how well the monolayers and hydrated lime were mixed during production. As for HeatSavr, there are economic and environmental issues associated with the large scale use of solvents on water storages (Barnes 2008). In addition, the effects of hydrated lime or isopropanol on the efficacy of the monolayer film in terms of its evaporation suppressing ability and spreading characteristics are largely unknown.

It is also worth noting that new monolayer products are currently being developed through the Cooperative Research Centre (CRC) for Polymers. The CRC for Polymers aims to create new monolayer chemicals which are more durable and more effective in reducing evaporation, however, commercialisation of these products is still some time off. In light of the above information and the fact that a suitable liquid form monolayer

¹Information with regards to Flexible Solutions International's products, WaterSavr and HeatSavr, can be found at: <http://www.flexiblesolutions.com/products/>

product is not currently available, the development of a suitable monolayer product for all of the empirical work for this PhD was seen as a necessity. In the development of a suitable product, the author collaborated with Michael Herzig (a PhD student from University of Queensland in Brisbane). Mr. Herzig was instrumental in the selection of suitable monolayer materials, testing their efficacy and producing them in large enough quantities for this PhD work.

4.3 Materials and methods

A complete description of the materials and methods employed to produce the empirical results presented in Section 4.4 can be found in Herzig et al. (2011). However, in order to maintain the integrity of the results and their interpretation a summary of Herzig's materials and methods are provided.

C16OH and C18OH, both puriss grade (*geq*99% GC) were obtained from Fluka. C20OH, for synthesis grade (*geq*96% GC) was obtained from Merck. These alcohols were purified by recrystallising with spectroscopic grade hexane from Ajax. The emulsifier, Brij78 (polyoxyethylene (20) stearyl ether) was obtained from Sigma-Aldrich and used without further purification. Milli-Q water with 18.2 M ω cm resistivity was used in the emulsions and for the subphase. The emulsions were made by melting the alcohol and Brij78 together and then adding hot water (at approximately 70°C) while stirring. The emulsions were then allowed to cool with continued stirring. Emulsions contained 3-5% alcohol with a 5:1 alcohol to emulsifier ratio. All the emulsions were stable for at least 6 months except the C16OH emulsion which started visibly separating after approximately one month.

The surface pressures were measured in a PTFE Langmuir trough and barrier using a Wilhelmy plate cut from Whatman 1 Chr chromatography paper, attached to a NIMA (NIMA Technologies, Coventry, UK) force sensor. Water was thermostated and maintained at a constant temperature of 25°C. Emulsion was applied carefully to the water surface as a single drop from a pipette. The volume of emulsion used for each of the spreading measurements was between 2-20 μ L. Evaporation resistances were

measured using a modified Langmuir-Schaefer method as described by (Barnes, Costin, Hunter & Saylor 1980).

4.4 Results and discussion

The spreading of powdered C16OH and C18OH on water using 6 times the amount needed for a single monolayer (6x application) was measured and is shown in Figure 4.1. A 6x application quantity was used as this reflects the typically monolayer requirement in the field (at least 3x, Morrison et al. 2008). During the first few minutes after application, there was no measurable change in the surface pressure because the monolayer was in a gaseous phase. It is not until the surface concentration becomes high enough to form a condensed monolayer that the surface pressure increases. The difference between the spreading rate of C16OH and C18OH in powdered form are considerable (Figure 4.1). The fast spreading rate of C16OH has led to its use in many field trials, while the spreading rate of C18OH is considered slow and thus it is rarely used (Barnes 2008). Powdered C20OH spread much slower than C18OH, taking approximately 15 hours to reach 25 mN/m (not shown on graph).

The spreading of the emulsions made with Brij78 were measured and compared to the spreading of the powder alcohols (also shown in Figure 4.1). When the emulsions were first applied to the surface there was a sharp increase in surface pressure to approximately 10 mN/m. This was mostly due to the emulsifier increasing the surface pressure quickly, as a similar pressure increase occurs when applying a drop of water containing emulsifier only. The pressure then increased at a slightly reduced rate as the alcohol in the emulsion spreads. All the emulsions spread to a higher surface pressure than the corresponding equilibrium spreading pressure of the powders.

While there was no clear improvement in the spreading rate of the emulsified C16OH, the results make it clear that the emulsion formulations of C18OH and C20OH have much faster spreading rates than the powders. The fast spreading rate of the emulsion makes it feasible to use C18OH on large water storages.

By comparing the monolayers spread from powder and emulsion, the effect of the Brij78

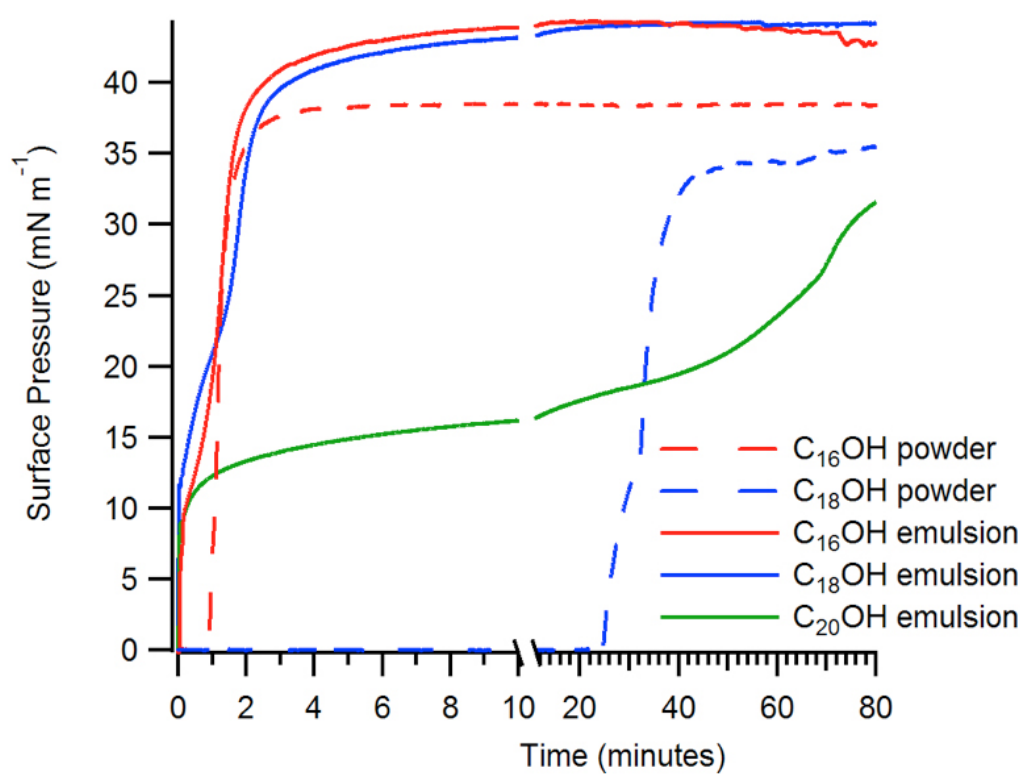


Figure 4.1: Spreading of the alcohol emulsions made with Brij78 compared to powdered alcohols using a 6x application. Reproduced from Herzig et al. (2011).

on evaporation resistance can be seen (Figure 4.2). Considering that monolayers of pure Brij78 used in the present research have zero evaporation resistance, there is a possibility of reduced evaporation resistance when combining the long-chain alcohols with the Brij78. However, the evaporation resistance of long-chain alcohols increases with increasing surface pressure, so it might be expected that emulsion application would result in higher evaporation resistance than powder application.

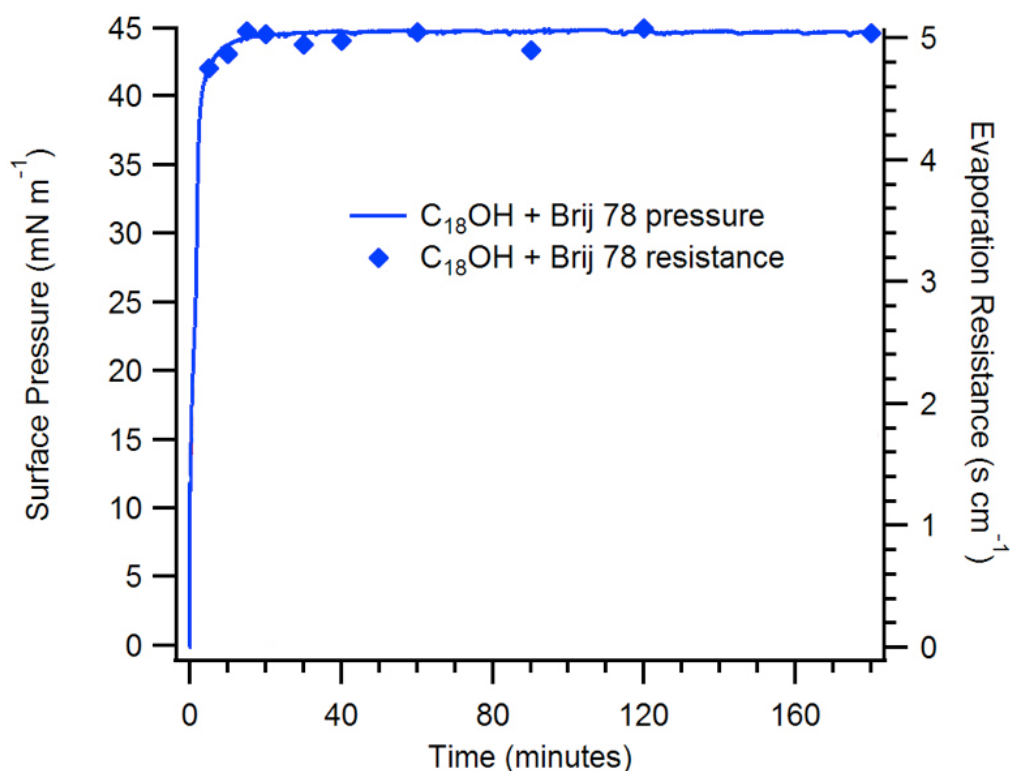


Figure 4.2: A comparison of evaporation resistances of monolayers spread from powder and emulsion using a 6x application amount. These emulsions were made with Brij emulsifiers. Reproduced from Herzig et al. (2011).

4.5 Conclusions

Using emulsions to apply monolayers to water surfaces has clear advantages over powder application. Most notable is the improvement in spreading rate which will allow the use of monolayers with much higher evaporation resistances. However there are a number

of other issues that need to be considered when evaluating the potential for practical application. Choosing an emulsifier that does not interfere with the evaporation resistance of the monolayer is essential and ensuring that the monolayer material stays at the surface rather than dispersing into the bulk is important to prevent unnecessary wastage of material.

Although emulsion's are essentially particles dispersed in water and typically have a similar density to water, there is always likely to be some submergence (which in this case is assumed to be loss into the bulk water due to particle dispersion). With purified C18OH and Brij78 in water-emulsion there appeared to be no evidence of submergence, however with unpurified C18OH (which was used for all of the experimental work in this Thesis), 33 to 50% of the C18OH was being lost to submergence. Despite this potential for product loss to submergence, which can largely be mitigated by ensuring the dispersed particles within the emulsion are kept as small as possible and is gently applied to the water surface (Herzig et al. 2011), the C18OH and Brij78 in water-emulsion is still a very promising method for practical application of evaporation retardants to large scale water storages.

Chapter 5

Monolayer Spreading (without wind stress)

5.1 Introduction

Effective evaporation suppression of water by a monomolecular film is fundamentally dependent on the maintenance of that film over the great majority of the water surface. In the laboratory under controlled conditions complete cover can easily be established, however, in the field under natural weather conditions, this is very difficult to both achieve and maintain. Across all the readily-available publications to date reporting the in-field performance of monolayer, it would be near impossible to find one that does not make reference to the deleterious effects of wind. Wind is the principle factor negatively affecting the persistence of monolayer on the water surface (Crow 1963). Wind increases film volatilisation, surface drift downwind, beaching on the lee shore and waves, which can break-up or submerge the film (Fitzgerald 1964, Frenkiel 1965, Reiser 1969).

Vines (1960*b*) reported that wind induced drift of a monolayer film across the water surface starts to occur at wind speeds of around 3.2 km/h. McArthur (1962) and Crow & Mitchell (1975) have reported similar values. Above this threshold wind speed, it is well known that a monolayer film will drift downwind at a speed of about $3.5(\pm 0.6)\%$ of the wind speed (Hale & Mitchell 1997). The general approach to maintaining a

continuous film cover during wind speeds >3.2 km/h has been to apply monolayer continuously at a rate equal to which it is removed (Frenkiel 1965, Crow 1963, Reiser 1969). However, even a ‘constant’ wind is highly dynamic and, of course, varies from location to location and in speed and direction. Also, periods of calm (defined here as wind speeds <3.2 km/h) may persist for hours or even days. Therefore, an effective monolayer application system should be capable of non-continuous application during periods of calm and also continuous application during periods of wind (Brink et al. 2010).

Central to the design of the application system and appropriate application strategies is knowledge of the spatial distribution of monolayer applied to the water surface; and in turn this requires a fundamental understanding of the characteristics of monolayer movement under different wind conditions. Thus, in order to characterise monolayer movement, it is necessary to achieve this for both low wind conditions, <3.2 km/h, and for a range of wind conditions >3.2 km/h. Using the C18OH and Brij78 in water-emulsion (described in Chapter 4) as a benchmark monolayer material, this Chapter reports experimental results with zero wind stress at a range of scales (using laboratory water tanks of diameter 0.3 m, 2 m and 6 m); and Chapter 6 reports experimental results for a range of windspeeds (at the 6m diameter tank scale). The present methodology was designed to bridge between centimeter-scale, clean room laboratory experimentation (e.g. a petri dish and Langmuir trough) and the desired field conditions, i.e. on extensive open water storages, where experimentation is particularly challenging, principally due to lack of environmental control. By this means the validity of extrapolation of the results to field (hectare) scale is argued.

5.2 Background

During low wind conditions, there would be little if any influence by the wind on monolayer movement, therefore, rate of coverage will largely be dictated by the natural spreading rate of the monolayer. As monolayer molecules are amphiphilic (each has a hydrophobic part and hydrophilic part), they anchor themselves to the water surface causing a decrease in surface tension (Barnes 2008). When a monolayer-

forming material is first placed on the water surface it creates a surface tension gradient between the film-forming material and the water surface causing rapid initial spreading (Myers 1992). This phenomenon of fluid flow caused by surface tension gradients is known as Marangoni flow (Jensen 1995, Dussaud & Troian 1997, Tarasov et al. 2006, Berg 2009). The speed of spreading is controlled by the initial spreading force (Davies & Rideal 1963), which can be determined using equation 2.1 (in Section 2.2).

As indicated in Chapter 4, although surface chemists measure spreading rate in terms of relative changes in surface pressure, which allows prediction of whether spreading will occur and the rate at which spreading will occur, this does not provide a direct measurement of spreading rate (Hale & Mitchell 1997). More recently engineering researchers have been concerned with the dynamics of spreading of monomolecular films in industry and science, as they provide an interesting transport mechanism for technological processes (Berg 2009). In this field, spreading at the air-water interface is measured according to the speed of advance of the leading edge (edge between clean and monolayer covered water surface), which is usually identified using small tracer particles (such as talcum powder).

The spreading dynamics at the air-water interface of a deep liquid (which we are exclusively dealing with in this chapter) are different to those for a thin liquid (Berg 2009). A simple force balance first proposed by Fay (1969) determines the advance of the leading edge of a thin film spreading on a deep liquid in the surface-tension regime. Fay (1969) and Dussaud & Troian (1997), reasoned that the force per unit length driving the spreading process is the spreading force, which is opposed by the viscous drag force exerted on the film by the subsurface boundary layer.

The full theory for spreading is complicated and in most cases full solutions are numerical (Jensen 1995, Chebbi 2001, Berg 2009). However, Dussaud & Troian (1997) show that where the spreading film is non-volatile, immiscible in water, has a constant concentration source and is expanding radially on deep water, the leading edge position is given by:

$$d(t) = K \frac{(\mu\rho)^{1/4}}{S^{1/2}} t^n \quad (5.1)$$

where:

$d(t)$	=	distance travelled by the leading edge	[m]
K	=	spreading coefficient	[dimensionless]
μ	=	dynamic viscosity of water	[Pa*s]
ρ	=	density of water	[kg/m ³]
S	=	spreading force	[N/m]
t	=	elapsed time	[seconds]
n	=	scaling exponent	[dimensionless]

The value of the scaling exponent n has been determined numerically by Foda & Cox (1980) and Jensen (1995) to be 0.75, and verified experimentally by Camp & Berg (1987), Dussaud & Troian (1997) and Tarasov et al. (2006) to be $0.75(\pm 0.01)$. The implication from these results is that the exponent may be universal for all non-volatile immiscible films (for an infinite source of monolayer). However, for volatile and/or miscible films, or a finite source spreading other than radially, this exponent has found to be lower (Dussaud & Troian 1997).

(Berg 2009) reports that the spreading coefficient K is 1.1547 for axisymmetric geometry, which is in excellent agreement with Chebbi (2001) who calculated K to be 1.15 through numerical analysis. However, Camp & Berg (1987) and Dussaud & Troian (1997) report values in the range of 0.67 to 1.06. Following Dussaud & Troian (1997), K can be calculated from empirical data using:

$$K = \frac{S^{1/2}}{(\mu\rho)^{1/4}} k_D \quad (5.2)$$

in which k_D is determined from a power trend line fit to experimental data when plotted as $d = k_D f(t)$, i.e.

$$d(t) = k_D t^n \quad (5.3)$$

Berg (2009) reports that the spreading dynamics of the leading edge of monolayer is overwhelmingly reported to follow the power law equation 5.3.

5.3 Experimental objectives

Of the relevant studies found in literature, all were conducted on small surface areas ($<3 \text{ m}^2$) and over very short time spans (<5 seconds) - Camp & Berg (1987); Dussaud & Troian (1997); Tarasov et al. (2006); Berg (2009). Thus, the experimental objectives of the present study has been to measure spreading rate of the C18OH and Brij78 in water-emulsion at different scales over different time durations (i.e. spreading periods) and compare with the spreading rates predicted using equation 5.1 and equation 5.3. To the best of the author's knowledge a spreading coefficient for C18OH has not previously been reported, despite this material being used extensively in evaporation mitigation research. In addition, the value of the spreading exponent needs to be confirmed for C18OH (when applied as a monolayer in water-emulsion) to validate extrapolation to full-scale water storages.

5.4 Materials and methods

5.4.1 Monolayer material and application amounts

A C18OH and Brij78 in water-emulsion the same as that described in Chapter 4 was used in all tests. A detailed description and performance assessment of the C18OH and Brij78 in water-emulsion used can also be found in this Chapter.

As the monolayer application requirement in the field will be different for different size reservoirs it is necessary to determine the effect of different application amounts on spreading rate. In addition, application rates greater than the theoretical value required for still water (i.e. 1x) are necessary in order to compensate for material losses due to volatilisation and/or submergence (Vines 1962, Frenkiel 1965, Reiser 1969, Crow & Mitchell 1975) as well as the increased surface area due to both gravity and capillary

waves. Denoting the theoretical (still water) value for monomolecular layer formation as ‘1x’ ($= 2.3\text{mg}/\text{m}^2$ for the C18OH and Brij78 in water-emulsion), the equilibrium surface pressure was measured for three different application amounts, 1x, 3x and 6x, as set out in Table 5.1¹. Surface pressure was measured using a Wilhelmy plate cut from Whatman 1 Chr chromatography paper, attached to a NIMA (NIMA Technologies, Coventry, UK) force sensor. Section 4.3 provides a more detailed description of the method used for measuring surface pressures and Section 2.2 provides a detailed description of monolayer surface pressure theory.

Table 5.1: Surface pressures measured for C18OH and Brij78 in water-emulsion at different application amounts.

No. of Monolayers Applied:	π (equilibrium surface pressure) [mN/m]:
1	13
3	42
6	43

5.4.2 Measurement of initial spreading force

The initial spreading force S for the C18OH and Brij78 in water-emulsion was determined by measurement of force balance on a custom-built PTFE Langmuir trough and barrier. An immiscible film-forming material (C18OH, dissolved in hexane) was applied to the water surface of the trough and then compressed to a high surface pressure (i.e. $>50\text{ mN}/\text{m}$) by reducing the water surface area with the barrier. Once compressed, a drop of the C18OH and Brij78 in water-emulsion was placed on top of the C18OH film that was first formed and compressed. Due to the high surface pressure of the C18OH film first formed, the drop of C18OH and Brij78 in water-emulsion did not spread. The barrier was then moved backwards, thereby increasing the water surface area and decreasing the surface pressure of the C18OH film first formed. Surface pressure mea-

¹Although the equilibrium surface pressure for a monolayer like C18OH is considered to be fixed for application amounts 1x and greater, it was found to increase slightly with increasing application amount for the C18OH and Brij78 in water-emulsion. A consequence of the varying proportion of Brij78 present in the different application amounts.

measurements taken during this process indicated that the drop of the C18OH and Brij78 in water-emulsion started to spread at a surface pressure of $14(\pm 1)$ mN/m (at a water temperature of 23°C): this was taken to be the initial spreading force.

5.4.3 Experimentation with 0.3 m diameter tank

Experiments were conducted in a round polypropylene plastic bin, 0.3 m in diameter and 0.37 m deep, which was lined with a dark green polythene plastic bin liner (Figure 5.1a). This improved the visual contrast between talcum powder and monolayer during measurements, and also allowed the bin liner and water to be replaced for every spreading test, negating the need to clean the water surface of residual surfactant. This procedure, with the assumption that the surface pressure of the clean tap water was <4 mN/m, avoided the need to measure the initial surface pressure with indicator oils (which would have required sacrifice of a substantial portion of the surface area). A plastic ruler was placed on the water surface after each spreading rate test for calibrating the digital rulers used during video analysis.

For each test the water was left for an hour to settle before applying monolayer and all replicate tests for each application amount were all run on the same day to minimise temperature differences - water temperature is known to affect the spreading rate of monolayer, (McArthur 1962). Temperature variation within each set of replicates was measured to be less than 1°C .

Prior to monolayer application the water surface was dusted with a very thin layer of Sigma-Aldrich Technical Talc powder (following Davies & Rideal (1963); Lange & Huhnerfuss (1978); Hale & Mitchell (1997)). Although O'Brien et al. (1976) report that the use of talcum powder underestimated spreading rates of oleic acid by $<10\%$ compared to rates measured using thermistors, Hale & Mitchell (1997) state that measurement error in his study accounted for much of this difference. During this study, the layer of talcum powder applied to the water surface was kept as thin as practically possible in order to minimise any potential errors imposed by its use. A hand-held Gilmour pesticide duster proved to be an effective method for applying a very fine layer of talc to the water surface (Figure 5.2). The temperature of the top 10 mm of water was also



(a)



(b)

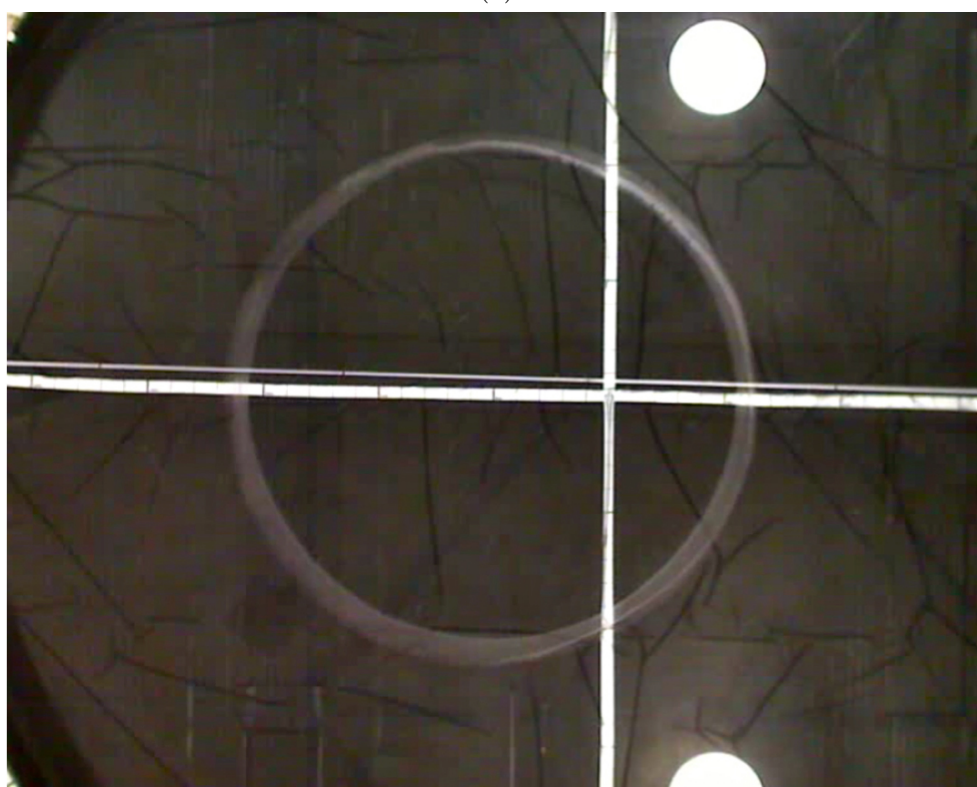
Figure 5.1: (a) Polypropylene plastic bin, diameter 0.3 m; and (b) polyethylene cattle trough, used for spreading rate tests. The trough is shown with a measuring tape suspended across the top for calibrating the digital rulers used during video analysis.

measured before the application of monolayer with a K-type thermocouple and Lutron TM-905 digital thermometer.

Monolayer was applied from approximately 15 mm above the water surface in the middle of the tank by hand with a micropipette. All spreading rate tests were recorded with a Canon Digital IXUS 80IS digital camera mounted above the centre of the tank from a wall bracket. Video was recorded at 30 frames per second and at a resolution of 640 x 480 pixels, and manually analysed (using Adobe Flash software) (Mitchell et al. 1995). The spreading front and time were measured relative to the first point of contact of monolayer with the water surface.



(a)



(b)

Figure 5.2: (a) Talcum powder application (prior to monolayer application) to visualise the spreading characteristics of the monolayer on the water surface; and (b) monolayer spreading in a circular pattern as is identified by the talcum powder collecting around the edges of the spreading front (both shown here for the 6 m diameter tank).

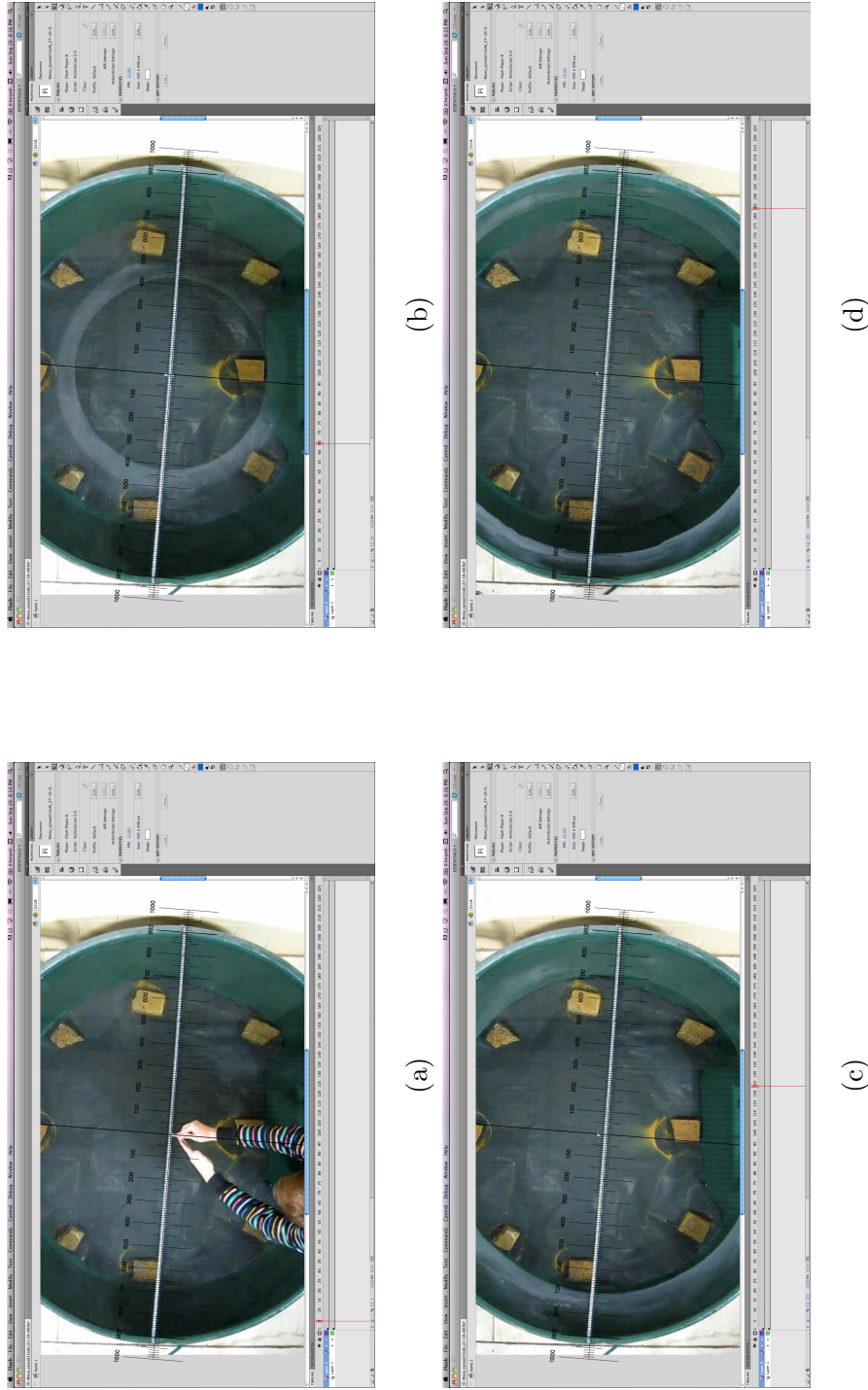


Figure 5.3: Screen shots of video analysis using Adobe Flash (2 m diameter tank shown): (a) First point of contact at $t = 0$ seconds (no monolayer has been applied yet); (b) Radius of the monolayer 5 seconds after application; (c) Radius of monolayer 10 seconds after application; (d) Radius of monolayer 15 seconds after application.

Monolayer surface pressures were measured 20 minutes after application using a range of calibrated indicator oils, each comprising a different proportion of dodecanol (C₁₂OH) in mineral oil such that it spreads at a specific water/monolayer surface pressure. The range used spanned 4 mN/m to 22 mN/m in 1 mN/m steps, plus 24, 28, 32 and 34 mN/m.

5.4.4 Experimentation with 2 m diameter tank

The second set of experiments was conducted similarly in a round polyethylene plastic cattle trough, 2 m in diameter and 0.7 m deep, which had a black polythene plastic sheet fixed to the bottom of the tank, again to improve the contrast between talcum powder and monolayer. A measuring tape was suspended across the top of the tank and fixed on opposing sides of the tank rim (Figure 5.1b). The measuring tape was placed so that the middle of the tape intersected the middle of the tank. The water level was always kept below the height of the measuring tape so as not to touch the water surface.

The tank was filled with tap water until overflowing and until the water surface was thoroughly cleaned of impurities and residual monolayer. When the surface appeared clean, the water interfacial surface pressure was tested with calibrated indicator oils. If the water surface was measured to be <4 mN/m, the cleaning process was stopped, but again only after all of the indicator oil was allowed to overflow over the edge of the tank². Three hours settlement time was allowed for each measurement, thereby reducing the influence of water currents set-up during the cleaning process (following Hale & Mitchell (1997)). Again, in order to minimise the effect of temperature, as water temperature was not regulated, replicates for each application amounts were all run on the same day. Temperature variation was contained to within 2°C for all sets of replicates.

Again, as monolayer is not visible to the human eye, an empirical method of determining

²Although every effort was made to ensure the water surface was clean prior to application, it is almost impossible to achieve a completely clean water surface at this experimental scale. However, any surface active impurities still present after cleaning were measured to have a surface pressure of <4 mN/m.

if the water surface was clean of monolayer was necessary (Timblin et al. 1962, Grundy 1962, McArthur 1962). A very thin layer of Sigma-Aldrich Technical Talc powder was also applied to the water surface before application of monolayer using the method described in Section 5.4.3. The temperature of the top 10 mm of water was also measured before the application. Monolayer was then applied from approximately 15 mm above the water surface in the middle of the tank by hand with a calibrated medical syringe. After 20 minutes the application of monolayer the interfacial surface pressure was again checked with the indicator oils. All spreading rate tests were recorded with the same digital camera and analysed in the same manner as described in Section 5.4.3.

5.4.5 Experimentation with 6 m diameter tank

The third and final set of experiments was conducted similarly in a round water tank, 6 m in diameter and 0.3 m deep, fitted with an impervious black polyethylene (PE) liner. Two thick strips of cloth tape, (silver in colour) with ruler markings every 100 mm were fixed to the liner in a criss-cross pattern with the intersection point of the strips of tape in the centre point of the liner (Figure 5.4).

The tank was filled with tap water until overflowing. As in the 2 m diameter trough tests, before every test the water surface was thoroughly cleaned of impurities and residual monolayer by overflowing and repeated scraping to the overflowing edge of the tank with a 5 m long 90 mm diameter polyethylene (PE) pipe. This cleaning process usually continued for 45 minutes until the water interfacial surface pressure was measured to be <4 mN/m (measured in a portion of the water surface sectioned off with the PE pipe so that the oil was contained and subsequently flushed over the edge of the tank to remove it). Again, after cleaning, the water was left for 3 hours to settle and because water temperature was not regulated during testing, replicates for each application amount were all run on the same day to minimise temperature variations. At this scale, with a much greater diameter-to-depth ratio for the water body, the water temperature variation could be contained to within 1°C for all sets of replicates.

Talcum powder was again applied to the water surface before monolayer application

by the same method detailed in Section 5.4.3, and the temperature of the top 10 mm of water measured before the application of monolayer. Monolayer was then applied at the centre of the tank using a calibrated medical syringe operated remotely at the end of a 3 m long 25 mm diameter aluminium pole (Figure 5.4-inset). Application was at approximately 20 mm above the water surface.



Figure 5.4: 6 m diameter water tank (lined with a black polyethylene liner) used for spreading rate tests. Monolayer is being then applied (by the author) with a calibrated medical syringe fixed to the end of a 3 m long aluminium tube for reach. Another aluminium tube, inside the larger diameter aluminium tube, is used to push down on the syringe plunger to apply monolayer.

The interfacial surface pressure was again checked 20 mins after the application of monolayer using the calibrated indicator oils. All spreading rate tests were recorded with a Logitech Webcam Pro 9000 digital camera suspended from the roof 5.5 m above the centre of the tank. Video was recorded at 25 fps and at a resolution of 960 x 720 pixels, and likewise manually analysed.

5.5 Results

At each experimental scale (0.3 m, 2 m and 6 m) the spreading rate results are only valid up to the time when the edge of the tank starts to affect the spreading rate. It was observed that for all three tanks that the spreading rate would drop to zero abruptly when the leading edge of the monolayer was close to the edge of the tank (e.g. Figure 5.5), at radius distances of approximately 110 mm, 700 mm and 2600 mm respectively. Hence valid data was restricted to the first 1 s, 10 s and 55 s for the 0.3 m, 2 m and 6 m tanks respectively.

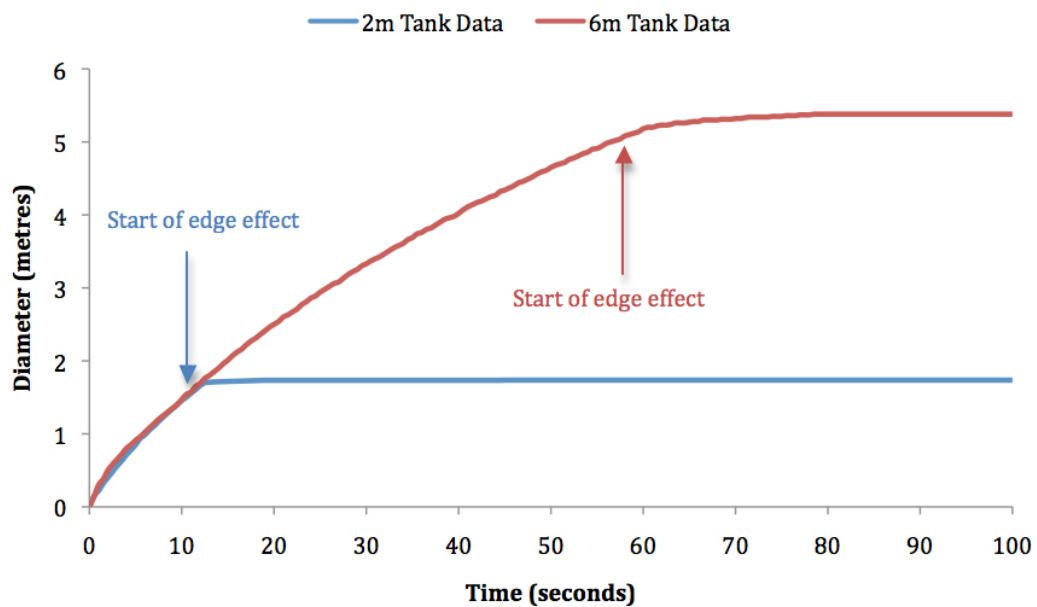


Figure 5.5: Radius increase versus time for monolayer spreading on the 2 m and 6 m diameter tank. As is visible in both tanks, the monolayer spreads until nearing the edge of the tank where the spreading rate drops to zero.

As the monolayer spread such that the leading edge was clearly close to a perfect circle every time, the radius was repeatedly measured from the first point of contact of monolayer with the water surface to the leading edge in a single direction for operational convenience. However, the validity of the perfect circle assumption was quantified at each tank scale by making one set of spreading front radius measurements along four orthogonal directions outwards from the first point of monolayer application. The average variation was 1.3%, 1.3% and 2.0% for the 0.3 m, 2 m and 6 m diameter tanks

respectively.

Three replicate tests were carried out for each application amount to ensure reproducibility. The data from the three replicates for each application amount was then averaged and plotted for radius versus time. The results from the 0.3 m, 2 m and 6 m diameter tanks are shown in Figures 5.6, 5.7 and 5.8 respectively. For the 2 m and 6 m tanks average uncertainty was 2.10 and 2.48% respectively across the three replicate experiments for each: this compares with the uncertainty of $\leq 2\%$ arising from the simple technique of radius estimation.

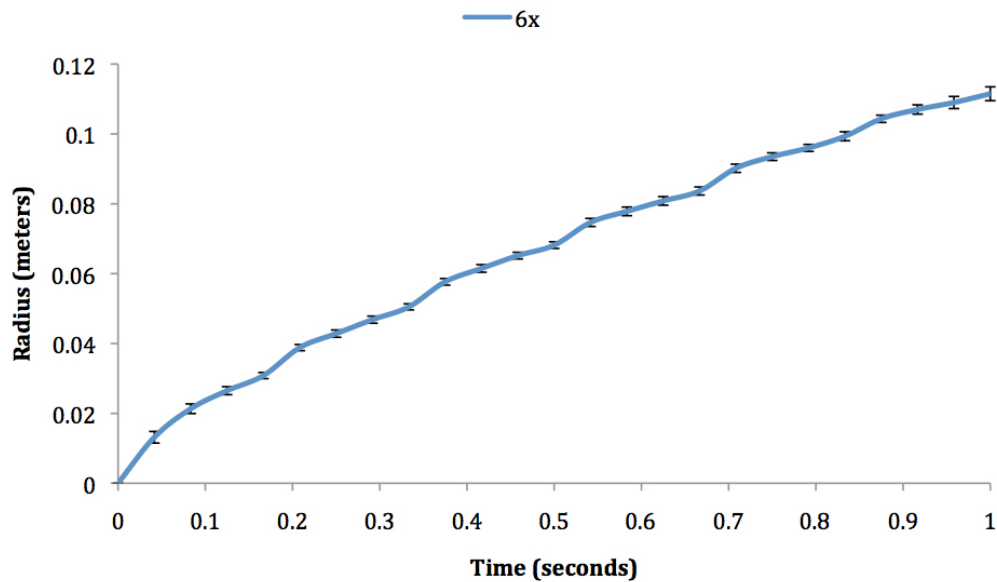


Figure 5.6: The leading edge radius versus time for a 6x application of monolayer placed at the centre of the 0.3 m diameter tank (at time = 0). At each timestep the error bars represent the mean and standard deviation of five replicate experiments. The average standard deviation is 0.0045 m.

The power law $d(t) = k_D t^n$, (equation 5.3) was fitted for each set of replicate tests and the results, plus the calculated spreading coefficients (eq. 3) are set out in Table 5.2. As noted in Section 5.4.2, the initial spreading force S for the C18OH and Brij78 in water-emulsion used in this study was determined to be $14(\pm 1)$ mN/m (at a water temperature of 23°C).

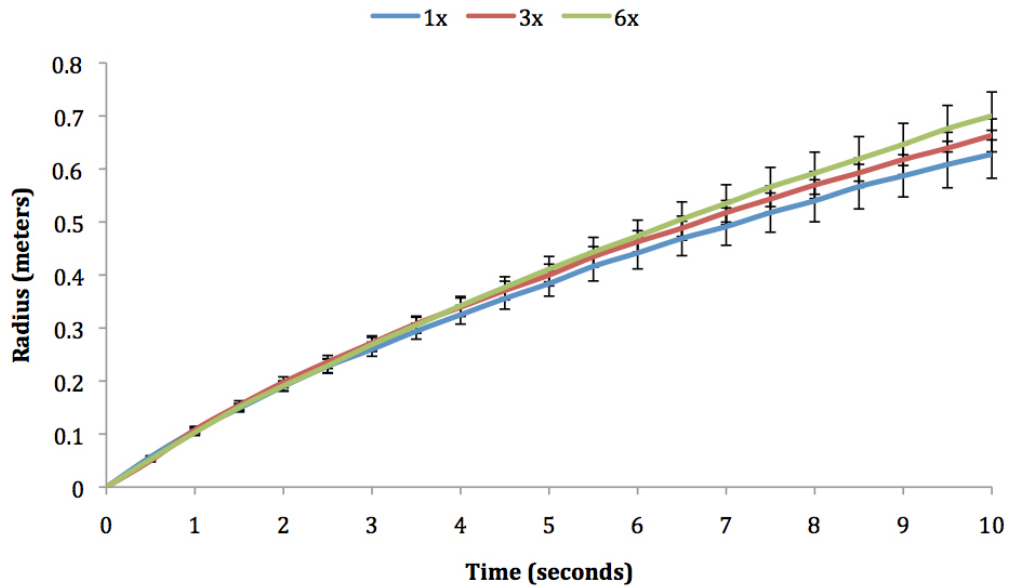


Figure 5.7: The leading edge radius versus time for three different application amounts of monolayer (1x, 3x and 6x) placed on the 2 m diameter tank (at time = 0). At each timestep the mean and standard error resulting from replicate experiments is shown.

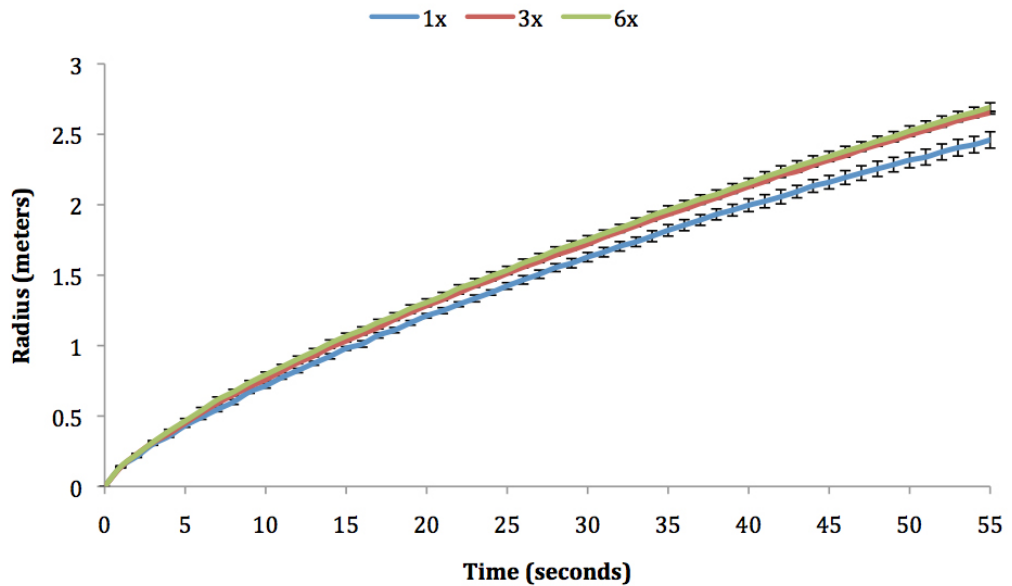


Figure 5.8: The leading edge radius versus time for three different application amounts of monolayer (1x, 3x and 6x) spread on the 6 m diameter tank (at time = 0). At each timestep the mean and standard error resulting from replicate experiments is shown.

Table 5.2: Summary of monolayer quantities applied and water temperatures during testing, including the constants and exponents derived from the 0.3, 2 and 6 m diameter tank results.

No. of Monolayers:	Monolayer Quantity (mg):	Water Temp. (°C):	Fitted factor k_D (eq. 5.3)	Fitted exponent n (eq. 5.3)	R ² :	Spreading Coefficient K (eq. 5.2):
0.3m Diameter Tank						
6	1.1	23	0.108	0.769	0.996	0.898
2m Diameter Tank						
1	7.0	19	0.107	0.788	0.998	0.907
3	20.0	18	0.105	0.825	0.994	0.896
6	40.0	18	0.103	0.849	0.998	0.881
Mean (\pm std. error):			0.105 (\pm 0.001)	0.821 (\pm 0.018)	-	0.895 (\pm 0.008)
6m Diameter Tank						
1	60.8	19	0.1333	0.7325	0.9996	1.1340
3	182.4	21	0.1380	0.7416	0.9999	1.1600
6	364.6	21	0.1436	0.7351	0.9997	1.2066
Mean (\pm std. error):			0.138 (\pm 0.003)	0.736 (\pm 0.003)	-	1.167 (\pm 0.021)

Finally, to inform comparison across size scales and the possible effect of application amount, a direct comparison was performed in which the same quantity of monolayer, 7.0 mg, was applied to both the 2 m and the 6 m tank. Water temperatures were 19°C and 23°C respectively. The results are shown in Figure 5.9 and discussed below.

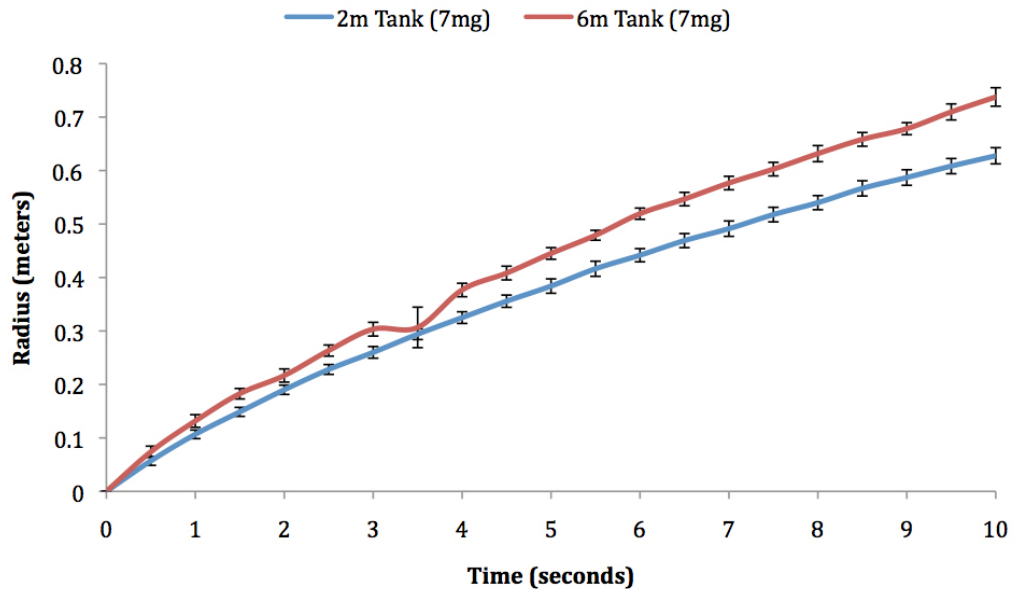


Figure 5.9: Comparison of radius increase over the first 10 seconds for 7 mg of emulsion spread on the 2 m and 6 m diameter tanks. Each line represents the average of three replicates. The error bars represent the standard deviation for the three replicates. The standard deviations are 0.024 and 0.027 for the 2 m and 6 m tanks respectively. The influence of surface area on spreading rate is clearly evident. (The data for the 6m tank at $t=3.5$ s is anomalous and attributed to an erroneous measurement rather than a physical effect.)

5.6 Analysis and discussion

5.6.1 Comparison with theoretical parameters

The theoretical spreading curve according to equation (5.1) using the Chebbi (2001) values of $K = 1.15$ and the spreading exponent $n = 0.75$ is plotted in Figures 5.10, 5.11 and 5.12 (upper curve in each). For the three size scales respectively, this theoretical

curve is compared directly with the empirical data; and also with equation (5.1) using the appropriate empirically derived K and n values (Table 5.2) for the 6x application. This latter curve was added to assess the quality of fit as a precursor to extrapolation across experimental scales (below).

In all calculations spreading force S was taken to be 14 mN/m, and values for dynamic viscosity and density of water were calculated using the average water temperature recorded for 6x application at their respective tank scale.

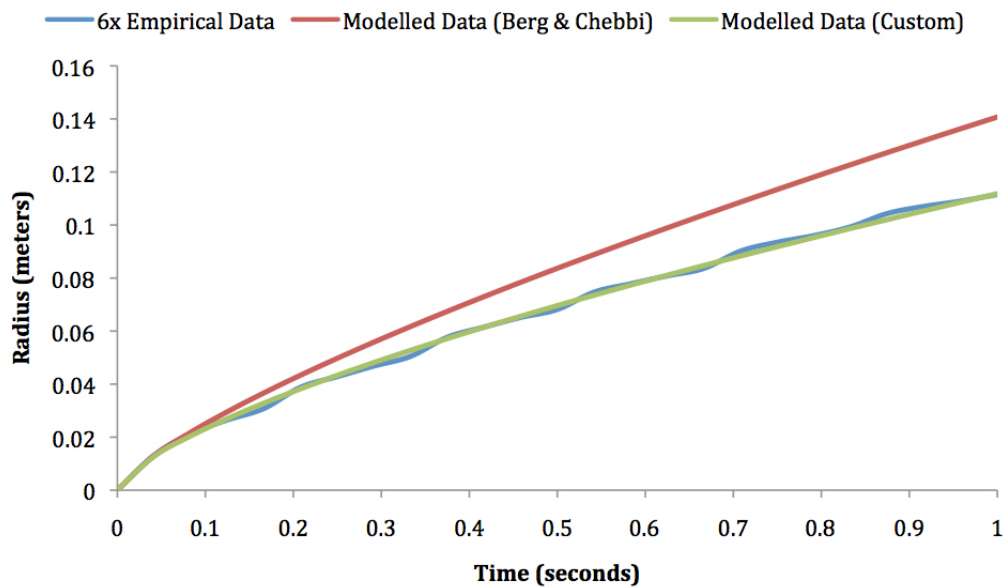


Figure 5.10: Comparison of measured spreading front radius versus time for the 0.3 m diameter tank, (i) measured data, (ii) equation (5.1) with $K = 1.15$ and $n = 0.75$ (Berg and Chebbi values), and (iii) equation (5.1) with K and n values from Table 5.2.

5.6.2 Comparison and reconciliation across different experimental scales

The duration of the spreading observed for the 0.3 m, 2 m and 6 m tanks was 1 s, 10 s and 55 s respectively (Figures 5.10, 5.11 and 5.12). To facilitate comparison, and exploration of the implications for extrapolation to field scale, the three empirical curves were compared directly by extrapolation of each curve out to 100 s duration as shown in Figure 5.13.

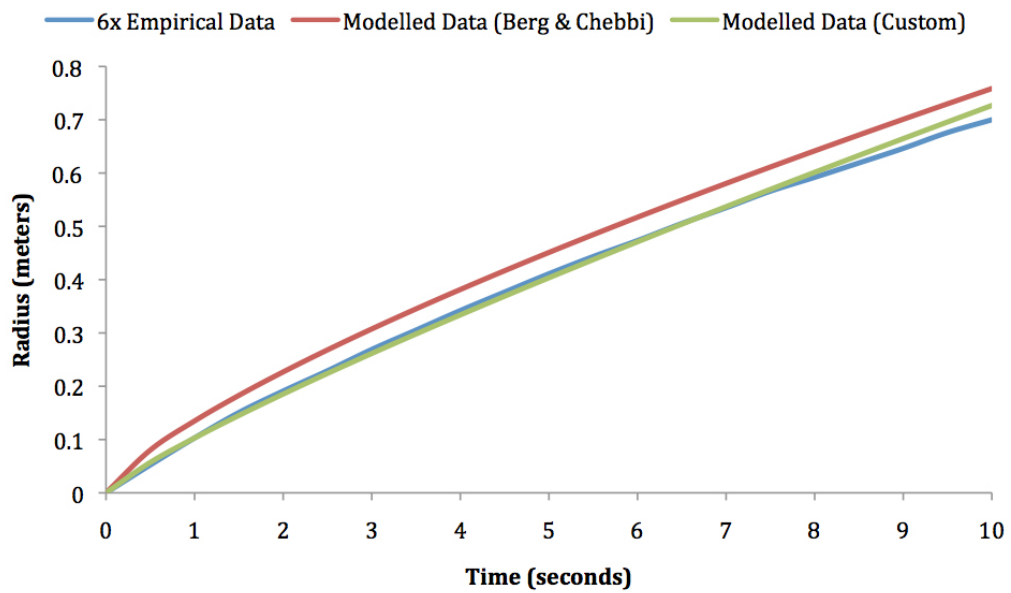


Figure 5.11: Comparison of measured spreading front radius versus time for the 2 m diameter tank at a 6x monolayer application, (i) measured data, (ii) equation (5.1) with $K = 1.15$ and $n = 0.75$ (Berg and Chebbi values), and (iii) equation (5.1) with K and n values from Table 5.2.

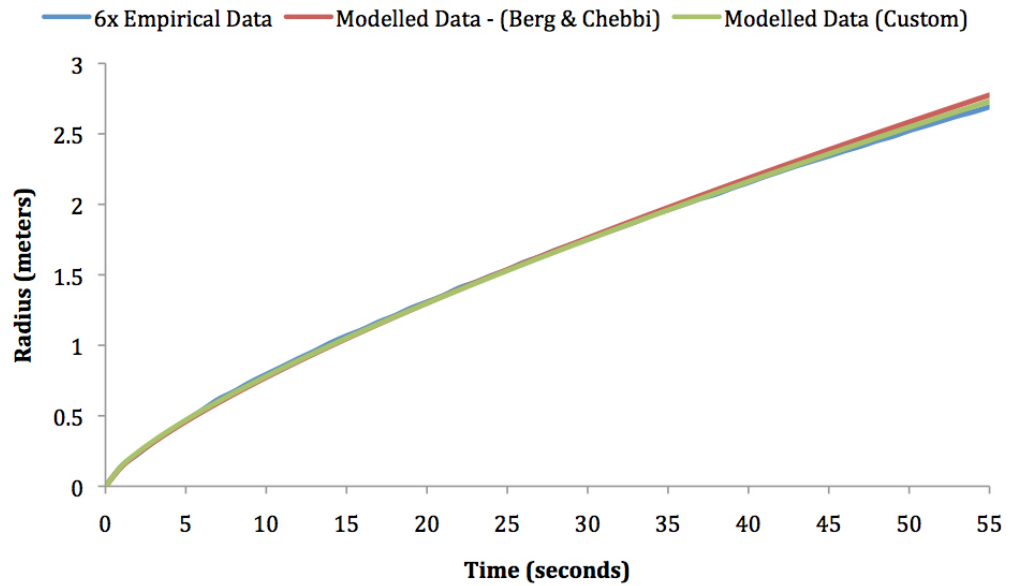


Figure 5.12: Comparison of measured spreading front radius versus time for the 6 m diameter tank at a 6x monolayer application, (i) measured data, (ii) equation (5.1) with $K = 1.15$ and $n = 0.75$ (Berg and Chebbi values), and (iii) equation (5.1) with K and n values from Table 5.2.

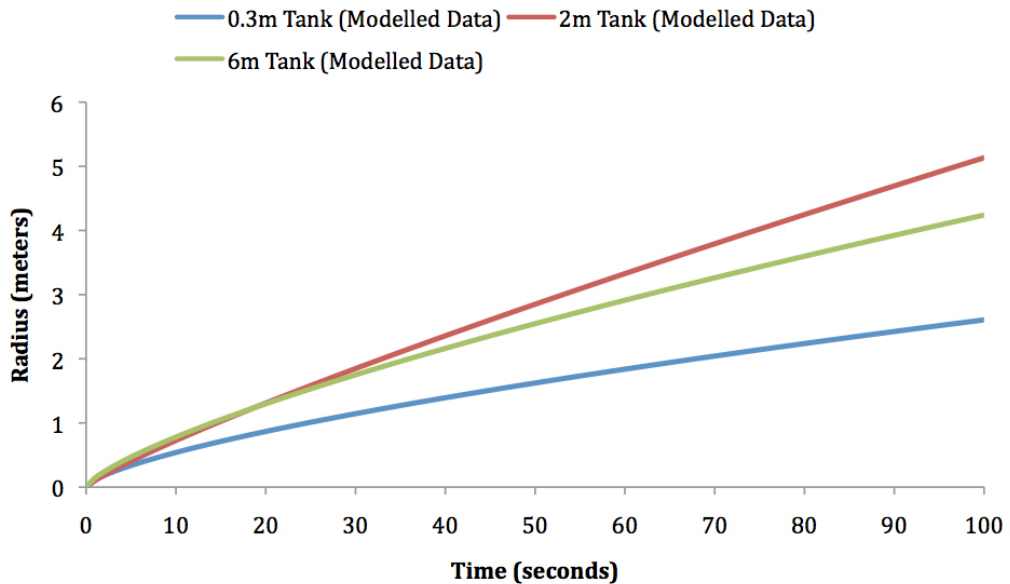


Figure 5.13: Comparison of the predicted spreading front radius versus time derived from the three different tanks scales by extrapolation to 100 s duration via equation (5.1). Each extrapolation used the empirically-derived K and n values (Table 5.2) for the 6x application.

Figure 5.13 indicates that the predicted spreading radii diverge, as might be expected, especially for the 0.3 m tank results which involve a 100-fold extrapolation; and at extended times (after approximately 30 s, extrapolations do not differ monotonically with experimental scale (0.3 m - 2 m - 6 m) as might have been expected. Clearly such extrapolation is heavily dependent on the value of the spreading exponent n , and Dussaud & Troian (1997) noted that the 0.75 value for non-volatile systems is not always reproducible.

Two further comparisons were undertaken. Firstly, assuming equal validity for the exponent n derived at all three experimental scales, a second reconciliation was attempted by using the global average empirically-derived exponent $n = 0.78 \pm 0.03$ and the resulting comparison is shown in Figure 5.14.

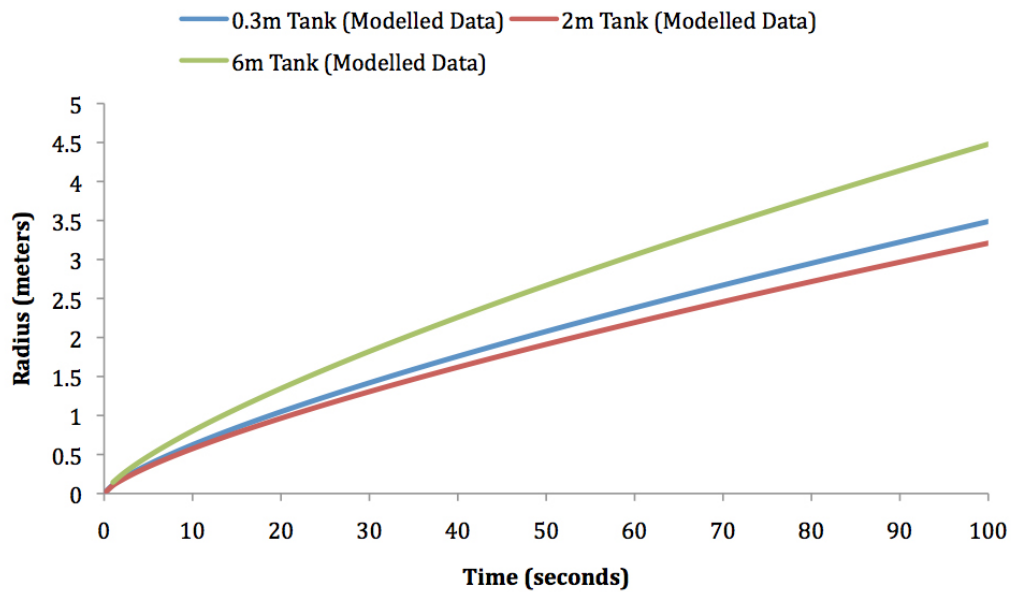


Figure 5.14: Comparison of the predicted spreading front radius versus time derived from the three different tanks scales by extrapolation to 100 s duration via equation (5.1) using scale-dependant K values (Table 5.2) with the global mean empirical scaling exponent $n = 0.78$.

In comparison with Figure 5.13, Figure 5.14 indicates the divergence is reduced between the 0.3 m and 2 m tanks but increased for the 6 m tank, which is expected from the differing empirical values of the coefficient K (Table 5.2). As noted, the 0.3 m tank results are highly extrapolated and undertaken at a different temperature, but closer

agreement might have been expected between the 2 m and 6 m tanks which were essentially at the same water temperature. A possible explanation for this difference is that the initial spreading rate may have been enhanced in the 6 m tank by the significantly larger amount of monolayer applied, or inhibited in the 2 m tank by the closer proximity of the tank edge. To investigate this the final experiment yielding the results of Figure 5.9 was undertaken. Figure 5.9 clearly shows different performance, but this is compounded by the 4°C water temperature difference.

Finally, the results show that the K values for the three tank scales do not follow the expectation that monolayer spreads faster at higher water temperature: it would have been expected that the value for K in the 0.3 m tank would have been greater than that for the 2 m and 6 m tanks. However, in comparison with the significant literature, the higher K value for the 6 m tank (Table 5.2), is in excellent agreement with those of Berg (2009) and Chebbi (2001); whereas the K values for the 0.3 m and 2 m tanks are in good agreement with those of Camp & Berg (1987) and Dussaud & Troian (1997).

5.7 Conclusions

It has been demonstrated that the formula of Dussaud & Troian (1997) and others, equation (5.1), is applicable to the spreading of ‘bulk’ monolayer from a centre point on circular, open water surfaces of scale 0.3 m, 2 m and 6 m diameter and that, as expected, under still conditions, monolayer spread in a uniform circular pattern outwards centred on the point of application. ‘Bulk’ application involved the placement of enough material to form layers either 1x, 3x or 6x monomolecular. Hitherto this has not been demonstrated at these scales and with these ‘overdosed’ material quantities, i.e. scales which come closer to that required for monolayer application for the evaporation mitigation of practical open water storages.

However, although characteristically similar across the three experimental scales, replicated results showed that the spreading rate varied slightly between the different scales, resulting in slightly different fitted values of the spreading coefficient K and spreading exponent n . No consistent explanation for these differences was indicated from the

limited range of data, but exploration of the spreading performance indicated by extrapolation and comparison from the smaller scales (0.3 m and 2 m, with respect to 6 m) indicated a mean spreading exponent value of $n = 0.78$. This was close to, and not significantly different from, the generally accepted value of $n = 0.75$.

Chapter 6

Monolayer Spreading and Drift (with wind stress)

6.1 Introduction and Background

As a monolayer film is only ~ 2 nm thick, coupled to the top layer of water surface by its hydrophilic head (Barnes, 2008), it is subject to transport by the wind (Crow 1963, Fitzgerald 1964, Vines 1962, Frenkiel 1965, Reiser 1969). The cause of this surface transport/drift is a consequence of two main components; the wind induced shear stress and Stokes mass transport related to wave characteristics (Lange & Huhnerfuss 1978, Dobroklonskiy & Lesnikov 1972). However, the Stokes mass transport component in most laboratory water tanks is usually $<10\%$ of the total surface drift rate (Wu 1975, Dobroklonskiy & Lesnikov 1972). The ratio of total surface drift speed (u_s) of clean water (i.e. no monolayer) to wind speed (u_w) has been reported by many researchers (Table 6.1). The average of the measurements for this ratio (u_s/u_w) from laboratory studies is 0.035 ± 0.008 .

Table 6.1: Comparison of various laboratory studies investigating the relationship between clean water surface drift speed (u_s) and wind speed (u_w). Field studies in lakes and open oceans have been omitted from this table as u_s is generally greater, most likely due to an increase in Stokes mass transport by developed deep-water waves (Lange & Huhnerfuss 1978). Adapted from (Lange & Huhnerfuss 1978) and (Hale & Mitchell 1997).

Source:	Length (m):	Depth (m):	Method:	Wind Speed Range (km/h):	Ratio of u_s/u_w :
Keulegan (1951)	20	0.14	Paraffin flakes	10.8-43.2	0.033
Fitzgerald (1964)	1.83	0.15	Talcum powder	12.6-27	0.03
Wu (1968)	14	1.2	Spheres and disks	12.6-48.2	0.028-0.048
Plate et al. (1969)	13.7	0.11	Wax paper disks	13-46	0.032
Wright & Keller (1971)	4.9	0.28	Plastic spheres and disks	8-28.4	0.038-0.045
Dobroklonskiy & Lesnikov (1972)	25	0.8	Polystyrene spheres	25.2-43.2	0.026-0.03
Shemdin (1972)	45.7	0.92	Paper disks	11.2-32.8	0.026-0.029
Mizuno & Mitsuyasu (1973)	13.4	0.35	Paper disks	9.0-36.0	0.030-0.034

Whereas, when the water surface is damped by the presence of a monolayer film, this ratio has been found to rise linearly from 0.03 then tend to a constant of 0.045 (Fitzgerald 1964). Fitzgerald is the only researcher, to the authors knowledge, who has quantified surface drift speed for clean water surface and monolayer covered surface with respect to wind speed during the same study. He suggested that the increase in the ratio of u_s/u_w was related to the surface concentration of the monolayer added. However, the results of Lange & Huhnerfuss (1978) and Hale & Mitchell (1997) indicate the exact opposite. They both found this ratio to decrease from ~ 0.041 then tend to a constant of ~ 0.03 . Reiser (1969) on the other hand found this ratio to be constant. Quite clearly, there is no general consensus between researchers for the ratio and trend of u_s/u_w for a monolayer covered surface. The average of measurements for this ratio from laboratory studies is 0.035 ± 0.006 , which is exactly the same average as that for clean water surface. This suggests that there is little if any difference in the surface drift velocity whether monolayer is present or not. A comparison table detailing various laboratory studies which have investigated this ratio of u_s/u_w can be found in Section 2.5.2.

As monolayer films are so readily transported by wind the general approach has been to apply monolayer continuously at a rate equal to which it is transported (Frenkiel 1965, Crow 1963, Reiser 1969). However, wind is highly dynamic and varies from location to location and in speed and direction, therefore, an effective application system should be capable of satisfying this demand. For which non-autonomous application methods (i.e. aerial application) generally do not. Also, application of monolayer in a liquid form is considered advantageous over powders (Barnes & Gentle 2005). A handfull of prototypical application systems have been developed which satisfy the above requirements. All generally use a number of applicators or application points strategically arranged around the perimeter and/or floating within the water body (McArthur 1962, Crow 1963, Reiser 1969, Crow & Mitchell 1975). The number of applicators/application points used and their strategic arrangement would have been influenced by the spreading characteristics of monolayer under wind stress. However, there is no general consensus for spacing between applicators/application points, their arrangement or detailed information with regards to spreading characteristics of monolayer under wind stress, which ultimately determines this spacing. A table summarising

the relevant information from studies employing application systems for monolayer in a liquid form and the spacing between applicators used can be found in Section 2.6.2.

McArthur (1962) reports that the width of a slick spread in the direction of the wind depends on the initial spreading rate of the source, which must overcome the lateral stress of the wind. Higher wind velocities, all other factors remaining constant, give narrower slicks. McArthur only provides some general measurements of slick width for winds between 8-14.4 km/h on water at 9-11°C. Further to this, Crow & Mitchell (1975) produced some film coverage maps based on hourly observations made by an observer using a plane table and alidade¹ from a vantage point atop a 27.4 m tower (Figure 6.1). As can be seen in Figure 6.1 the monolayer appears to spread in wedge shape out from the points of application before converging together. They also noted three intervals of wind speed that significantly affected the film cover: (i) 100% coverage for wind speeds <4.8 km/h, (ii) spreading of film over large areas between 4.8 and 20.8 km/h, and (iii) at winds >20.8 km/h application rate to maintain film cover was considered to be excessive.

6.2 Experimental objectives

To the author's knowledge, the coverage maps shown in Figure 6.1 are the only published documentation depicting the spreading characteristics of monolayer under wind stress. In addition, the drift rate of monolayer has only ever been characterised for a single application of a finite concentration, which would not be representative of in-field conditions where continuous application of monolayer would be desirable. Therefore, the following large-scale laboratory water tank and wind experiment was conducted to characterise:

1. the spreading angle of monolayer under wind stress, and
2. the drift rate of monolayer being continuously applied under wind stress.

¹An alidade is a device that allows one to sight a distant object and use the line of sight to measure the angle to the object from some reference point. Angles measured can be horizontal, vertical or in any chosen plane.

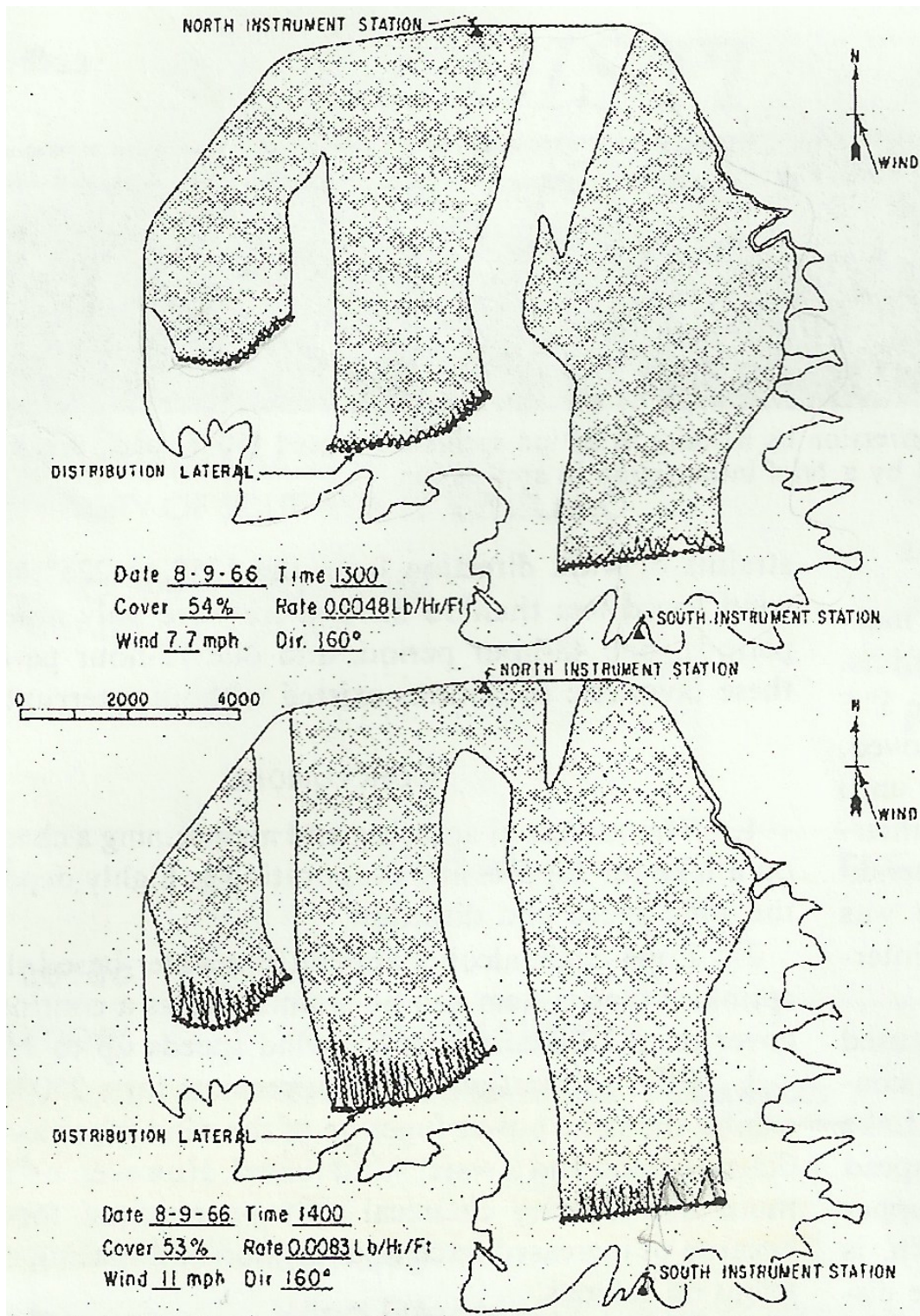


Figure 6.1: Monolayer coverage maps based on hourly observations made by an observer using a plane table and alidade from a vantage point atop a 27.4 m tower. The above map shows coverage achieved under a 12.4 km/h wind speed and the map below shows coverage during a 17.7 km/h wind speed. Reproduced from Crow & Mitchell (1975).

Although the primary objective of this study was to characterise spreading angle, it seemed necessary to also characterise drift rate during continuous application in order to compare with existing figures quoted in literature to see if there was a detectable difference.

6.3 Materials and methods

6.3.1 Water tank and wind apparatus

All experiments were conducted in a round water tank, 6 m in diameter and 0.3 m deep, fitted with an impervious black polyethylene liner. Wind was provided by an axial-flow fan, from which air was ducted through a 0.6 m diameter flexible air duct into an expansion chamber. The entry of the expansion chamber had a cross-section of 0.6 m by 0.2 m and an outlet cross-section of 2.7 m by 0.2 m. The expansion chamber outlet was placed at one end of the water tank so that the bottom surface of the expansion chamber sat at the water level of the tank. The expansion chamber was set-up to be level with the water in the tank so that air exiting the expansion chamber was travelling parallel to the water surface. The inlet of the expansion chamber was fitted with an adjustable wind vane apparatus and the outlet was filled with an arrangement of 90 mm diameter PVC tubes for air straightening. The apparatus is detailed in Figure 6.2 and illustrated in Figure 6.3.

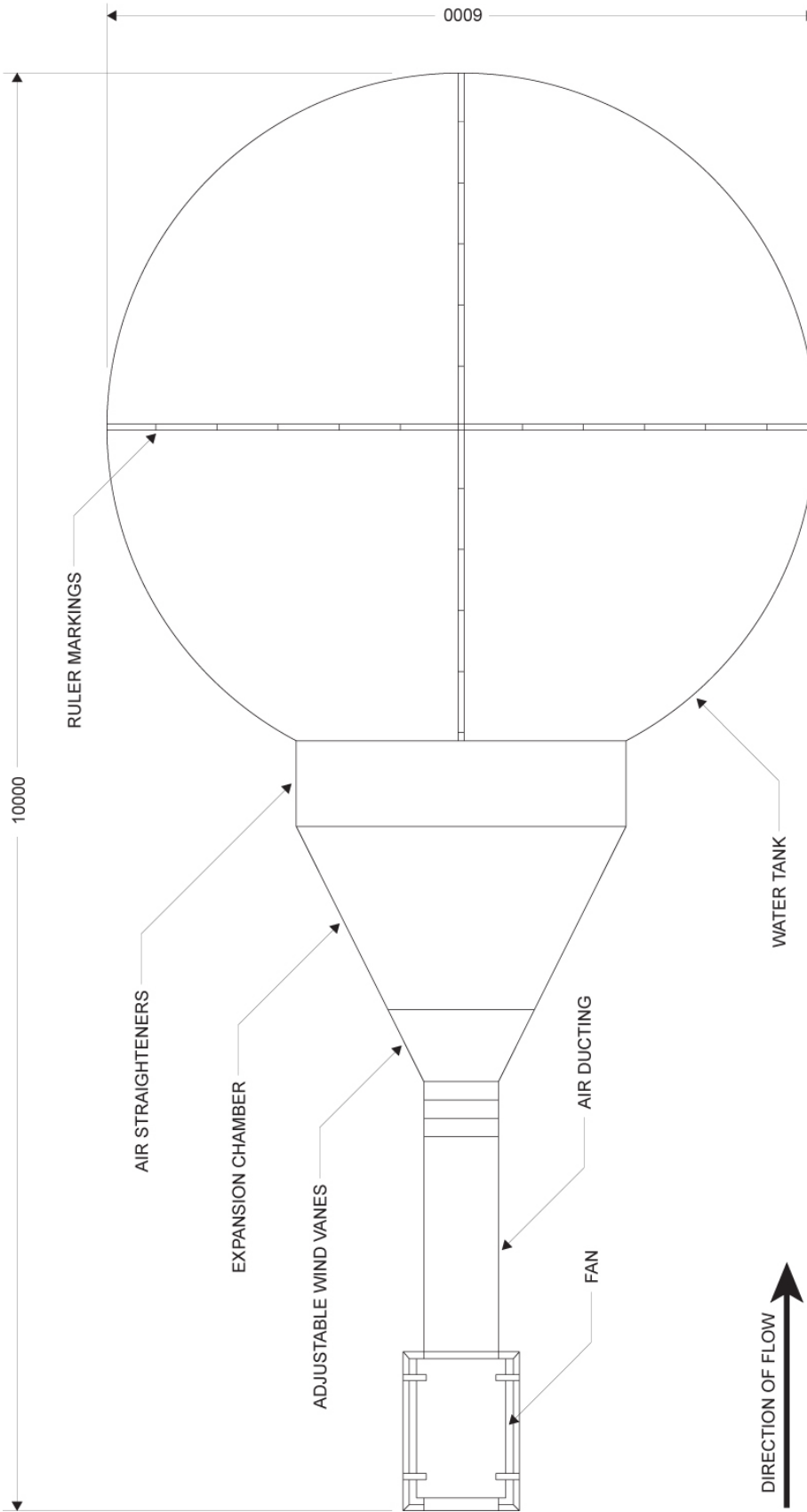


Figure 6.2: Diagrammatic overview of experimental set-up, shown in plan view, comprising axial-flow fan, air duct, adjustable wind vanes, expansion chamber, air straighteners and water tank.

In order to achieve a uniform wind profile across the face of the outlet duct of the expansion chamber, an adjustable wind vane apparatus was placed at the entry of the expansion chamber (Figure 6.4). The adjustable wind vane apparatus detailed in Figure 6.4 consists of a tapered four-sided box (1), within which four individual vanes (2) are evenly spaced apart from each other. The downwind ends of the vanes are fixed in position by a hinge (3), whereas the upwind ends of the vanes are moveable and are locked in position by a pin (4). This allows the fine adjustment of the angle of each vane. When the vanes are evenly spaced apart equal volumes of air are projected outwards to fill the volume of the expansion chamber. Vanes can then be adjusted individually to help achieve a uniform wind velocity profile at the outlet.

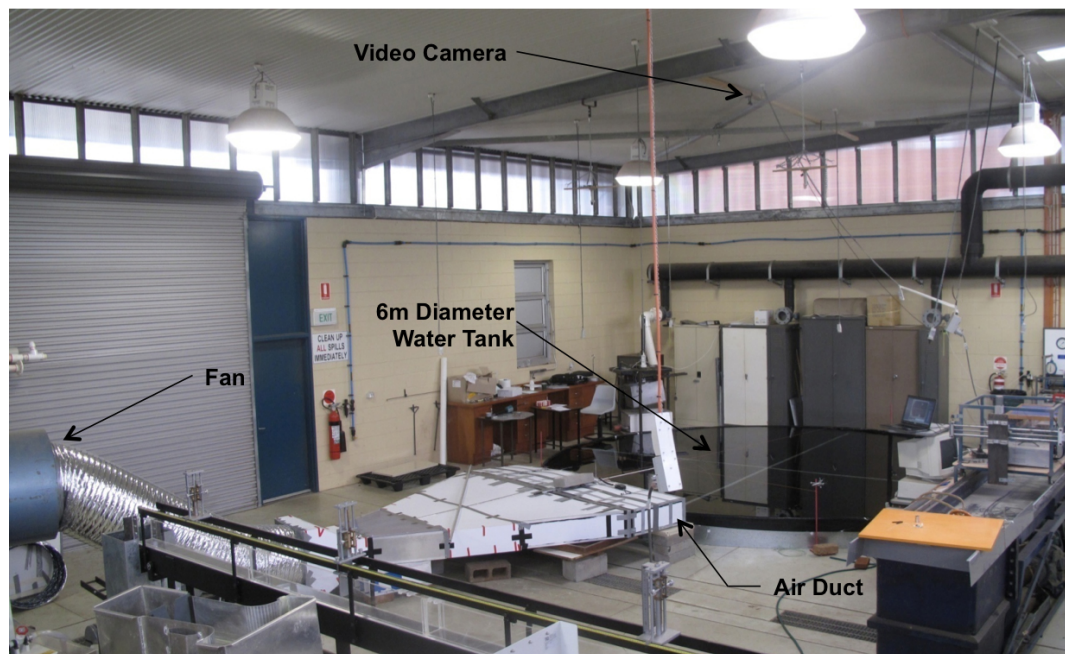


Figure 6.3: Experimental set-up in the laboratory.

6.3.2 Monolayer material and application

A C18OH and Brij78 in water-emulsion the same as that described in Chapter 5.4.1 was used in all tests. The monolayer water-emulsion was applied at a continuous rate during all tests with an Aqua 24v DC peristaltic pump PER-RS 01-03. Monolayer was applied at a continuous rate for all tests, as this is representative of what is required in the field under wind conditions >3.2 km/h in order to maintain monolayer coverage

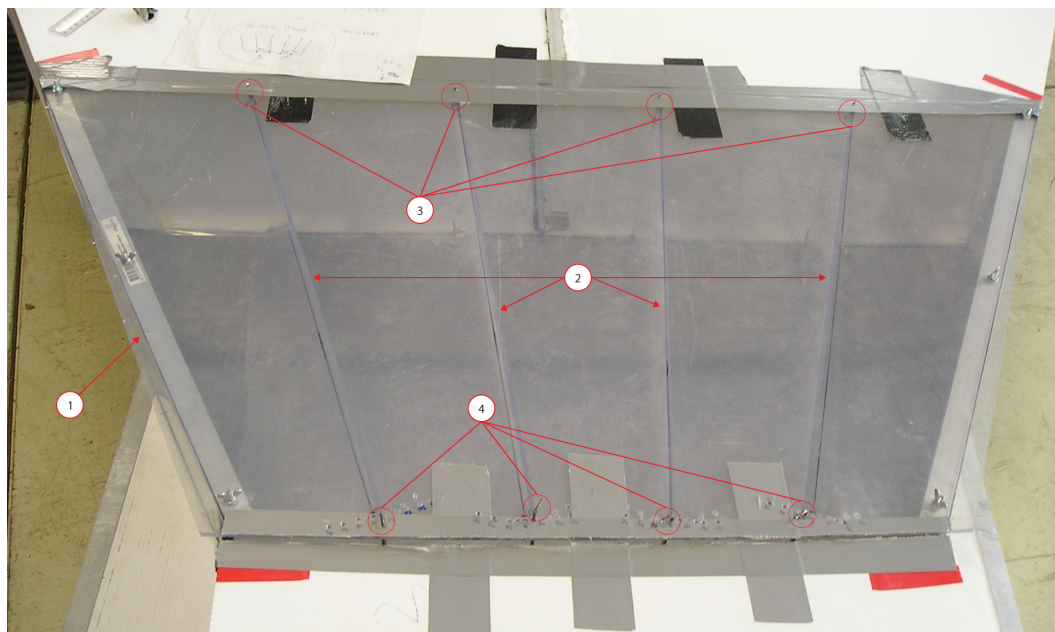


Figure 6.4: Adjustable wind vane apparatus allowing control over the direction of air flow to evenly fill the volume of the expansion chamber. This apparatus was necessary in producing a uniform wind velocity profile at the outlet.

(Vines 1962, McArthur 1962, Crow 1963, Frenkiel 1965, Reiser 1969, Crow & Mitchell 1975). The peristaltic pump allowed the application rate to easily be changed with voltage. The voltage was regulated and adjusted with a GW Instek laboratory DC power supply. To assess the effect of application rates on drift rate and spreading angle, the following application rates were used for each wind speed: $8v = 16.8$ mL/min, $12v = 24.5$ mL/min, $19v = 41.5$ mL/min and $24v = 51.3$ mL/min. The outlet tube from the peristaltic pump was suspended in place at the water/air interface to ensure minimal product loss into the bulk.

6.3.3 Water surface cleaning process

Before each test the water surface was thoroughly cleaned of impurities and residual monolayer by overflowing the tank. The water surface was also repeatedly scraped to the overflowing edge of the tank with a 5 m long 90 mm diameter polyethylene (PE) pipe. This cleaning process was usually continued for 45 minutes or until the water surface appeared clean. Before the cleaning process was stopped, a portion of the tank

water surface was sectioned off with the PE pipe and the interfacial surface pressure tested with calibrated indicator oils (as detailed in Section 5.4.3). If the water surface was measured to be <4 mN/m, the cleaning process was stopped. As the indicator oil were always used in a sectioned off portion of the tank, the oil was always contained and overflowed over the edge of the tank to remove it. Once the cleaning process was stopped the hose was removed from the tank and the water was left for 3 hours to settle, thereby reducing the influence of drift currents set-up during the cleaning process.

6.3.4 Wind velocities and velocity profiles

All wind velocity measurements were made with a Comark KM 4007 thermistor probe with an accuracy of $\pm 3\%$. Four different wind velocities, 3.7, 4.5, 5.2 and 8.3 m/s were used for determining the dispersion angle of monolayer, however, only three were used to characterised monolayer drift velocity, 3.7, 5.2 and 8.3 m/s. All wind velocities were measured at a standard height of 0.1 m above the water surface and 1 m from the outlet of the middle of the duct. Velocity profiles were characterised for each wind velocity in both the vertical (z) and horizontal planes (x and y) above the water surface (without monolayer present). Vertical wind velocity measurements were made at distances of 1 m and 3 m from the outlet of the expansion chamber. At each 1 m and 3 m location the vertical profile included 10 individual wind velocity measurements. Vertical velocity profiles are shown in Figure 6.5.

Horizontal wind velocity measurements were made by hand at approximately 20 mm above the water surface (without monolayer) at 88 individual locations marked out by a grid temporarily strung across the water surface. The temporary grid spanned 2.5 m (x -plane) by 4.5 m (y -plane). Temporary grid marker string was placed 0.25 and 0.5 m apart in the x and y planes respectively. Wind velocity measurements were made at the intersections of the strings. After analysis of the horizontal wind velocity profiles a workable wind area was designated where the wind velocity did not differ more than 30% in both the x and y directions. The designated workable wind area started 1 m from the face of the duct outlet, measured 2 m in width and extended 4 m downwind. The averaged horizontal wind velocity profiles for the designated workable wind area is shown for the four-test wind velocities in Figure 6.6.

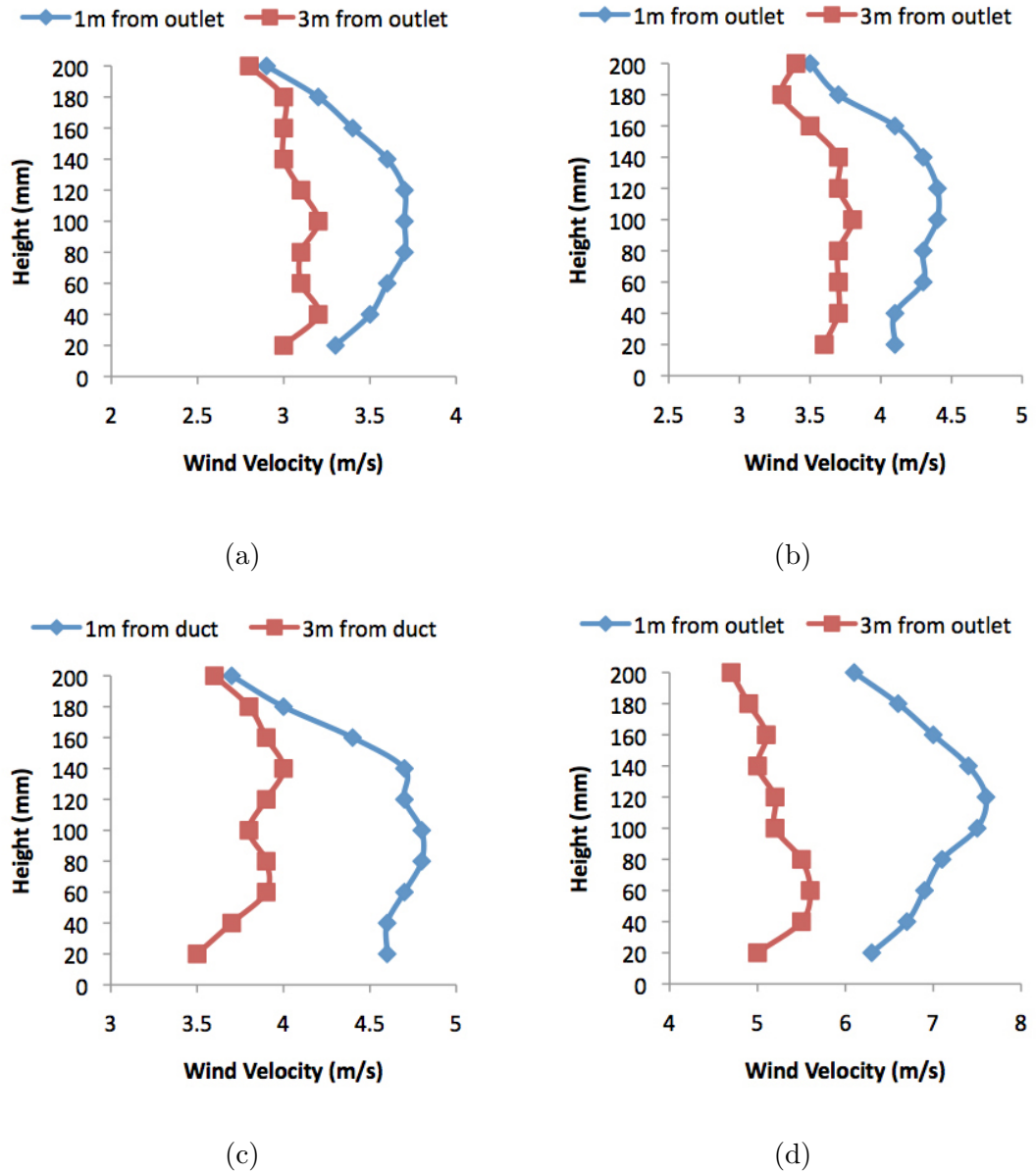


Figure 6.5: Vertical velocity profiles measured at 20 mm intervals above the water surface for 1 m and 3m distances from the middle of the outlet of the duct: (a) velocity profile for 3.8 m/s wind velocity; (b) velocity profile for 4.5 m/s wind velocity; (c) velocity profile for 5.2 m/s wind velocity; (d) velocity profile for 8.3 m/s wind velocity.

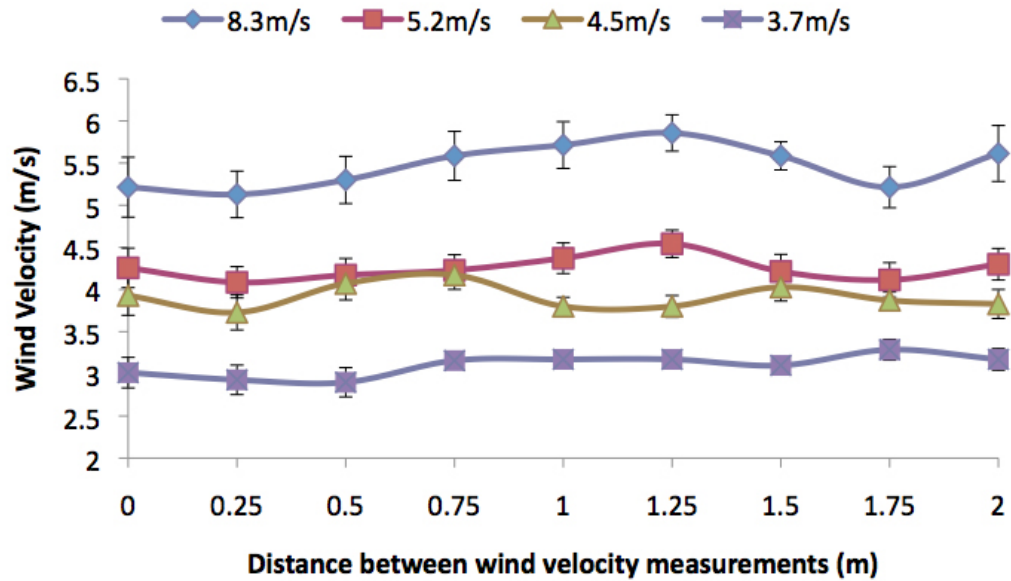


Figure 6.6: The average of the horizontal wind velocity profiles (i.e. the average of all 88 individual wind velocities measured in the x and y direction) for the four test wind velocities of: 3.7, 4.5, 5.2 and 8.3 m/s. Error bars represent the standard deviation of 7 individual measurements for each point.

6.3.5 Drift velocity tests

Although the drift rate of monolayer was initially characterised using both paper disks (5 mm diameter) and polyethylene spheres (7 mm diameter), the polystyrene spheres proved easier to detect on the water surface, making them more reliable especially with wave formation at the higher wind velocities. In addition, according to Wright & Keller (1971), neither float size nor shape (other than float depth) effects drift velocity. As there is a dependence on float depth, an analysis of the float depth was conducted. The polyethylene spheres were found to float with approximately 50% below the water and 50% above (Figure 6.7). Therefore, the centroid of the submerged portion of the sphere would be at a depth of approximately 1.75 mm below the water surface.

In two previous studies by Wu (1975) and Wright & Keller (1971) the surface drift velocity of pure water was characterised using drift indicators (floats) that float at different depths from 0.2 to 3.2 mm below the water surface (measured at the centroid of the submerged portion of the float). Both researchers found that drift velocity decreases



Figure 6.7: The float depth of a 7 mm diameter polyethylene sphere, which were used as an indicator for the drift velocity of the water surface. The centroid of the submerged portion of the sphere was estimated to be 1.75 mm below the water surface.

almost linearly with depth below the water surface. Although the drift velocity in this study was only measured with one size float with a centroid depth below the water of 1.75 mm, the difference in drift velocity at this depth and those reported by Wu and Keller & Wright for the surface (centroid depth = 0) would be expected to be on average $0.043(\pm 0.025)$ m/s slower. However, as monolayer was continuously applied during this study, and not in Wu and Keller & Wright's, it would be expected that the deficit in the drift velocity measured would be compensated for by the added velocity caused by the spreading force of the monolayer.

To account for the drift velocity error attributed to the added force exerted by the wind on the portion of the polystyrene sphere floating approximately 3 mm above the water surface, the following analysis was conducted. A boundary layer based on the wind velocity profiles at 3 m from the duct (Figure 6.5) was defined for the best case (fully laminar boundary layer) and worst case (fully turbulent boundary layer). The boundary layer thickness was estimated based on the length Reynolds number and the freestream velocity at 3 m. For the laminar boundary layer, the sinusoidal boundary layer velocity profile was used, while the 1/7 boundary layer velocity profile was used for the turbulent boundary layer: these were used to estimate the wind speed at 3 mm above the surface. From this wind speed, the diameter-Reynolds number for a sphere was calculated to determine the drag coefficient. The drag coefficient for water was also calculated, based on the drift speed in Figure 6.11. Setting the drag force from the air to be equal to that for water, the error in drift velocity can be determined. For the 3.7 m/s wind case, the error for a fully turbulent boundary layer was 51%, while for a fully laminar boundary layer it was 21%; for the 8 m/s wind case, the corresponding errors were 28% and 14%. Note that for the 3.7 m/s case, the boundary layer is most likely to be close to fully laminar (approx 25% error); for 8 m/s, the boundary layer should be turbulent, but accounting for the short distance that it is turbulent, the error should be less than for the 3.7 m/s case.

During testing, monolayer was continuously applied as the polystyrene spheres were gently placed on the water surface (spaced about a metre apart) by hand at the upwind side of the tank and allowed to drift downwind. Drift velocity tests were also run for each wind speed without applying monolayer to determine the drift velocity of pure

water. All tests were recorded with a Logitech Webcam Pro 9000 digital camera mounted above the water tank. Four replicate measurements of drift velocity were made for each wind velocity and application rate. Only measurements of drift velocity within the designated workable wind area were included. Distance measurements were made by taking a float position near the upwind end (near the start of the workable wind area) and then a position at the downwind side (near the end of the workable area) and measuring between these two positions. The time for the distance travelled by the float was measured by dividing the number of video frames between the two float positions by the frame rate of the digital camera. All measurements of distance and time were taken from digital recordings analysed using Adobe Flash software.

6.3.6 Spreading angle tests

Due to a decrease in water surface tension by application of the monolayer (Barnes 2008), a defined wave calming effect was observed between the covered (monolayer) and uncovered (no monolayer) water surface. This effect was easily definable for all of the wind velocities, except for the lowest, 3.7 m/s, because at this wind velocity there was too little contrast between the waves on the covered and uncovered surface. To overcome this, small amounts of talcum powder were applied during these tests to aid in detecting the edges between covered and uncovered surface.

For all tests the fan was turned on first and allowed to reach the predetermined test wind velocity before the continuous application of monolayer was started. Once monolayer application was started it would take between 20-50 seconds, depending on the wind speed and application rate, for the dispersion angles to steady (i.e. the equilibrium spreading angle). Once this equilibrium spreading angle was achieved, monolayer application was continued for at least 60 seconds. Figure 6.8 shows the evolution of a spreading angle test.

All tests were recorded with the same digital camera as described in Section 6.4.1 and analysed using Adobe Flash software to determine the equilibrium spreading angles. Angles were manually determined by fitting a line to each defined edge between calm and wavy water surface (Figure 6.9b). The fit of these lines was checked for a period

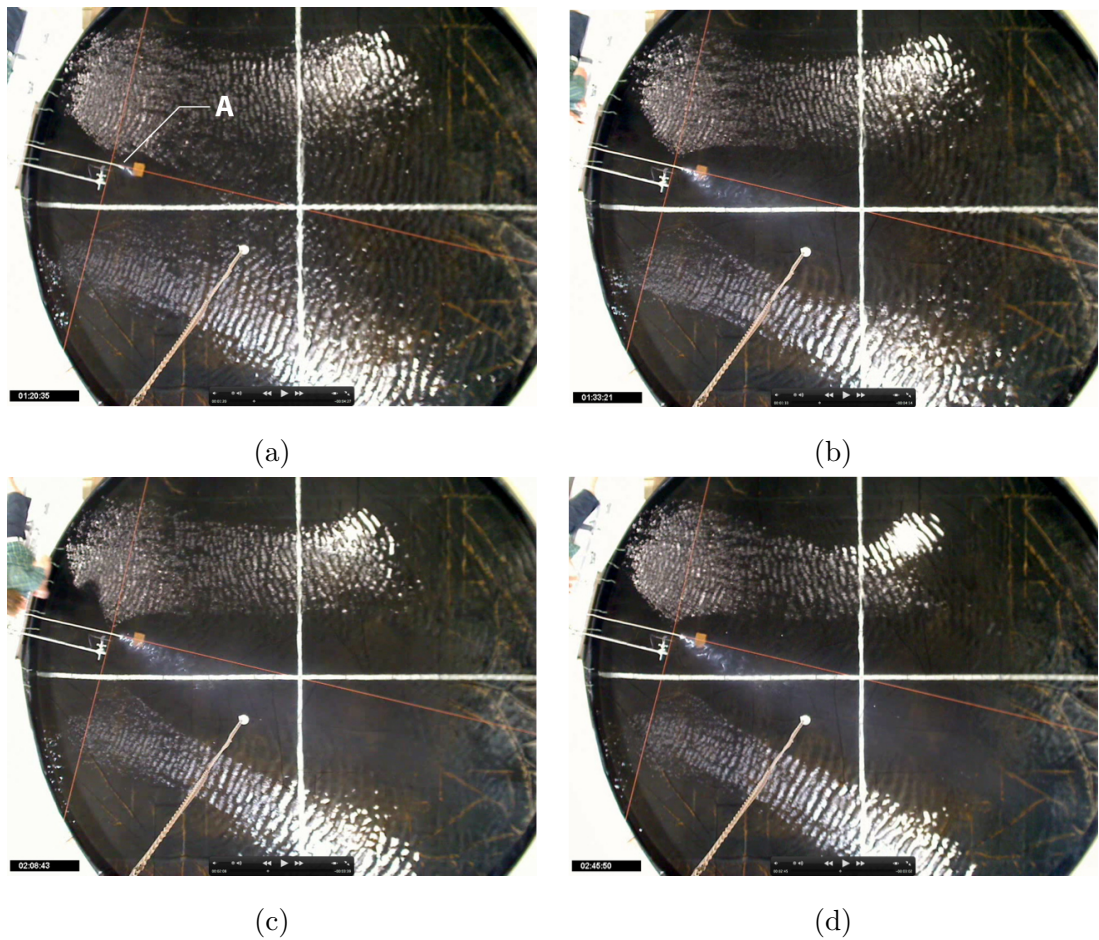


Figure 6.8: Snap shots from video showing the evolution of the spreading of monolayer continuously applied under a uniform imposed wind velocity of 4.5 m/s: (a) predetermined wind velocity has been reached and monolayer application has just begun at A; (b) monolayer is now spreading laterally and drifting down wind; (c) spreading angles have now equilibrated and measurement of the angle can begin; (d) the equilibrium spreading angle is maintained, even after almost 60 seconds.

of 60 seconds by stepping through the video (Figure 6.10c). These lines of best fit were only fitted to edges within the workable wind area (Figure 6.9a). A digital angle template was then positioned over the lines of best fit to determine the angle (Figure 6.10d).

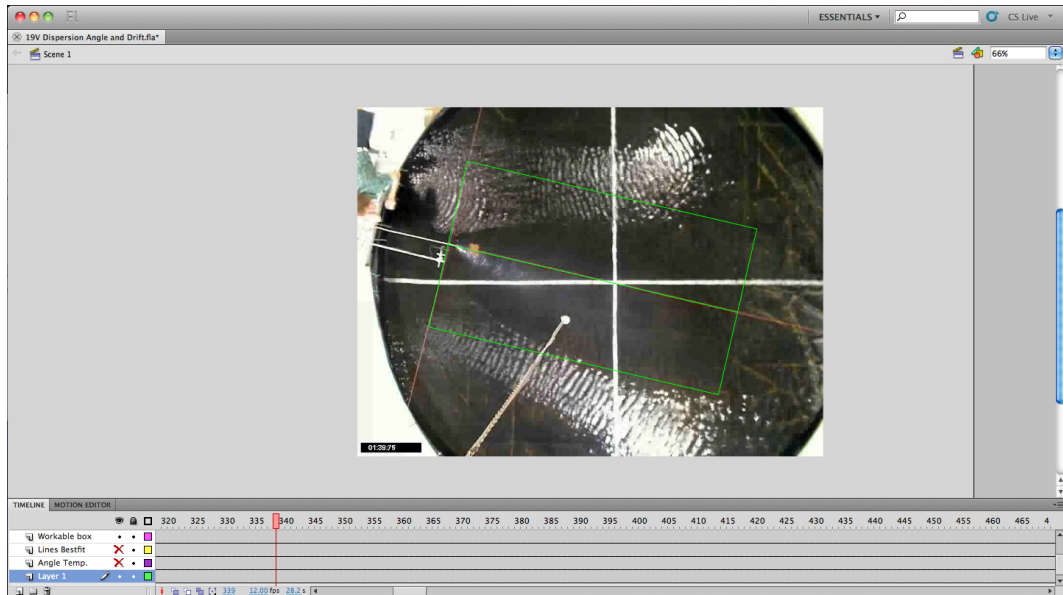
6.4 Results

6.4.1 Drift velocity

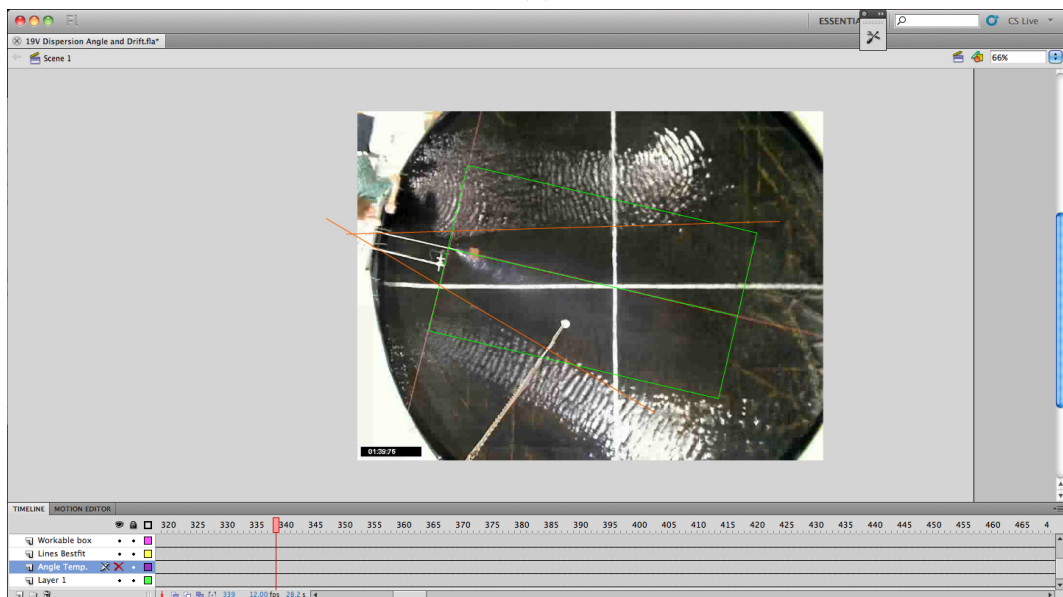
Drift velocity tests were conducted at three different reference wind velocities and Table 6.2 summarises the application rates used for each reference wind velocity. The results for these drift velocity tests are plotted as a function of application rate in Figure 6.11. As can be seen in Figure 6.11 the average of the standard deviations for the drift velocities measured for the different application rates at each reference wind velocity are less than 10% of the measured drift velocity. As the drift velocities were so minimally affected by application rate the drift velocities for all the different application rates at each reference wind speed were averaged. These averaged drift velocities will be referred to as the measured sphere velocity from now on.

Table 6.2: Summary of the drift velocity test application rates used for each reference wind velocity.

Reference Wind Velocity (m/s):	Application Rates (mL/min):
3.7	16.8, 41.5 and 51.3
5.2	16.8, 25.8, 41.5 and 51.3
8.3	25.8, 41.5 and 51.3

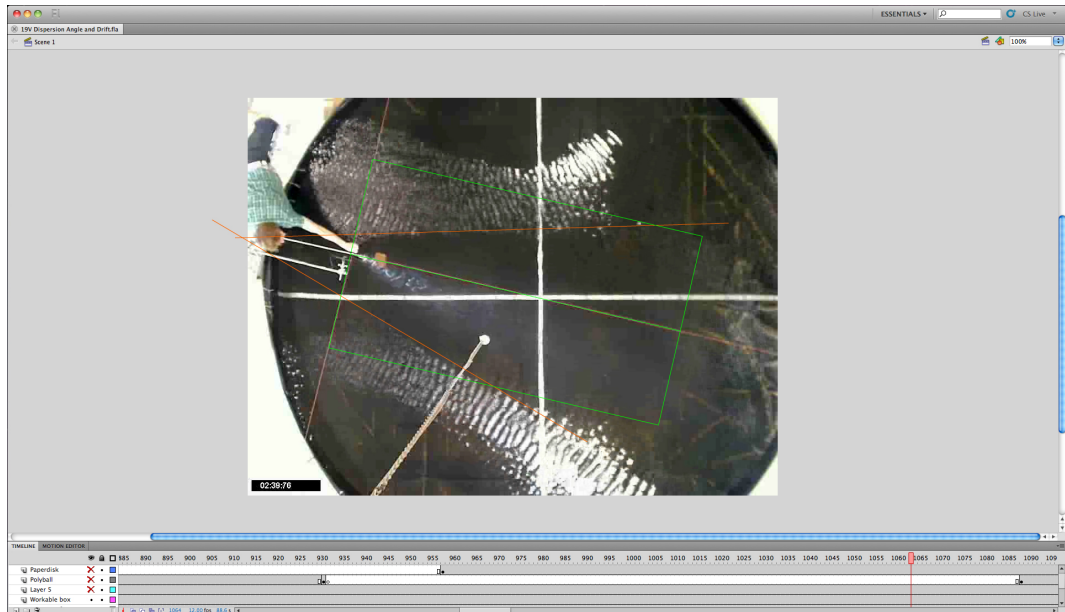


(a)

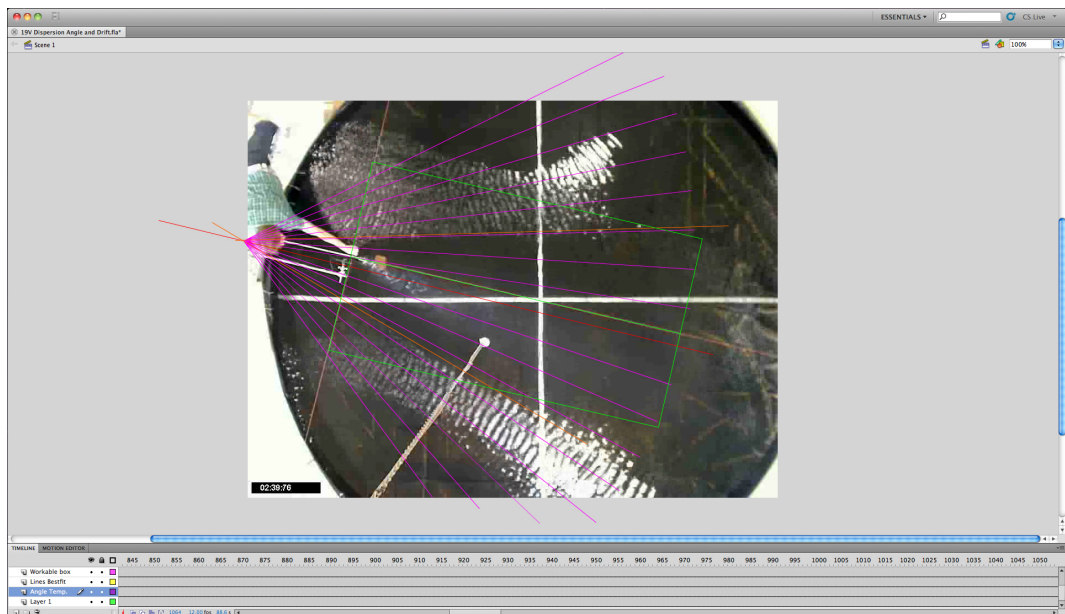


(b)

Figure 6.9: Video analysis process for determining the spreading angles of monolayer (Part 1): (a) a box representing the boundaries of the designated workable wind area is overlaid over the video; (b) a line of best fit is manually fitted to each defined edge between calm and wavy water surface by eye.



(c)



(d)

Figure 6.10: Video analysis process for determining the spreading angles of monolayer (Part 2): (c) the fit of the line is manually checked for at least 60 seconds of video; (d) an angle template is then fitted over the lines of best fit, by eye, to determine the spreading angle.

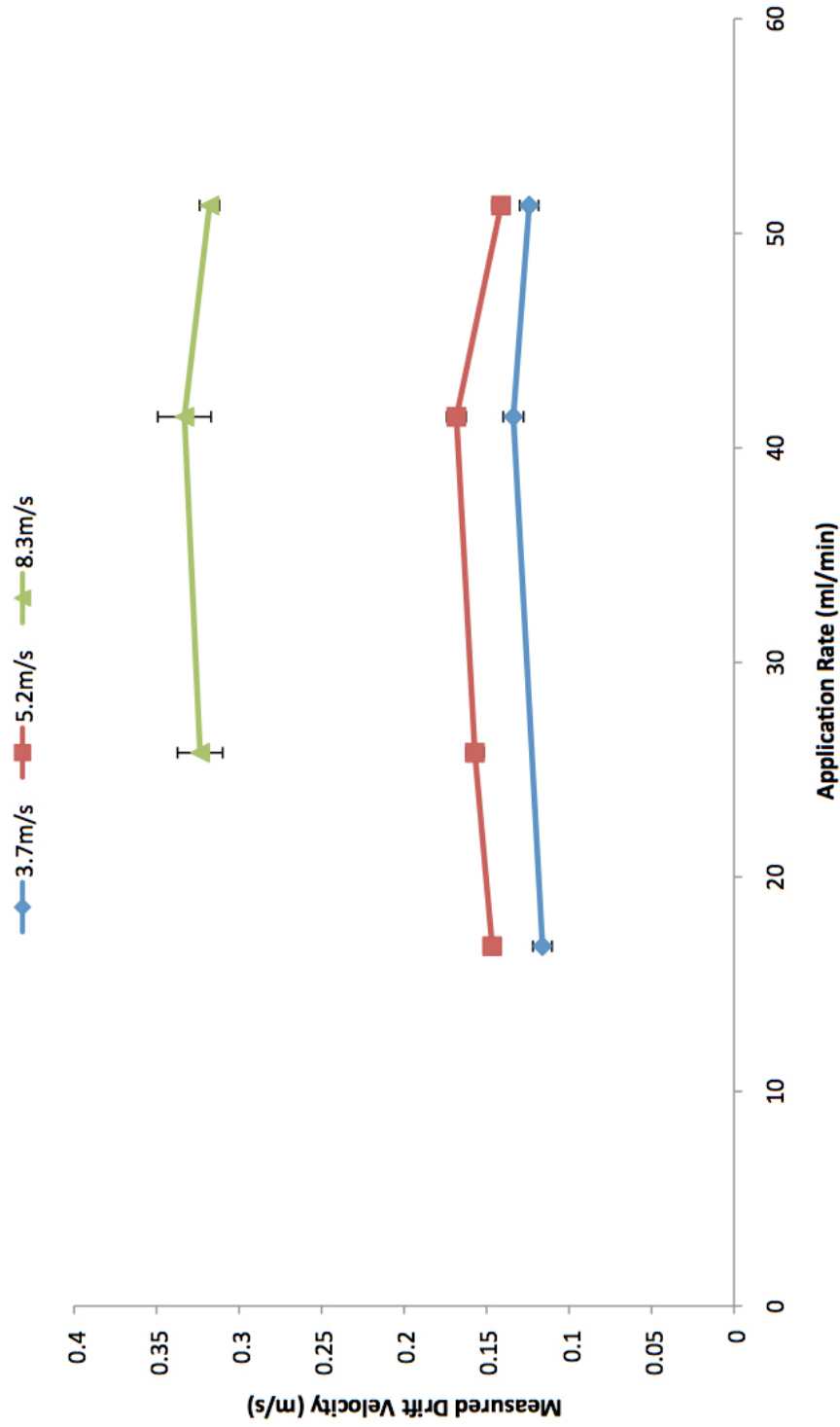


Figure 6.11: Comparison of the drift velocities at three reference wind velocities plotted as a function of application rate. Each point on the graph represents the average of four replicates. Error bars represent the standard deviation of the four replicates for each point.

The measured sphere velocity is shown in Figure 6.12 plotted as a function of the reference wind speed. Also shown in Figure 6.12 is the measured sphere velocity without the presence or application of any monolayer. As monolayer was continuously applied the measured sphere velocity would not only be a result of the wind shear and Stokes transport, but also due to the spreading force of the monolayer (to an unknown degree). As indicated by the results in Chapter 5, the spreading rate of the monolayer (and therefore the impact of the spreading force) would be diminishing over time.

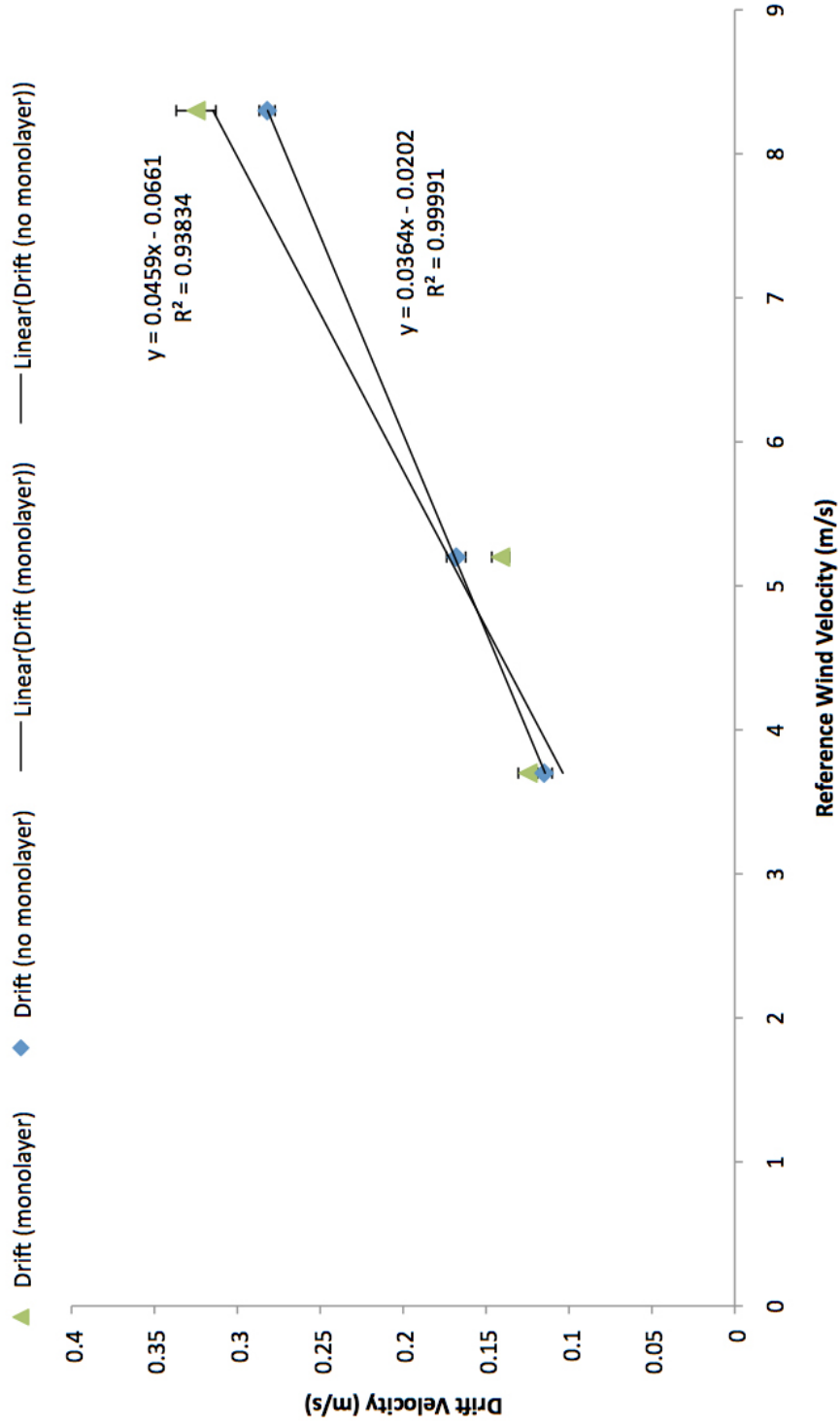


Figure 6.12: Comparison of measured sphere velocity with continuous application of monolayer, and without the presence or application of monolayer, plotted as a function of the reference wind velocity.

6.4.2 Spreading angle

When monolayer is continuously applied under wind stress, initially it starts to spread in an elliptical teardrop pattern (Figure 6.8a) that grows greater in size parallel to the wind direction than it does perpendicularly. This growth continues until the edges (between clean water and monolayer) of the teardrop normal to the wind direction start to flatten to form two edges that splay diagonally outwards across the wind. This behaviour then continues until the diagonal edges of what now is a wedge shaped spreading pattern start to stabilise at a certain angle. The angle of these diagonal edges then seem to remain fairly stable, in what appears to be a relative state of equilibrium (i.e. force balance). A series of still images, from the digital video, depicting the growth stages of the monolayer spreading pattern under wind stress is provided in Figure 6.13.

In each test the angle at which these diagonal lines splayed outwards apart from each other appeared to be a function of the wind velocity. The angle is decreased by higher wind velocities and increased by lower wind velocities. This *spreading angle*, as it will be referred to from here on, was characterised at four different wind velocities and at least three different application rates for each wind velocity. Spreading angle tests were conducted at four different reference wind velocities and Table 6.3 summarises the application rates used for each reference wind velocity. The results for each of these spreading angle tests were plotted as a function of application rate and are shown in Figure 6.14.

Table 6.3: Summary of the spread angle test application rates used for each reference wind velocity.

Reference Wind Velocity (m/s):	Application Rates (mL/min):
3.7	16.8, 41.5 and 51.3
4.5	16.8, 24.5, 41.5 and 51.3
5.2	25.8, 41.5 and 51.3
8.3	16.8, 25.8, 41.5 and 51.3

As there appeared to be little if any influence of application rate on the spreading angles, the average of all the spreading angles at each wind velocity were taken and used from here on. These averaged spread angles were then plotted as a function of

reference wind velocity and are shown in Figure 6.15. As is also shown in Figure 6.15, the spreading angles appeared to follow a power law, therefore a trend line of this form was fitted to the data with an agreement of $R^2 = 0.987$. The equation for this trend line is also shown in Figure 6.15.

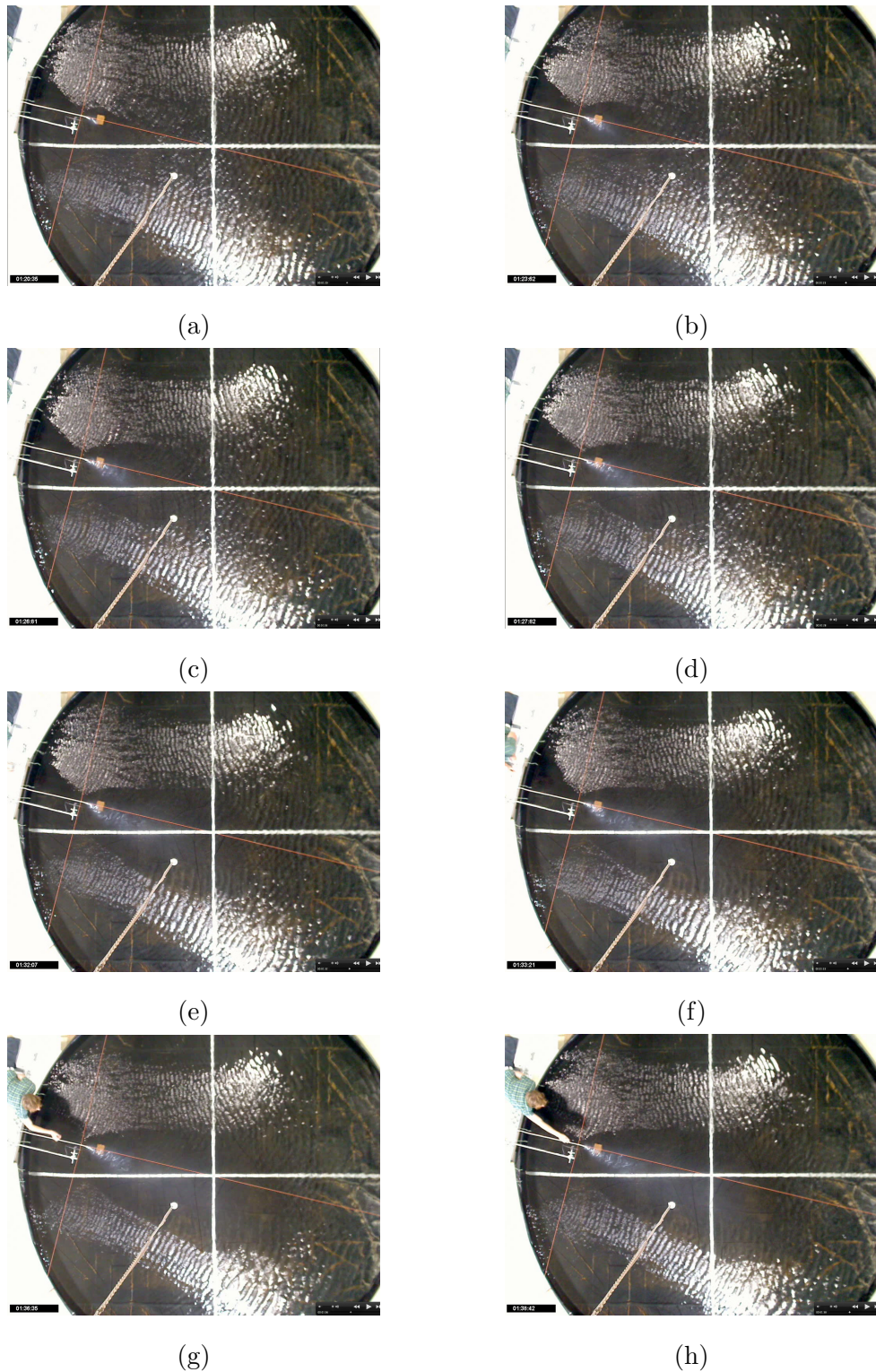


Figure 6.13: Series of still images depicting the growth stages of the monolayer spreading pattern under wind stress: (a) spread pattern about 1 second after application was initiated; (b) after 4 seconds; (c) after 7 seconds; (d) after 9 seconds; (e) after 13 seconds; (f) after 14 seconds; (g) after 17 seconds; (h) after 20 seconds.

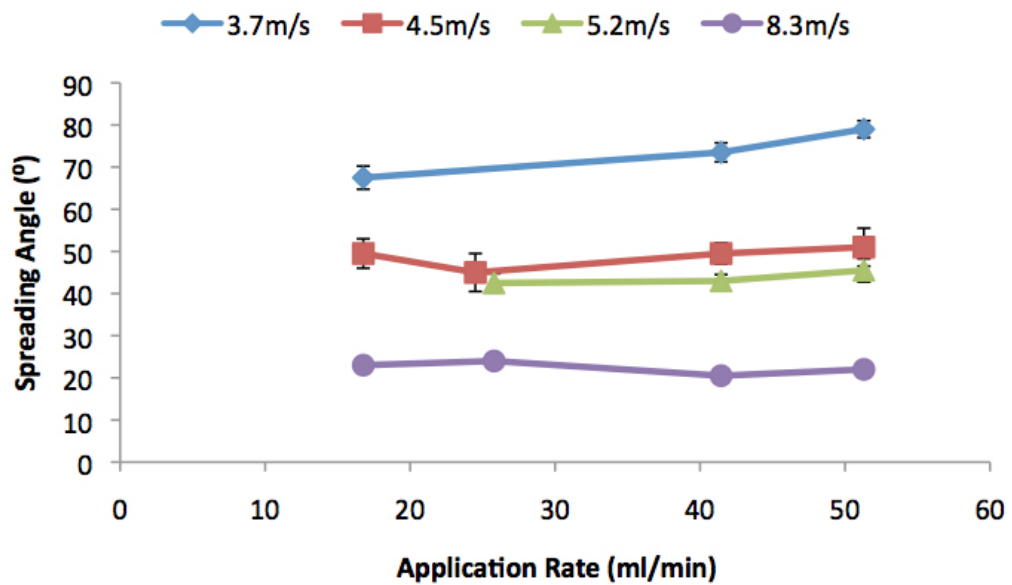


Figure 6.14: Relationship between spreading angle and application rate at the four reference wind velocities. Error bars represent the standard deviation of the angle measurement for each test.

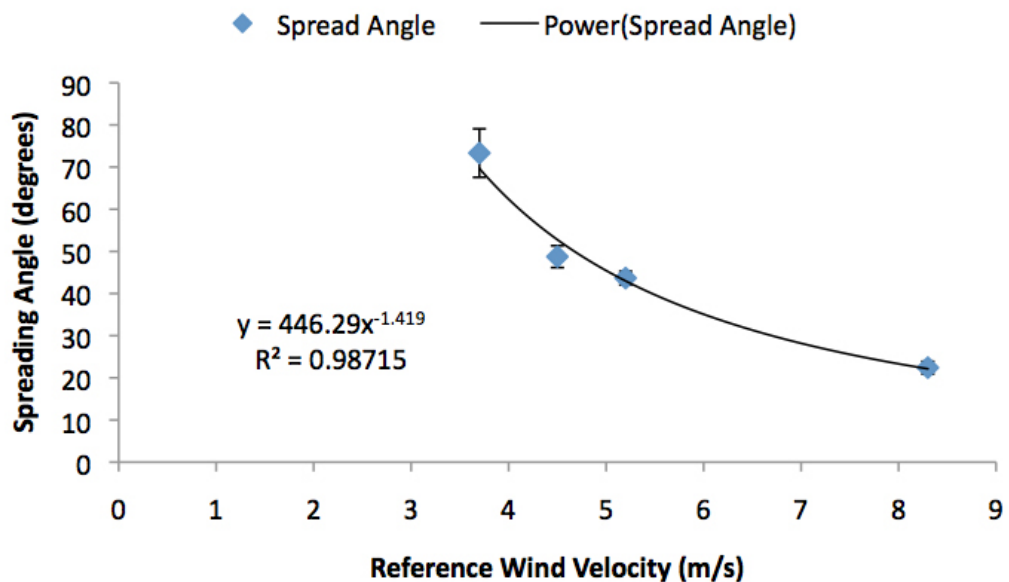


Figure 6.15: Relationship between spreading angle and reference wind velocity.

6.5 Analysis

6.5.1 Relationship between drift velocity and wind velocity

The results for drift velocity of monolayer applied continuously (Figure 6.12) appear to more closely follow an exponentially increasing trend rather than the linearly increasing trend as suggested by Lange & Huhnerfuss (1978) and Hale & Mitchell (1997). However, with only three data points, even though each data point represents at least 12 replicate measurements, it is impossible to conclude that the drift rate follows an exponentially increasing trend. Therefore, as suggested by other researchers observations, a linear trend line was fitted to the data for both monolayer covered water and clean water (Figure 6.12). The equations for both lines and the R^2 for the fit of the line to empirical data are also shown in Figure 6.12.

When drift velocity for a monolayer covered surface and a clean water surface is calculated using their respective equations for the lines of best fit and the results are divided by the reference wind velocity to derive a ratio of u_s/u_w , both data sets follow an increasing trend tending to a constant (Figure 6.16). This trend is consistent with Wu (1968) for clean water surface and, the trend for the monolayer covered water surface is consistent with Fitzgerald (1964).

The results in Figure 6.16 indicate that at a wind velocity of 3.7 m/s the drift velocity is relatively similar for both monolayer and no monolayer covered water surfaces. Then at a wind velocity of 5.2 m/s, the monolayer covered water surface appears to drifting faster than the clean water surface. At wind velocities of about 8 m/s, the clean water and monolayer covered water surfaces appear to be tending towards a constant of about 3.4% and 3.8% of the reference wind velocity respectively.

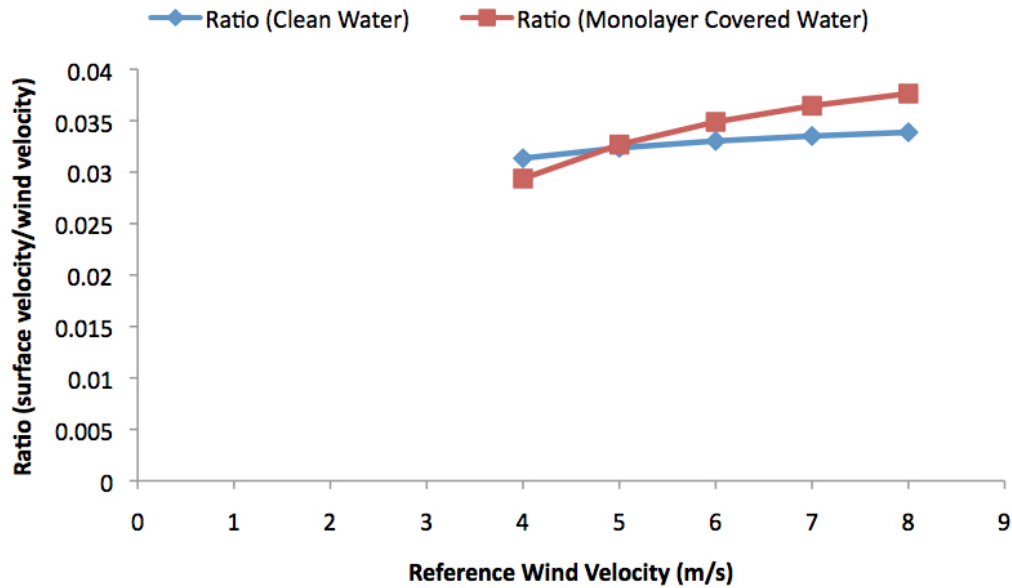


Figure 6.16: Comparison of measured sphere velocity with continuous application of monolayer and without the presence or application of monolayer plotted as a function of the reference wind velocity.

6.5.2 Spreading angle and empirical relationship

When a monolayer is continuously applied under wind stress after a period of time, depending on the wind velocity, the monolayer appears to create a wedge shaped spreading pattern (Figures 6.8 and 6.13). Although the monolayer spreading force, S , is omnidirectional, and has been shown to spread radially without wind stress (Section 5.5), when sufficient wind stress is applied the resistance of S is overcome so that it forms a wedge shape (i.e. circular segment). The edge of this wedge can be predicted by taking the resultant or net force, F_{net} , of the wind shear force, τ_u , and the net spreading force, S_{net} , acting on the edge of the wedge (Figure 6.17).

The relationship between the spreading angle and the wind stress has been characterised (Figure 6.15). However, the equation for the trend line shown in Figure 6.15, would only hold true for a monolayer material that exerted the same S as that used in this study. S for the C18OH and Brij78 in water-emulsion (used in this study) was measured to be 14 mN/m (Section 5.4.2 of Chapter 5). In order to relate the effect of spreading force on drift velocity and spreading angle, the spreading kinetics formula (Equation 5.1) of

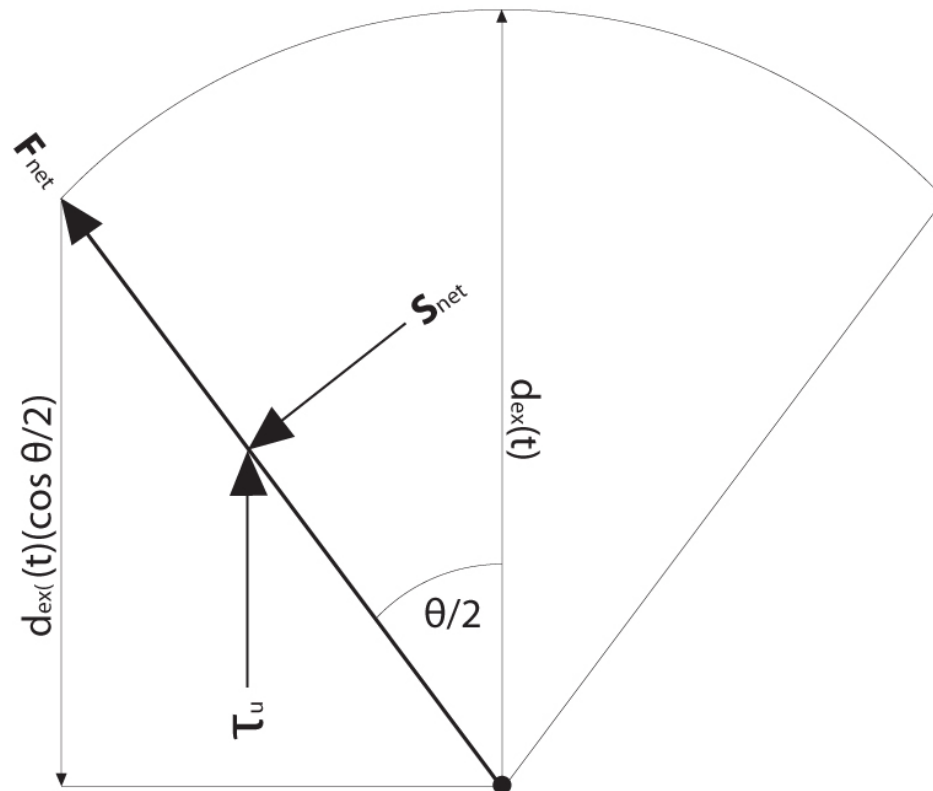


Figure 6.17: Diagram of the wedge (i.e. circular segment) shaped spread pattern of monolayer under wind stress. The length of the edge of the wedge is calculated from the drift rate measured in Section 6.4.1, and denoted as, $d_{ex}(t)$. Also shown is the resultant or net force, F_{net} , of the wind shear force, τ_u , and the net spreading force, S_{net} , acting on the edge of the wedge, thereby creating the internal angle of the half-wedge ($\theta/2$).

Dussaud & Troian (1997) was used: this formula has been experimentally validated for zero-wind conditions for the C18OH and Brij78 in water-emulsion (Section 5.5), and provides the monolayer spread distance at any point in time, $d(t)$. Empirical values for K and n in this instance were taken as 1.167 and 0.736 respectively, as calculated for monolayer applied at 6x dosage in the 6 m diameter tank (Table 5.2 in Section 5.5).

Without wind stress a monolayer molecule moves in a direction normal to the (subsequently considered) windward direction, however, when wind stress is sufficiently strong this molecule moves at an angle to the windward direction (i.e. in-line with the F_{net} shown in Figure 6.17). Although the distance this molecule travels in the windward direction is proportional to the theoretical $d(t)$ for quiescent conditions, it was found to scale by the product of an empirical constant, C , of 0.45 and the wind velocity U :

$$d_{ex}(t)\cos\frac{\theta}{2} = CUd(t) \quad (6.1)$$

from which:

$$\theta = 2\cos^{-1}\left(\frac{d_{ex}(t)}{d(t)}CU\right) \quad (6.2)$$

C was calculated by taking the ratio of $d_{ex}(t)$ and $d(t) \times (\cos\frac{\theta}{2})$ for all replicates at the three different reference wind velocities, 3.7, 5.2 and 8.3 m/s. Each ratio was then divided by its corresponding wind velocity. The resulting values were then averaged to derive the empirical constant 0.45 ± 0.014 .

6.6 Discussion

Although Fitzgerald (1964) related surface velocity to the surface concentration of the monolayer added, in this study no dependence of surface velocity to surface concentration could be detected (Figure 6.11). This is most likely due to the fact that in this study, monolayer was being overdosed at all times (i.e. surface concentration of monolayer was at a maximum for all application rates). Therefore, this leads to the general

conclusion that when monolayer is overdosed (exceeding the minimum amount to reach equilibrium surface pressure) at a continuous rate, surface velocity is not dependent on dosage volume.

The higher surface drift velocity of monolayer covered water for wind velocities >5.2 m/s, in this study, would suggest that the dynamics of air flow near the water surface is markedly different to that for a clean water surface, mainly due to the wave damping effect of the monolayer (Wu 1971*b*). One explanation is that a more laminar flow regime may be created by a water surface damped by monolayer, therefore increasing the wind drag coefficient. Another possible explanation may be that a wavy water surface (i.e. no monolayer present) creates zones of high and low pressure between the waves, which can act to pull the water surface backwards in the opposite direction of the air flow (Jeffreys 1925). This would effectively decrease the surface drift velocity of clean water.

Monolayer spread under wind stress was found to initially create a teardrop shape whose sides soon flattened after a period of time, depending on the wind velocity, to create a wedge shaped spread pattern. This wedge pattern would then be maintained for at least one minute. The edges of the wedge were easily detectable due to the wave damping provided by the monolayer. The internal angle of the wedge were measured and plotted as a function of wind velocity. The internal angle of the wedge was found to follow a power law, which decreased with increasing wind speed. Therefore, internal angle of the wedge is a result of a force equilibrium between the lateral force of the monolayer spreading outwards and the linear force of the wind opposing the lateral spread.

An empirical relationship was derived between the drift velocity and the spreading angle results in this study, using the widely accepted spreading kinetics formula (Equation 5.1). For this relation an empirical constant (C) of 0.45 was selected and used to determine the empirical relationship, Equation 6.2, shown in Section 6.5.2. It is the author's belief that equation 6.2 would hold true for similar monolayer materials to C18OH (i.e. non-volatile, immiscible in water and spread rapidly upon the water surface) for the range of wind velocities used in this study. Therefore, either the $d(t)$ or $d_{ex}(t)$ or θ could be determined using equation 6.2 as long as two of either one of the three parameters, $d(t)$ or $d_{ex}(t)$ or θ , were known.

6.7 Conclusions

In this study, the drift velocity and spreading angle of monolayer continuously applied under wind stress was characterised.

The ratio of surface drift velocity (u_s) and wind velocity (u_w) for a monolayer covered water surface appeared to follow an increasing trend from 0.03 at 4 m/s, tending towards a constant of 0.038 at 8 m/s. Although this trend was found to be the same for a clean water surface (i.e. no monolayer present), the ratio for clean water increased from 0.031 at 4 m/s and tended towards a constant of 0.034 at 8 m/s. Therefore, for wind velocities >5.2 m/s, the ratio of u_s/u_w for the monolayer covered water surface exceeds that for clean water. This increase in surface velocity for a monolayer covered water surface, at wind velocities >5.2 m/s, was attributed to the alteration of the flow dynamics near the water surface due to the wave damping effect provided by the monolayer. The author hypothesises that this may be due to:

- i. a more laminar flow regime being created by a water surface damped by monolayer, therefore increasing the wind drag coefficient; and/or
- ii. a wavy water surface (i.e. no monolayer present) creating zones of high and low pressure between the waves, which is pulling the water surface backwards in the opposite direction of the air flow, effectively decreasing the surface drift velocity of clean water.

Furthermore, an empirical relationship was derived between the drift velocity and the spreading angle results in this study. With this equation it would be possible to predict the spreading angle of other monolayer materials as long as the spreading velocity (without wind stress) and drift velocity (with wind stress) was known.

Chapter 7

Monolayer Simulation Platform

7.1 Introduction

Before the decision was made to develop a customised monolayer simulation platform, a brief review and investigation of currently available oil dispersion models was undertaken. This research has shown that the monolayer simulation platform requirements were not able to be satisfied by the reviewed oil dispersion models for the use of a monolayer on a farm dam with respect to:

- spreading rate,
- wind driven transport,
- coverage area and coverage pattern, and
- application rate calculation.

This chapter sets out to develop models that address the above requirements by first describing the mechanisms for oil dispersion.

7.1.1 Spreading rate

Oil dispersion models are designed for modelling the spread of very large volumes of oil (i.e. barrels of oil and each barrel contains 0.159 m^3 or 159 L of oil) spilled by tankers, offshore platforms, drilling rigs, wells and the like. The oil spreading situation is mostly governed by a very different set of physical phenomena compared to that for monolayer materials, such as C18OH. According to Foda & Cox (1980), Camp & Berg (1987) and Chebbi (2001), the spreading of a large volume of oil is initially driven by gravitational forces and resisted by inertial forces. As time elapses, viscous drag due to the substrate replaces inertia as the opposing force. Then in the terminal stages of spreading, when the oil layer is very thin (possibly molecularly thin), surface tension replaces gravity as the driving force. The spreading process for monolayer materials, on the other hand, is largely governed by surface tension forces due to the small volumes of material required to produce a molecularly thick¹ surface film. (Camp & Berg 1987, Fay 1969, Berg 2009).

7.1.2 Wind-driven transport

According to Lehr et al. (1984) and Chao et al. (2001), most oil dispersion models currently employ the wind-driven drift ratio of 3% for surface drift velocity divided by wind velocity. However, this is an underestimation of monolayer drift rate according to literature reviewed (Section 2.5.2) and the empirical studies conducted in this present work (Section 6.5.1). The average of all values for the ratio of surface drift velocity divided by wind velocity presented by researchers is 3.5% and the ratio determined in the author's own empirical studies was found to increase from 3-3.8% as wind speed increases.

The difference in the ratio of surface drift velocity divided by wind velocity between oils and monolayer materials (suitable for evaporation mitigation) is most likely due to the differing properties of their surface chemistry. Oils vary in grade, viscosity and the chemicals within them (Bobra 1990, Fingas et al. 1995). According to Clark & Brown (1977), crude oil contains somewhere between 50 to 98% hydrocarbons with the rest

¹In this context, 'molecularly thin' refers to a surface film that is monomolecular (i.e. one molecule thick).

of the fraction containing organic compounds that provide the necessary surfactants that cause spreading. As oils are never pure, compared with a monolayer like C18OH for evaporation mitigation, their surface active molecules may pack on the surface in a more random disordered fashion, whereas a pure monolayer material will form an ordered densely packed surface film by virtue of their strong intermolecular Van der Waals attraction (Henry et al. 2010). The author speculates that a monolayer like C18OH may dampen wave action to a greater degree than oils, therefore alter the air flow dynamics across the water surface to a greater degree and hence the drift rate (Jeffreys 1925). Further information in regards to wave damping by monolayer and the resultant effect on wind-driven transport of monolayer is detailed in Section 6.5.

7.1.3 Coverage area and coverage pattern

Oil spill models normally calculate coverage area and coverage pattern through a random walk procedure where the initial spill area is divided into a grid of x and y coordinates which then diffuse randomly from their origin (Chao et al. 2001). The shape and track of each grid node from their origin is then calculated at every time-step based on the governing spread rate equation and wind-driven and current-driven transport equations. An in-depth review of the governing equations can be found in Chao et al. (2001). Typically, the evolution of oil coverage area and the coverage pattern is modelled over long periods of time (i.e. days).

For the modelling of monolayer coverage area and coverage pattern in the present work, the coverage areas and patterns were characterised in a series of empirical studies under varying levels of wind stress. Through this empirical work it was found that over short periods of time (i.e. minutes) when monolayer is applied continuously, monolayer spreads in a uniform pattern whose coverage pattern grows down-wind in a parallel direction to the wind. In addition, the tracking of monolayer coverage over hourly periods is more appropriate as application rate and origin of application would most likely change on an hourly time-step (based on averaged on-site wind conditions). Thus, modelling of monolayer coverage area and coverage pattern on lakes and dams would be far less random over short time periods compared to that for oil spills.

7.1.4 Application rate calculation

Continuous application is a requirement for the maintenance of a monolayer film on the water surface during periods of wind stress (Frenkiel 1965, Crow 1963, Reiser 1969). In addition, the application rate required under a particular wind condition is calculated according to the effective area to be covered based on the recommended application rate of the monolayer product, the spreading rate and wind-driven drift rate. Furthermore, this application rate will need to be varied according to the number of application points used, their location and the overlap of monolayer coverage area between application points (to avoid double-up of monolayer material). In contrast, oil dispersion models calculate oil coverage according to a finite amount of oil spilled as specified by the user before the simulation is initiated.

Considering the above information, the decision was made to develop a customised simulation platform around the unique needs and requirements for monolayer application on a lake or dam. Furthermore, the simulation platform could be calibrated with the empirical work conducted to characterise the spreading characteristics of monolayer under varying levels of wind stress.

7.2 Rationale, formulation and overview

As monolayer is so readily transported by wind automated re-application of monolayer is required to maintain surface cover in order to suppress evaporation (Frenkiel 1965, Crow 1963, Crow & Mitchell 1975, Reiser 1969). The more effective application systems incorporate many application points around and within the water storage (Section 2.6.2). As stated in Section 3.2.2, if the design principle of employing a series of applicators or application points strategically placed around and within a given waterbody is adopted, a number of issues are immediately raised: (i) how many applicators are needed, (ii) how far are they to be spaced apart, and (iii) how are they to be arranged on-site. In addition, the application strategies to be employed on-site (i.e. which applicators to apply from for a specific wind direction and the amount of monolayer each needs to apply for a specific wind speed) is another issue.

As noted during the formulation of the UDF, Chapter 3, resolving these issues is not so straight forward. The optimal number of applicators to be used, their spatial arrangement, and the application strategies to be employed will vary for every situation and will depend on the size, shape and orientation of the storage, the site's unique prevailing wind conditions and the user's requirements. Therefore, the approach was taken to develop a simple simulation platform that would allow the spatial distribution of monolayer to be predicted/estimated. Flexibility of the simulation platform would be a pre-requisite (i.e. the capability of different user inputs), to allow different user scenarios to be modelled. The effect of different site conditions and user requirements on system layout, applicator numbers and application rate could be rapidly conducted with a desktop simulation platform of this nature. Another benefit is that a tailored application system design (number of applicator types required and their on-site layout) could be determined before any physical hardware is built or installed at that particular site.

Central to the accuracy of the simulation platform in predicting/estimating the monolayer coverage under a range of different wind conditions, are algorithms describing the distribution characteristics of monolayer. The monolayer algorithms required for the model have been determined through a series of large-scale laboratory studies during this present research. The algorithms that have been derived from these laboratory studies are as follows:

- spreading rate and pattern of monolayer distribution under quiescent conditions (Section 5.2);
- spreading angle of monolayer as a function of wind speed (Section 6.4.1); and
- drift rate of monolayer as a function of wind speed (Section 6.4.2).

The basic inputs, outputs and simulation requirements of a simple simulation platform, as described above, are illustrated in Figure 7.1.

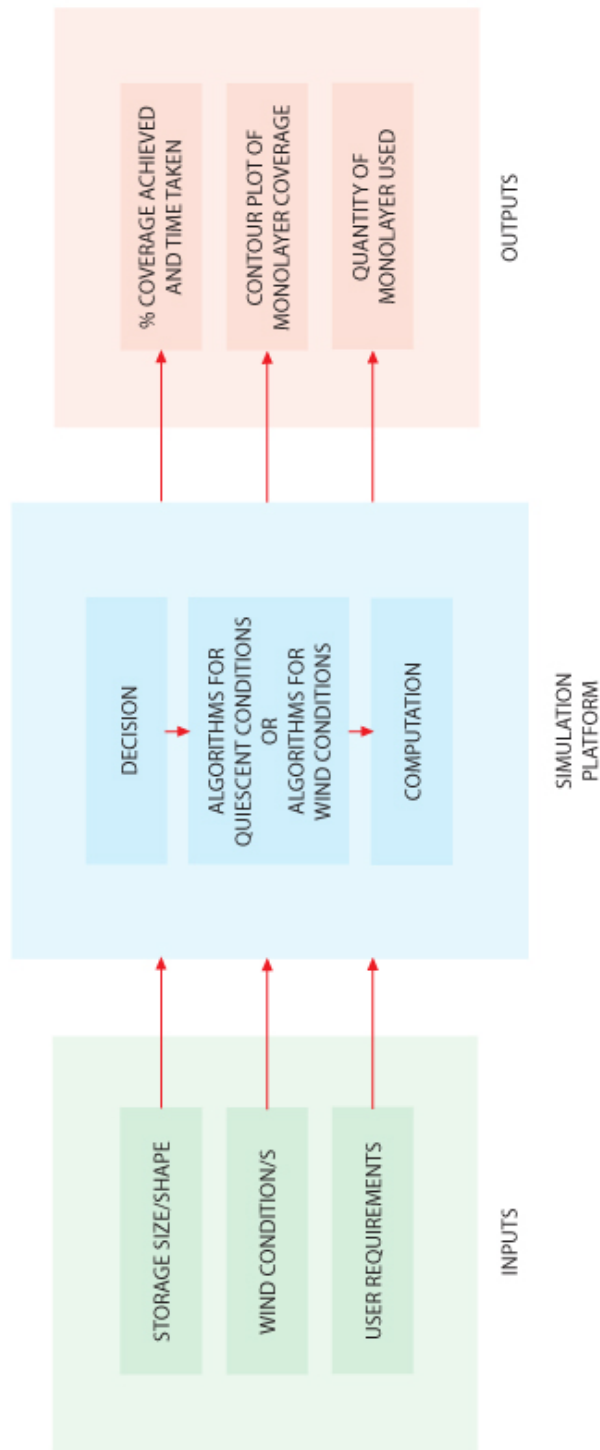


Figure 7.1: Illustrative overview of the basic model inputs, outputs and simulation requirements.

7.3 Simulation platform structure

The simulation platform was developed in MATLAB 7.10.0 as it has all the necessary functionality required, namely matrix manipulation, plotting of functions and data, and implementation of algorithms. The simulation platform developed is essentially a two-dimensional numerical model, which has been designed to operate in one of either two monolayer dosing states, non-continuous and continuous application. The decision of which state to operate in is based on user input wind speed (U). Non-continuous application is prescribed when U is less than or equal to the minimum wind speed threshold (U_{MIN}). Continuous application on the other hand, is prescribed when U is greater than the minimum wind speed threshold and less than or equal to the maximum wind speed threshold (U_{MAX}).

The reason the model has been set-up to operate in these two different dosing states is that many researchers report that wind-induced drift of a monolayer film starts to occur at wind speeds of $U_{MIN} = 3.2$ km/h (Vines 1962, McArthur 1962, Crow & Mitchell 1975). Below this wind speed the coverage rate of the water surface with monolayer will be dependent on the spreading rate of the monolayer (as detailed in Chapter 5). Whereas, at wind speeds >3.2 km/h the coverage rate of the water surface with monolayer will be assisted by wind-induced drift (as detailed in Chapter 6). Hence, the model has two different dosing states and the transition point between the two states is at a wind speed of 3.2 km/h.

Many researchers also indicate that the application of monolayer becomes impractical at a certain threshold wind speed (Fitzgerald 1964, Crow 1963, Walter 1963, Reiser 1969, Nicholaichuk 1978). Therefore, monolayer application should be stopped once that wind speed is reached. The average of all the threshold wind speed values sighted in literature to date is $26.4(\pm 5)$ km/h (refer to Section 2.5.2 for further detail). Hence, this application cut-off value has been used in the model (i.e. $U_{MAX} = 26.4$ km/h).

As the model operates in two different dosing states, the calculation of monolayer spatial distribution is very different for both. Therefore, the details of the distribution calculations are handled in a separate section for each. Although distribution of monolayer is calculated differently for each state, the fundamental aim of the modelling

process is the same, addressing the following:

1. selection of which applicators from which to best apply the monolayer,
2. quantify the monolayer surface coverage, and
3. the application rate.

The assumptions, inputs, distribution and application calculations made in the model, and the outputs from the model are then detailed.

7.3.1 Assumptions

The simulation platform makes the following major assumptions:

1. Wind speeds and wind directions specified by the user are considered constant by the simulation platform (i.e. wind increases, decreases or turbulence is not taken into account)².
2. Water surface temperature is even across the whole storage at a constant 20°C (i.e. a temperature greater than this would increase spread rate, whereas a lower temperature would decrease spread rate).
3. Water surface pressure at the start of monolayer application is always below 4 mN/m (i.e. surface pressures greater than this would impede the spreading ability of the monolayer).
4. All monolayer reaching the downwind shore is lost to beaching.
5. There is no volatilisation, submergence or biodegradation of the monolayer material.

²In particular it is acknowledged firstly that the upwind dam wall will cause an edge effect arising from different airflow conditions at the upwind waters edge, and that this may extend downwind for many metres (dependent on windspeed, wall height, slope of dam batter, and perhaps also other factors). And secondly it is acknowledged that turbulence in the airflow and its interaction with the water surface (causing wave generation) will normally change as the airflow extends over the water surface. The modeling of each of these phenomena is beyond the scope of this thesis.

6. There is no long-term residual surface drift or under-water currents set-up over the simulation period.
7. There is no residual surface coverage from the previous time-step (i.e. at every next time step monolayer surface coverage is reset to zero).
8. The model is calibrated with the surface transport characteristics for a C18OH in water-emulsion (this monolayer material is detailed in Chapter 4).

If a monolayer material with a different spreading force other than that exerted by the C18OH in water-emulsion used in this study, the spreading characteristics will most likely be different (Jensen 1995, Dussaud & Troian 1997, Tarasov et al. 2006, Berg 2009). If a monolayer material other than C18OH was used, in order to calibrate and improve the accuracy of the model, it would be recommended that this material be characterised with respect to spread without wind stress (as detailed in Chapter 5), and spread and drift under wind stress (as detailed in Chapter 6).

7.3.2 Inputs

The outcomes of the modelling process (as detailed in Section 7.3) can be significantly altered by the user specified inputs. The model is set-up to allow customisation of a number of inputs, these are as follows:

- Water storage length and width.
- Wind speed.
- Wind direction.
- Number of applicators and their locations.
- Duration of application period.
- Monolayer application density (mg of monolayer per m² of water surface).

A deeper level of control of the modelling processes and/or alteration of the three key variables is available through a number of customisable model parameters. These are as follows:

1. Density of the numerical matrix (resolution of the model).
2. Minimum wind speed threshold (U_{MIN}).
3. Maximum wind speed threshold (U_{MAX}).
4. Percentage of monolayer loss at the perimeter (due to beaching).
5. Limit of coverage allowed off the water by applicators.

Parameter **1** can be adjusted to increase or decrease the number of nodes used to quantify monolayer coverage, which alters the resolution of the model. Parameter **2** is the transition point for the two different dosing states, for wind speeds $\leq U_{MIN}$ a single application is prescribed and for wind speeds $> U_{MIN}$ continuous application is prescribed (as detailed in Section 7.3). Parameter **3** is the wind speed cut-off point for the application of monolayer (Section 7.3). Parameter **4** determines the amount of monolayer that is lost to beaching when reaching the perimeter of the storage. Currently this parameter is set to 100% as there is no study, to the author's knowledge, that has characterised this phenomena. Parameter **5** is the proportion of coverage, as calculated in Section 7.3.5, that is allowed to be off the water by an applicator in order for it to be used for dosing (i.e. off water = monolayer expected to be lost to beaching). Increasing this limit would allow a larger proportion of the coverage provided by the applicators to be off the water, and thereby possibly altering the decision of which applicators to apply from. Currently this parameter is set to 50%.

7.3.3 Simulation platform processes

Once the above inputs and parameters have been set, the model begins by calculating the number of nodes required by dividing the length and width of the storage by the numerical matrix density. The model then creates two arrays, one containing the 'x'

coordinates and another containing the ‘y’ coordinates for each node. These nodes are then used to quantify the spatial distribution of monolayer. Nodes return a ‘0’ for no monolayer and a ‘1’ where monolayer is present. Monolayer coverage is calculated in two different ways, depending on the user-specified wind speed. For all wind speeds $\leq U_{MIN}$ monolayer distribution is calculated as described in Section 7.3.4 below, and for all wind speeds $> U_{MIN}$ and $\leq U_{MAX}$ monolayer distribution is calculated as described in Section 7.3.5 below.

7.3.4 Distribution calculation for quiescent conditions

For all wind speed conditions $\leq U_{MIN}$ all applicators are used for dosing regardless of wind direction since monolayer is not subject to wind-induced drift at these wind speeds (Vines 1962, McArthur 1962, Crow & Mitchell 1975). The potential surface area that can be covered by each applicator is calculated for the user-specified application period according to the spreading characteristics derived from empirical results in Chapter 5. According to empirical results monolayer spreads radially, therefore, monolayer coverage is modelled as a circle. The diameter of the circle is calculated for the user-specified application period using the following equation:

$$d = 0.2816t^{0.7384} \quad (7.1)$$

where:

$$\begin{aligned} d &= \text{diameter of monolayer coverage} \quad [\text{m}] \\ t &= \text{user-specified application period} \quad [\text{s}] \end{aligned}$$

The predicted diameter is then used in calculating the surface area of coverage for each applicator. This is done by creating a matrix of node indices from each applicator, then interrogating the matrix to determine which of the nodes, according to their indices, are within a distance of half the diameter. This is done for each applicator. The node indices within half the diameter from each applicator return a ‘1’ indicating the extent of monolayer coverage.

7.3.5 Distribution calculation for wind conditions

For all wind speed conditions $> U_{MIN}$ but $\leq U_{MAX}$ monolayer spreads in a wedge shape according to empirical results in Section 6.4.2. Therefore, monolayer coverage under wind conditions is modelled as a wedge (i.e. a circular segment). The wedge for each applicator is modelled in the same direction (spreading downwind) and parallel to the user-specified wind direction. The angle of the wedge is different for every wind speed and has been characterised empirically in Section 6.4.2. The following equation is used to determine the angle of the wedge according to the user-specified wind speed:

$$\theta_S = 152.77e^{-0.233U} \quad (7.2)$$

Where:

$$\begin{aligned} \theta_S &= \text{spreading angle} && [\text{degrees}] \\ U &= \text{user-specified wind velocity} && [\text{m/s}] \end{aligned}$$

To model the wedge from each applicator, simple trigonometry is used to interrogate the matrix containing the node indices for each applicator. Once the nodes that sit within this wedge normal to the wind direction are determined, a comparison of the wedge area on the water surface is made with the area that would be expected to be off the water surface. The area expected to be off the water surface is calculated by using trigonometry and the longest length of one edge of the wedge area on the water surface to calculate the complete surface area. The complete surface area calculated minus the wedge area on the water surface equals the off water surface area. An illustration of the calculated wedge on-water and off-water surface coverage areas is provided in Figure 7.2.

The decision of which applicators to use to dose monolayer from, is made according to the proportion of the wedge surface area that is on the water surface and off the water surface. Only applicators that have a wedge surface area $\geq 50\%$ on the water surface are used for dosing monolayer. This threshold is a user-customisable parameter, which is currently set at 50% (Section 7.3.2).

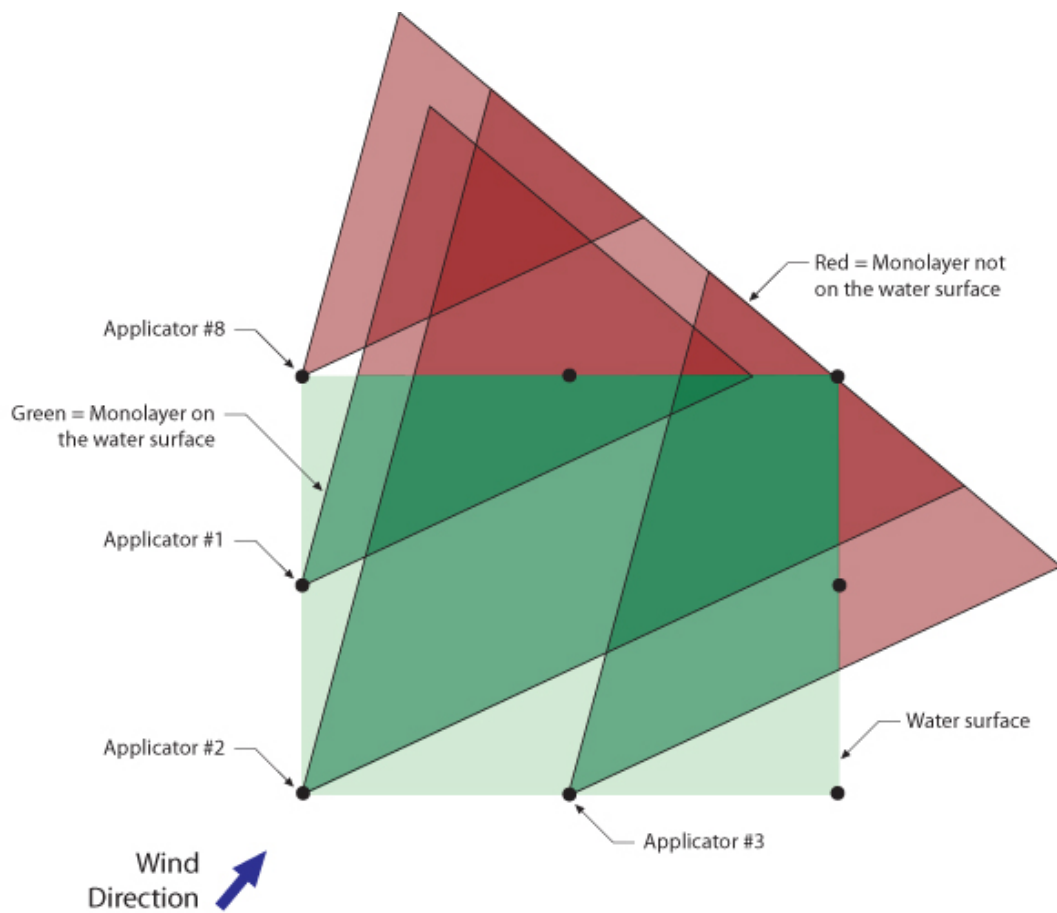


Figure 7.2: Illustration of the wedge on-water (green) and off-water (red) surface areas for each applicator at a user-specified wind speed and wind direction. Only applicators 2 and 3 have an on-water coverage area of $\geq 50\%$. Whereas applicators 1 and 8 have an on-water coverage area of $< 50\%$. Therefore, under this scenario, applicators 2 and 3 will be used for dosing.

The wedge on-water surface area calculated for one applicator may overlap with other applicators (as illustrated in Figure 7.2). To stop this from happening coverage overlap between applicators is divided up according to the number of applicators contributing and the proportion each contributes to the overlap (as illustrated in Figure 7.3). The reason this is done is to ensure there is no error in calculating the required application rate, which is calculated according to the total effective coverage area provided by all the applicators (Section 7.3.6).

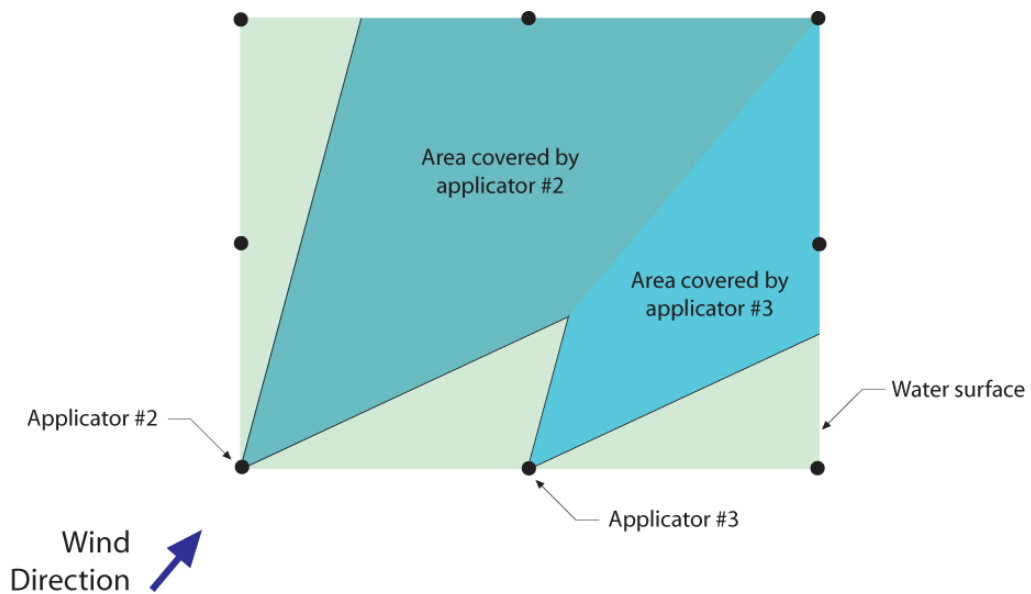


Figure 7.3: Illustration of the effective water surface area that each applicator will cover with monolayer at a user-specified wind speed and wind direction. The coverage area overlap between applicators 2 and 3 has been divided up by the proportion each contributes to the overlap so that there is no double-up when calculating the application rate.

7.3.6 Application calculations

The monolayer application amount for quiescent conditions is calculated by multiplying the monolayer application density by the surface area of the storage. This is reported as an amount in kilograms and not a rate as only a single application is required. This total application amount is evenly divided up by the number of applicators. Whereas, for wind conditions, application amount is reported as a rate in kg/s and is usually different for each applicator as the effective surface area able to be covered by each

applicator is likely to be different. The effective surface area is calculated for each applicator as outlined in Section 7.3.5. Once the effective surface area is known for each applicator, the application rate is calculated for each applicator using Equation 7.3:

$$m = \frac{\rho A_e U}{L} \quad (7.3)$$

where:

m	=	application rate	[kg/s]
ρ	=	monolayer coverage density	[kg/m ²]
A_e	=	effective area covered (calculated in 7(d))	[m ²]
U	=	drift speed of the monolayer film (a function of wind speed)	[m/s]
L	=	length of monolayer coverage path over water	[m]

Then the respective application rates for each applicator are simply added together to derive a total application rate.

7.3.7 Outputs

The simulation platform outputs the following information:

1. Graph of the percentage of surface coverage over time (Figure 7.4).
2. Distribution graph of monolayer coverage at the end of the simulation period (Figure 7.5).
3. Table of applicator locations and their corresponding monolayer output over the simulation period (Table 7.1).

The sample outputs below have been simulated for a 350 x 450 m size rectangular storage, with a total of eight shore based applicators, under a wind speed of 20 km/h coming from the South West, and over an application period of 2.5 hours.

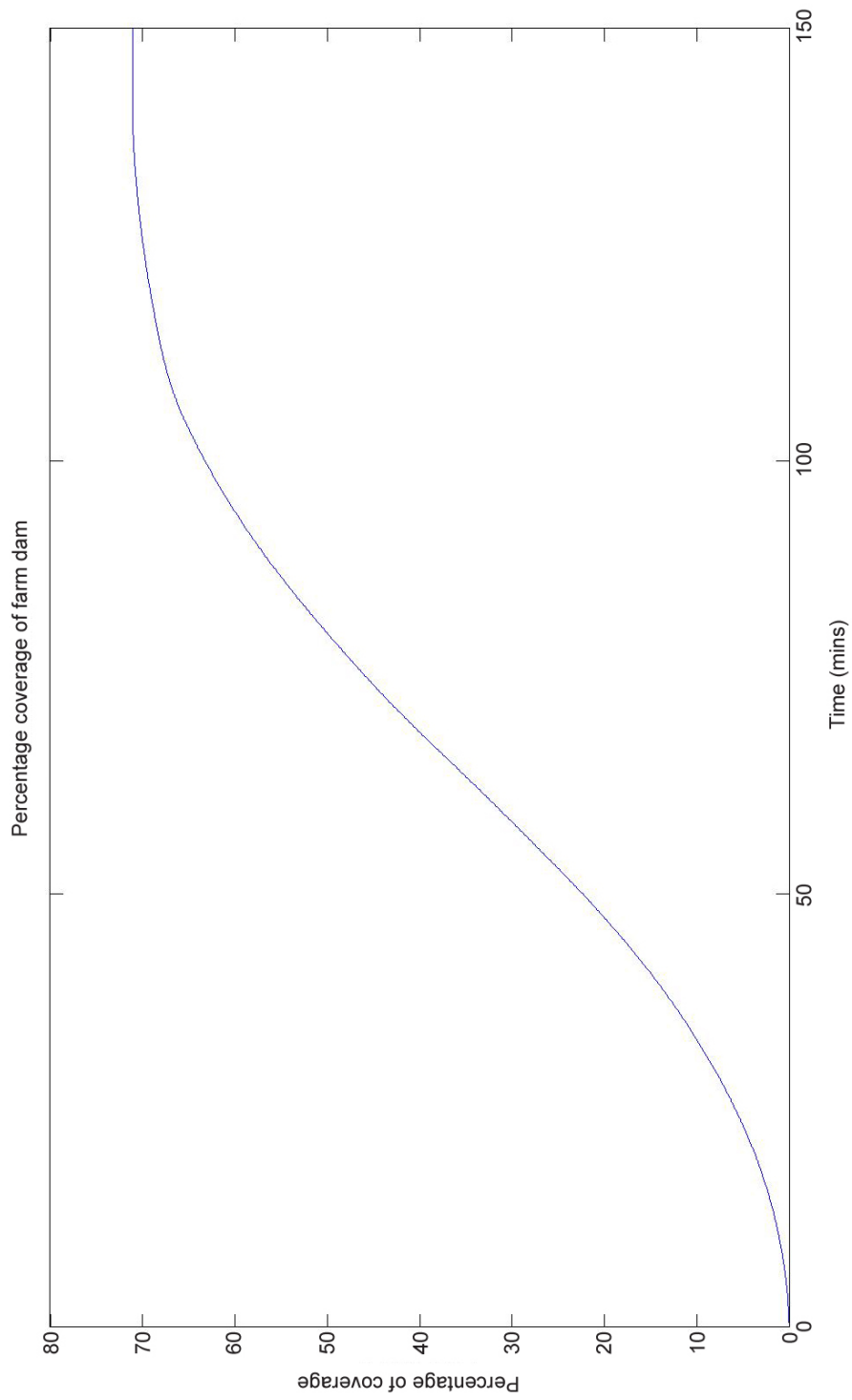


Figure 7.4: Graph of the percentage of surface coverage over time as output from the MATLAB simulation platform.

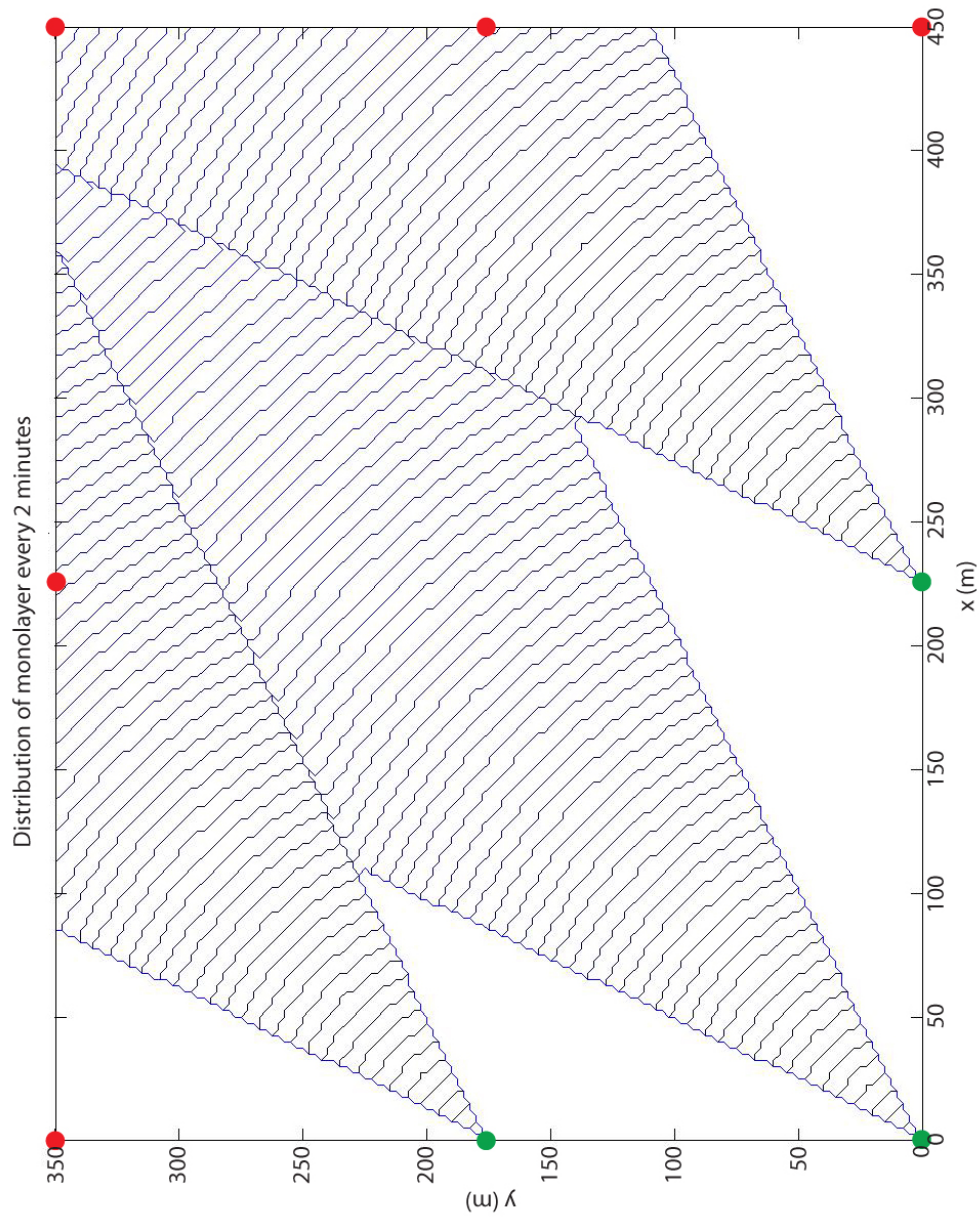


Figure 7.5: The distribution of monolayer coverage at the end of the simulation period as output from the MATLAB simulation platform. Although there are actually 8 applicators here, only 3 are shown to be applying monolayer for this wind speed and wind direction (green = applicators on; red = applicators off).

Table 7.1: Table as output from the MATLAB simulation platform showing the Cartesian coordinates (x and y location) of each applicator and the corresponding total amount of monolayer applied for that applicator. Applicator locations are listed anti-clockwise, starting from the bottom left-hand corner of the distribution graph (Figure 7.5).

Applicator locations (m):		Monolayer applied (kg):
x coordinate:	y coordinate:	
0	0	0.53
225	0	0.32
450	0	0.00
450	175	0.00
450	350	0.00
225	350	0.00
0	350	0.00
0	175	0.25

7.4 Discussion

The simulation platform currently makes a number of major assumptions (Section 7.3.1), namely:

1. no residual surface coverage from the previous time-step (i.e. at every next time step monolayer surface coverage is reset to zero), and
2. all monolayer reaching the downwind shore is lost to beaching.

These assumptions are not correct as there will be residual coverage from the previous time step that will need to be taken into consideration and not all monolayer will be beached at the downwind shore. Therefore, the application rate/s calculated by the model are quite pessimistic (i.e. a worst case scenario).

Further development of the computer code to account for dynamic wind conditions and pre-established coverage between time-steps will largely correct assumption (1). However, the effect of assumption (1) could largely be mitigated by not dosing from applicators within the waterbody (i.e. not on the shore) once steady-state conditions are reached (i.e. maximum possible coverage has been achieved by all applicators for a particular wind condition). This is because once steady-state conditions are reached the added coverage that was initially provided by applicators within the waterbody will largely be negated by the applicators near the shore (Figure 7.6). Whereas, assumption (2) will need to be characterised for different shore batters and compositions for a range of wind and wave conditions. A satisfactory shoreline absorption model will need to be developed to allow the prediction of beaching and or/ redistribution of monolayer product after a wind shift to be determined.

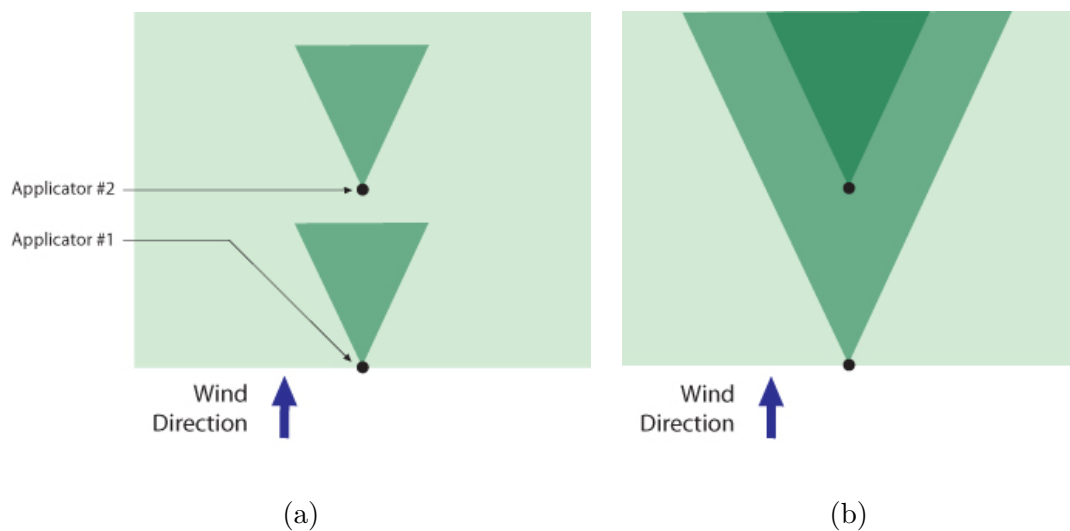


Figure 7.6: (a) Illustration of 'pre' steady-state conditions, the applicator within the waterbody is providing added coverage. (b) Illustration of 'post' steady-state, the applicator within is now not providing any additional coverage to that already being provided by the applicator near the shore.

The coverage results produced assume that monolayer continues to spread as a wedge outwards from the point of application and this would need to be confirmed in the field. However, it is unlikely that this perfect wedge shaped spread pattern will be maintained, especially under dynamically changing wind conditions in the field. The wedge spread pattern could be altered due to a low-wind zone, which is sometimes

created near the shore by the freeboard of the dams batters. Then again, the angles of the wedge shaped spread pattern could started to flatten after a certain distance effectively reducing coverage. The large scale effects are largely unknown and the spatial distribution/monolayer spread pattern would need to be verified for different wind conditions in a full-scale field trial and calibrated accordingly.

Despite the major assumptions in the simulation platform, as discussed above, the main purpose of the model is to allow the effect of different application system arrangements (i.e. number and location of applicators) under different wind speeds, wind directions and storage sizes on the spatial distribution of monolayer coverage to be predicted. The model allows the user to change applicator positions, specify more or less applicators and predict the coverage and application rate for different wind conditions. Even though there are likely to be significant errors associated with the major assumptions, it is unlikely that these errors will significantly alter the net result of how many applicators are needed and of which type (i.e. shore-based or floating) and where are they best located on-site to provide optimal coverage. For the purposes of the UDF, this model is sufficient.

7.5 Conclusion

The model simplifies a number of natural and highly dynamic phenomena that may be significantly different for every situation. This simulation is the first-step towards providing some indicative insights into the spread and coverage rate of monolayer on large water surfaces under changing wind conditions. Although a fully dynamic and much more complex model is required to go beyond this, the simulation platform does allow the determination of a number of novel insights, as set out in Chapter 8 and Chapter 9.

Chapter 8

Indicative Modelling of Monolayer Distribution

8.1 Introduction, rationale and overview

A monolayer simulation platform has been developed (Chapter 7) to allow the prediction of coverage rate and application rate of monolayer for different applicator arrangements (both number of applicators and their layout) on different size water storages, under different wind conditions (both strength and direction) and over different application periods. With the requirements of the Universal Design Framework (UDF) in mind (Section 7.2), the simulation platform will allow many different user scenarios to be modelled while also allowing each user to develop an optimised applicator arrangement according to their unique site and user requirements.

Hence, the purpose of this Chapter is twofold:

1. to explore the effect of different size storages, wind conditions and application periods on the coverage and application rates provided by a number of symmetrical applicator arrangements, and
2. to demonstrate the benefits of developing an asymmetrical applicator arrangement optimised for a particular storage size, site-specific wind conditions and

user performance criteria (as would be the requirement for a user of the UDF).

With regard to (1), this study involved the use of two different site-specific sets of wind data, one for a relatively calm location (Amberley, Queensland) and another for a windier one (Moree, New South Wales). Three different size square storages, 50 x 50 m, 500 x 500 m and 5000 x 5000 m, were specified and tested for both sets of wind data. Due to the significant differences in scale between the three water storages, the following criteria was considered for each storage:

- unique applicator arrangements (3 different symmetrical applicator arrangements for each size storage),
- unique application periods (1, 3, and 5 hours were selected and used for the 50 x 50, 500 x 500 and 5000 x 5000 m storages respectively).

Results for each combination (i.e. storage size, applicator arrangement and application period) were obtained by performing simulations, with the simulation platform, for 31 different combinations of wind speed and direction (i.e. wind conditions). To moderate the simulated results according to each site's unique historical wind condition frequencies, which were obtained from Bureau of Meteorology (BOM) wind rose data, a post-process (set out in Section 8.2.2) was used. This post-process involved weighting the simulated results by the BOM wind condition frequencies for that particular site to determine the average percentage of time a particular percentage of coverage is achieved, including the aggregate application rate for each combination.

With regard to (2), the two optimised asymmetrical applicator arrangements were developed for the 500 x 500 m storage and moderated with Moree's historical wind condition frequencies. Both applicator arrangements were designed for the 500 x 500 m storage as this represents the closest typical storage size best suited for evaporation mitigation by monolayer (Craig et al. 2007). Both asymmetrical arrangements were designed to satisfy two different sets of user performance criteria, (i) $\geq 80\%$ coverage at least 80% of the time for a 3 hour application period, and (ii) $\geq 80\%$ coverage at least 80% of the time for a 6 hour application period.

Although only one size storage, one set of wind conditions and two different user performance criteria were used in study (2), the process could simply be replicated for any other set of site-specific conditions and user requirements.

8.2 Materials and methods

8.2.1 Study (1)

To determine a suitable application period for the simulations to be run in study (1), for each storage size, a basic analysis was performed with the simulation platform to determine the time taken for each applicator arrangement to achieve steady-state conditions (i.e. maximum coverage by all applicators is never reached for a particular wind condition) for the standard 31 different wind conditions (as set out in Section 8.2.3). Based on these results, a suitable application period, for each storage size, was selected by the criteria that steady-state conditions are not reached by an applicator arrangement in any wind condition. This was done to ensure that the differences in the extent and speed at which coverage was achieved by each applicator arrangement is clearly identifiable. These differences are substantially decreased, and therefore harder to identify, once steady-state conditions are reached. Accordingly, the following application periods were selected for modelling: 1, 3, and 5 hours for the 50 x 50, 500 x 500 and 5000 x 5000 m storages respectively.

The simulation platform (Chapter 7) was then used in study (1) to determine:

- the percentage of surface cover and application rate for all three of the applicator arrangements, for each size storage, for 31 different wind conditions and the respective application period for each size storage. (i.e. 3 different applicator arrangements, by 3 different size storages, by 31 different wind conditions, which is a total of 279 individual simulations);
- the results were then grouped, according to their respective applicator arrangement (9 individual groups), and moderated for the two wind site's unique historical wind condition frequencies (Section 8.2.3), using the Post-Process 1 (set out

in Section 8.2.2) to determine the percentage of time a particular percentage of cover is achieved (9 groups of results, by 2 wind site's wind frequencies, is a total of 18 groups);

- the percentages of time a particular percentage of coverage is achieved, was then plotted for each group at their respective storage sizes (as set out in Section 8.3).

8.2.2 Post-Process 1

All data output from the simulation platform, for both study 1 and 2, were further analysed in Post-Process 1, which involves the following procedures:

- Coverage results for each of the 31 different wind conditions (strength and direction) are moderated, using BOM wind rose data (Section 8.2.3), to determine a percentage of time that each wind condition occurs.
- The respective percentages of time are then summed according to their percentage of coverage, which are grouped in 10% steps from 10% to 100%.
- This produces the percentage of time that a particular percentage of coverage will occur.

For example, to determine the percentage of time at least 80% coverage is achieved, suppose five simulations (each with a different wind condition) achieve this target and the percentage of time each wind condition occurs is 5%, then at least 80% coverage will be achieved 25% of the time.

In conjunction with this analysis, the application rate for each simulation was averaged to determine the average application rate corresponding to that application period.

8.2.3 Storage size and wind site selection

Three square storages of sizes 50 x 50 m, 500 x 500 m, 5000 x 5000 m were simulated using wind data from two different sites. The two different wind sites were: Amberley,

QLD as a low-wind site (Figure 8.1) and Moree, NSW as a high-wind site (Figure 8.3). Outputs from the simulation were applied to statistical wind speed, direction and frequency data from these two locations using Post-Process 1 (Section 8.2.2). Annual wind roses for both 9 am and 3 pm and the data used to produce them was obtained from the BOM (see Figures 8.2 and 8.4), with the average of the frequencies from both times used to specify the likelihood of each wind speed and direction occurring. The frequency tables generated, and used in Post-Process 1, can be found in Appendix C.

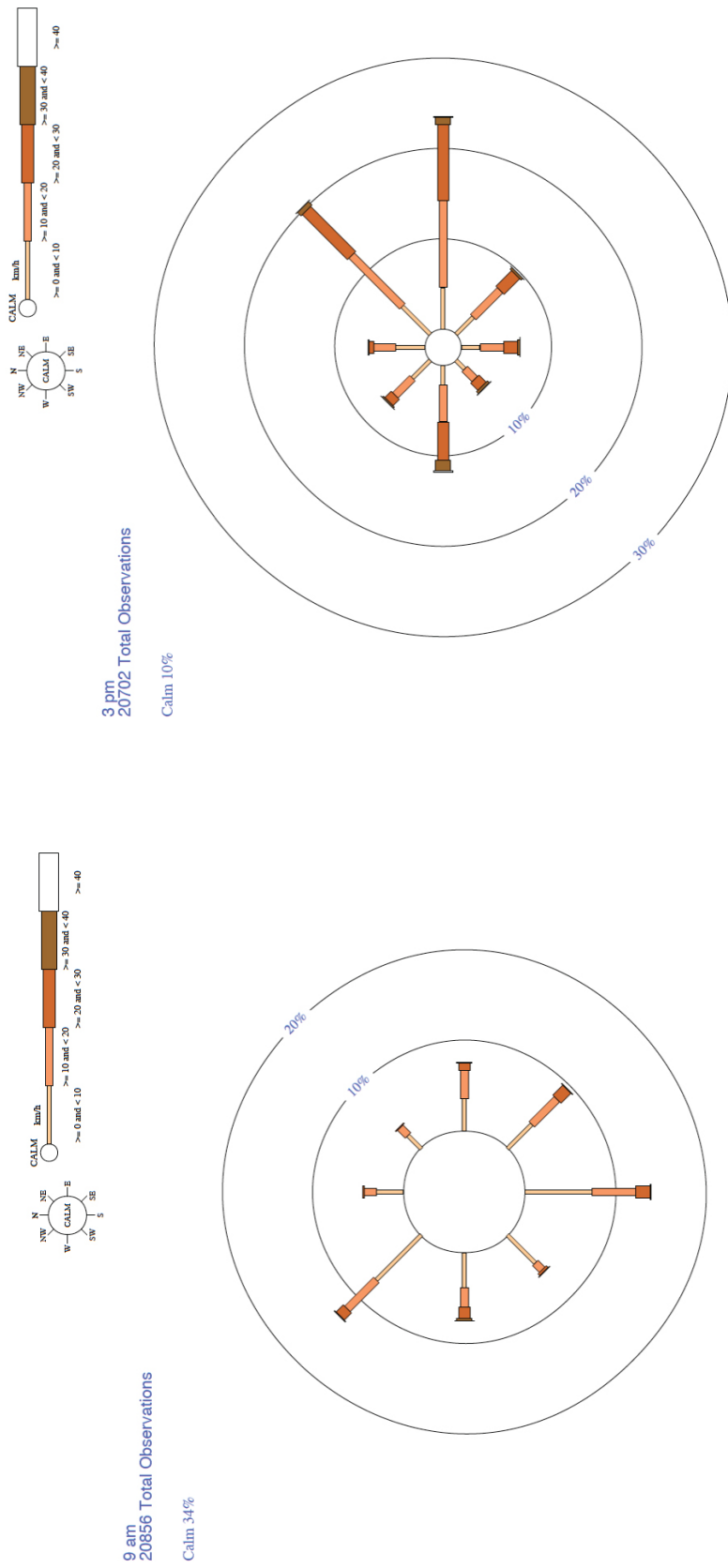
The BOM wind rose data is based on ranges of wind speeds at 45° compass points. Therefore the centre point of each range of wind speeds has been used as the input for the simulation (see Table 8.1). For wind speeds >30 km/h the simulation platform does not apply product (based on U_{MAX} as detailed in Section 7.3.2), therefore both coverage and application rate are taken as zero. Wind directions were limited to the standard 8 different directions matching that of the BOM wind rose (i.e. N, NE, E, SE, S, SW, W, NW). As all the storages are square and applicator arrangements symmetrical, the effects of these 8 directions are accounted for by the two N and NE wind directions. The wind frequency data used in this analysis for the two locations, as received from the BOM, can be found in Appendix C.

Table 8.1: BOM wind rose speed ranges and the corresponding wind speeds used in modelling.

BOM Wind Rose Speed Ranges (km/h):	Modelled Wind Speed (km/h):
Calm	0
0-10	5
10-20	15
20-30	25
30-40	30
>40	30



Figure 8.1: Amberley, QLD (low-wind site) is located 51 km West of Brisbane, 53 km East of Gatton, 89 km East of Toowoomba and 433 km North East of Moree.



(a)

(b)

Figure 8.2: BOM annual wind roses for Amberley, QLD (low-wind site): (a) 9 am wind rose; and (b) 3 pm wind rose.

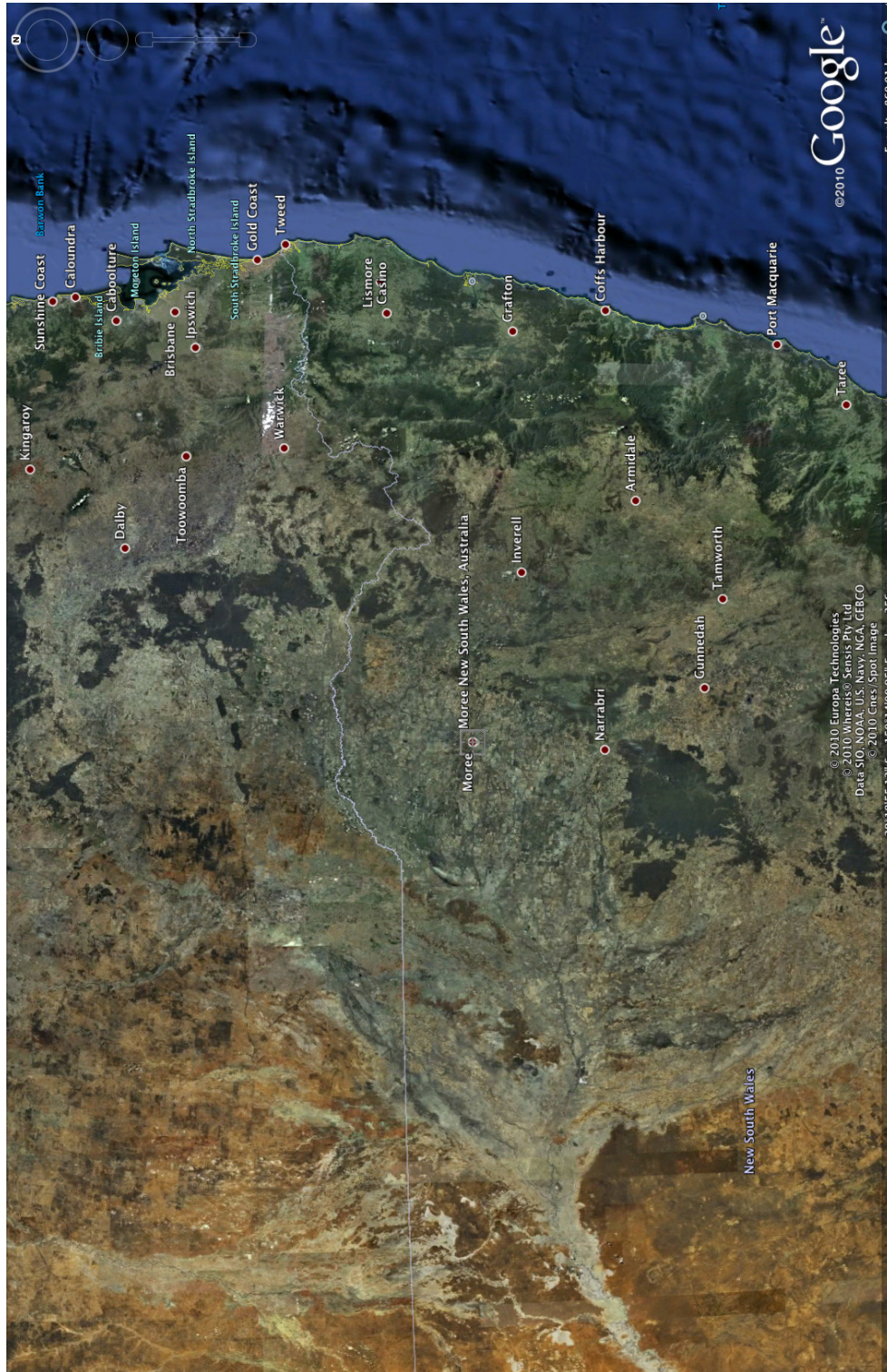


Figure 8.3: Moree, NSW (high-wind site) is located 473 km South West of Brisbane, 381 km North East of Dubbo and 639 km North West of Sydney.

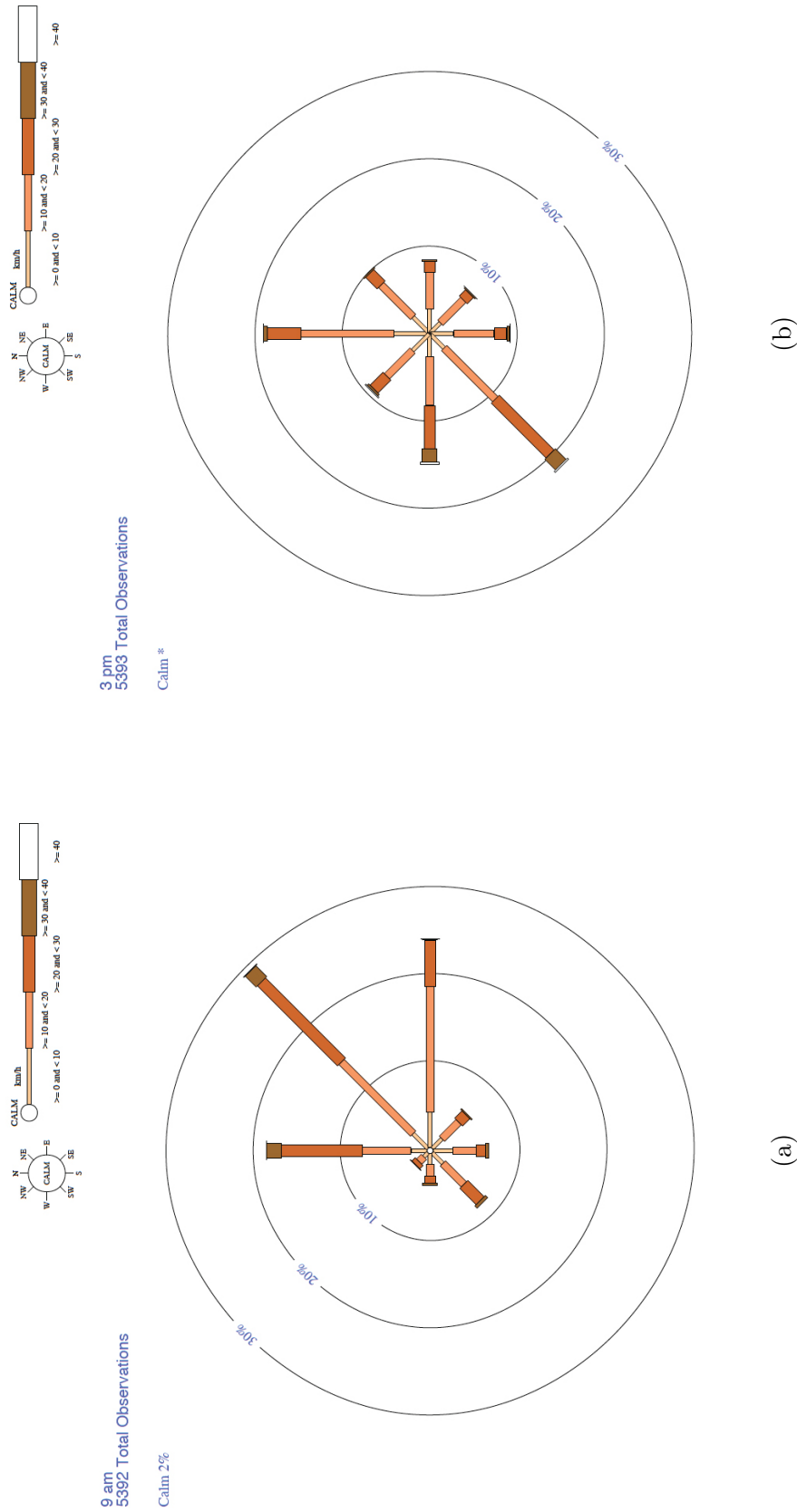


Figure 8.4: BOM annual wind roses for Mores, NSW (high-wind site): (a) 9 am wind rose; and (b) 3 pm wind rose.

8.2.4 Applicator arrangements

Various applicator spacing and arrangements were modelled for each of the storage sizes. A combination of applicators around the perimeter of the storage (i.e. shore-based) and applicators within the storage (i.e. floating) were used on regular, evenly-spaced grids (i.e. symmetrical). Applicator arrangements for the 50 x 50 m, 500 x 500 m and 5000 x 5000 m storages are detailed in Figures 8.5, 8.6 and 8.7 respectively.

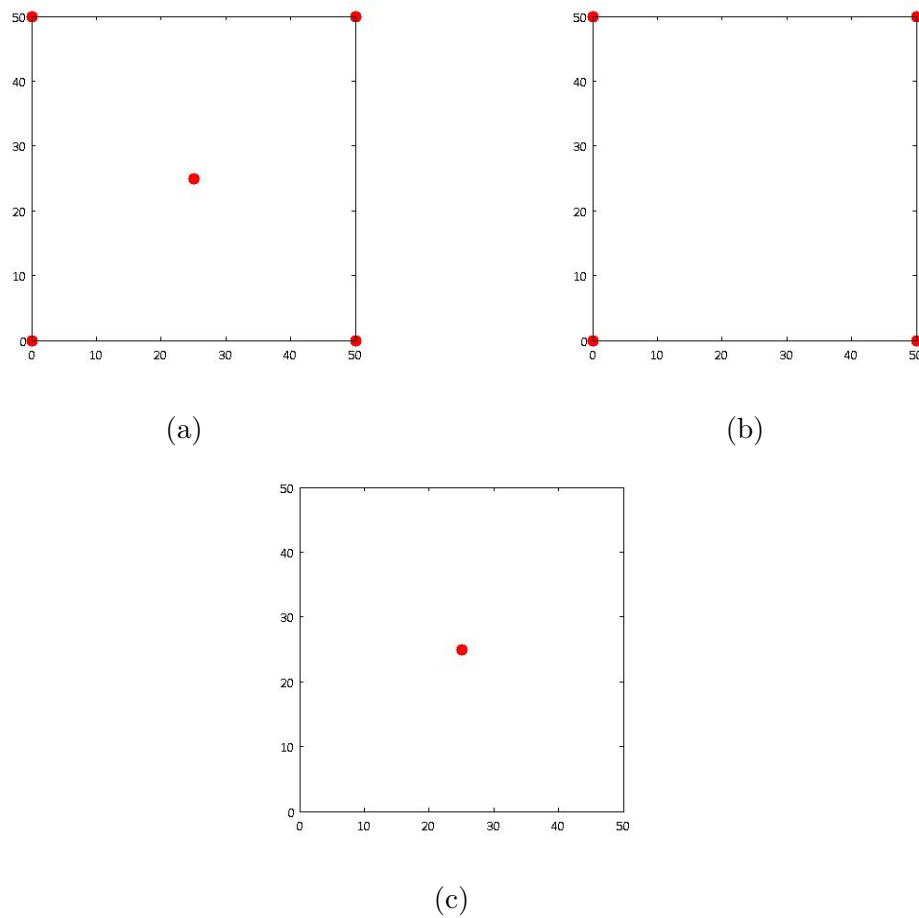


Figure 8.5: 50 x 50 m storage applicator arrangements: (a) 4 + 1, an applicator in each corner plus 1 in the centre of the storage; (b) 4 applicators placed in each corner; and (c) 1 applicator placed in the centre of the storage.

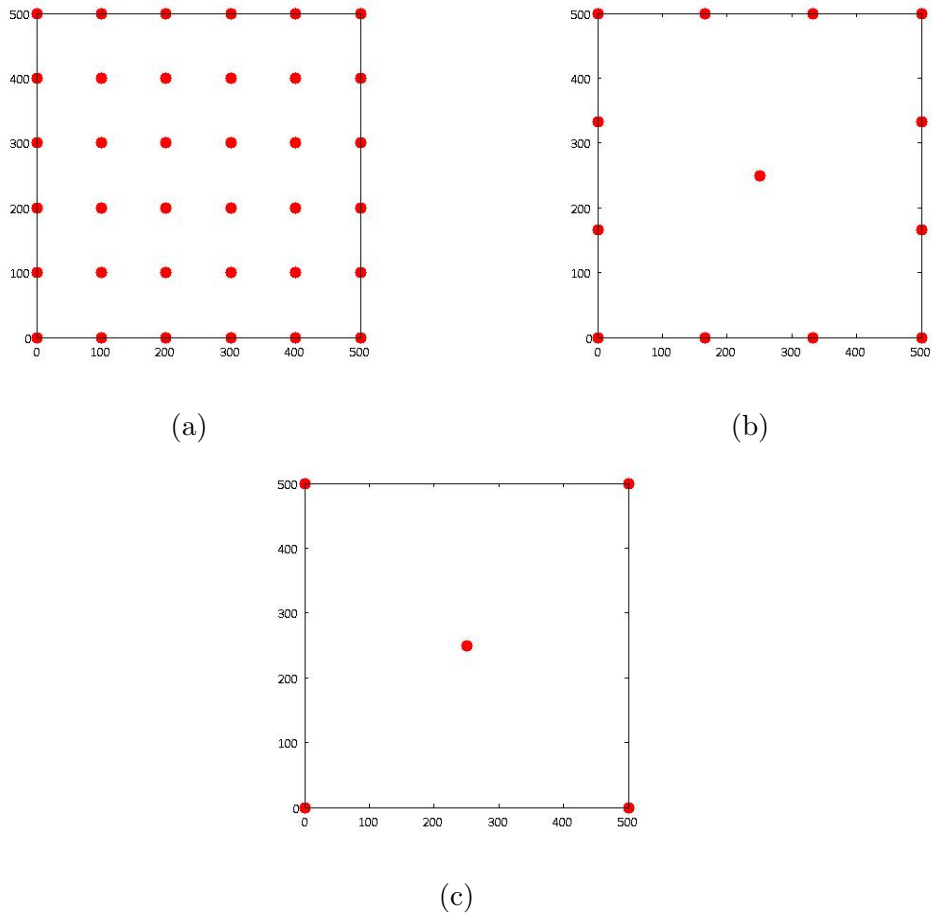


Figure 8.6: 500 x 500 m storage applicator arrangements: (a) 6 x 6 applicator grid, with 100 m spacing between applicators; (b) 12 + 1, four applicators on each side plus 1 in the centre of the storage; (c) 4 + 1, an applicator in each corner plus 1 in the centre of the storage.

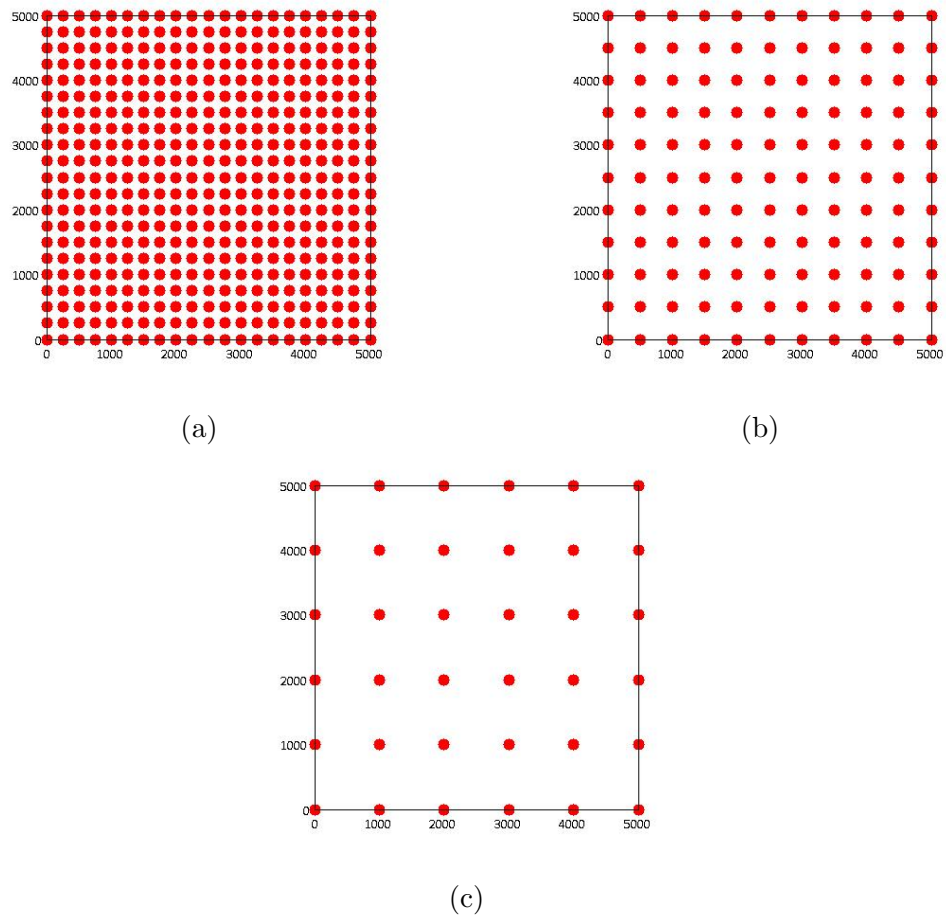


Figure 8.7: 5000 x 5000 m storage applicator arrangements: (a) 21 x 21 applicator grid (441 applicators), with 250 m spacing between applicators; (b) 11 x 11 applicator grid (121 applicators), with 500 m spacing between applicators; and (c) 6 x 6 applicator grid (36 applicators), 1000 m between applicators.

8.2.5 Study (2)

As a first step in study (2) towards developing two optimised applicator arrangements, the BOM wind rose data for the annual wind speed and direction frequencies for Moree were plotted to determine the major prevailing wind direction/s (Figure 8.8). As the majority of wind is predominately from the North and North Eastern directions the general approach was taken to concentrate applicator numbers near the North and North East shores. During the design process many different arrangements were simulated to determine the optimal number of applicators and their arrangement to satisfy user performance criteria.

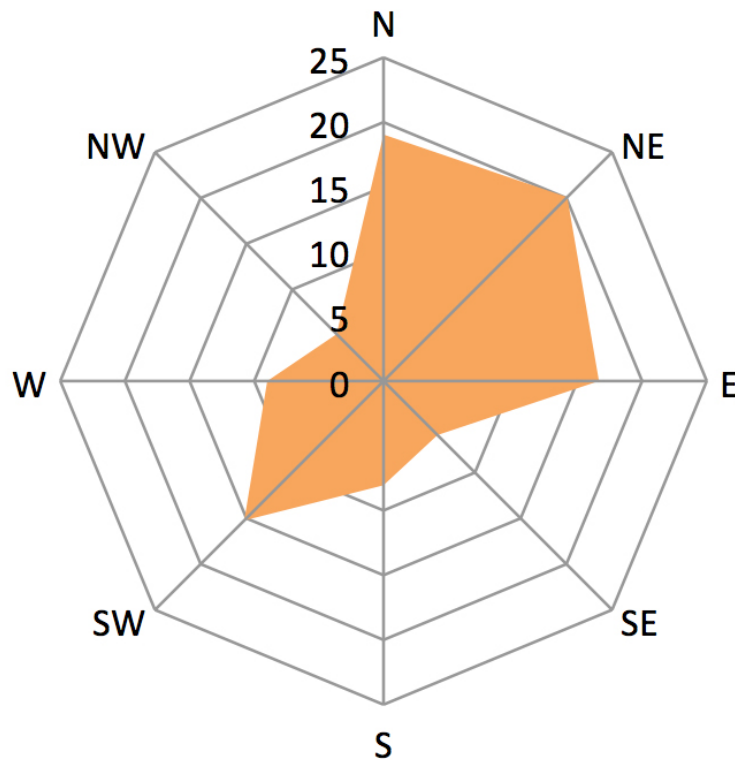


Figure 8.8: Wind rose of the BOM annual wind speed and direction frequencies for Moree, NSW.

For demonstration purposes, two sets of user performance criteria were specified and used for developing and optimising an applicator arrangement for each. The two sets of user performance criteria are that the applicator arrangement must provide:

Set 1 a minimum of 80% coverage at least 80% of the time for a 3 hour application period;

Set 2 a minimum of 80% coverage at least 80% of the time for a 6 hour application period.

The first arrangement comprises a total number of 16 applicators, 15 shore-based and 1 floating (Figure 8.9a). The second arrangement is made up of 30 applicators, 18 shore-based and 12 floating (Figure 8.9b). As can be seen, both applicator arrangements are asymmetrical and quite different from each other. The first requires many more floating applicator in order to achieve the 80% coverage level 80% of the time (in 3 hours), whereas only one is needed to achieve this level of coverage after 6 hours. The total number of shore-based applicators for each arrangement varies only slightly.

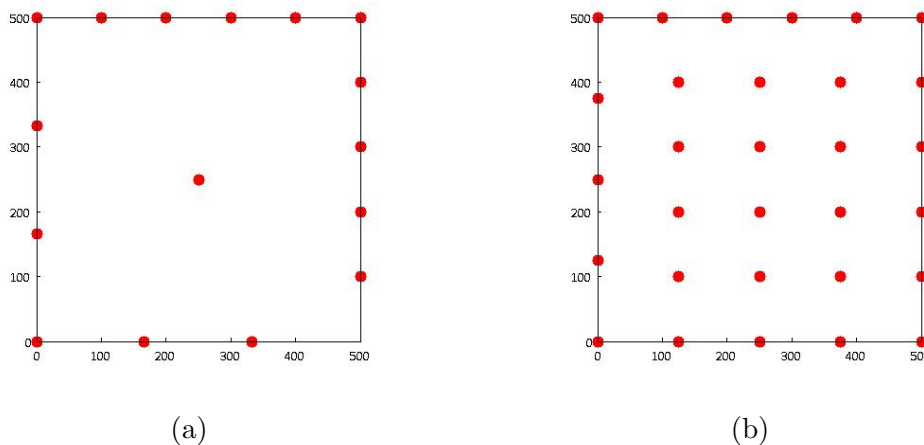


Figure 8.9: 500 x 500 m storage asymmetrical applicator arrangements: (a) 15 + 1, 15 strategically located applicators on the shore and 1 floating applicator in the middle; (b) 18 + 12, 18 strategically located applicators on the shore and 12 evenly spaced apart floating applicators.

8.3 Results

The results for three different application arrangements for each size storage, and moderated with wind data for two different wind sites, are set out in Sections 8.3.1, 8.3.2 and 8.3.3 for the 50 x 50, 500 x 500 and 5000 x 5000 m storages respectively. Also, the

results for two asymmetrical applicator arrangements, optimised for the 500 x 500 m storage and the windy site's conditions, are set out in Section 8.3.4.

8.3.1 50 x 50 m storage

Results for the percentage of time a minimum area is covered for the three different applicator arrangements are shown for both the Amberley and Moree wind sites for a 1 hour application period (Figure 8.10). The actual numbers used to produce the graph in Figure 8.10 are detailed in Table 8.2. Also shown in the table is the average percentages of time coverage is achieved, the aggregate application rate and the total amount of monolayer material applied by each applicator arrangement.

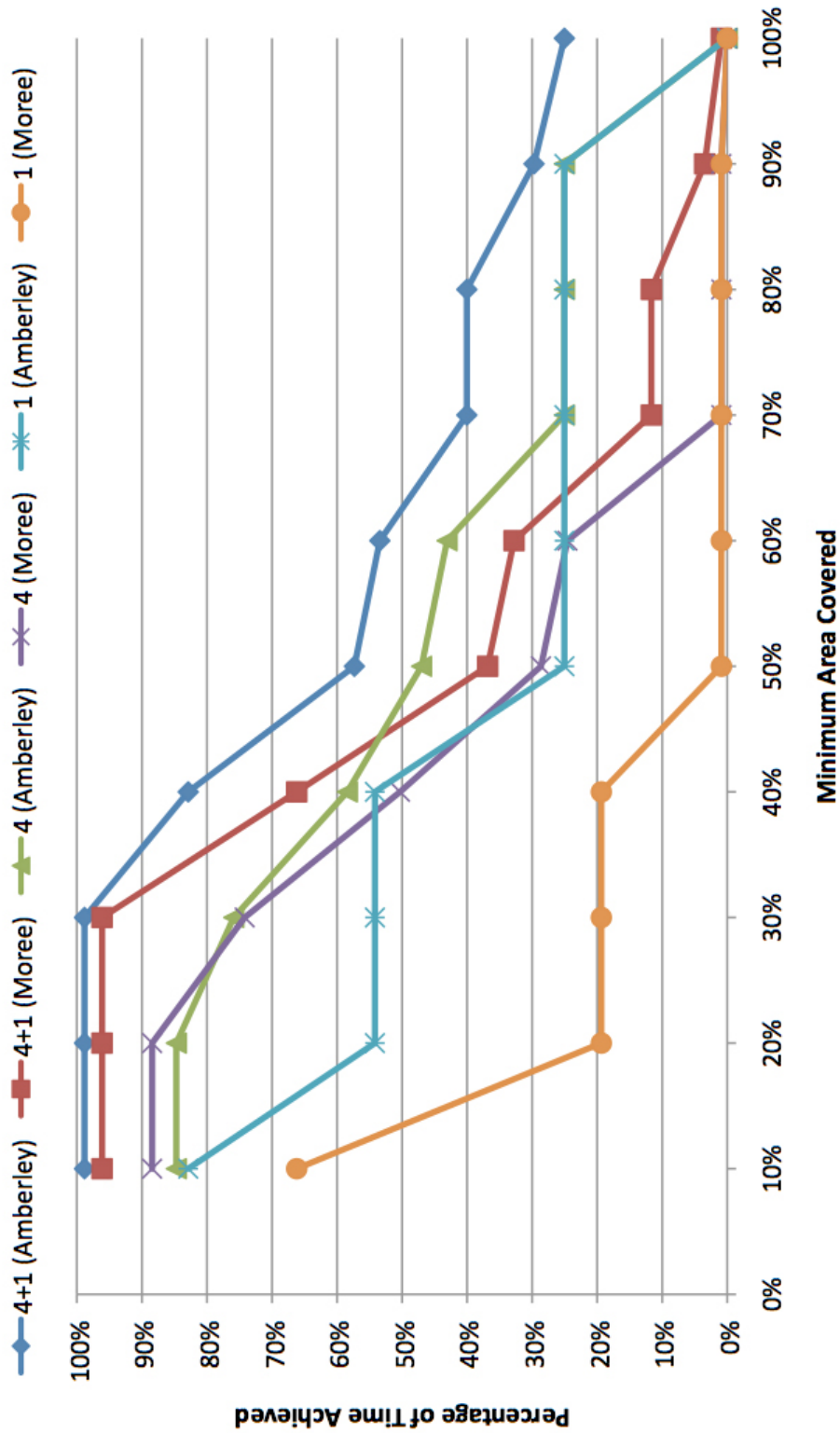


Figure 8.10: Percentage of time a minimum area is covered for the 50 x 50 m storage after 1 hour of application. Results are shown for all three application arrangements, 4 + 1, 4 and 1, for both Amberley and Moree wind conditions.

Table 8.2: Percentage of time a minimum area is covered for the 50 x 50 m storage after 1 hour of application. Including the average of the percentages of time, the aggregate application rate over that period and the total amount of monolayer applied for each arrangement. Results calculated using BOM average annual wind speeds and directions for both Amberley and Moree.

Area Covered (%):	Amberley			Moree		
	4+1	4	1	4+1	4	1
	% of Time:					
10	98.8	84.7	90.0	96.1	88.4	81.9
20	98.8	84.7	54.2	96.1	88.4	19.4
30	98.8	75.9	54.2	96.1	74.2	19.4
40	90.0	75.9	54.2	81.9	74.2	19.4
50	75.1	68.8	34.7	62.6	58.5	7.9
60	53.4	53.4	25.0	32.8	32.8	0.9
70	53.4	53.4	25.0	32.8	32.8	0.9
80	40.0	40.0	25.0	11.7	11.7	0.9
90	40.0	40.0	25.0	11.7	11.7	0.9
100	28.3	28.3	25.0	3.8	3.77	0.9
Average % of Time:	67.7	60.5	41.2	52.6	47.6	15.2
Application Rate (kg/h):	0.1	0.1	0.1	0.2	0.1	0.1
Total Applied (kg):	0.1	0.1	0.1	0.1	0.1	0.1

8.3.2 500 x 500 m storage

Results for the percentage of time a minimum area is covered for the three different applicator arrangements are shown for both the Amberley and Moree wind sites for a 3 hour application period (Figure 8.11). The actual numbers used to produce the graph in Figure 8.11 are detailed in Table 8.3. Also shown in the table is the average percentages of time coverage is achieved, the aggregate application rate and the total amount of monolayer material applied by each applicator arrangement.

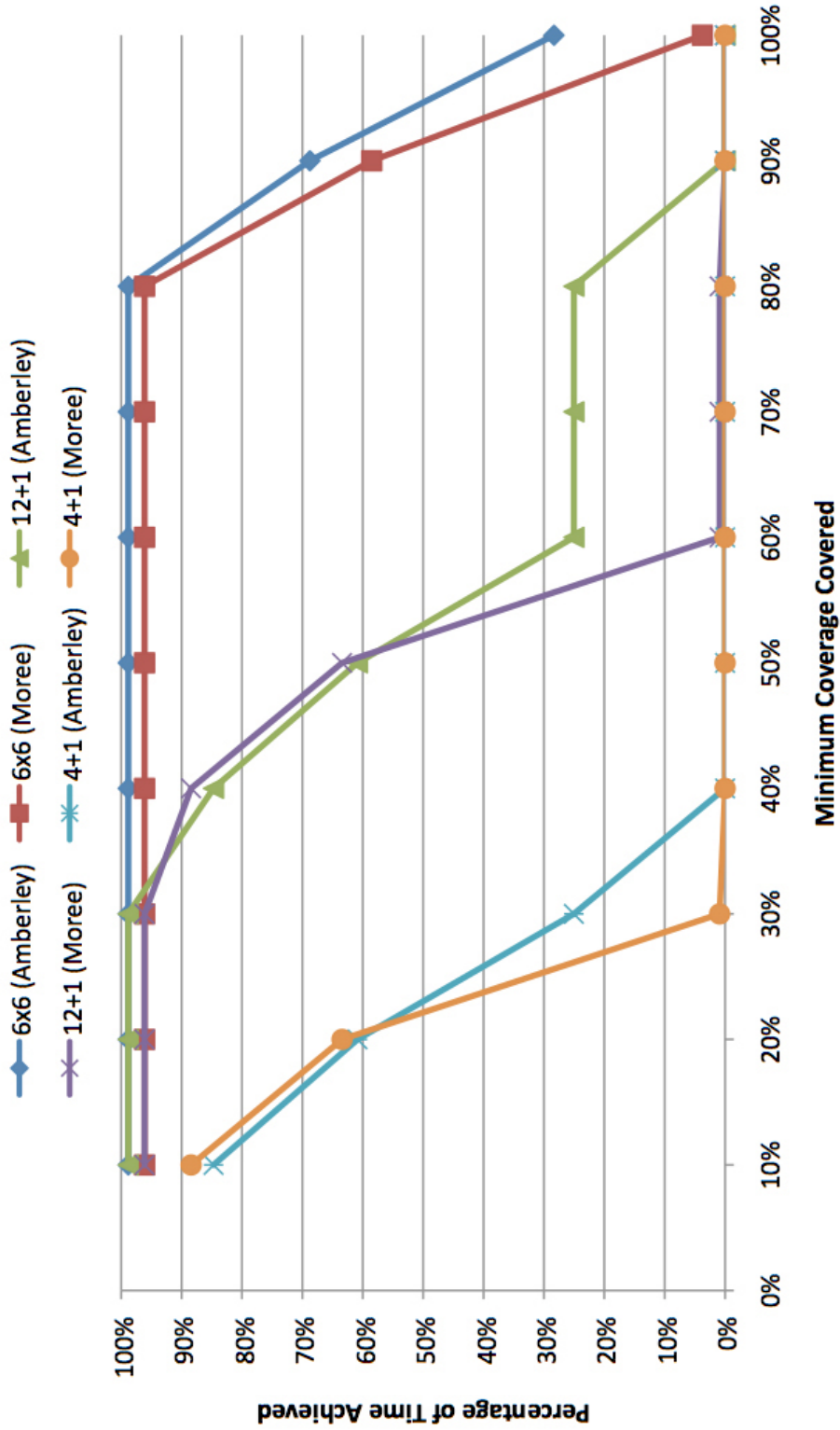


Figure 8.11: Percentage of time a minimum area is covered for the 500 x 500 m storage after 3 hours of application. Results are shown for all three application arrangements, 6 x 6, 12 + 1 and 4 + 1, for both Amberley and Moree wind conditions.

Table 8.3: Percentage of time a minimum area is covered for the 500 x 500 m storage after 3 hours of application. Including the average of the percentages of time, the aggregate application rate over that period and the total amount of monolayer applied for each arrangement. Results calculated using BOM average annual wind speeds and directions for both Amberley and Moree.

Area Covered (%):	Amberley			Moree		
	6x6	12+1	4+1	6x6	12+1	4+1
	% of Time:					
10	98.8	98.8	84.7	96.1	96.1	88.4
20	98.8	98.8	60.9	96.1	96.1	63.4
30	98.8	98.8	25.0	96.1	96.1	0.9
40	98.8	84.7	0.0	96.1	88.4	0.0
50	98.8	60.9	0.0	96.1	63.4	0.0
60	98.8	25.0	0.0	96.1	0.9	0.0
70	98.8	25.0	0.0	96.1	0.9	0.0
80	98.8	25.0	0.0	96.1	0.9	0.0
90	68.8	0.0	0.0	58.5	0.0	0.0
100	28.3	0.0	0.0	3.8	0.0	0.0
Average % of Time:	88.8	51.7	17.1	83.1	44.3	15.3
Aggregate Rate (kg/h):	2.7	2.2	1.4	4.1	3.2	1.8
Total Applied (kg):	8.1	6.6	4.2	12.3	9.6	5.4

8.3.3 5000 x 5000 m storage

Results for the percentage of time a minimum area is covered for the three different applicator arrangements are shown for both the Amberley and Moree wind sites for a 5 hour application period (Figure 8.12). The actual numbers used to produce the graph in Figure 8.12 are detailed in Table 8.4. Also shown in the table is the average percentages of time coverage is achieved, the aggregate application rate and the total amount of monolayer material applied by each applicator arrangement.

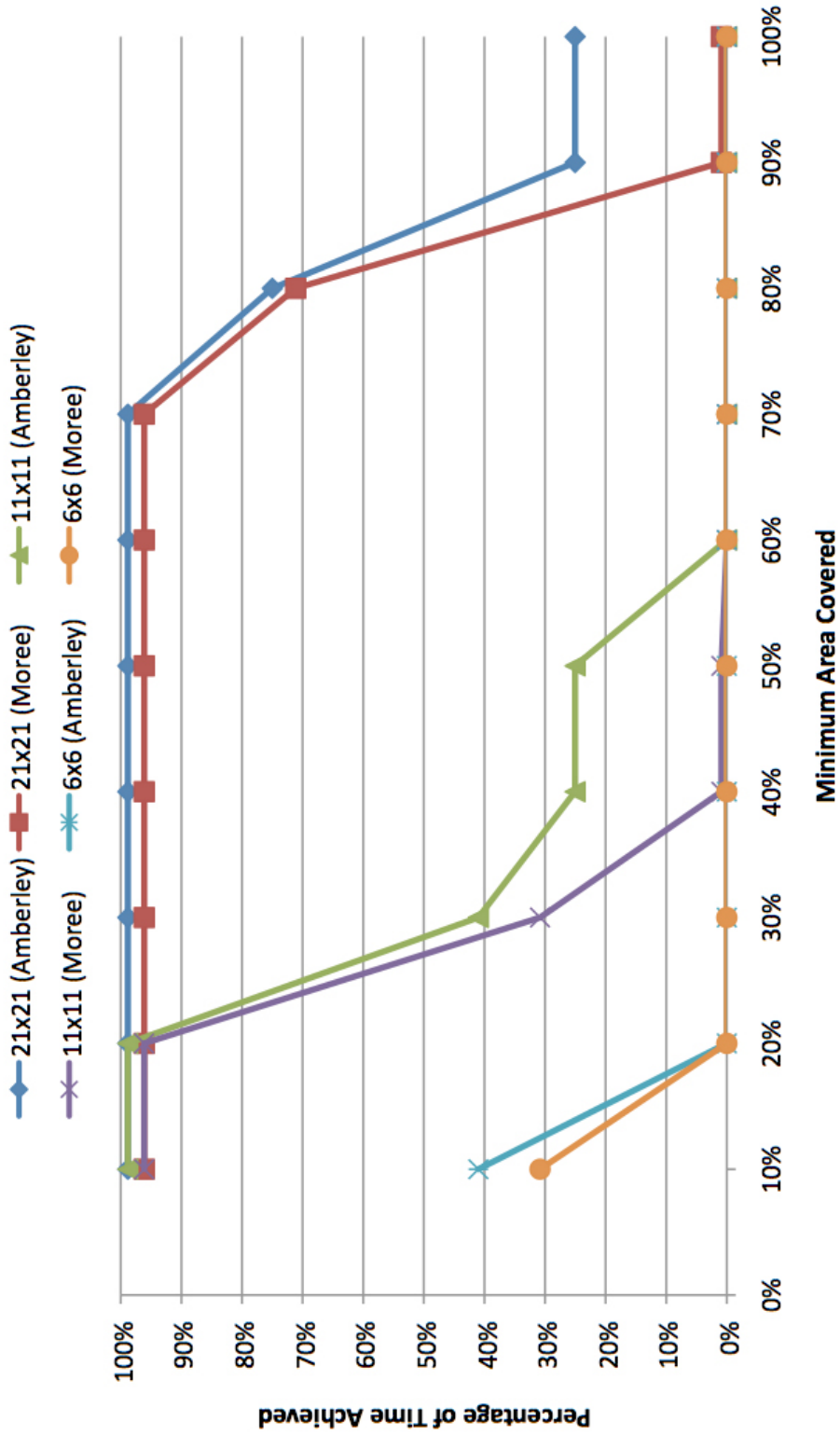


Figure 8.12: Percentage of time a minimum area is covered for the 5000 x 5000 m storage after 5 hours of application. Results are shown for all three application arrangements, 21 x 21, 11 x 11 and 6 x 6, for both Amberley and Moree wind conditions.

Table 8.4: Percentage of time a minimum area is covered for the 5000 x 5000 m storage after 5 hours of application. Including the average of the percentages of time, the aggregate application rate over that period and the total amount of monolayer applied for each arrangement. Results calculated using BOM average annual wind speeds and directions for both Amberley and Moree.

Area Covered (%):	Amberley			Moree		
	21x21	11x11	6x6	21x21	11x11	6x6
	% of Time:					
10	98.8	98.8	41.0	96.1	96.1	30.8
20	98.8	98.8	0.0	96.1	96.1	0.0
30	98.8	41.0	0.0	96.1	30.8	0.0
40	98.8	25.0	0.0	96.1	0.9	0.0
50	98.8	25.0	0.0	96.1	0.9	0.0
60	98.8	0.0	0.0	96.1	0.0	0.0
70	98.8	0.0	0.0	96.1	0.0	0.0
80	75.0	0.0	0.0	71.1	0.0	0.0
90	25.0	0.0	0.0	0.9	0.0	0.0
100	25.0	0.0	0.0	0.9	0.0	0.0
Average % of Time:	81.7	28.9	4.1	74.6	22.5	3.1
Aggregate Rate (kg/h):	47.8	45.4	41.3	52.2	48	41
Total Applied (kg):	239	227	206.5	261	240	205

8.3.4 Optimised applicator arrangements

The results for the asymmetrical applicator arrangements are presented in Table 8.5, and are shown in comparison to the 6 x 6 arrangement (which was simulated for both 3 and 6 hour application periods and moderated for Moree's wind conditions).

8.4 Discussion

8.4.1 50 x 50 m storage

According to the results in Section 8.3.1, there was no detectable difference in the aggregate application rate for all three application arrangements for both wind sites over a 1 hour application period. There was also very little difference in the average percentage of time that coverage is achieved between the 4 + 1 and 4 applicator arrangements, even for windier conditions. Whereas, the difference between the 4 and 1 applicator arrangements at both wind sites is much greater. The difference in the average percentage of time that coverage is achieved between the 4 and 1 applicator arrangements for the windier storage is quite substantial (a 32.4% reduction).

As was expected the windier conditions reduced the average percentage of time that coverage is achieved for all three applicator arrangements. The difference for each application arrangement when comparing results for calm (Amberley) and windy (Moree) conditions is:

- 15.1% reduction for the 4 + 1 arrangement,
- 12.9% reduction for the 4 arrangement, and
- 26% reduction for the single applicator.

The 4 corner applicator arrangement for the 50 x 50 m square storage proved least affected by the windier conditions of Moree and provided comparable levels of coverage with the 4 + 1 arrangement at both wind sites (i.e. only 7.2 and 5% less for Amberley and Moree's wind conditions respectively).

Table 8.5: Percentage of time a minimum area is covered for the 500 x 500 m storage after 3 and 6 hours, the average of the percentages of time, the aggregate application rate over that period and the total amount of monolayer applied for each arrangement. Results calculated for Moree only.

	3hr Response		6hr Response	
	Symmetrical 6 x 6 % of Time:	Asymmetrical 18 + 12 % of Time:	Symmetrical 6 x 6 % of Time:	Asymmetrical 15 + 1 % of Time:
Area Covered (%):				
10	96.13	96.13	96.13	96.13
20	96.13	96.13	96.13	96.13
30	96.13	96.13	96.13	96.13
40	96.13	96.13	96.13	96.13
50	96.13	96.13	96.13	96.13
60	96.13	96.13	96.13	96.13
70	96.13	96.13	96.13	91.26
80	96.13	79.27	96.13	80.68
90	58.51	56.34	66.20	31.62
100	3.77	0.90	3.77	0.90
Average % of Time:	83.13	80.94	83.90	78.12
Application Rate (kg/h):	4.1	4	4.1	3.4
Total Applied (kg):	12.3	12	24.6	20.4

8.4.2 500 x 500 m storage

Quite clearly there are substantially large differences in performance for each applicator arrangement. The most obvious trend being that when more applicators are used, more coverage is achieved and more monolayer product is used. The 6 x 6 applicator arrangement has substantially better coverage a greater percentage of the time compared to the 12 + 1 and 4 + 1 arrangements at both wind sites. However, this comes at a substantially greater monolayer requirement (Table 8.3. Also, the aggregate application rate was considerably increased for each application arrangement at the windier site. The aggregate application rate for the 6 x 6 arrangement at the windier site is 51% greater than for the calm site.

As was expected the windier conditions reduced the average percentage of time that coverage is achieved for all three applicator arrangements, however, not by much. The difference for each application arrangement when comparing results for calm (Amberley) and windy (Moree) conditions is:

- 5.7% reduction for the 6 x 6 arrangement,
- 7.4% reduction for the 12 + 1 arrangement, and
- 1.8% reduction for the 4 + 1 arrangement.

Interestingly, the 6 x 6 arrangement has 15 more floating applicators than the other two arrangements, which undoubtedly contributed to this arrangements very high levels of coverage.

8.4.3 5000 x 5000 m storage

Again, substantially large differences in performance exist between each of the applicator arrangements, which is mainly attributed to the number of applicators used. The 21 x 21 applicator arrangement has substantially better coverage a greater percentage of the time compared to the 11 x 11 and 6 x 6 arrangements at both wind sites. Clearly the 36 applicators of the 6 x 6 arrangement is sub-optimal, however, even the

121 provided by the 11 x11 applicator arrangement is only able to achieve an average percentage of time (cover is achieved) of 28.9% for the calm site.

Interestingly, the aggregate application rate does not correspond with the coverage levels achieved, as each applicator arrangement's aggregate rate is not substantially different (Table 8.4). In addition, the difference in the aggregate application rates between the calm and windy sites are not significantly different.

Again, windier conditions only slightly reduced the average percentage of time that coverage is achieved for all three applicator arrangements, 7.1, 6.4 and 1.0% reduction for the 21 x 21, 11 x 11 and 6 x 6 arrangements respectively.

8.4.4 Optimised applicator arrangements

As can be seen from the 3 hour application period results, in Table 8.5, there are no significant improvements to be had from the asymmetrical arrangement over the 6 x 6 arrangement. Although the average percentage of time coverage is achieved has been very slightly reduced with the asymmetrical arrangement, the target of 80% coverage achieved 80% of the time is still achieved with 6 less applicators. There is also a 0.1 kg/h monolayer product saving with the asymmetrical arrangement. These improvements, represent a capital and maintenance cost saving to the user over the service life of the hardware.

The results for the 6 hour application period time show that 80% coverage can be achieved 80% of the time with only 16 applicators strategically located, compared to 36 for the 6 x 6 arrangement. A direct comparison with the 6 x 6 applicator arrangement shows that there is only a drop in the percentage of time at 80, 90 and 100% levels of cover. Data from Table 8.5 suggests that the greatest reduction in the percentage of time appears at 90% coverage, which is really insignificant in light of the overall benefits. The average for the percentages of time, for the asymmetrical arrangement, are only slightly less than for the 6 x 6 arrangement. The slightly reduced percentages of time and the significant reduction in the number of applicators afford the asymmetrical arrangement a 0.5 kg/h monolayer product saving over the 6 x 6 arrangement.

In summary, the results for the asymmetrical applicator arrangements indicate that to achieve >80% coverage at least 80% of the time in a 3 hour application period, a ratio of 0.83 is required (i.e. an applicator every 0.83 ha). With an aggregate application rate of about 4 kg/h. Whereas, for an application period of 6 hours this ratio can be reduced to 1.56 (almost half the number of applicators), with a reduction in the application rate of 0.4 kg/h. Again it can be seen that shore-based applicators provide the majority of surface coverage and floating applicators mainly reduce the time taken to achieve the coverage. The key message from the results is that an asymmetrical applicator arrangement should be optimised for a particular size storage and its on-site wind conditions according to a specific set of user performance criteria.

8.5 Conclusion

Indicative analyses of the effect of different applicator numbers and arrangements for different size storages, wind conditions and application periods on the percentage of cover and the percentage of time that cover is achieved can be conducted using the simulation platform described in Chapter 7. Each one of these variables can be altered in the simulation platform to determine the effect on the percentage of cover achieved and the percentage of time that cover is achieved. This also allows the optimisation of an asymmetrical applicator arrangement for a particular size storage, set of wind conditions and user requirements. The key findings to date are as follows:

- When the average application rates for each of the three different size storages are compared proportionally (i.e. kg/h per ha), application rate appears to decrease as storage area is increased. This is mainly due to increased product beaching over short fetch distances.
- Significantly greater application rates are required for wind site compared to calm site for the 500 x 500 m size storage, but not for the 5000 x 5000 m storage.
- Shore-based applicators provide the majority of surface cover and floating applicators mainly reduce the time taken to achieve coverage.

- An asymmetrical applicator arrangement should be developed according to on-site conditions (namely, storage size and prevailing wind conditions) and user specified performance criteria (namely, minimum application period, minimum area to be covered and the minimum percentage of time that area is to be covered) in order to reduce the number of applicators required to achieve cover and the monolayer requirement, while potentially increasing coverage levels.
- For the 500 x 500 m storage with the asymmetrical applicator arrangements developed for the windy site's wind conditions, reducing the application period from 6 to 3 hours (i.e. the time taken to re-establish coverage from zero), requires almost twice as many applicators. Mostly floating applicators were required.

It is the author's recommendation that the UDF analyses involving the simulation platform and Post-Process 1, begin with collation of the following information: (1) size and orientation of the storage, (2) BOM annual historical wind speed and direction frequency analysis for the site, (3) user-specified minimum application period, area covered and percentage of time that area is covered. Once this information has been given, a number of iterative simulations can be undertaken to develop an asymmetrical applicator arrangement optimised to meet the above key performance criteria as specified by the user.

Chapter 9

Scope of the ‘Universal Design Framework’

9.1 Introduction

The Universal Design Framework (UDF), although not yet refined or in integrated software form, encapsulates the processes involved in determining key information the user (being anyone choosing to employ a monolayer-based evaporation mitigation system) would want to know.

The processes outlined requires a number of inputs, principally user performance criteria, water storage factors, monthly climate data, and water quality and biological factors. This necessary information is used in four key analysis stages, which involve the simulation platform (as detailed in Chapter 7) in combination with two post-processes (Post-Process 1 is detailed in Chapter 8 and Post-Process 2 is detailed in Section 9.6 below) and a monolayer product decision table (detailed below in Section 9.3). The required inputs used in the four key analysis provide important information for the design, planning, installation and operation/management of the monolayer application system. An overview of the UDF processes is illustrated in Figure 9.1.

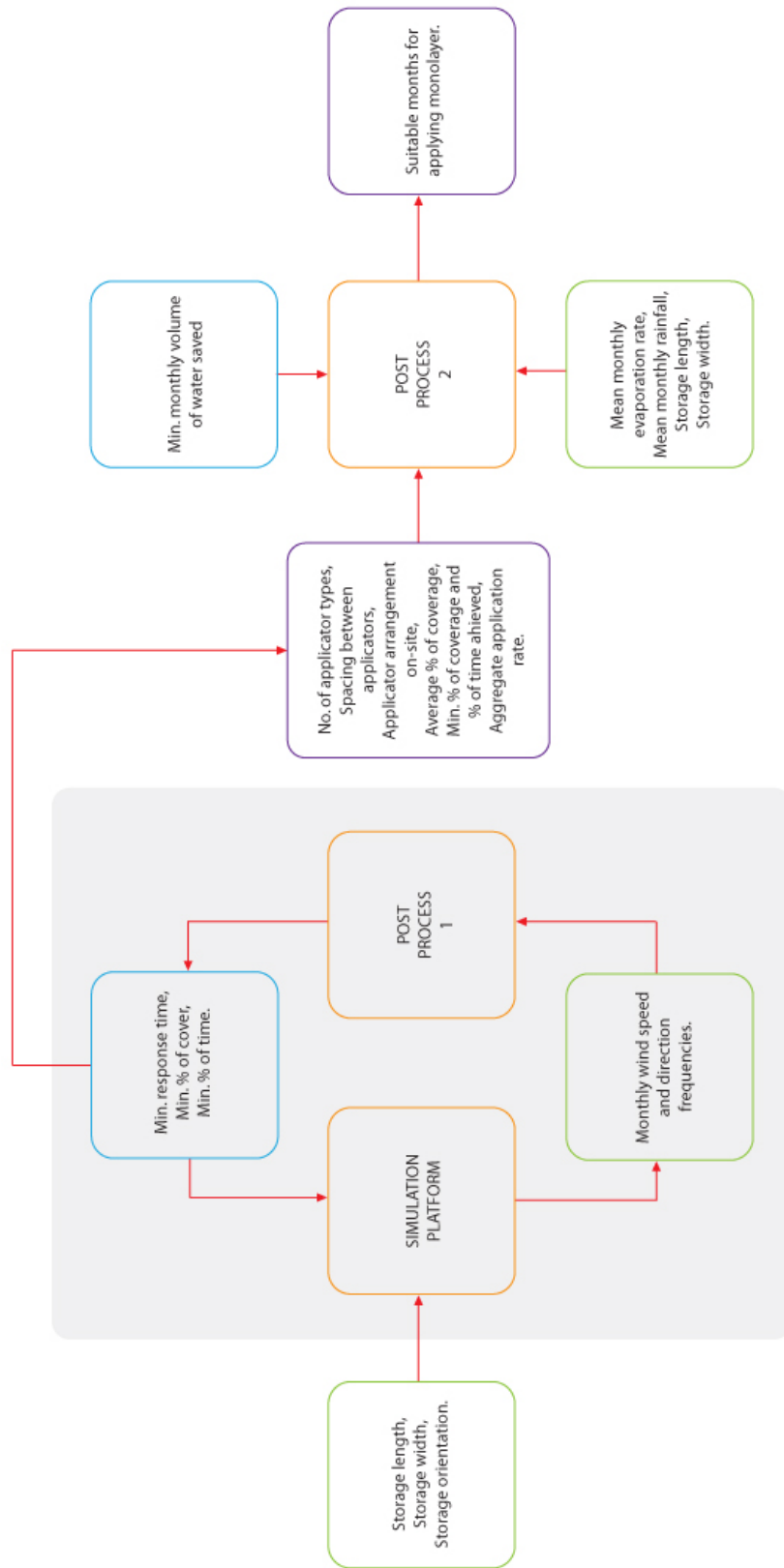


Figure 9.1: Overview of the UDF processes, which involves input of necessary information, analysis of the information to inform design, planning, installation and operation/management of a monolayer application system. Green boxes represent inputs, orange boxes represent analysis, blue boxes represent user performance criteria and purple boxes represent outputs. The grey box represents the iterative modelling process.

The required inputs are effectively the major influencing factors and/or indicators that when considered together as a whole, within the UDF processes, provide important insights into the expected monolayer performance characteristics. This is an important step forward, especially when considering that the poor performance of many field trials can be reasonably attributed to a limited understanding of the degree to which some factors can influence monolayer performance. Therefore, the significance of each of these influencing and/or indicating factors on the monolayer performance is explored in this chapter, including how each of them is used within the UDF and in which analysis.

This chapter concludes with a ‘demonstration’ of the UDF (Section 9.7) to illustrate the process.

9.2 Overview of analyses

The analyses incorporated within the UDF processes have been specifically developed during this research to allow a deeper understanding of the effect of the influencing factors on monolayer performance to be gained. These analyses are as follows:

Analysis 1 is monolayer product/s selection via a decision table. Although this analysis is not shown in Figure 9.1, it is a relatively straight forward process, which involves input of site-specific water quality and biological factors which are then matched within a decision table to determine a suitable monolayer product/s (Section 9.3).

Analysis 2 is performed with the simulation platform, and provides an estimate of surface coverage (with monolayer) and the application rate for a range of different wind conditions. This information is then analysed in Post-Process 1, using BOM wind frequency data, to determine the percentage of time a specific percentage of coverage will be achieved. This allows the user to determine a suitable monolayer application system design (Section 9.7.4).

Analysis 3 is also performed with the simulation platform, but with much more detailed wind conditions (841 compared to the standard 33 as used in Analysis 2), to

provide an estimate of surface coverage, which applicators to use and their respective application rate for each wind condition. This information is then used as a decision table to inform the real-time application strategies on-site (Section 9.5).

Analysis 4 The fourth analysis, which is basically Post-Process 2, allows determination of which months are suitable for applying monolayer using information output from the second analysis (Section 9.7.6).

As indicated by the grey box in Figure 9.1, the analyses that occur with the simulation platform and Post-Process 1 may need to be re-run a number of times in order to satisfy the user specified performance criteria. The majority of outputs are derived from this iterative modelling process. Each of the output/s from the UDF processes are critical pieces of information that will inform:

- planning: number of applicators required, expected performance according to the aggregate application rate, average percentage of cover, monthly volume of water saved and suitable months for monolayer application.
- design: the physical form of the applicators and the specification of componentry capable of satisfying the application requirements.
- installation: optimal placement of applicators on-site.
- operation: hour-by-hour monolayer application (yes/no decision) based on maximum and minimum wind speed thresholds, expected drift rates and spreading angles under wind conditions (or spreading rate under zero-wind conditions); which applicators to apply monolayer from according to wind direction and the application rate for those applicators.

9.3 Monolayer product decision table

As indicated in Chapter 3, a number of key indicators that best predict the performance of a specific monolayer product applied to a reservoir have been selected for use in a decision support system. These key indicators are algal blooms, UV absorbance, water colour and storage size. The significance of each of these indicators are as follows:

- Algal blooms: have the potential to disrupt artificial monolayers by increasing the population of monolayer-degrading bacteria, and by producing surface-active compounds.
- UV absorbance: high concentrations of UV-absorbing organics in the water also increase the activity of monolayer-degrading bacteria and the concentration of surface-active compounds.
- Water colour: is an indicator for the amount of dissolved humified organics (low UV absorbance). Colours of interest are dark browns or blacks, which indicate high levels of humified organics and the likelihood of monolayer degrading bacteria and surface-active compounds. Most other colours indicate low levels.
- Storage size: a large storage is an indicator of the volume of water held. A large volume of water indicates a low concentration of dissolved humified organics.

A decision table capturing the key indicators for each of the three SEQ benchmark reservoirs and the best match monolayer product for the combination of these indicators has been produced (Table 9.1). This decision table allows the user to make numerical comparisons between the SEQ benchmark reservoirs and their own (once characterised with respect to the key indicators) to determine a best match. The best match will then identify the most suitable monolayer compound/s for their reservoir.

Table 9.1: Decision table capturing the water quality attributes of three water storages in south-east Queensland (Pittaway & van den Ancker 2010) were matched with the performance specifications of three monolayer compounds to predict which product will best perform on a given storage.

Water Storage:	Algal Bloom:	UV Absorbance:	Water Colour:	Storage Size:	Suitable Monolayer/s:
Cooby Dam	no	0.14	clear	306ha	C16OH, C18OH or C18E1
USQ Ag. Plot	yes	0.31	pink	0.01ha	C18OH
Narda Lagoon	no	0.45	brown	2ha	C18OH

The monolayer compound C16OH is susceptible to bacterial degradation, but less susceptible to brown water microlayer disruption. The C18E1 monolayer is more micro-

bially resilient, but very susceptible to brown water microlayer disruption. The C18OH compound is more resistant to both microbial degradation and brown water disruption and is suitable for use on water reservoirs with a wider range of water quality attributes (Table 9.1). As indicated by Table 9.1, the large volume of water held in Cooby Dam indicates a low concentration of dissolved humified organics and the low risk of algal bloom formation indicates that all three monolayer products could be considered for use. However, for the USQ Agplot, which was known to be affected by algal blooms, currently only the C18OH product is suitable. C18OH is also the only suitable product for Narda Lagoon reservoir as it has high concentrations of UV-absorbing organics and a dark brown water colour.

Although only three monolayer products have been assessed in the laboratory with respect to microbial degradation and microlayer disruption, as new monolayer products become available, they can be run through the same tests and entered into the UDF to expand the capacity of the current decision table. Nevertheless, prospective users can enter the basic water quality attributes of their water storage to compute the best product match to ensure optimal product performance.

9.4 Iterative modelling and Post-Process 1

The objective of this analysis is to develop a customised applicator arrangement through an iterative modelling process until the user-specified performance criteria is satisfied. This analysis involves the use of the simulation platform, which is thoroughly detailed in Chapter 7, and Post-Process 1, as detailed in Chapter 8. The first step in the process is to input the following into the simulation platform: length and width of storage, storage orientation, number of applicators and their locations and the desired response time. Then a series of wind interval data is input into the simulation. The standard wind intervals used are 5, 10, 15 and 25 km/h wind speeds for every 45 degree wind direction and one for 0 km/h, which is a total of 33 different wind conditions. Output data is then grouped according to their respective wind conditions and includes the percentage of coverage, aggregate application rate and time to steady-state for each.

This output data from the simulation platform is further analysed in Post-Process 1 for each month according to monthly wind speed and direction frequency data (available from the BOM). Post-Process 1 basically determines the percentage of time that a particular percentage of cover will occur for each month. This data is then checked against the user-specified performance criteria of minimum percentage of cover, the minimum percentage of time that cover is achieved and the minimum response time.

This process is basically repeated until the user-specified performance criteria has been satisfied with the minimum amount of applicators in the best possible arrangement. It is with this arrangement that the average percentage of cover, the aggregate application rate and the percentage of time that a particular percentage of cover occurs must be determined for each month (using the respective BOM monthly wind speed and direction frequency data). Once this has been done the floating applicators are then removed from the simulation platform inputs and only the shore-based applicators are kept. The same analysis is then run to determine the aggregate application rate for each month, again using the respective monthly wind speed and direction frequency data.

9.5 Detailed wind condition modelling

This stage involves a more through analysis using a full set of wind intervals. The wind intervals used are 0 and 4 to 27 km/h wind speeds for every 10 degree wind direction, which is a total of 841 different wind conditions. One simulation is run for all applicators and another for only shore applicators, using the 841 different wind conditions for each. This produces two tables. *Table A*, which uses all applicators, is effectively the application strategy to be used after a high wind speed or rainfall event to re-establish steady-state conditions. *Table B*, which uses only shore-based applicators, is the application strategy to be used once steady-state conditions have been achieved.

The information within each table details the applicators that were and were not used for dosing and the application rate for each for all 841 different wind conditions. This information is key to the real-time automation of the application system as it can be

matched with a wind condition being experienced on-site to determine which applicators to use for dosing and the application rate for each applicator. Therefore, these data constitute a decision table for the real-time automation of the application system which will provide variable dosing according to on-site wind speed and direction. An illustrative example of both Tables A and B are detailed in Appendix D, and an example of their use in real-time to automate the application of monolayer on-site is detailed in Section 9.7.5.

9.6 Post-Process 2

The objective of this analysis is to provide the user with an indication of: (1) monthly expected volume of water saved, (2) monthly quantity of monolayer used and (3) most suitable months for monolayer application. These outputs are calculated by using data output from Section 9.4, specifically, the average percentage of coverage, aggregate application rate, time to steady-state (maximum coverage achieved by all applicators used for dosing) and aggregate application rate (for all applicators and for when only shore-based applicators are used). This data is provided for each month of the year. In addition to data used from Section 9.4, historical monthly mean evaporation and rainfall days ≥ 1 mm are also used in this analysis.

(1) monthly expected volume of water saved is determined by using the mean monthly evaporation rate then multiply that by the surface area of the storage to calculate the volume of water lost in that month. This volume of water lost is then multiplied by the average percentage of coverage for the month. This is now the volume of water saved according to the average coverage, assuming the average coverage provided the monolayer is 100% effective at reducing evaporation. However, as is well known from previous field trial results, monolayer is not 100% effective at reducing evaporation and is highly variable. Therefore, to calculate a more representative amount of water saved by the monolayer, a monolayer evaporation reduction factor (ERF) of 0.3 is applied to the volume of water saved by the average coverage. For example, if the monthly evaporation rate was 0.3 m, the average cover provided by the monolayer is 50% and the surface area of the storage is 100,000 m² then the volume of water saved by the

monolayer is 4.5 ML.

(2) monthly quantity of monolayer used is determined by multiplying the aggregate application rate (for all applicators) by the time to reach steady-state and then by the number of rain days and/or high wind speed event ($> U_{MAX}$) for the month. This provides a quantity of monolayer that has been applied for every rain day or high wind speed event according to the time taken to re-establish a steady-state condition. This is done as it is assumed all monolayer coverage is lost after a rainfall day or high wind speed event, therefore coverage needs to be re-established from zero. For example, if the aggregate application rate for the whole storage is 5 kg/h, the time to reach steady-state is 5 hours, there are 5 rainfall days in the month and no wind speed events $> U_{MAX}$, then the amount of product applied is 125 kg and the total time elapsed to reach steady-state is 25 hours. This represents the total amount of product applied when all applicators were used in dosing and the total time that all applicators were used to dose.

Once steady-state conditions have been re-established it is assumed that the floating applicators can be turned-off until another rainfall or high wind speed event occurs. As was concluded in Chapter 8, floating applicators mainly provide quick response in establishing coverage, whereas shore-based applicators provide the majority of coverage. Therefore, it is assumed that once steady-state conditions have been re-established the shore-based applicators would be capable of maintaining coverage. This strategy provides a significant monolayer product saving as once steady-state conditions are reached the coverage provided by the floating applicators largely overlap the coverage provided by shore-based applicators. Hence, once steady-state conditions have been reached, there is little to no benefit in continued dosing from floating applicators.

The amount of product used by the shore-based applicators once steady-state conditions have been reached is then determined by multiplying the aggregate application rate for shore-based applicators only by the time these applicators are used for dosing. The time these applicators are used for dosing is calculated by subtracting the rainfall days from the total days in the month, then multiplying the days left by the number of hours in the day. It is assumed that the application system is active for 24 hours a day. Then the total time all the applicators are used for dosing (which was calculated previously)

is subtracted from the time that only shore-based applicators are used. This time is then the total time all the applicators are used for dosing. For example, if the aggregate application rate for shore-based applicators only is 2.5 kg/h, there are 5 rainfall days, 30 days in the month and the total time all applicators are used for dosing is 25 hours, then the total amount of product applied by shore-based applicators only is 1,437.5 kg.

Then the total amount of product applied by all applicators is added to the total amount of product applied by shore-based applicators. This represents the total amount of monolayer applied in the month.

(3) most suitable months for monolayer application is determined by comparing each months volume of water saved to the user-specified performance criteria of minimum acceptable volume of water saved. The months that satisfy this criteria are the months suitable for monolayer application.

9.7 Demonstration of the UDF

9.7.1 Site selection

The user in this demonstration of the UDF comes from Amberley in Queensland and owns a regular rectangular ring tank water storage. This dam is fairly typical of the types of storages to be found throughout most agricultural areas in Australia. A ‘Google Earth’ satellite image of the dam is provided in Figure 9.2.

9.7.2 Gathering necessary information

The storage length and width has been measured using the standard ‘Google Earth’ measurement tool. The storage measures 300 meters in width by 460 meters in length, which gives a surface area of 13.8 ha. As this storage is >10 ha in surface area it is a good candidate for monolayer based evaporation mitigation. The storage is located 27°38’48” South longitude and 152°44’21” East latitude. This storage’s longest fetch is oriented at 14° clockwise from North.



Figure 9.2: ‘Google Earth’ satellite image of the rectangular ring tank storage used in this demonstration. The storage is located at Amberley in Queensland and has a width of 300 meters and a length of 460 meters, which is a surface area of 13.8 ha.

Monthly wind speed and direction frequency data is available from the BOM; however, at the time of this analysis this data was not free and was purchased at a modest cost of AU\$33. The closest BOM automatic weather station to this storage was found to be Amberley Airport, Qld, 27.63° South and 152.70° East (BOM station number: 040004) 2.6 km away from the storage and as this is open plains country unimpeded by significant woodland this provides a good indication of the historical wind conditions for this site. Historical data for monthly mean rainfall days ≥ 1 mm were also gathered for this weather station from the BOM online at no cost¹. Data for the monthly evaporation rate for this location was gathered via the ‘NCEA Ready Reckoner’ at no cost online².

Next, a number of user-specified performance criteria were nominated by the user for the UDF analyses to be conducted. The following user criteria were specified:

- Minimum response time: 3 hours
- Minimum surface coverage: 60%
- Minimum percentage of time coverage is achieved: 90%
- Minimum acceptable volume of water saved: 10 ML/month

Although water quality and biology information was not available for this site, key indicators required for the monolayer product selection were nominated by the author to demonstrate a theoretical analysis. The following key indicators were specified:

- Algal blooms: yes
- UV absorbance: 0.3
- Water colour: light brown
- Storage size: 13.8 ha

¹Bureau of Meteorology online climate database: <http://www.bom.gov.au/climate/data/>

²The National Centre for Engineering in Agriculture Ready Reckoner is available online at this address: <http://www.readyreckoner.ncea.biz/>

9.7.3 Determination of suitable monolayer product/s

The water quality and biological indicators as specified by the user were matched with the water quality and biological indicators for the three SEQ benchmark storages in Table 9.1. The Amberley storage best matched the USQ Ag. Plot as it suffers for algal blooms and has a similar UV absorbance. Although its water colour did not match with any of the three benchmark storages, it did not have brown water, which usually indicates low levels of humified organics (see Section 9.3). The water volume, although not as large as Cooby Dam's, is substantially greater than Narda Lagoon's, which means that any monolayer-degrading bacteria or surface active compounds should not be too concentrated. However, the overriding key indicator is algal bloom and since this storage suffers from them, there is a high chance of monolayer-degrading bacteria. Therefore, the C18OH monolayer product would be the best suited for this storages water quality and biology.

9.7.4 Determination of optimal application system

As a first step, in designing a customised arrangement, a wind rose of the annual wind speed and direction frequencies for Amberley was plotted to determine the major prevailing wind direction/s (Figure 9.3). As the majority of wind is predominately from the North East and Easterly directions the general approach was taken to concentrate applicator numbers near these shores. The next step was to specify a number of applicators and their locations and this is done completely at the users discretion. As a first go, a 4 x 5 symmetrical grid style applicator arrangement was specified (i.e. 20 applicators in total). However, a number of simulations were run and each time the number and locations of the applicators were altered until the user-specified 60% minimum surface cover at least 90% of the time was achieved with the least number of applicators. Before any of these simulations were run the storage length, width and minimum response time were also set.

After a number of iterative simulations an asymmetrical applicator arrangement, reduced to 17 applicators, was found to satisfy the performance criteria (Figure 9.4). Table 9.2 details the data output by the simulation platform for this applicator ar-

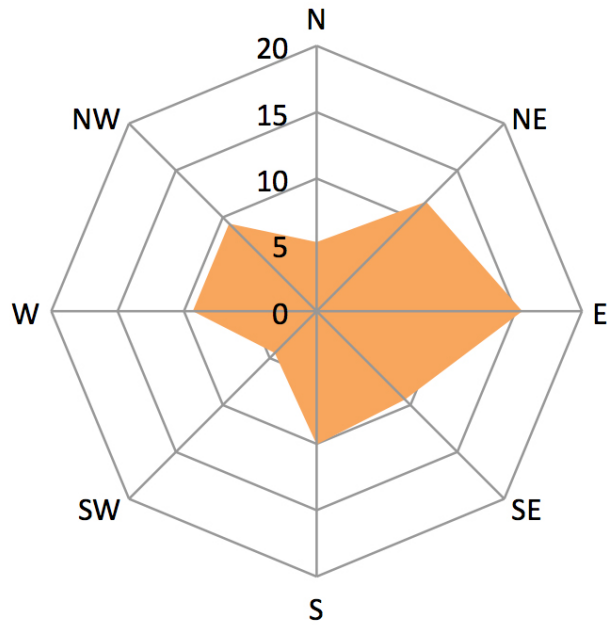


Figure 9.3: Wind rose of the annual wind speed and direction frequencies for Amberley, QLD.

rangement, which was then analysed in Post-Process 1 to determine the percentage of time a certain level of coverage is achieved (Table 9.3). As can be seen in Table 9.3, the minimum coverage level of 60% is achieved 93% of the time within a 3 hour response time. Therefore, this applicator arrangement satisfied the user-specified performance criteria set out in Section 9.7.2.

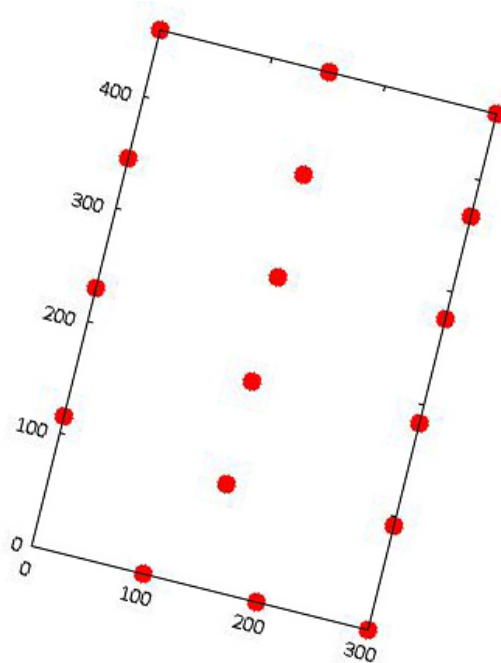


Figure 9.4: Asymmetrical applicator arrangement that satisfied the user-specified performance criteria by providing at least 60% cover at least 90% of the time within a 3 hour response time for the Amberley dam of Figure 9.2. As shown, a greater density of applicators are required on the East and South shores. (There is no applicator at the origin (0,0).)

9.7.5 Decision tables for real-time application

As described previously, one simulation is run for all applicators and another for only shore applicators, using the 841 different wind conditions for each. This produces two tables. One table will be called Table A and the other Table B from now on for illustrative purposes. Tables A and B are reproduced, in a truncated format due to their cumbersome size, in Appendix D: Table A has more applicators and therefore a higher general application rate, whereas Table 2 less applicators and a lower general application rate. Tables A and B can then be used in real-time by simply matching the on-site measured wind condition with the closest similar wind condition in the appropriate table to determine which applicators to use for dosing and the application rate for each. A real-time application strategy of the following form can be employed by using information within decision Tables A and B (Appendix D):

Table 9.2: Data output from the simulation platform, which details the percentage of cover achieved, the aggregate application rate and the time to steady-state for each wind condition.

Wind speed (km/h):	Wind Direction (°):	Area Covered (%):	Application Rate (kg/s):	Time to Steady State (hr):
0	0	100.00	0.0002	0
5	0	59.38	0.0000	0
15	0	76.73	0.0006	0
25	0	63.66	0.0009	0
5	45	77.39	0.0001	0
15	45	88.43	0.0007	0
25	45	75.73	0.0011	0
5	90	0.8067	0.0001	0
15	90	85.66	0.0008	0
25	90	71.56	0.0013	0
5	135	85.84	0.0001	0
15	135	90.52	0.0009	0
25	135	75.32	0.0014	0
5	180	61.85	0.0000	0
15	180	84.41	0.0006	0
25	180	75.49	0.0010	0
5	225	73.29	0.0001	0
15	225	82.89	0.0008	0
25	225	66.94	0.0011	0
5	270	81.33	0.0001	0
15	270	76.32	0.0008	0
25	270	58.15	0.0012	0
5	315	0.8000	0.0001	0
15	315	88.05	0.0009	0
25	315	68.79	0.0012	0

Table 9.3: Data output from Post-Process 1 using the percentages of cover for each wind condition, as output from the simulation platform (Table 9.2), and applying a weighting for the frequency of that wind condition occurring. The frequency weightings were derived from BOM wind speed and direction frequency data for Amberley, Qld.

Area Covered (%):	% of Time Achieved:
10	98.83
20	98.83
30	98.83
40	98.83
50	98.83
60	92.96
70	86.79
80	59.17
90	29.13
100	25.04

- *Calm conditions (≤ 4 km/h):* The application strategy for calm conditions would need to include two ‘if’ statements:
 1. if the last condition was a high wind or rainfall event assumes cover is zero (i.e. all pre-existing coverage was lost). Select the calm wind condition in Table A and initiate this application rate with the appropriate applicators, which for calm conditions all applicators are used;
 2. if the last condition was a wind condition, check the average percentage of cover to expected for that last wind condition to determine the coverage deficit. Apply the required amount of monolayer product for this deficit area with all applicators.
- *Wind conditions - After high wind or rainfall event (> 27 km/h or > 1 mm):* Determine the on-site wind condition and match it with the closest similar wind condition in Table A. Initiate this application rate with the appropriate applicators until steady-state is achieved or until the on-site wind conditions change again.
- *Wind conditions - After steady-steady state ($4 < U \leq 27$ km/h):* Determine the on-site wind condition and match it with the closest similar wind condition in Table B this time. Initiate this application rate with the appropriate applicators until the on-site wind conditions change again.

The above application strategy illustrates a simple way of employing data produced from UDF analyses to achieve variable dosing according to on-site wind conditions. This strategy could simply be looped through every 1, 15, 30, 60 or even 120 minutes (or any other appropriate time-step) to re-determine which applicators to dose with and the application rate for each according to on-site wind conditions.

9.7.6 Expected performance of application system

Once a suitable applicator arrangement has been selected based on the BOM annual average wind speed and direction frequency data, a similar analysis is now run for

monthly wind frequency data. This analysis also involves a number of iterative simulations with the simulation platform and Post-Process 1 until the time taken to reach steady-state for all of the 33 wind conditions is determined. For the Amberley dam theoretical analysis it was found that steady-state is achieved after 9 hours. Results are then recorded for the average percentage of cover and the aggregate application rate for each month.

Then, to determine the aggregate application rate once steady-state has been achieved, another analysis is performed with the simulation platform and Post-Process 1, however this time only with the shore-based applicators. This is done as once steady-state conditions are re-established, turning off the floating applicators reduces the aggregate application rate without compromising the average percentage of cover. The information gathered from both analyses, with all applicators and with only shore applicators, is summarised in Table 9.4. Also shown in Table 9.4 is the monthly historical climatic data required for the final analysis using Post-Process 2.

Table 9.4: Data required for Post-Process 2. These data were determined via the simulation platform and Post-Process 1 using monthly wind speed and direction frequency data from the BOM for Amberley, Qld. Simulations were run firstly for all applicators, and secondly for the shore-based applicators only.

Month:	Evap. Total (mm):	No. Rain Days:	No. Days:	Avg. Cover (%):	App. Rate All (kg/h):	App. Rate Shore (kg/h):
Jan	231.9	8.3	31	88.18	2	1.8
Feb	188.1	8.4	28	88.18	1.8	1.6
Mar	186.2	7.9	31	90.79	1.7	1.5
Apr	144.6	5.2	30	92.04	1.4	1.2
May	111.9	5.4	31	90.90	1.3	1.1
Jun	94.6	4.2	30	90.21	1.3	1.1
Jul	106.8	4.2	31	89.74	1.2	1
Aug	135.0	3.8	31	88.11	1.4	1.2
Sep	171.6	4.2	30	87.40	1.7	1.5
Oct	204.7	6.7	31	85.54	1.9	1.7
Nov	217.3	7.1	30	86.24	2	1.7
Dec	236.5	8.3	31	86.45	2	1.7

The information detailed in table 9.4 are necessary for conducting this last analysis to give the user an idea of the expected performance of the application system. This information is provided in the form of the potential monthly amount of water to be saved, the amount of monolayer product used and which months are suitable for monolayer application. This information is determined according to the user-specified performance criteria, namely, the monolayer based evaporation mitigation system must save a minimum of 10 ML of water a month and the monolayer has an evaporation reduction factor (ERF) of 30%. The results of this analysis are provided in Figure 9.5 and summarised in Table 9.5. When the results are compared with the user-specified performance criteria, a minimum of 10 ML of water to be saved each month, the months for cost effective monolayer application are September through to March.

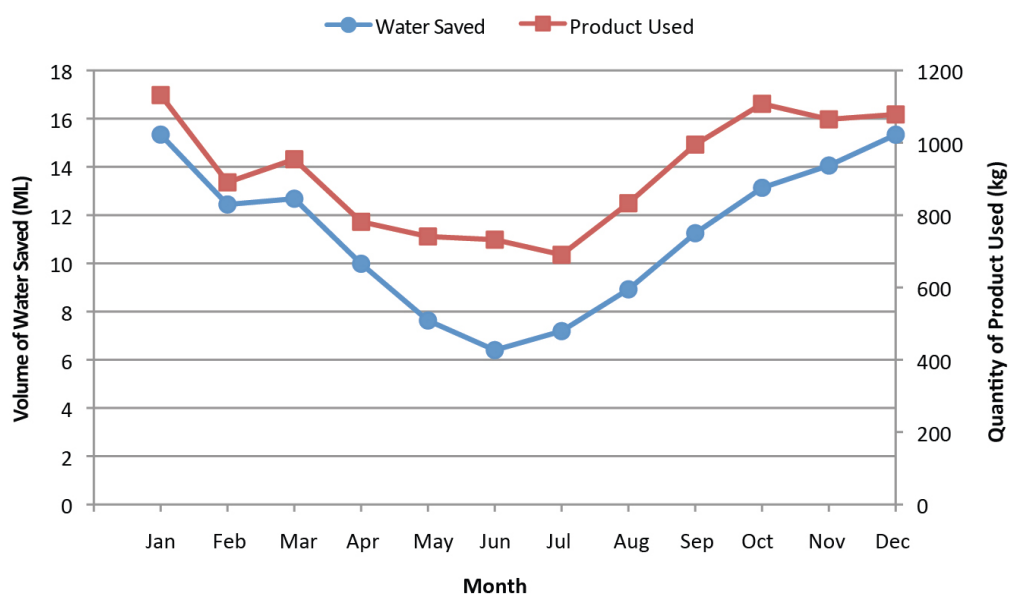


Figure 9.5: Volume of water saved by the monolayer for each month of the year and the quantity of monolayer product used to achieve these savings.

With this information the user could even start to do some economic calculations for the cost of the monolayer material used, which can be divided by the volume of water saved to determine a cost for every ML of water saved. This analysis was not done, as an accurate economic analysis involves the cost of a commercially available C18OH monolayer product, which is currently unavailable. It is envisaged that this analysis will be important for the user, from an economic point of view, as more monolayer

products become commercially available (such as the new CRC Polymers monolayer products).

Table 9.5: Data output from Post-Process 2 detailing the monthly quantity of monolayer product used and the volume of water saved.

Month:	Quantity of Product Used (kg):	Volume of Water Saved (ML):
Jan	1114.84	15.34
Feb	875.32	12.44
Mar	939.97	12.68
Apr	769.96	9.98
May	730.12	7.63
Jun	721.36	6.40
Jul	680.56	7.19
Aug	821.44	8.92
Sep	980.56	11.25
Oct	1091.71	13.13
Nov	1047.82	14.06
Dec	1061.26	15.33

9.8 Summary and conclusion

Through the holistic approach provided by the UDF it has been demonstrated that the evaporation suppressing performance of monolayer can be optimised according to a user's site-specific conditions and user requirements. The information provided by the UDF to the user (as demonstrated in the example in Section 9.7 above) will aid in the following ways:

Design: Application rates for each applicator gives the designer an idea of the expected flow rates for pump specification (if the monolayer is dosed as a liquid) or monolayer quantities for specification of another suitable type of mechanical apparatus. Storage reservoir volumes and/or top-up periods for each applicator can also be determined

from this information. Depending on the optimal applicator arrangement determined, some may be located near the shore (i.e. shore-based) whereas other may be located away from the shore (i.e. floating). This information will influence the physical form of the applicators. For instance, an applicator near the shore may have its monolayer storage reservoir located on the dam wall, whereas, an applicator located away from the shore might have its storage reservoir on board or tethered next to it. The physical form of shore-based or floating applicators could vary quite significantly (Appendix E).

Planning: Although the information provided by the UDF to aid in the design, specification and construction of the application system involves a fair amount of planning, information of the monthly application rate and volume of water saved allows the user to determine which months are potentially more feasible/suitable for monolayer application. This can also allow the user to do some economic projections (i.e. how much will the monolayer material cost and how much will it cost to save a megalitre of water).

Installation: Information of where to locate applicators on-site in order to achieve suitable levels of coverage (according to user specified performance criteria) is provided by the UDF. Therefore, the guess work of where to place applicators on-site is removed during installation.

Operation/Management: The two decision charts (e.g. Appendix D), which are determined for a specific application system that has been designed according to user specific conditions and performance criteria, enable real-time application strategies to be determined for almost every wind condition that can be encountered on-site. Specifically this allows strategic selection of applicators that are going to allow optimal surface coverage based on the wind direction, and also varying quantities of monolayer to be dosed by applicators based on the effective surface area that each can service for the wind speed and direction.

It is anticipated (although it cannot be proven without direct, full-scale experimentation) that through this approach the generally poor performance of monolayer in past field trials may be largely avoided.

Chapter 10

Conclusions and recommendations

A Universal Design Framework (UDF) has been created to allow anyone interested in implementing a monolayer-based system for evaporation mitigation to determine a suitable monolayer product/s, application system and appropriate application strategies for their site-specific environmental conditions and desired performance criteria. Central to the determination of the above information is a monolayer simulation platform, which allows the user to model different storage sizes, application rates, numbers of applicators, their locations and wind conditions, to predict/estimate monolayer surface coverage and amount of monolayer used.

The information determined from this framework will aid the user during both the design, planning and installation stage, and the day-to-day operations of employing a monolayer application system for evaporation mitigation.

In this chapter, the achievement of the research objectives (as outlined in Section 1.2.2) is discussed and the recommended further work is described.

10.1 Achievement of objectives

Objective 1 - Formulation of the UDF

Factors that influence monolayer performance have been identified, including those that will need to be taken into consideration for the design, planning, installation and operation/management of the application system. In addition, a working environmental range/boundaries for monolayer use as well as the UDF has been specified. A UDF has also been formulated, which incorporates all of the important influencing factors and environmental boundaries identified. To inform the next development stages of the UDF, certain information and processing requirements were then identified. All of the above information pertaining to the achievement of Objective 1 can be found in Chapter 3.

Objective 2 - Large-scale laboratory study of monolayer dispersion characteristics

Monolayer materials suitable for evaporation suppression have been identified (Chapter 2), with C18OH chosen as the best candidate monolayer material for experimental use. A C18OH in water-emulsion has also been formulated for ease of application in empirical laboratory work and for possible future field trials (Chapter 4). Using this C18OH water-emulsion, the following surface transport dynamics have been characterised:

1. spreading rate and spreading pattern for calm wind conditions (Chapter 4), and
2. drift rate and spreading pattern for a range of wind conditions when continuous application would be required (Chapter 6).

Algorithms have also been derived from this experimental work in order to calibrate the simulation platform.

Objective 3 - Simulation platform development and demonstration

A basic two-dimensional simulation platform has been developed, which allows the estimation/prediction of monolayer surface coverage and application rate for different applicator arrangements, wind conditions and spatial scales. The model was calibrated with the algorithms derived from the laboratory studies of the surface transport char-

acteristics of the C18OH in water-emulsion. All information pertaining to the development of the monolayer simulation platform can be found in Chapter 7 and Appendix B.

The simulation platform was then tested in a theoretical study using different wind conditions, storage sizes and application durations. Through this study the utility and robustness of the simulation platform was demonstrated, specifically its ability to estimate the percentage of monolayer cover; the percentage of time that cover is achieved/maintained; which applicators to apply from and their respective application rates for each scenario. A theoretical demonstration of the monolayer simulation platform can be found in Chapter 8.

Objective 4 - Scope and demonstration of the UDF

A decision table that allows the user to make numerical comparisons between the South East Queensland (SEQ) benchmark reservoirs and their own to determine the most suitable monolayer compound/s for their storage has been created. Furthermore, a process for using the UDF to determine a customised applicator arrangement with the simulation platform has been developed. The monolayer product decision table has been incorporated as part of this process. The capability of the UDF to determine suitable monolayer product/s, optimal application system, decision criteria for real-time application and the expected performance of the application system was then demonstrated in a theoretical study.

All of the above research pertaining to the achievement of Objective 4 can be found in Chapter 9.

10.2 Recommended further work

10.2.1 Expand monolayer product decision table

The principal requirement here is to expand the current monolayer product decision table employed in the UDF to include the characterisation of more water storages with respect to the key indicators that influence monolayer performance. In addition,

more monolayer products will need to be assessed for their performance on these extra water storages to determine a best match. This will potentially provide the user with more monolayer product options, which have been matched to a larger variety of water storage key indicators.

10.2.2 Laboratory characterisation of more monolayer products

Determine the dispersion characteristics of more monolayer products on the water surface in the laboratory for different wind conditions. This would be done using the same materials and methods as those used to characterise the dispersion characteristics of C18OH. Ideally, all of the monolayer products included in the monolayer product decision table would be studied with respect to spreading rate, drift rate and spreading angle. Then algorithms would need to be derived from the study of these dispersion characteristics for each monolayer product.

10.2.3 Monolayer simulation platform development

Develop the simulation platform to enable the calculation of coverage and application rate for dynamic changes in wind conditions (i.e. hourly changes in wind conditions). This will reduce the application rate for floating applicators since they will be aware of existing product in their region of application. A satisfactory shoreline absorption model will also need to be developed to predict the amount of monolayer material lost and the amount available for redistribution after a wind shift. In addition, time-critical weathering effects such as volatilisation, submergence and biological degradation will also need to be characterised and modelled. This can be incorporated as a sub-model in the simulation platform.

10.2.4 Validation of the UDF

Validation of UDF - Planning mode

The UDF process should of course, be implemented and validated in full-scale monolayer field trials to verify the potential performance benefits, to identify any shortcomings or omissions, and to generally optimise/calibrate the UDF. A range of different sized water storages will need to be selected, then characterised with respect to the water quality and biology indicators to determine a best match monolayer product/s. Then a suitable monolayer application system design and application strategies will need to be determined and installed at each water storage. The appropriateness of each system will need to be evaluated for each water storage and the unique environmental conditions for each.

Validation of UDF - Operational mode

The application system, as determined by the UDF, will need to be constructed, installed and run on-site. In addition to the application system, a suitable system for detecting the presence and/or effectiveness of the monolayer, in real-time, will also need to be installed to validate monolayer coverage for certain wind conditions as compared to that predicted by the model. At this time, technology for the extensive aerial detection of monolayer presence is unfortunately not yet available. However, when such measurement technology is developed the information can then be used to calibrate the position and application rates of each applicator to optimise performance. Furthermore, the simulation platform can also be calibrated to reflect the real-world coverage conditions.

References

- ABS (2004), Year book australia, Technical report, Australian Bureau of Statistics, Canberra, ACT, 2617, Australia. Cat. No. 1301.0.
- Alpers, W. & Huhnerfuss, H. (1989), ‘The dampening of ocean waves by surface films: a new look at an old problem’, *Journal of Geophysical Research* **95**, 6251–6265.
- Angioletti, A. (1980), ‘Floating breakwater’. US patent 4,234,266 November 1980.
- Archer, R. J. & La Mer, V. K. (1954), ‘The effect of monolayers on the rate of evaporation of water’, *New York Academy of Sciences* **58**, 807–829.
- Archer, R. J. & La Mer, V. K. (1955), ‘The rate of evaporation of water through fatty acid monolayers’, *Journal of Physical Chemistry* **59**, 200–208.
- Baier, R. E. (1972), ‘Organic films on natural waters: Their retrieval, identification, and moes of elimination’, *Journal of Geophysical Research* **77**, 5062–5075.
- Baker, W. H. (1977), ‘Wave-quelling float’. US patent 4,052,755, October 1977.
- Baltaxe, R. (1967), ‘Air flow patterns in the lee of model windbreaks’, *Journal Theoretical and Applied Climatology* **15**, 287–312.
- Barnes, G. T. (2008), ‘The potential for monolayers to reduce the evaporation of water from large water storages’, *Agricultural Water Management* **95**, 339–353.
- Barnes, G. T., Costin, I. S., Hunter, D. S. & Saylor, J. E. (1980), ‘On the measurement of the evaporation resistance of monolayers’, *Journal of Colloid and Interface Science* **78**, 271–273.

- Barnes, G. T. & Gentle, I. (2005), *Interfacial science: an introduction*, Oxford University Press, Oxford.
- Berg, S. (2009), ‘Marangoni-driven spreading along liquid-liquid interfaces’, *Physics of Fluids* **21**.
- Blanchard, D. C. & Woodcock, A. H. (1975), ‘Bubble formation and modification in the sea and its meteorological significance’, *Tellus* **9**, 145–158.
- Bobra, M. (1990), A study of the formation of water-in-oil emulsions, *in* ‘Proceedings of the 13th Arctic Marine Oil Spill Program (AMOP) Seminar’.
- BOM (2007), ‘Annual australian climate statement 2005’. [accessed 16 February, 2009].
URL: <http://www.bom.gov.au/lam/climate/levelthree/ausclim/ausclim.htm>
- Boshammer, M. (2007), Aquatain liquid anti-evaporation film. independent trial results, Technical report, Total Ag Services Pty Ltd, Dalby, QLD, 4405, Australia. [*unpublished*].
- Bowley, W. W. (1974), ‘Floating wave barrier’. US patent 3,848,419 November 1974.
- Brink, G. & Symes, T. (2010), Monolayer application systems: design, control and application strategies, Technical report, National Centre for Engineering in Agriculture, Toowoomba, QLD, 4350, Australia. [*unpublished*].
- Brink, G., Symes, T. & Hancock, N. (2011), ‘Development of a ‘smart’ monolayer application system for reducing evaporation from farm dams – introductory paper’, *Australian Journal of Multidisciplinary Engineering* p. [*in press*].
- Brink, G., Wandel, A., Pittaway, P., Hancock, N. & Pather, S. (2010), A ‘universal design framework’ for installation planning and operational management of evaporation-suppressing films on agricultural reservoirs, *in* ‘International Conference on Agricultural Engineering’.
- Brooks, J. H. & Alexander, A. E. (1960), Losses of evaporation and solution from monolayers of long-chain aliphatic alcohols, *in* ‘3rd International Congress of Surface Activity Cologne 1960’, Vol. 5, pp. 196–201.
- Camp, D. W. & Berg, J. C. (1987), ‘Spreading of oil on water in the surface-tension regime’, *Journal of Fluid Mechanics* **184**, 445–462.

- Casey, G. J. (1976), 'Containment boom'. US patent 3,973,406 August 1976.
- Cerasari, N. P. (1974), 'Floating boom'. US patent 3,800,542 April 1974.
- Chao, X., Shankar, J. N. & Cheong, H. F. (2001), 'Two- and three-dimensional oil spill model for coastal waters', *Ocean Engineering* **28**, 1557–1573.
- Chebbi, R. (2001), 'Viscous-gravity spreading of oil on water', *The American Institute of Chemical Engineers* **47**, 288–294.
- Clark, R. C., J. & Brown, D. W. (1977), Petroleum: Properties and analyses in biotic and abiotic systems, in D. C. Malins, ed., 'Effects of petroleum on Arctic and subarctic marine environments and organisms', Vol. 1, Academic Press.
- Cluff, C. B. (1966), 'Evaporation reduction investigation relating to small reservoirs', *Agricultural experimental station. University of Arizona, Tucson, Arizona*.
- Coop, P. (2011), Detection of Monolayers, PhD thesis, University of New England.
- Coop, P., Lamb, D., Fellows, C. & Bradbury, R. (2007), Assessment of monolayer detection methods, Technical report, School of Science and Technology, The University of New England, Armidale, NSW, 2351, Australia. [*unpublished*].
- Coop, P., Lamb, D., Fellows, C. & Bradbury, R. (2008), Automatic detection of evaporation reducing monolayers, Technical report, Cooperative Research Centre for Irrigation Futures, Toowoomba, QLD, 4350, Australia. [*unpublished*].
- Craig, I. (2006), Evaporation mitigation technologies: manufacturers liason report, Technical report, National Centre for Engineering in Agriculture, Toowoomba, QLD, 4350, Australia. [*unpublished*].
- Craig, I., Aravinthan, V., Bailee, C., Beswick, A., Barnes, G., Bradbury, R., Connell, L., Coop, C., Fellows, C., Fitzmaurice, L., Foley, J., Hancock, N., Lamb, D., Morrison, P., Misra, R., Mossad, R., Pittaway, P., Prime, E., Rees, S., Schmidt, E., Solomon, D., Symes, T. & Turnbull, D. (2007), 'Evaporation, seepage and water quality management in storage dams: A review of research methods', *Environmental Health* **7**, 81–94.

- Craig, I., Green, A., Scobie, M. & Schmidt, E. (2005b), Controlling evaporative loss from water storages, Technical report, National Centre for Engineering in Agriculture, Toowoomba, QLD, 4350, Australia.
- Craig, I., Schmidt, E. & Hancock, N. (2005a), Crc-if first stage rp2 research proposal: evaporation mitigation tools, Technical report, National Centre for Engineering in Agriculture & CRC for Irrigation Futures, Toowoomba, QLD, 4350, Australia. [*unpublished*].
- Crow, F. R. (1961), 'Reducing reservoir evaporation: application of surface films cuts losses', *Agricultural Engineering* **42**, 240–243.
- Crow, F. R. (1963), The effect of wind on evaporation suppressing films and methods of modification, in 'International Union of Geodesy and Geophysics. International association of scientific hydrology. General Assembly of Berkeley', California, pp. 26–37.
- Crow, F. R. & Mitchell, A. L. (1975), 'Wind effects on chemical films for evaporation suppression at lake hefner', *Water Resources Research* **11**, 493–495.
- CSIRO (2008), 'Climate change - projections for australia'. [accessed 16 February, 2009].
URL: <http://www.dar.csiro.au/publications/projections2001.pdf>
- Cutnell, J. D. & Johnson, K. W. (2001), *Physics*, John Wiley and Sons, United States.
- Davies, J. T. & Rideal, E. K. (1963), *Interfacial Phenomena*, 2 edn, Academic Press: New York.
- Davies, J. T. & Rose, R. W. (1965), 'On the dampening of capillary waves by surface films', *Proceedings of the Royal Society of London Series A* **286**, 218–234.
- de Boer, J. H. (1953), *The Dynamical Character of Adsorption*, London: Clarendon at the University Press.
- Deo, A. V., Kulkarni, S. B., Gharpurey, M. K. & Biswas, A. B. (1961), 'Compressibility and specific evaporation resistance of the monolayers of long-chain alcohols and glycol monoalkyl ethers', *Nature* **191**, 378–379.

- Deo, A. V., Kulkarni, S. B., Gharpurey, M. K. & Biswas, A. B. (1962), 'Rate of spreading and equilibrium spreading pressure of the monolayers of n-fatty alcohols and n-alkoxy ethanols', *Physical Chemistry* **66**, 1361–1362.
- Deo, A. V., Sanjana, N. R., Kulkarni, S. B., Gharpurey, M. K. & Biswas, A. B. (1960), 'New compounds for the control of water evaporation', *Nature* **187**, 870–871.
- Dobroklonskiy, S. V. & Lesnikov, B. M. (1972), 'A laboratory study of the surface layers in drift currents', *Academy of Sciences, Izvestiya, USSR., Atmospheric and Oceanic Physics* **8**, 686–692.
- Dressler, R. G. & Guinat, E. (1973), 'Evaporation control on water reservoirs', *Industrial and Engineering Chemical Research* **12**, 80–82.
- Dressler, R. G. & Johanson, A. G. (1958), 'Water reservoir evaporation control', *Chemical Engineering Progress* **54**, 66–69.
- Duncan, D. P. (1950), Tree windbreaks for the orchard, Technical report, Minnesota Horticulturalist, Minnesota, United States.
- Dussaud, A. M. & Troian, S. M. (1997), 'Dynamics of spontaneous spreading with evaporation on a deep fluid layer', *Physics of Fluids* **10**.
- Eddy, R. C. (1996), 'Wave suppressor'. US patent 5,520,562, May 1996.
- Eimern, J. V., Karschon, R., Razumova, L. A. & Robertson, G. W. (1964), *Windbreaks and Shelterbelts: Technical note no.59*, Secretariat of the World Meteorological Organisation, Geneva, Switzerland.
- Fay, J. A. (1969), 'The spread of oil slicks on a calm sea', In 'Oil on the Sea' (Ed. Hoult, D.).
- Fietz, T. R. (1959), Water-loss investigations: Lake hefner - 1958. evaporation reduction investigations, report of the collaborators., Technical report, U.S. Bureau of Reclamation, Washington DC, United States.
- Fietz, T. R. (1970), Engineering aspects of evaporation reduction for small surface water storages, Technical report, Water Research Foundation of Australia Limited, Acton, ACT, 0200, Australia. ISBN: 0858380013.

- Fingas, M., Kyle, D. & Tennyson, E. (1995), The use of chemicals in oil spill response, *in* P. Lane, ed., 'Dispersant effectiveness: Studies into the causes of effectiveness variations', pp. 92–132.
- Fitzgerald, L. M. (1964), 'The effect of wave-damping on the surface velocity of water in a wind tunnel', *Australian Journal of Physics* **17**(184-188).
- Fitzgerald, L. & Vines, R. (1963), 'Retardation of evaporation by monolayers: Practical aspects of the treatment of large storages', *Australian Journal of Applied Science* **14**, 340–346.
- Florey, C. S. (1965), 'Apparatus for large scale application of monomolecular layers to water surfaces using melted material'. US patent 3,184,789, May 1965.
- Foda, M. & Cox, R. G. (1980), 'The spreading of thin liquid films on a water-air interface', *Journal of Fluid Mechanics* **101**, 33–51.
- Frenkiel, J. (1965), *Evaporation reduction: physical and chemical principles and review of experiments*, UNESCO, Paris, France.
- FSI (2007). [accessed 16 February, 2009].
URL: <http://www.flexiblesolutions.com>
- Geist, J. J. (1977), 'Articulated floating barrier'. US patent 4,033,137 July 1977.
- Gill, H., Prime, E. & Solomon, D. (2010), Efficacy of selected micro- and mono-layer products on evaporation. IAA National Conference, Irrigation Australia Limited, Sydney, Australia.
- Gladyshev, M. (2002), *Biophysics of the surface microlayer of aquatic ecosystems*, IWA Publishing: London.
- Green, T. & Houk, D. F. (1979), 'The removal of organic surface films by rain', *Limnology and Oceanography* **24**, 966–970.
- Grundy, F. (1962), 'Some problems of maintaining a monomolecular film on reservoirs affected by winds', *In* 'Retardation of Evaporation by Monolayers: Transport Processes' (Ed. La Mer, V. K.), 213–218.

- Hale, M. S. & Mitchell, J. G. (1997), 'Sea surface microlayer and bacterioneuston spreading dynamics', *Marine Ecology Progress Series* **147**(269-276).
- Hancock, N. (2008), personal communication. 16th November.
- Hancock, N. H., Pittaway & Symes, T. W. (2011), 'Assessment of the performance of evaporation suppressant films – analysis and limitations of simple trialling methods', *Australian Journal of Multi-disciplinary Engineering* p. (In press).
- Harbeck, G. E. & Koberg, G. E. (1959), 'A method of evaluating the effect of a monomolecular film in suppressing reservoir evaporation a method of evaluating the effect of a monomolecular film in suppressing reservoir evaporation', *Journal of Geophysical Research* **64**(89-93).
- Henry, D. J., Visham, D. I., Prime, E. L., Qiao, G. G., Solomon, D. H. & Yarovsky, I. (2010), 'Monolayer structure and evaporation resistance: A molecular dynamics study of octadecanol on water', *Journal of Physical Chemistry B* **114**, 3869–3878.
- Herzig, M. A., Barnes, G. T. & Gentle, I. R. (2011), Improved spreading rates for monolayers applied as emulsions to reduce water evaporation. submitted to Journal of Colloid and Interface Science.
- Hobbs, P. V. & Kezweeny, A. J. (1967), 'Splashing of a water drop', *Science* **155**, 1112–1114.
- Huhnerfuss, H., Alpers, W., Garrett, P., Lange, P. & Stolte, S. (1983), 'Attenuation of capillary and gravity waves at sea by monomolecular organic surface films', *Journal of Geophysical Research* **88**, 9809–9816.
- Jaffrennou, B. E. & Cessou, M. C. (1984), 'Flexible floating boom comprising transverse stiffeners of variable stiffness'. US patent 4,430,955 February 1984.
- Jeffreys, H. (1925), On the formation of water waves by wind, *in* 'Proceedings of the Royal Society of London. Series A, Containing Papers of a Mathematical and Physical Character', Vol. 107, pp. 189–206.
- Jensen, O. E. (1995), 'The spreading of insoluble surfactant at the free surface of a deep fluid layer', *Journal of Fluid Mechanics* **293**.

- Jones, F. (1992), *Evaporation of Water with Emphasis on Application and Measurements*, Lewis Publishers: Chelsea Michigan, USA.
- Kajlich, A. J. (1977), 'Turbulence inhibitors'. US patent 4,048,677, September 1977.
- Kajlich, A. J. (2006), 'Equipment for faster swimming pools'. US patent 7,100,219, September 2006.
- Kann, K. C. (1998), 'Wave suppression system'. US patent 5,827,011 October 1998.
- Keulegan, G. H. (1951), 'Wind tides in small closed channels', *Journal of Research of the National Bureau of Standards* **46**, 358–381.
- Kiefer, A. G. (1967), 'Turbulence-reducing device for swimming pools'. US patent 3,304,560, February 1967.
- Kiefer, J. K. (1990), 'Wave suppression means'. US patent 4,894,873, January 1990.
- Kinase, T., Yano, I., Okubo, K., Kitakoga, H. & Tayama, H. (1976), 'Oil fence'. US patent 3,971,220 July 1976.
- Koberg, G. E. (1969), 'Underwater gravity-type monomolecular film dispenser and method of use'. US patent 3,425,791, February 1969.
- Kodairo, S. T. & Kunitachi, Y. I. (1976), 'Floating breakwater'. US patent 3,991,576 November 1976.
- La Mer, V. K., Healy, T. W. & Aylmore, L. A. G. (1964), 'The transport of water through monolayers of long-chain n-paraffinic alcohols', *Journal of Colloid and Interface Science* **19**, 673–684.
- Lahav, N. & Alto, P. (1984), 'Method and apparatus for treating the surface of a body of liquid'. US patent 4,455,266, June 1984.
- Lange, P. & Huhnerfuss, H. (1978), 'Drift response of monomolecular slicks to wave and wind action', *Journal of Physical Oceanography* **8**, 142–150.
- Langmuir, I. & Schaefer, V. J. (1943), 'Rates of evaporation of water through compressed monolayers on water', *Journal of The Franklin Institute* **235**, 119–162.

- Lehr, W. J., Cekirge, H. M., Fraga, R. J. & Belen, M. S. (1984), 'Empirical studies of the spreading of oil spills', *Oil and Petrochemical Pollution* **2**, 7–11.
- Levich, V. G. (1940), 'The damping of waves by surface-active materials (in russian)', *Pis'ma v Zhurnal Eksperimental'noi i Teoreticheskoi Fiziki* **10**, 1296–1304.
- Lowe, E. G. (1974), 'Wave suppression device for swimming pools'. US patent 3,849,807, November 1974.
- Lunkenheimer, K. & Zembala, M. (1997), 'Attempts to study water evaporation retardation by soluble surfactants', *Journal of Colloid and Interface Science* **188**, 363–371.
- MacRitchie, F. (1969), 'Evaporation retarded by monolayers', *Science* **163**(929-931).
- Magill, J. W. (1953), 'Portable floating type breakwater unit for effective wave energy dissipation'. US patent 2,658,350 November 1953.
- Mansfield, W. W. (1955), 'Influence of monolayers on the natural rate of evaporation of water', *Australian Journal of Applied Science* **175**, 247–249.
- Mansfield, W. W. (1959), 'The influence of monolayers on evaporation from water storages', *Australian Journal of Applied Sciences* **10**(73-84).
- Mansfield, W. W. (1962), 'Aspects of evaporation control', In *Retardation of Evaporation by Monolayers: Transport Processes* (Ed. La Mer, V. K.), 133–136.
- McArthur, I. K. H. (1962), 'Cetyl alcohol monolayers for water conservation', *Research Applied in Industry* **15**, 230–238.
- McJannet, D., Cook, F., Knight, J. & Burns, S. (2008), Evaporation reduction by monolayers: overview, modelling and effectiveness, Technical report, CSIRO, Clayton South, VIC, Australia, 3169. [*unpublished: in draft*].
- Miles, J. W. (1957), 'On the generation of surface waves by shear flows', *Journal of Fluid Mechanics* **3**, 185–204.
- Miles, J. W. (1959), 'On the generation of surface waves by shear flows, 2.', *Journal of Fluid Mechanics* **6**, 568–582.

- Mitchell, J. G., Pearson, L., Bonazinga, A., Dillon, S., Khouri, H. & Paxinos, R. (1995), 'Long lag times and high velocities in the mobility of natural assemblages of marine bacteria', *Applied Environmental Microbiology* **61**, 877–882.
- Mito, M. T. (1974), 'Floating breakwater for attenuating seas'. US patent 3,791,150 February 1974.
- Morey, B. J., Cammaert, A. B. & Frampton, G. (1995), 'Prediction of floating breakwater performance', *Transaction on the Built Environment* **8**, 351–358.
- Morrison, P., Gill, R., Symes, T., Misra, R., Craig, I., Schmidt, E. & Hancock, N. (2008), Small-scale evaporation mitigation trials, 2007-2008, Technical report, National Centre for Engineering in Agriculture, Toowoomba, QLD, 4350, Australia. [*unpublished: in draft*].
- Myers, D. (1992), *Surfactant science and technology*, 2nd edn, VCH Publishers: New York.
- Naegeli, W. (1953), 'Untersuchungen uber die windverhaltnisse im bereich von schilfrorwanden', *Mitteil. Schweiz. Anstalt Forstl. Versuchswesen* **29**, 213–266.
- Nicholaichuk, W. (1978), 'Evaporation control on farm-size reservoirs', *Journal of Soil and Water Conservation* **33**, 185–188.
- Nicholaichuk, W. & Pohjakas, K. (1967), 'A wind-operated automatic powder dispenser for evaporation suppressants', *Canadian Journal of Soil Science* **47**, 79–80.
- Nielsen, E. C. (1977), 'Fending device for oil containment boom'. US patent 4,000,532 January 1977.
- O'Brien, R. N., Feher, A. I. & Leja, J. (1976), 'Spreading of monolayers at the air-water interface – a new method of measuring the spreading rate', *Journal of Colloid and Interface Science* **56**, 469–473.
- Olsen, J. O. (1975), 'Floating breakwater system'. US patent 3,877,233 April 1975.
- Pauken, M. T., Jeter, S. M. & Abdel-Khalik, S. I. (1996), 'Apparatus for large scale application of monomolecular layers to water surfaces using melted material'. US patent 5,558,845, September 1996.

- Phillips, O. M. (1957), ‘On the generation of surface waves by turbulent wind’, *Journal of Fluid Mechanics* **2**, 417–445.
- Pittaway, P. (2008), NPSI workshop presentation in Melbourne. 6th November.
- Pittaway, P. A. & van den Ancker, T. R. (2010), ‘Properties of natural microlayers on australian freshwater storages and their potential to interact with artificial monolayers’, *Marine and Freshwater Research* **60**, 1083–1091.
- Plate, E. J., Chang, P. C. & Hindy, G. M. (1969), ‘Experiments of the generation of small water waves by wind’, *Journal of Fluid Mechanics* **35**, 625–656.
- Rademacher, T. P. (1986), ‘Aquatic turbulence suppression device’. US patent 4,616,369, October 1986.
- Reiser, C. O. (1969), ‘A system for controlling water evaporation’, *Industrial and Engineering Chemical Research* **8**, 63–69.
- Reiser, C. O. (1970), ‘Method and apparatus for retarding evaporation from water surfaces’. US patent 3,528,764, September 1970.
- Rideal, E. K. (1925), ‘On the influence of thin surface films on the evaporation of water’, *Journal of Physical Chemistry* **29**, 1585–1588.
- Robertson, Q. L. (1966), ‘Apparatus for distributing material to reduce evaporation from water storages’. US patent 3,285,692, November 1966.
- Rosano, H. L. & La Mer, V. K. (1956), ‘The rate of evaporation of water through monolayers of esters, acids and alcohols’, *Journal of Physical Chemistry* **60**, 348–353.
- Ruhlman, J. R. (1972), ‘Water barrier floatation curtain’. US patent 3,691,773 September, 1972.
- Saylor, J. & Handler, R. (1999), ‘Capillary wave gas exchange in the presence of surfactants’, *Experiments in Fluids* **27**, 332–338.
- Saylor, J. R. (2001), ‘Determining liquid substrate cleanliness using infrared imaging’, *Review of Scientific Instruments* **72**, 4408–4414.

- Saylor, J., Smith, G. & Flack, K. (2000), 'The effect of a surfactant monolayer on the temperature field of a water surface undergoing evaporation', *International Journal of Heat and Mass Transfer* **43**, 3073–3086.
- Shemdin, O. H. (1972), 'Wind-generated current and phase speed of wind waves', *Journal of Physical Oceanography* **2**, 411–419.
- Shukla, R. N. & Kulkarni, S. B. (1962), 'The effect of wind speed on water evaporation reduction by the monolayers of alkoxy ethanols and n-alkyl alcohols', *Journal of Scientific and Industrial Research* **21B**, 276–277.
- Skidmore, E. L. & Hagen, L. J. (1970), 'Evaporation in sheltered areas as influenced by windbreak porosity', *Agricultural Meteorology* **7**, 363–374.
- Smith, D. I. (1962), *Structural geometry in the selection of retardants and dispersants for use in water evaporation suppression*. In: *La Mer, V.K. (Ed.), Retardation of Evaporation by Monolayers: Transport Processes*, Academic Press, New York.
- Smith, D. I. (1998), *Water in Australia: resources and management*, Oxford University Press, Melbourne.
- Smith, R. D. (1992), 'Floating boom'. US patent 5,120,159 June 1992.
- Stanwood, D. A. (1970), 'Turbulence dispelling float device and string'. US patent 3,540,063, November 1970.
- Tarasov, V. V., Kovalenko, N. F., Shcherbakova, G. S. & Zhang, D. (2006), 'Linear and radial marangoni flows of surfactants', *Theoretical Foundations of Chemical Engineering* **40**(111-115).
- Thurman, R. K. (1973), 'Floating oil containment boom'. US patent 3,751,925 August 1973.
- Timblin, L. O., Florey, Q. L. & Garstka, W. U. (1962), 'Laboratory and field reservoir evaporation reduction investigations being performed by the bureau of reclamation', In '*Retardation of Evaporation by Monolayers: Transport Processes*' (Ed. La Mer, V. K.), 177–192.
- Tokyo, T. M. & Matsudo, Y. M. (1976), 'Floating breakwaters'. US patent 3,969,901 July 1976.

- Treloar, H. A. (1959), 'Means for preventing evaporation from reservoirs or the like'. US patent 2,878,098, March 1959.
- van der Linde, R. J. (1958), Tree outside the forest, chapter of the fao-report: Forest influences, Technical report, Food and Agriculture Organization of the United Nations, Rome, Italy. FAO Forestry Paper - 140.
- Vidal, S. P. (1967), 'Liquid film maintaining apparatus'. US patent 3,353,610 November 1967.
- Vines, R. G. (1960a), 'Recent developments in the control of water evaporation', *Wool Technology and Sheep Breeding* **7**, 136–139.
- Vines, R. G. (1960b), 'Reducing evaporation with cetyl alcohol films: a new method of treating large water storages', *Australian Journal of Applied Sciences* **11**(200-204).
- Vines, R. G. (1962), 'Evaporation control: A method for treating large water storages', In *'Retardation of Evaporation by Monolayers: Transport Processes'* (Ed. La Mer, V. K.), 137–160.
- Walket, M. C. (1973), 'Turbulence suppression apparatus for a body of water'. US patent 3,755,829, January 1973.
- Walket, M. C. (1974), 'Swinging baffle element for water turbulence suppression system'. US patent 3,786,521, January 1974.
- Walter, J. (1963), The use of monomolecular films to reduce evaporation, in 'International Union of Geodesy and Geophysics. International association of scientific hydrology. General Assembly of Berkeley', California, pp. 39–48.
- Wolbeer, H. J. (1963), The calculated efficiency of monolayers in relation to increased water temperature, in 'International union of Geodesy and Geophysics. International association of scientific hydrology. International union of Geodesy and Geophysics. International association of scientific hydrology. General Assembly of Berkeley', pp. 13–23.
- Wright, J. W. & Keller, W. C. (1971), 'Doppler spectra in microwave scattering from wind waves', *Physics of Fluids* **14**, 466–474.

-
- Wu, J. (1968), 'Laboratory studies of wind-wave interactions', *Journal of Fluid Mechanics* **34**, 91–112.
- Wu, J. (1971*a*), 'An estimation of oceanic thermal-sublayer thickness', *Journal of Physical Oceanography* **1**, 284–286.
- Wu, J. (1971*b*), 'Evaporation retardation by monolayers: Another mechanism', *Science* **174**, 283–285.
- Wu, J. (1975), 'Wind-induced drift currents', *Journal of Fluid Mechanics* **68**, 49–70.

Appendix A

Literature Reviewed

A.1 Introduction

The through review detailed in this Appendix ranges from methods to measure evaporation and monolayer materials through to systems for applying monolayer and structures for wave calming or reducing wind speed. A summary to this literature review is provided in Chapter 2 of the dissertation.

A.2 Methods for estimating evaporation

A number of different methods have been developed for measuring or estimating evaporation from water storages such as the water balance method, Class A evaporation pans, automatic weather station (AWS) based estimates (utilising Penman-Monteith type "combination" formulae), Bowen Ratio measurement and Eddy Correlation, infrared (IR) large aperture spectroscopy (LAS) or laser radar (LIDAR). A study of these various methods was conducted by the NCEA in 2005 to determine the appropriateness of each method for measuring the effectiveness of an evaporation mitigation system in reducing evaporation. A summary of the advantages and disadvantages of the various methods reviewed by the NCEA is provided in Table A.1 and A.2.

Most of the methods for measuring evaporation reviewed by the NCEA were considered to be suitable for open storages but not for covered (e.g. covered with a monolayer surface film). As it is difficult to measure evaporation from a covered storage, the favored method needed to be simple, affordable and easy enough to install at existing storages.

Table A.1: Summary of the advantages and disadvantages of various methods for measuring evaporation from farm water storages (Part 1). Overview based on Craig and (Hancock 2008)

Method	Brief Description	Advantages	Disadvantages	Appropriateness to PhD
1. Water balance using PST technology.	A very accurate pressure sensitive transducer is used to record small changes in water depth with time.	Simple, robust, millimetre (depth) accuracy (with custom temperature compensation); able to place several sensors in several storages at a reasonable cost.	Dependent on the ability to separate seepage from evaporation. Require several days of data to obtain reliable evaporation and seepage rates.	Very appropriate as uncertainties in atmospheric demand measurements are avoided.
2. Simulation using an 'Class A' evaporation pan	Simple pan of water, refill rate is a measure of the evaporation rate. Related to crop ET via a simple 'pan factor'.	Standardised apparatus and procedure, simple & robust, have been widely used for irrigation scheduling purposes.	Pan factors determined from daily data are highly variable, even with good pan siting and rigorous maintenance (citeAllenetal198here).	Poor, but might serve as a general indicator.

Continued on Table A.2.

Table A.2: Summary of the advantages and disadvantages of various methods for measuring evaporation from farm water storages (Part 2). Overview based on Craig and (Hancock 2008)

Method	Brief Description	Advantages	Disadvantages	Appropriateness to PhD
Continued from Table A.1.				
3. Atmospheric measurement using Penman-Monteith type combination equation (FAO 56)	‘FAO56’ is accepted standard method for estimating general <i>crop</i> evaporation from standard (single height) meteorological data (radiation, humidity, windspeed) as provided by a low-cost automatic weather station (AWS).	FAO 56 is now widely established and used; FAO 56 is considered superior to other ET formulae, e.g. Blaney-Criddle, Priestly-Taylor	(i) Combination equation theory assumes adequate (aerodynamic) fetch, i.e. extensive area if surface such that there is no advected energy; & (ii) uses a ‘reference crop’ as the potential evaporation and this is not optimised for open water evaporation.	Potentially inaccurate, especially for small dams where advected energy may be expected to have a major influence on evaporation; but superior to an evaporation pan.
Continued on Table A.3.				

Table A.3: Summary of the advantages and disadvantages of various methods for measuring evaporation from farm water storages (Part 3). Overview based on Craig and (Hancock 2008)

Method	Brief Description	Advantages	Disadvantages	Appropriateness to PhD
Continued from Table A.2.				
4. Atmospheric measurement using Bowen Ratio (BR) method	Measures temperature and humidity gradient across two heights close to evaporating surface.	Accurate, but only with high accuracy sensors and with good fetch, i.e. uniform surface to extending at least 100x measurement height upwind of the measurement point (such that there is no advected energy).	(i) Fetch requirement is critical; & (ii) Humidity sensors of the required accuracy, e.g. matched pair of aspirated or cooled mirror hygrometers, plus precision net radiometer, are very expensive.	Superseded by eddy covariance technique.
Continued on Table A.4.				

Table A.4: Summary of the advantages and disadvantages of various methods for measuring evaporation from farm water storages continued (Part 4). Overview based on Craig and (Hancock 2008)

Method	Brief Description	Advantages	Disadvantages	Appropriateness to PhD
Continued from Table A.3.				
5. Atmospheric measurement using Eddy Covariance/Correlation (EC)	Uses 3 axis sonic anemometry and fast response infra-red sensors to detect the net upward water vapour flux (i.e. point evaporation).	(i) Now well established using essentially standard apparatus with integral software; & (ii) advected energy (due to change of surface) does not invalidate the technique, i.e. measurements are essentially <i>independent</i> of upwind fetch.	Expensive (typically A\$50,000); must be installed over the water surface; & provides essentially a 'point' measurement which may not be representative of the whole water surface.	Appropriate (with the assumption that variations in water vapor flux across the surface will be small).
Continued on Table A.5.				

Table A.5: Summary of the advantages and disadvantages of various methods for measuring evaporation from farm water storages continued (Part 5). Overview based on Craig and (Hancock 2008)

Method	Brief Description	Advantages	Disadvantages	Appropriateness to PhD
Continued from Table A.4.				
6. Optical line/area based methods	Large Aperture Scintillometry (LAS); IR/FTIR/UV absorption spectroscopy; LIDAR; Microwave radar; Remote sensing Airborne survey.	Laser techniques provide line-integration horizontally, i.e. through the humidity plume of a whole dam, permitting the mapping of variability of water vapour concentration across a water surface and hence assessment of fetch/advection effects.	(i) Accuracy questionable when the vertical energy flux is substantially latent heat, i.e. as vapourised water, (because the sensed atmospheric scintillation arises principally from the sensible heat flux); and (ii) high cost of apparatus requiring extensive scientific support.	Potentially appropriate, but probably beyond the requirements of this study.

Through the NCEAs detailed assessment of methods for measuring evaporation from both open and covered water storages they identified the water balance using pressure sensitive transducer (PST) technology and eddy covariance method as the most appropriate. The NCEA noted that the PST is the only method that can be applied to a covered storage and the instrumentation is both affordable and robust enough for use on operating farm storages in remote sites (Craig et al. 2005b).

The PST method looks at factors that increase and decrease the water volume as seen in Figure A.1.

$$\text{Evaporation} = \text{Inflow} + \text{Rain} - \text{Outflow} - \text{Seepage} - \text{Change in Volume} \quad (\text{A.1})$$

For periods when there is no inflow, outflow or rainfall and for small incremental time steps when the surface area is constant, the equation simplifies to:

$$\text{Change in water depth (mm)} = \text{Evaporation (mm)} + \text{Seepage (mm)} \quad (\text{A.2})$$

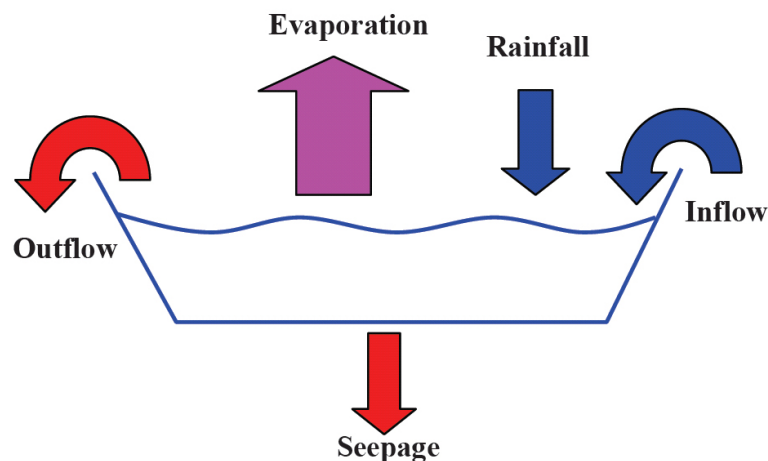


Figure A.1: Factors that effect a change in water volume (Craig et al. 2005b)

The PST is a device which when placed at the bottom of a dam is capable of measuring depth by means of water pressure. It outputs a millivolt reading which can then be

converted to millimetres of depth. Each PST has an individual mV-to-mm conversion factor which is obtained during bench calibration testing. It has also been found that the PST calibration is affected by temperature and although the changes are within specification, this can lead to significant errors of up to several millimeters depth. However, the relationship between sensor output and temperature is linear, thus it was able to determine a temperature correction factor for each PST. When this temperature correction is applied to the raw data the quality improves which shows more accurately the evaporative loss over time. Figure A.2 shows an individual PST. The preferred PST used throughout the NCEA evaporation mitigation trials is the Druck 4030 which was modified to include a fourth wire singly for signal return. The working range of this unit is 0 – 3569 mm and sensitivity is ± 0.5 mm (Morrison et al. 2008).



Figure A.2: Druck 4030 pressure sensitive transducer (Craig et al. 2005b)

Simple mV-to-mm conversion requires a multiplication of the raw data (voltage V_0) by the conversion factor K . However, to ensure ± 0.5 mm accuracy a temperature correction is required as follows:

$$\text{depth} = KV_0 - kT(20 - \text{PST temperature}) \quad (\text{A.3})$$

Where kT is the temperature correction factor derived in laboratory calibrations for each PST. A reference temperature is usually set according to trial location and is a generalised average temperature.

Although the NCEA identified the water balance method using PST technology, described above, to be the best way of measuring the actual evaporation from an open

and covered storage, if a method for comparison with PST water balance data is desired or all necessary components of a water balance are not available, then the eddy covariance method is considered to be the best available (Hancock 2008).

A.3 Monolayer materials

Monolayers are films that are one molecule thick formed at a phase boundary such as the air/water interface. These molecules are amphiphilic as each has a hydrophilic part (attracted to water) and a hydrophobic part (repels water). The hydrophobic part of the amphiphile renders the whole molecule insoluble in water while the hydrophilic part serves to anchor each individual molecule to the water surface. This tends to prevent the molecules from piling on top of one another (Barnes & Gentle 2005).

Monolayers can exist in a number of different surface states, but the ones most appropriate for evaporation mitigation are the condensed states, where the molecules are packed closely together: primarily the solid state and liquid condensed states, Figure A.3.

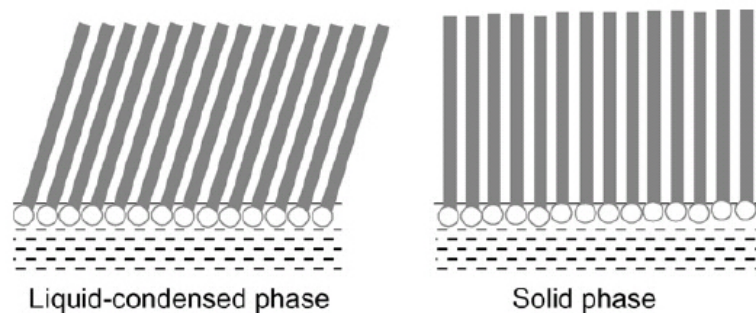


Figure A.3: Schematic diagram showing the structures of the liquid-condensed and solid monolayer phases. The hydrophilic groups are shown as open circles, and the hydrocarbon (alkyl) chains as grey lines (Barnes 2008)

A.3.1 Monolayer spreading properties

There are several techniques for spreading monolayers on a water surface, some of which may be suitable for use in the field. However, before considering these techniques it should be emphasised that in spreading these monolayer compounds it is necessary to generate and maintain a high surface pressure if the evaporation of the sub phase water is to be reduced. A lower surface pressure, due to a lack of condensed monolayer film present on the water surface, would indicate higher evaporation of the sub phase water.

The spreading rate is important in field applications as the material must spread, usually from a single application point across a large surface area before being deposited on the lee shore. There are two steps in the spreading process: transfer from bulk solid to monolayer on the water surface, and movement of monolayer across the surface. It is generally assumed that the rate-limiting step is the first one but few measurements have been made. For the first step, spreading rate is proportional to the length of line of contact between the solid and the water surface, so the finer the solid has been ground the faster it will spread (Barnes 2008).

A.3.2 Monolayer forms

Early monolayer field trials have been dominated by the preferred use of long-chain alcohols, mainly hexadecanol (cetyl alcohol) and octadecanol (stearyl alcohol). One particular reason for this is that evaporation resistance is exponentially increased when the chain length of these alcohols is increased. However, when chain length is increased there is a decrease in spreading rate (La Mer et al. 1964). To compensate for a slower spreading rate and to try retain the improved evaporation resistance, hexadecanol and octadecanol were sometimes applied together as a mixture. The hexadecanol would increase the spreading rate while the octadecanol would increase the evaporative resistance.

Although most useful monolayer materials for evaporation mitigation are solids at room temperature, they can be dissolved in a solvent to create a liquid solution. This is said to make application easier. One of the simplest methods for applying monolayer as

a solution is by gravity feed through a fine-gauge piping from calibrated containers. However, solvents pose a number of limitations as the monolayer tends to suffer from contamination by retained solvent. The spreading pressure of a concentrated solution is only half that of solid cetyl alcohol. In addition, solvents are generally expensive and environmentally undesirable (Barnes 2008).

Monolayer compounds can also be spread from aqueous slurries which may have some advantages in handling and distribution, but have been criticised due to spreading problems associated with prolonged contact with water. This is further confirmed by the NCEA during a field trial to evaluate the performance of a monolayer based evaporation mitigation system. It was noted that the WaterSavr powder appeared to lose its spreading ability.

A further method was trialled by Smith (1962), which involved mixing the monolayer with water and oil into an emulsion. Of the many formulations tested a mixture of hexadecanol (the 'oil'), glyceryl monostearate (dispersing agent), and water in the ratio 10:1:100 was selected because it was sufficiently fluid for application as a liquid. Although promising evaporation results were achieved on moderate size reservoirs (Reiser 1969) and (Dressler & Guinat 1973).

A.3.3 Evaporative resistance of monolayers

Much of the early laboratory studies of water evaporation through monolayers were simply surveys searching for monolayers that could reduce the evaporation rate (Rideal 1925). Experiments followed which also aimed at developing an understanding of the mechanism by which monolayers reduce water evaporation. In particular, Langmuir & Schaefer (1943) followed by Archer & La Mer (1954) and Archer & La Mer (1955) developed the concept of evaporation resistance and the means for measuring it.

Of the large number of amphiphiles investigated during this time, insoluble amphiphiles were found to be most appropriate for reducing evaporation as nearly all of the soluble amphiphiles investigated showed no measurable effect on evaporation rate (Lunkenheimer & Zembala 1997). More specifically insoluble amphiphiles that exhibit a usefully high

evaporation resistance have a long unbranched, fully saturated, alkyl chain with a polar group at one end (Barnes 2008).

Relevant examples include the long-chain fatty acids, long-chain alcohols, alkoxy ethanols, some methyl and ethyl esters of fatty acids, and calcium salts of long-chain fatty acids. These all form monolayers that give a solid phase at high surface pressures. Substances with double bonds in the hydrocarbon chain (cis or trans) or which contain a large hydrophilic group do not generally form a solid phase and have very low evaporation resistances (Rosano & La Mer 1956).

A.3.4 Existing product performance

There are two main chemical film products commercially available in Australia, they are Aquatain and WaterSavr. WaterSavr is a true monolayer product while Aquatain is better described as a microlayer product (much more than one molecule thick). Details of the two products are given in Table A.6. One further monolayer compound, which is not a commercial monolayer product, is C18E1 (Ethylene glycol mono-octadecyl ether). This material has excellent properties for evaporation mitigation (Deo et al. 1962, Deo et al. 1960, Deo et al. 1961), and has been of particular interest to the NCEA in their small-scale evaporation mitigation trials (Morrison et al. 2008).

Aquatain has claimed evaporation savings of 50% based on an independent trial conducted by Total Ag Services Pty Ltd over a three week period at a 0.4 ha dam at Tarcoola near Dalby (Boshammer 2007). However, due to inaccuracies in the measurement of evaporation and a dosage rate well in excess of the recommended rate, this trial is of questionable validity. An independent study of the evaporation reduction achieved using WaterSavr on a 4 ha dam at Korong Vale over a 3 week period claimed evaporation savings of 30%. Results from this trial again need to be treated with caution due to inaccuracies in seepage and evaporation estimation (McJannet et al. 2008).

The most accurate estimation of expected product performance between Aquatain, WaterSavr and C18E1 has been determined by the NCEA through their small-scale evaporation mitigation trials from 2007 to 2008 (Morrison et al. 2008). The performance

Table A.6: Commercially produced chemical film products currently available in Australia (CSIRO 2008)

	Aqautain (microlayer)	WaterSavr (monolayer)
Chemistry	Siloxane	Cetyl/stearyl alcohol
Approximate cost (bulk supply including GST)	\$16.00 per litre	\$10.00 per kg
Application rate	2 litres/ha	0.35 kg/ha
Re-application period	10 days	Daily
Claimed savings	50%	30%
Recommended application method	Aerial spraying	Applicator

of these three products were evaluated during 6 phased trials using 2.85 m diameter buckets (0.064 m² surface area) and 1.93 m diameter cattle troughs (2.93 m² surface area) and 10 m diameter tanks (78.5 m² surface area). However, the 10m diameter tank trials were not continued as there were large differences from the troughs and buckets for no discernable reason (Morrison et al. 2008).

Evaporative loss was determined by measuring water depth after a fixed time interval (bucket trials) or continuously logged (tank and bucket trials) using PSTs. Troughs and buckets had at least one replicate for each and with, of course, zero seepage in contrast to most practical storages. Different monolayer products were all tested at manufacturers recommended application rate and frequency of application, then also at 3x and 5x recommended application rate and at different application frequencies of anywhere from every 2-14 days.

The data presented below, Figure A.4, are from the Trial 6 trough trial, which is believed to be the most appropriate as experimental procedures were continually refined throughout. Application rate of C18E1 was increased from every 10 days to every 2 days in an attempt to move towards the potential savings achieved in previous bucket trials. Trough application rates were as follows:

1. Aquatain (Si Oil) - 12mL (40L per ha) every 10 days
2. WaterSavr (C16 Hexadecanol) - 0.9g (3 kg per ha) every 2 days
3. C18E1 - 45mL (15mg of active compound per ha) every 2 days

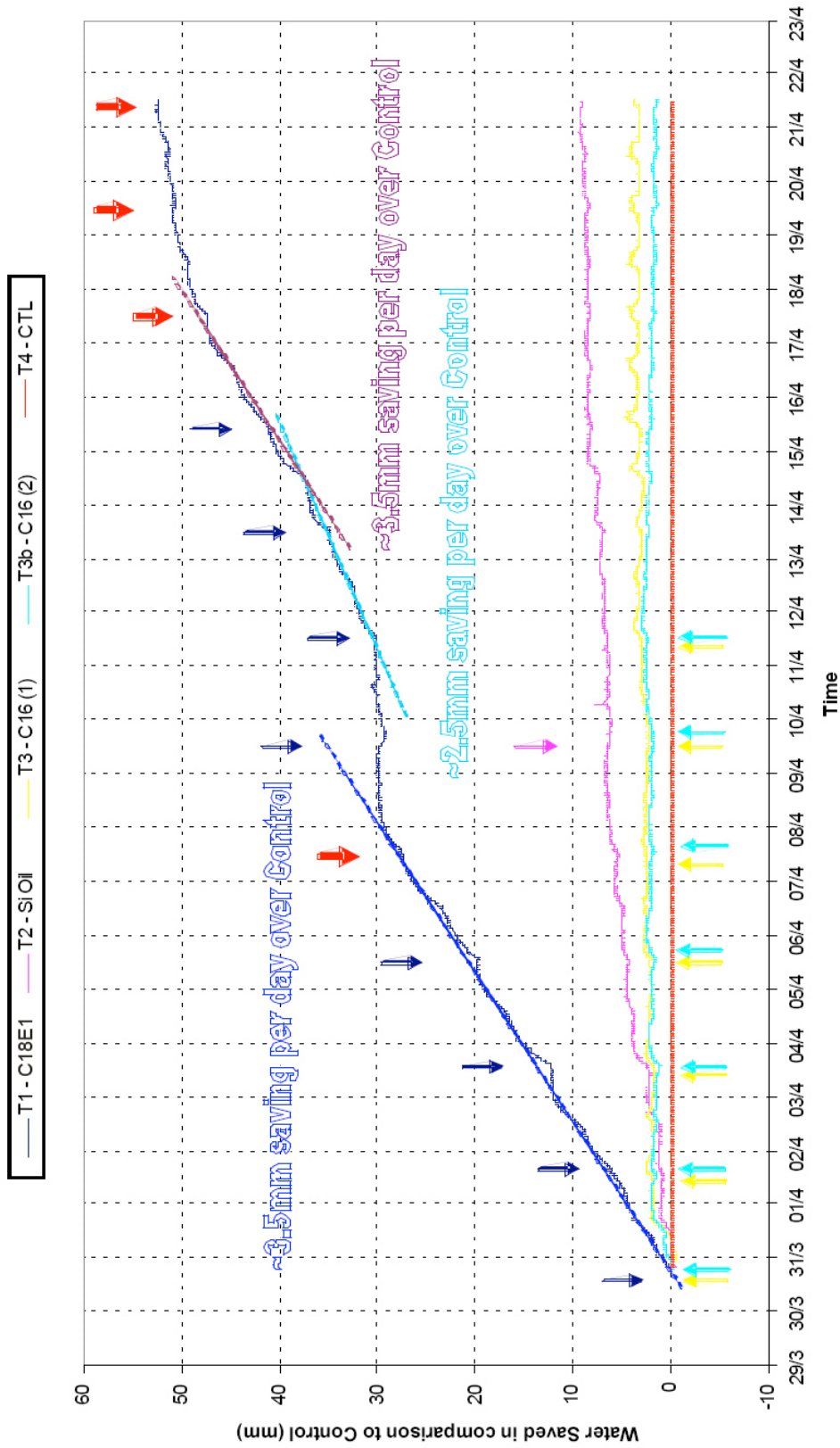


Figure A.4: The evaporative reduction performance of three monolayer products during trough Trial 6, T1=C18E1; T2=Silicone oil (Aquatain); T3=C16 (WaterSavr at the recommended application rate); T3b=C16 (WaterSavr at 2x recommended); T4=Control (no monolayer), are presented as the depth deviation from the control. The blue arrow indicate when product was applied, and the bolder red arrows represent missed applications for C18E1 (Morrison et al. 2008)

Overall it was concluded that despite closely replicated trials and techniques to manage potential systematic error, there appears to be considerable variability in the evaporation mitigation performance of all of the monolayer products tested. There is evidence that this variability is in part related to the condition of the water. However, the variations in product performance, and apparent performance, are likely also to be greatly influenced by the existence and evolution of natural microlayers existing on all natural waters and the micro-scale differences of temperature across the surface, their diurnal variation and their dependence on weather and on water body size (Morrison et al. 2008).

In addition, laboratory studies of the microbial resilience of C18E1 have been conducted by Dr. Pam Pittaway at the University of Southern Queensland. The results of which are presented in Figure A.5. In comparison to the commonly used C16OH (cetyl alcohol) and C18OH (stearyl alcohol), as used in WaterSavr, it is clear that C18E1 has greater resilience to microbial attack.

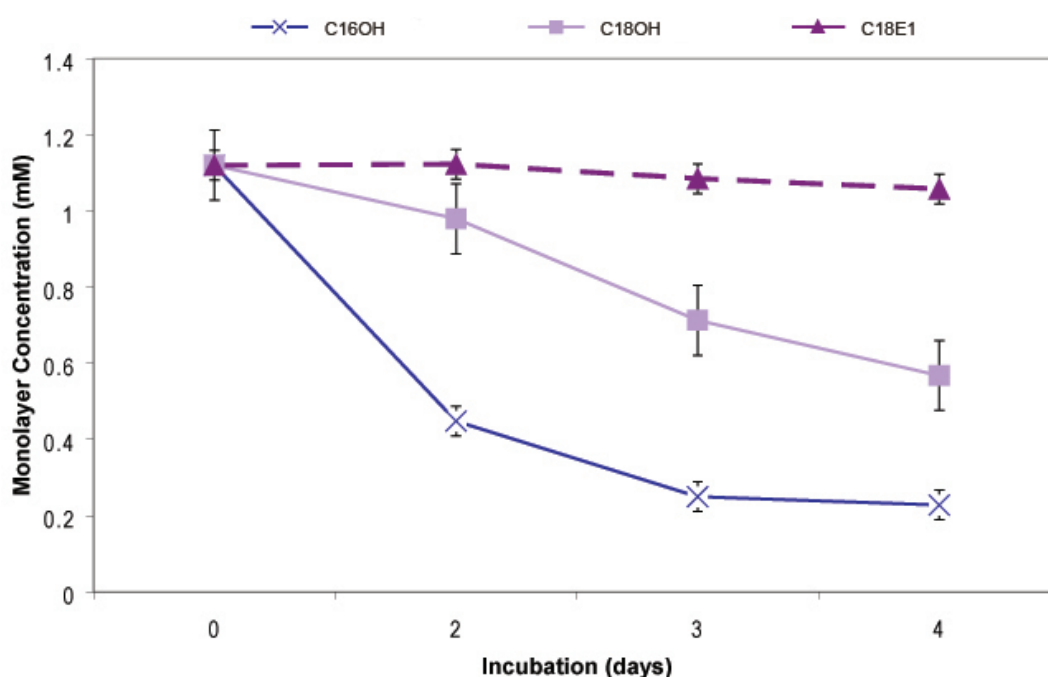


Figure A.5: Microbial degradation rates of C16OH, C18OH and C18E1 (Pittaway 2008)

It is also worth noting that the spreading rate of C18E1 is remarkably higher than that of C16OH, Figure A.6. In the intermediate range the curves run roughly parallel and here the rate of spread of C18E1 is about ten times higher than that of C16OH.

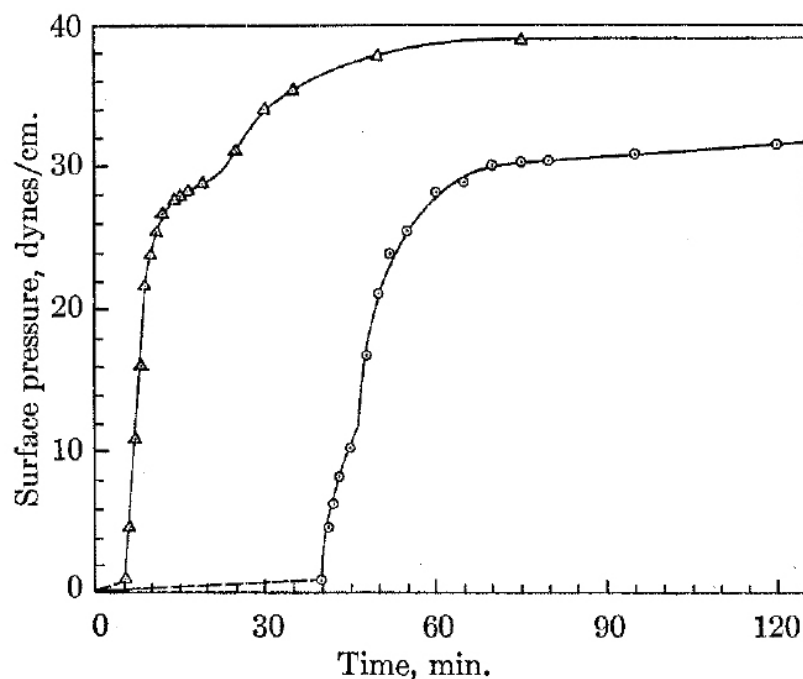


Figure A.6: Surface Pressure vs. Time for Δ – C16OH and O – C18E1. It is significant that C18E1 reaches a higher surface pressure in a much shorter time than C16OH, which indicates that C18E1 spreads more rapidly. Graph reproduced from Deo et al. (1962)

A.4 Monolayer application technologies

A large number of monolayer based application systems and technologies have been developed and trialled since the 1950s. Many of the application systems developed during this time period were rather crude working prototypes that incorporated simple mechanical components. Although monolayer related research seemed to taper off for a short time, severe drought and water shortages facilitated a renewed interest in monolayers.

More recently a number of systems have been developed by Flexible Solutions International (FSI) Pty Ltd for their WaterSavr product. Ultimate-Agri Products have also developed two application systems for their Aquatain product. Bio-Systems Engineering designed and built an application system for the NCEA to conduct a large scale monolayer field trial. In addition, the NCEA recently developed a demonstration application unit for further monolayer field trials.

This section provides a review of all the available application systems and technologies found in literature, patents and on-line for applying monolayer to open water surfaces.

A.4.1 Solution application (liquid)

Gravity feed appears to be a favoured method for solvent application as it is low-tech and reliable with no moving or mechanical components to service. This is also the standard method of spreading a monolayer in the laboratory and was first trialed in the field at Stephen's Creek Reservoir in Australia. Commercial cetyl alcohol was dissolved in a volatile petroleum fraction and ethyl alcohol. The solution was applied by means of gravity feed through fine-gauge piping from containers with calibrated holes which simply allowed the solution to drip onto the water surface. Similarly gravity feed solvent application systems have been trialed in India, Africa, Spain and the United States.

Two alternative devices for applying cetyl alcohol mixed with a volatile spirit were proposed by Howard Treloar and Jack Dunstan. The first device is a wind valve controlled application unit that floats on the water surface. The application unit is attached to a square stake by two square collars so that the unit can move freely up and down the post with the water level. Also supported by the application unit is a valve which has an inlet connected to a supply tank and an outlet pipe that projects down to have an opening just above the water surface, Figure A.7.

“The valve is normally closed by a spring 12 pressing on the plunger 13 to cause it to seat on the outlet 7, but this plunger 13 may be lifted to bring its sealing face 14 clear of the outlet 7 to allow a flow of liquid through same, the plunger being lifted when wind pressure on the vane 15, which is mounted on the arm 16 in turn pivoted to the valve by the pin 17, overcomes the pressure of the spring 12, Figure A.7” (Treloar 1959).

The second device is for dispensing an evaporation preventing substance onto the exposed surface of a moving stream of water. This applicator unit is also attached to a square stake by two square collars so that the unit can move freely up and down the

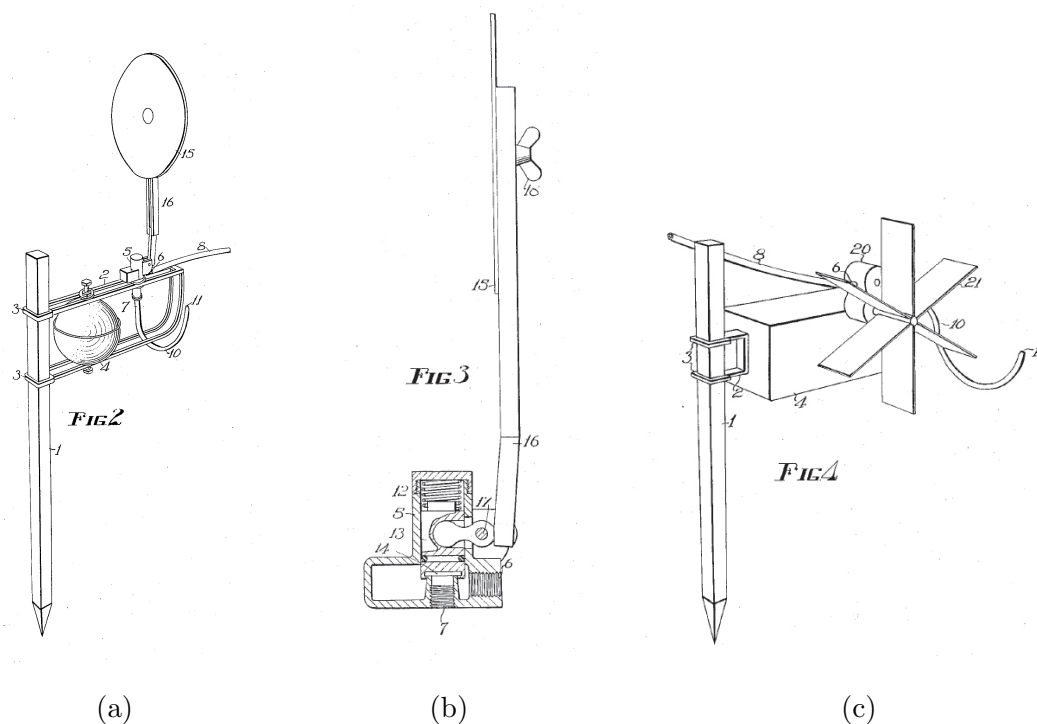


Figure A.7: Floating application units for application of monolayer in a solvent form. (a) Floating solvent application unit. (b) Detailed section of wind valve for application unit. (c) Floating gear driven water-wheel pump for solvent application. (Treloar 1959)

post with the water level. However, this unit comprises a small gear or other pump that is driven by a water wheel to control rate of application according to the rate of flow of water in the stream, Figure A.7. This unit is intended more for directional water flow, such as in streams or at a reservoir intake where it is desired to measure the inflow to replenish the protective liquid lost in normal outflow over a weir or the like.

Most methods for monolayer application usually involve spreading the evaporation suppressing film onto the water surface by means of spraying, dripping and floating. An alternative to the norm is the underwater gravity-type monomolecular film dispenser designed by Gordon E. Koberg. Koberg found that evaporation suppressor could be released just below the water surface and the low-density material would float upwardly and spread across the water surface in a monolayer with little waste of the suppressor material (Koberg 1969).

Koberg's design consists of two containers, one securely located below the water surface near the shore line and the other above the water surface along the embankment of the reservoir. In the sub-surface container is an evaporation suppressor liquid which floats on a displacement liquid, such as water or other liquid having a greater specific gravity than the suppressor liquid. The displacement liquid is stored in the container on the embankment and is supplied to the sub-surface container from a sufficient height to create a hydrostatic or fluid head. This serves to pressurise the system and provide the driving force to release suppressor liquid from the sub-surface container when required (Figure A.8).

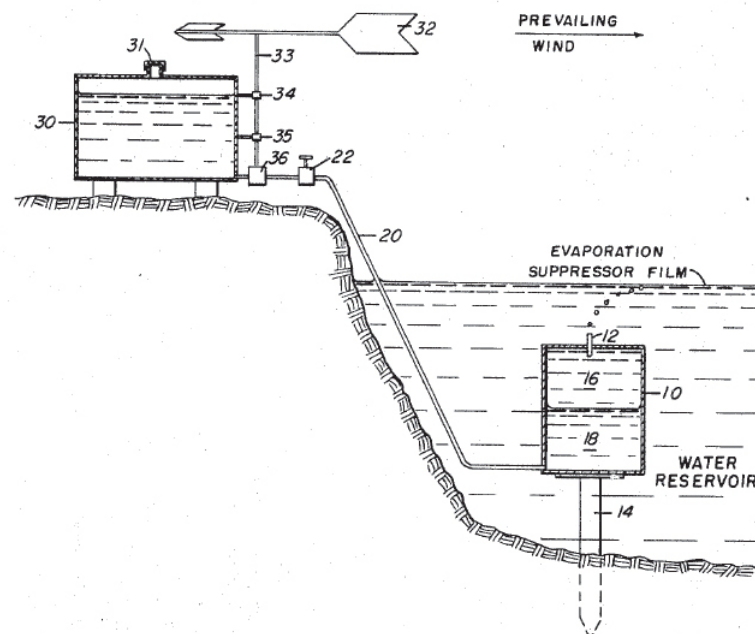


Figure A.8: Underwater gravity-type monolayer film dispenser (Koberg 1969)

The evaporation suppressor would usually be applied in response to wind speed and direction but may also be metered continuously or intermittently, or the wind vane apparatus may be used to increase the flow rate at certain times. Normally the sub-surface containers are spaced along a shore line at intervals of about 50 to 200 ft for best coverage of the reservoir.

Refilling of the storage tank and sub-surface container was accomplished by a number of different methods. One refill method is to connecting the outlet orifice to a supply of evaporation suppressing liquid and pressurising the sub-surface container which creates

a hydrostatic head in the refill connection and the displacement liquid would be returned to the storage tank. Another method would be to pump displacement liquid from the sub-surface container and return it to the storage container while simultaneously filling the sub-surface container with suppressor liquid from the supply tank through the outlet orifice.

A further variation for applying monolayer dissolved in a solution was designed by Michael T. Pauken, Sheldon M. Jeter and Said I. Abdel-Khalik. The device illustrated in Figure A.9 can basically be described as a film pump, for producing and spreading a monolayer of evaporation inhibiting film over large water surfaces. The device consists of an impeller which is disposed below and coplanar to the water surface. The impeller is connected to a hub and drive-shaft assembly which is powered by a variable speed electric motor. The speed of impeller rotation is controlled and adjusted to maintain a laminar flow at the edge of the impeller, thus providing a smooth interface for the application of the film to the water surface, and not disrupting the continuity of the monolayer (Pauken et al. 1996).

Film material is delivered to the water surface immediately above the impeller, and as close to the centre of the impeller as practical, and the film material is forced outward and spread over the surface of the body of water by the centripetal force created by the impeller, Figure A.9. Thus, it is not necessary to move the device about the body of water, but the device can remain in one position, unlike many of the prior art devices.

The only true liquid monolayer product commercially available is 'HeatSavr'. HeatSavr is basically octadecanol in solution with a combination of isopropanol-water azeotrope and n-butanol. HeatSavr is FSIs monolayer product for use as a solar blanket on swimming pools which also helps to reduce evaporative loss. FSIs HS115 Automatic Metering System appears to be the only commercially available dosing system specifically designed and sold for dosing of a liquid monolayer. This is a programmable dosage unit that incorporates a peristaltic pump configured to deliver a pre-set daily dosage.

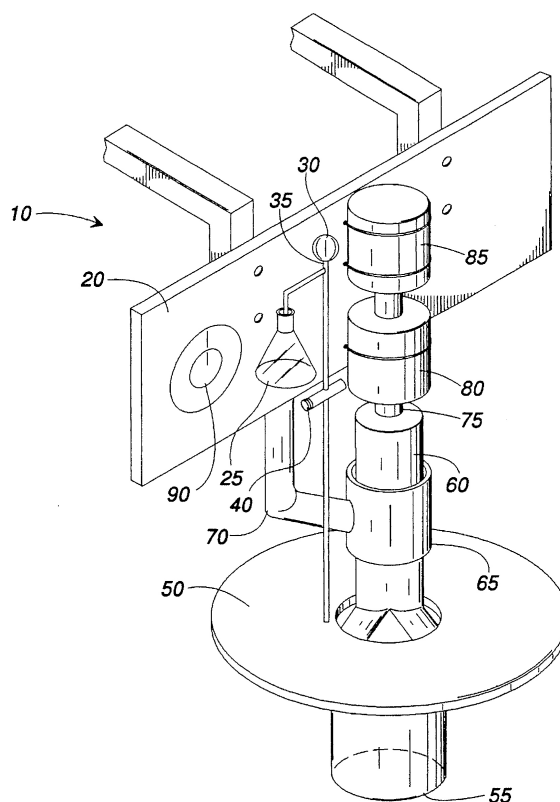


Figure A.9: Film pump for producing and spreading a monolayer (Pauken et al. 1996)

A.4.2 Oil application (liquid)

A modern variation of the gravity feed system is Ultimate-Agri Product's DS-1 dosing unit (Figure A.10a), which incorporates a programmable tap-timer control unit to meter Aquatain out for a pre-set length of time. As the DS-1 is a time calibrated gravity feed system, the flow rate will be higher when the Aquatain container is full than when it is nearly empty. Also, the ambient temperature can affect the viscosity of the Aquatain to some extent, resulting in a higher dose on very hot days than on cold days. It is suggested that the DS-1 is capable of servicing water storages of up to 1hectare in surface area.

A more accurate method of applying a liquid solution is by means of peristaltic pump. One such example is Ultimate-Agri Product's DS-2 (Figure A.10b), which is a programmable dosage unit that incorporates a peristaltic pump to apply accurate amounts of Aquatain at regular intervals. This unit is also solar powered for remote locations

with no on-site power source and is capable of servicing storages up to 20ha in size. For storages greater than 20ha it is recommended that multiple DS-2 dosing units be used. However, up to a certain size area, they suggest that aerial application may be economically more viable.

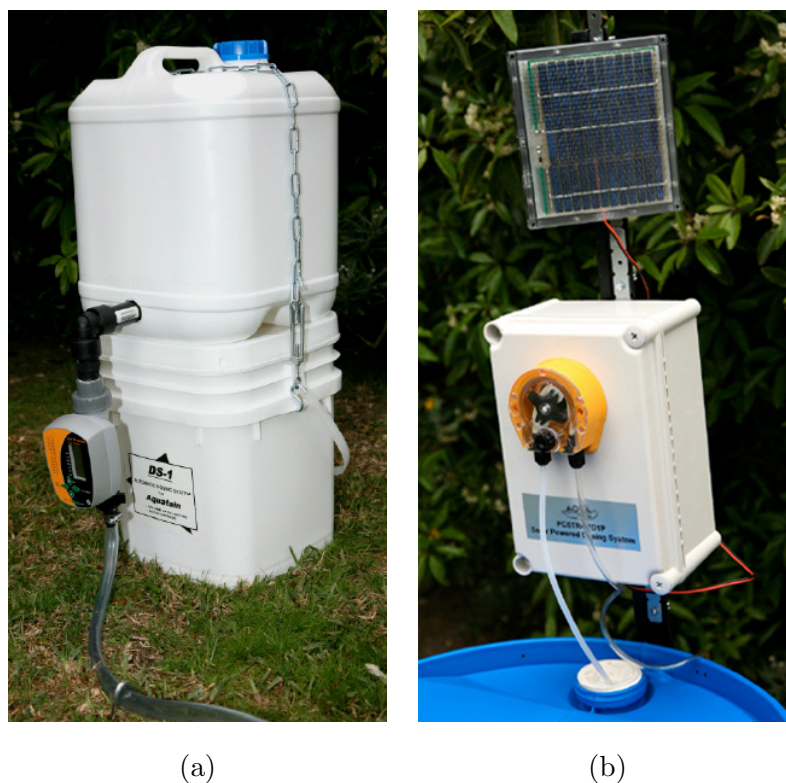


Figure A.10: Aquatain Dosing Units. (a) DS-1 gravity feed tap-timer system (b) DS-2 peristaltic pumping system

A further method for applying oil was developed by Noam Lahav and Palo Alto for treating the surface of a solar pond. In addition, they also developed a system for collecting and purifying the oil for re-use.

The application system comprises a number of wind activated nozzle units distributed along the periphery of the pond. Each nozzle unit includes a wind activated valve connected to an input pipe and to a pair of longitudinally spaced spray nozzles. The wind valve is rigidly attached to the stem of the valve and controls the opening and closing of the valve. The arrangement is such that the vane opens the valve whenever the wind direction lies within a predetermined azimuthal quadrant as indicated in Figure A.11 (Lahav & Alto 1984).

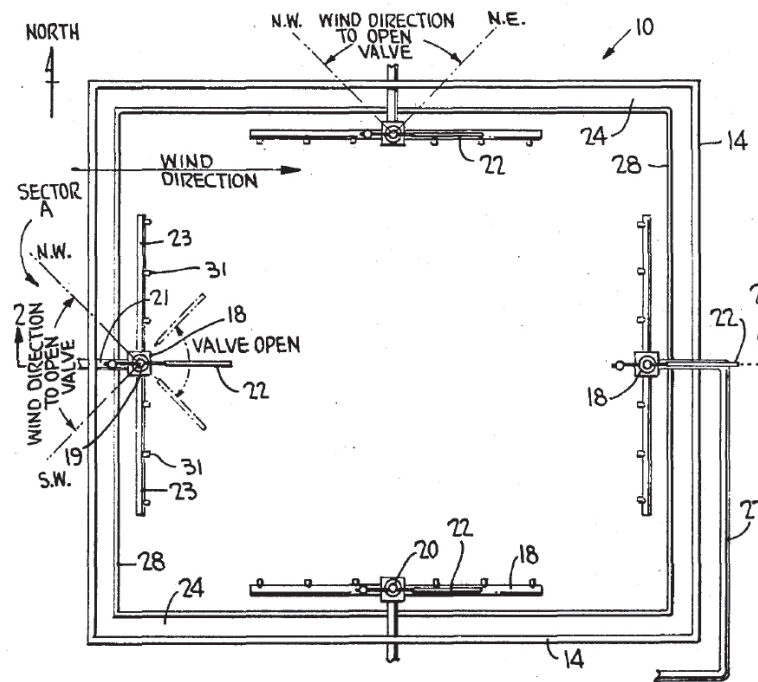


Figure A.11: Apparatus for applying oil to the surface of a solar pond (Lahav & Alto 1984)

The collection system comprises troughs or sinks located around the periphery of the pond and as the spreading oil reaches the downwind periphery, propelled by the prevailing wind, a layer of oil passes over the interior wall of the trough into its bottom. The collected oil in the troughs is then pumped a funnel or a coarse filter which separates macroscopic solid particles from the carrying liquid. The filtered oil is then passed through an inspection device for controlling the quality of the oil. After making the necessary determinations with the quality sensors, the quality of the oil is further improved by reconstitution. This is usually achieved through the addition of additives to the oil such that it has the desired properties prior to delivery to the spray nozzles, Figure A.12.

In this manner the oil application, collecting, purifying, controlling and recirculating system is unified into a continuous, generally closed circuit arrangement. It is claimed that a system of this nature saves both oil and labour by having a closed, continuous operating system (Lahav & Alto 1984).

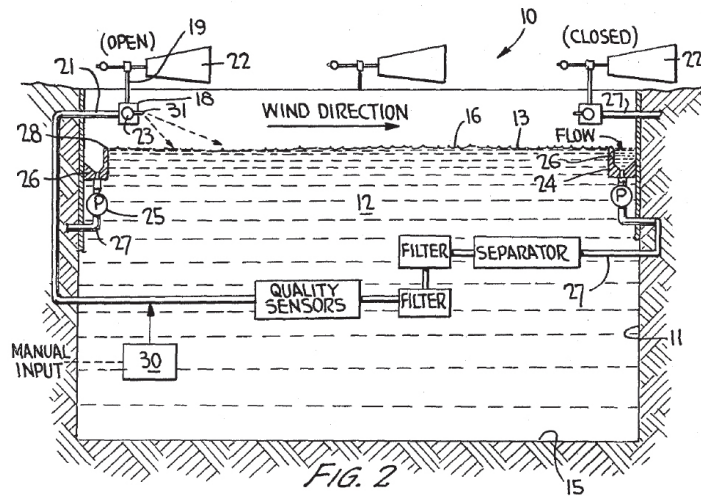


Figure A.12: Oil application, collecting, purifying, controlling and recirculating system (Lahav & Alto 1984)

A.4.3 Emulsion application (liquid)

The possibility of using water as an inert material to separate powder particles was studied by the US Bureau of Reclamation. Through preliminary experimentation Castle O. Reiser patented a method and apparatus for applying molten fatty alcohol emulsified with water. The general features of the apparatus include moving a stream of water at relatively high speed through a relatively narrow opening while at the same time delivering a molten fatty alcohol through a small orifice at the narrow opening. The fatty alcohol is introduced under lower pressure and at much lower speed than the speed of the water so that very small fragments of the fatty alcohol are sheared off for dispersal in the water stream, Figure A.13.

A certain amount of turbulence may also be affected immediately after introduction of the fatty alcohol media so that the very fine droplets of fatty alcohol are further split up into smaller fragments before stabilisation of a larger size particle can occur. This mixture of water and fatty alcohol is then applied to the water surface by a line of sprays individually activated in response to wind direction. This is done so that the sprays actually delivering the emulsion to the surface will always be on the windward side, Figure A.14.

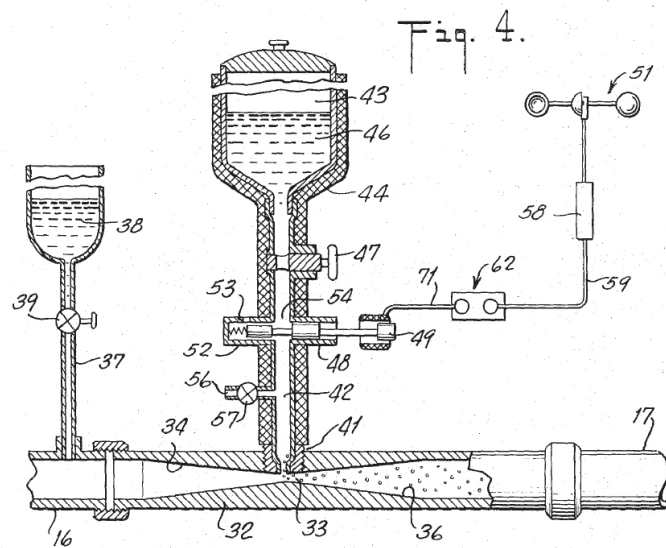


Figure A.13: Venturi style emulsion application of molten cetyl alcohol (Reiser 1970)

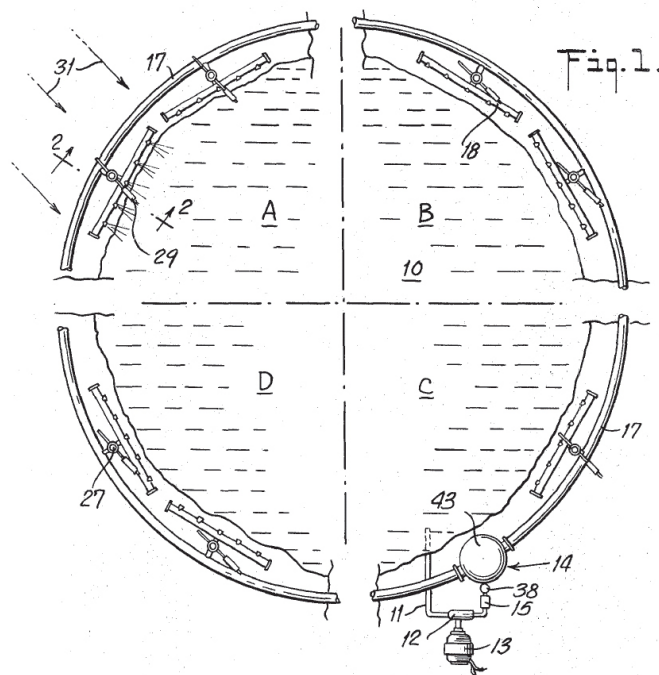


Figure A.14: Wind controlled apparatus for the application of emulsified cetyl alcohol (Reiser 1970)

In further detail,

“The emulsion is delivered from the emulsion line 17 to the distribution pipes 18 through a short connecting pipe 26 and the flow controlled by valve

27. The valve stem 28 carries wind vane 29 and the valve 27 is so constructed that when the wind blows windward of the valve's location, emulsion will be introduced to the distribution pipe 18 and to the spray heads 19. The wind vane 29 may be thought of having an arrow at its forward or long end and when this end is pointing out over the water, the valve associated with the vane will be opened to admit emulsion to the spray heads (Figure A.15)" (Reiser 1970)

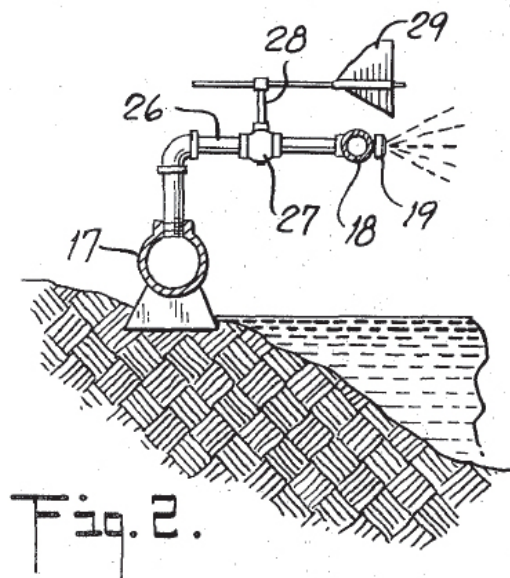


Figure A.15: Detail of wind controlled valve on the spray heads (Reiser 1970)

The principle of using water as a diluting and transporting medium for monolayer has also been employed in the JV-225 boat-mounted WaterSavr mixing system. The JV-225 is a manual application system that works on the premise of mixing the WaterSavr powder with water and then pumping it onto the water surface as a slurry. This spreading system needs to be mounted in a stable, flat bottomed (16ft) boat that requires a crew of two, one to drive the boat and the other to operate the spreading system. Technical specifications are detailed below:

Capacity:	225kg of WaterSavr
Power Source:	Liquid fuel combustion engine (outboard motor)
Crew Size:	2 People
Treatment Area:	60ha/hr
Dispensing Time:	3 hours and 20 minutes per 225kgs of WaterSavr
Current Pricing:	US \$3,400 plus shipping and handling

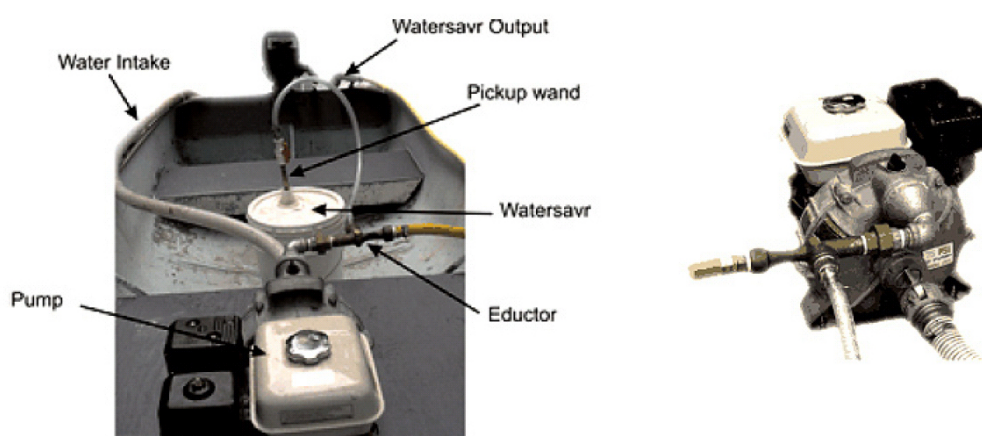


Figure A.16: JV-225 boat mounted WaterSavr mixing system (FSI 2007)

In more detail, water pressure is delivered by a 5-hp Honda pump to the water inlet and through a mazzei injector, creating a vacuum in the mixing chamber. Mazzei injectors are high-efficiency, venturi-type, and differential pressure injectors with internal mixing vanes. When a sufficient pressure difference exists between the inlet and outlet ports of the injector, a vacuum is created inside the injector body, which initiates suction of a liquid or gas through the suction port (Brink & Symes 2010).

Water is then directed through the mixing chamber control valve and Dole jet via delivery lines to the mixing chamber. Swirling water in the mixing chamber is then drawn into the mazzei injector and the hopper valve is then opened manually allowing dry WaterSavr to be drawn into the mixing chamber. Once the WaterSavr has been mixed with water, the solution is drawn back into the mazzei injector and directed through the outlet to be applied to the water surface (Brink & Symes 2010).

Another example is the Bio-Systems Engineering designed and built automatic monolayer mixing and distribution system (Figure A.17), commissioned by the NCEA for the application of WaterSavr to a 120ha water storage at Dirranbandi in Queensland.



Figure A.17: WaterSavr mixing system designed and built by Bio-Systems Engineering (FSI 2007)

In principle this is a mixing style system similar to that of the FSI spreaders for WaterSavr. This system meters the WaterSavr powder into a mixing chamber using a screw auger where the dry powder is mixed with water. From there the water/powder solution is pumped using a diesel Deutz pump into a grid of distribution pipes and evenly distributed on the water surface where the monolayer self spreads. The application system is designed to fill all of the pipes before distributing the water/powder solution, followed by a cool down which flushes all of the solution out of the pump and grid network of pipes.

The hopper holds enough monolayer for one week of application and it requires a knocker to stop the powder bridging. The hopper is located on top of the storage wall for ease of filling, while the pump is located lower down the wall closer to the water level to reduce suction height.

The grid system has nine outlets evenly spaced over the 120ha. This resulted in only one emitter per 13ha, a very large area covered per emitter but at relatively low installation cost. The main distribution lines are 50mm poly pipe and each riser has 10-20m of flexible hose with its own float. The poly pipe floats on the surface of the water and is tethered at either end to hold the outlet points in the prescribed position. However, the pipes ideally need to be placed on the bottom of the storage as the wind and waves were observed to place a great deal of strain on them.

Although the NCEA reported some initial problems with the applicator; air locks in the positive displacement pump and problems in metering the monolayer owing to bridging, the system generally worked very well for distributing the slurry mixture. However, due to the mixing of WaterSavr with water and the time taken for the slurry to get to the outlet points, the WaterSavr powder appeared to lose its spreading ability.

A.4.4 Molten application (liquid)

Frenkiel suggests that field studies on the behaviour of monolayer have indicated that the most efficient method for treating a reservoir under windy conditions would be by the use of automatic dispensers strategically placed around the banks and possibly within the reservoir which would distribute the retardant at rates proportional to the wind speeds (Frenkiel 1965).

A prototype dispenser of this kind was designed by Quentin L. Florey and Lloyd O. Timblin in the early 60s, which sprayed molten cetyl alcohol from a pressurised container heated by a small kerosene burner. The spray would solidify in the air creating a fine powder which fell on the water surface to form a monolayer. Two of the primary objectives for this apparatus, to provide a method for easy application of a finely divided powder to water surfaces while eliminating the handling problems associated with the direct application of fatty alcohols in a solid form.

The system reviewed (Figure A.18) comprises a storage and pressure tank 1, where a higher fatty alcohol evaporation retarding material is maintained as a molten liquid at a temperature of 150 to 160F by the heat from burner 2, having its fuel supplied from a tank 3. Other connections to tank 1 include a liquid level U-tube manometer type indicator 17 is connected to tank 1 to sense pressures at the top and bottom of the tank through connecting piping 18 and 19, joined to inlet means 10, and coupling 16, respectively (Florey 1965).

Also shown in Figure A.18 is spray nozzle 20 supplied with the molten higher fatty alcohol through outlet conduit 21, having a filter 22 therein, and connected to the coupling 16. Possible clogging of the nozzle by solidification of the higher fatty alcohol between

spray bursts is prevented by mounting the nozzle in a heated chamber, comprising a small sheet metal box in which a gas 'pilot light' is mounted about 8 inches below the nozzle (Florey 1965).

Mechanism 30, which is rotated to sense wind direction, is operative to maintain circuit 26 completed at switch 32, only when the direction sensed is within an arc of 90 degrees defining the limits in which dispensing of the retardant material would be effective to cover the water to be conserved. In operation, valve 23 is intermittently actuated by the controller mechanism 25 to cause a flow of molten higher fatty alcohol there through in short bursts. The frequency of the bursts and the direction of each are determined as functions of wind velocity (Florey 1965).

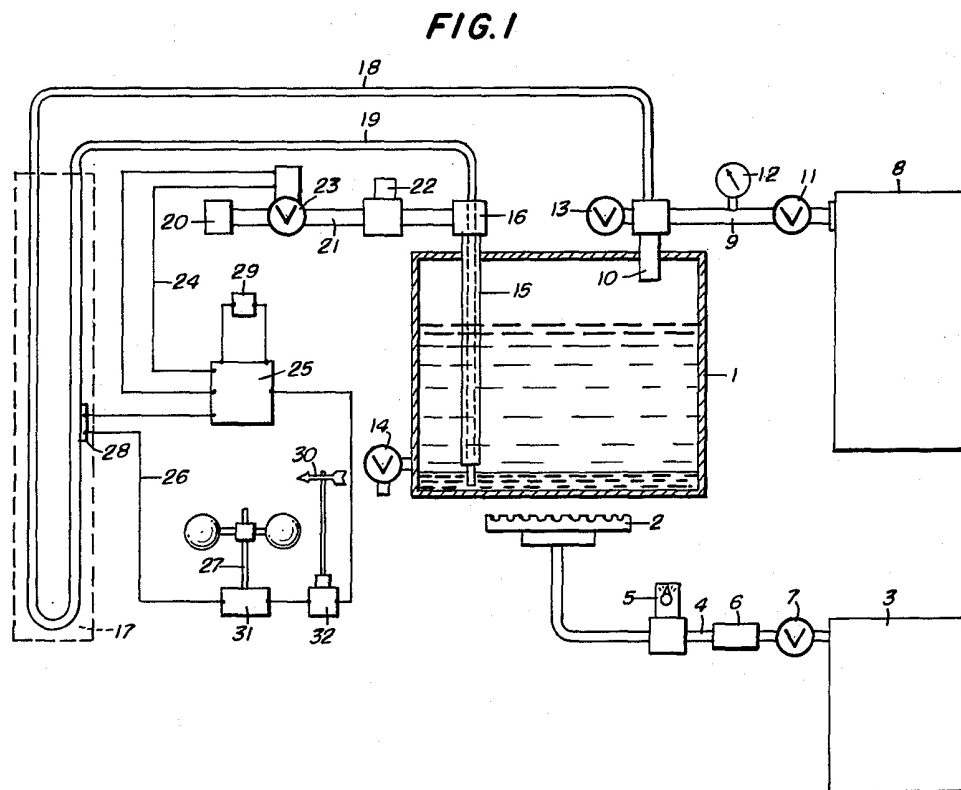


Figure A.18: Diagram of a Hot-Spray Application System (Florey 1965)

However, Frenkiel noted that the performance of these automatic dispensers was not satisfactory as malfunction of electrical and mechanical parts occurred repeatedly. In particular spray nozzles would freeze causing considerable difficulties. Consequently, the complexity of this equipment led the American's to abandon this method in favour

of non-automatic application (Frenkiel 1965).

A.4.5 Aerial application (liquid & solid)

In 1961, the Bureau of Reclamation undertook a study to determine the feasibility of applying evaporation retardants from the air. The first year was spent primarily in developing a dispenser that would handle the retardants in a liquid state. Subsequently, an applicator capable of applying the retardants in a powder form was also developed.

The two dispensers were tested at a number of different sites, finding that both powders and sprays most suited for aerial application appear to be in the 75 to 200 micron mean particle-diameter size. Particles smaller than 75 microns were susceptible to excessive wind drift, while powder particles larger than 200 microns are not as effective at forming a film.

A comparison between powder dispensers and liquid dispensers for aerial application reveals that powder dispensers have a number of advantages such as easier handling with less safety hazards (no hot liquids), low capital investment and less labour required. However, the powder had a tendency to clump and bridge across the outlet of the hopper.

In conclusion, aerial application of evaporation retardants appeared to be an effective delivery method for large reservoirs. However, no definitive preference for this method could be determined as further tests were required to quantify evaporation reduction performance and improve their aerial application techniques.

A.4.6 Powder application (solid)

During many of the earlier field trials it has become increasingly evident that the use of powdered materials, which are very effective in producing the film, present definite problems of handling and dispensing. In Australian trials, difficulties were also experienced with storing and transporting cetyl alcohol powder. Consequently as a remedy a fine 'spray dried' powder was produced in which the particles were globular

instead of 'flaky'. This material could be stored for long periods and transported over considerable distances with no deleterious effects. The powder would then be sieved through wire screens before being loaded into an agricultural duster on a boat, from which it was blown out over the water.

Another application method, the Robertson grinder-duster, was first trialled in Queensland, Australia, during the Lake Corella experiments 1959. It basically consists of a wire brush rotating at high speed to shred solid blocks of cast cetyl alcohol. This produces a very fine powder with excellent spreading properties, which is then blown through a delivery tube by a fan. As the equipment is mounted in a boat, the powder is not produced until actually required. The blocks of cetyl alcohol were cast on-site as required and cooled to 15C before use to increase their spreading ability.

In more detail the Robertson grinder-duster, Figure A.19, comprises a spindle 1 on which is mounted a cylindrical wire wheel type brush consisting of spaced annular stock members 2 of channel section carrying closely packed wire bristles. Axial-flow fans 7 are mounted at the ends of the spindle adjacent the brush assembly so as to be rotatable in unison with the spindle 1 (Robertson 1966).

To project a stream of finely divided particles of hexadecanol on to the water surface, a preformed block of material having a cross-section such that it will fit neatly into the hopper is pressed downward by hand through the feed hopper 19 on to the upper ends of the wire bristles, this causes disintegration of the block into small particles which will mainly consist of particles of a size not greater than 0.2mm, such particles being emitted from the casting through the outlet tube 20 (Robertson 1966). Further tests were carried out with the Robertson grinder-duster at Stephenson's Creek Reservoir and the Umberumberka Reservoir. At Stephenson's Creek, a speed boat capable of 20-25 M.P.H. was used to cover the entire surface area of more than 405ha in about an hour during light winds.

An automatic dispensing system was later developed by Nicholaichuk and Pohjakas at the Canadian Department of Agriculture, which consists of a wind-driven fan that supplies power to drive a powder dispensing unit, Figure A.20. A 60cm diameter fan drives a flyball governor which engages a disc clutch to transmit power through the

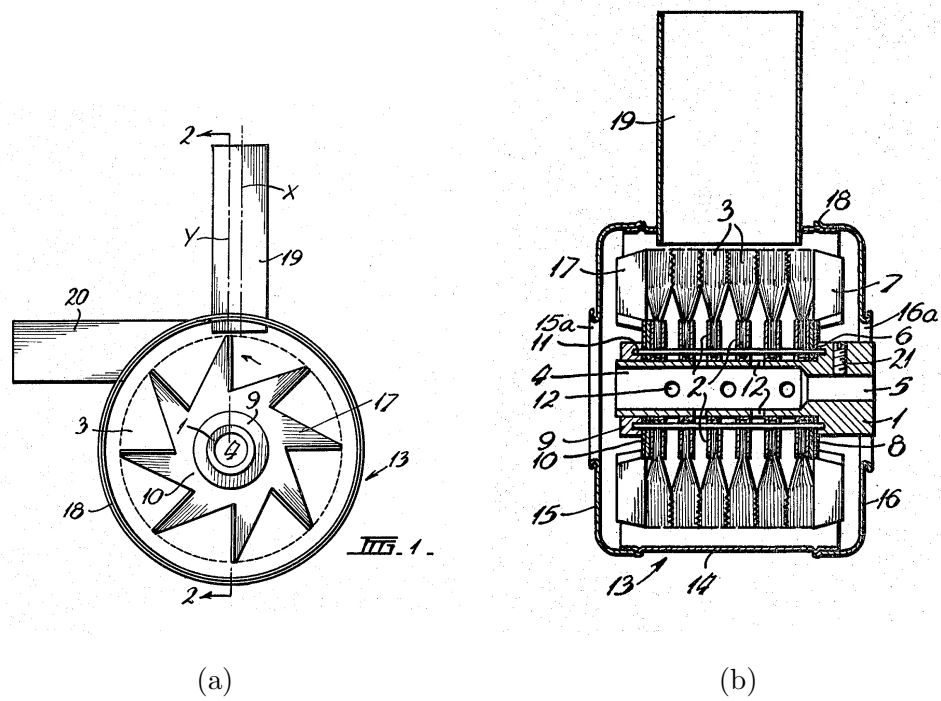


Figure A.19: Diagrams of a Robertson grinder-duster. (a) Detailed internal view (b) Section along 2-2 (Robertson 1966)

speed reducing gearbox. The 60cm diameter fan is sensitive to wind speeds as low as 4.8km/h. The flyball governor is set to interrupt transmission of power to the clutch when wind speeds above 16km/h are reached. The gearbox provides an overall speed reduction of 216:1. Power is then transferred by a right-angled semi-flexible driveshaft to the dispenser floating on the water surface approximately 3 meters away from the shore installation (Nicholaichuk & Pohjakas 1967).

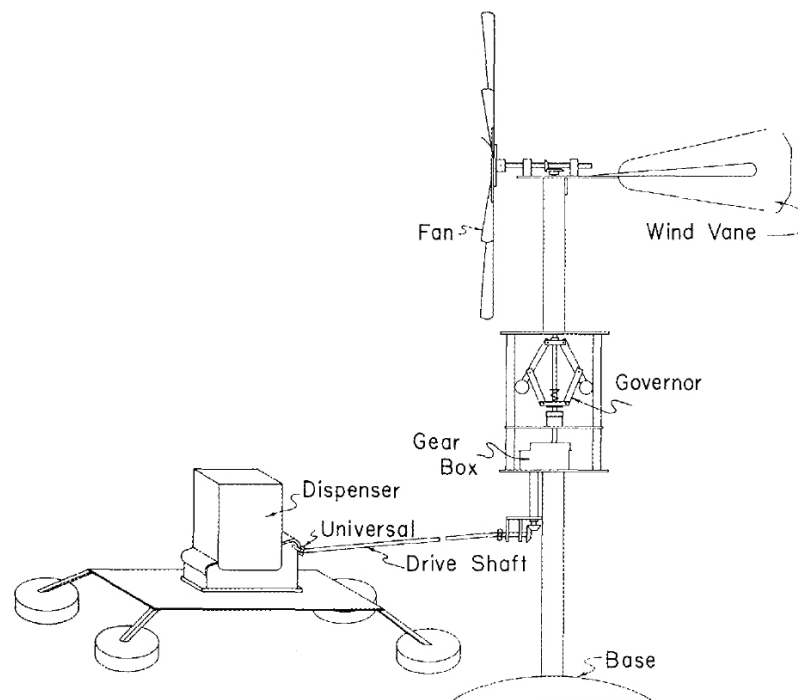


Figure A.20: Diagrammatic sketch of the wind operated powder dispensing system. Reproduced from: (Nicholaichuk & Pohjakas 1967)

The dispenser unit consists of a 300g capacity container with a notched flat belt that functions as a feed mechanism. An adjustable slide opening varies the dispensing rates from 0.012 to 0.024g per revolution of the drive shaft. The entire dispenser is mounted on a frame supported by four 25cm diameter floats. The rubber belt releases powder which drops through an opening in the dispenser platform to the water surface where it spreads to form a film (Nicholaichuk & Pohjakas 1967).

A further application system was developed by Nylex for the WaterSavr product, which utilised compressed air as a distribution medium for the powder. The powder from the hopper would fall into the distribution tube and then compressed air would be used

to force the powder through the distribution tube and delivered just below the water surface, Figure A.21.



Figure A.21: Nylex pneumatic spreader (Craig 2006)

Compressed air is pulsed through the distribution tube to reduce the chances of the WaterSavr powder clumping in the hopper. The powder is delivered just below the water surface to completely eliminate any chance of the powder being blown away by the wind, Figure A.22.

Through independent testing by Nylex and FSI, the pneumatic spreader proved quite effective for the distribution and application of powdered monolayer. Unfortunately, a pneumatic spreader was never commercialised.

Consequently FSI later developed an automated spreading system for WaterSavr, which is basically a pre-programmed hopper that agitates the WaterSavr powder (to reduce



Figure A.22: WaterSavr powder being pneumatically spread from just below the water surface (Brink & Symes 2010)

clumping) directly onto the water surface, figure A.23. Some of the M-60s basic specifications are listed below:

Capacity:	60kg of WaterSavr
Power Source:	12volt battery
Charging System:	Photovoltaic solar panel
Refill Period:	Every seven days on a 20ha storage
Current Pricing:	US \$3,400 plus shipping and handling



Figure A.23: M-60 Automatic Spreader (FSI 2007)

FSI suggest that one M-60 can treat a maximum of 20ha when the refill schedule is once a week. The M-60 can also be used in multiples, for example five M-60s can service 100 hectares (250 acres) or can be programmed to extend the refill cycle on 50 hectares (125 acres) to two weeks from one. This system is best suited for remote water storages up to 100 hectares in surface area.

A.5 Systems for monolayer detection

As a monolayer film is approximately 2 nanometers thick it is a very difficult thing to visualise let alone detect on the water surface of a dam. Despite this various methods have been devised for determining the presence and spatial distribution of a monolayer film. Frenkiel (1965) notes that the Bureau of Reclamation used indicator oils to determine the surface pressure of a monolayer film in comparison to the water surface pressure. However, through subsequent testing the indicator oil method proved misleading due to the difficulty of differentiating between monolayer and microlayer film pressures. Likewise, photographic techniques for film detection could not always be relied upon since many factors such as the angle at which the picture was taken, the position of the sun, and cloud and haze condition significantly influenced the indication of film coverage.

Bureau of Reclamation researchers also noted that even under calm conditions, through careful examination of the surface by an experienced observer, apparent or no-film slicks and fully compressed film slicks could usually be differentiated (Frenkiel 1965). Consequently, several methods were adopted by the Bureau of Reclamation during field tests to assess monolayer film coverage with maximum accuracy: (a) observations and photographs made from a vantage point above the water surface; (b) observing the location of the film when driving periodically around the lake; (c) aerial photographs coupled with shore observations (Frenkiel 1965). On the basis of all this information monolayer film coverage of the water would be determined and mapped two to five times a day, time and weather permitting.

Still another photographic technique was trialled, using a polarising filter, based on the property that a monolayer film on the water surface effects the rotary polarisation of the reflected light. It was found that this technique was helpful for locating the monolayer, determining its relative degree of compression, and the boundary between covered and uncovered portions of the water surface (Frenkiel 1965). Another possible monolayer detection method was reported by Saylor (2001), who used a nitrogen cooled infrared camera to visualise the difference in the change of surface viscosity between a water surface with and without monolayer present. However this technology for monolayer

detection was not considered practical for in-field use for the following reasons: (i) the Raytheon-Amber AE4256 IR camera used by Saylor is nitrogen cooled, (ii) it costs around \$20-40,000, and (iii) the changes being detected by the infrared camera are caused by changes in surface viscosity and many pollutants may have a similar effect on this as a monolayer film.

More recently a team of researchers from the University of New England (UNE), Paul Coop, David Lamb, Chris Fellows and Ron Bradbury, have been investigating and trialling methods for detecting the presence of an evaporation suppressive chemical film on the water surface. Through their previous research it had been noted that a chemical film increases surface tension which creates a calming effect on waves causing a change in the specular reflectance properties. This comparison can only be made when the water surface is partially covered. However if the film totally covers a water storage, or is totally absent, no comparison can be made and some type of referencing system is needed as part of an automatic detection system (Coop et al. 2007).

Their investigations to date have been focussed along two classes of assessment methods:

1. Remote sensing, which in principle could be used to map an entire storage, but in most embodiments would not be available for continuous monitoring.
2. Single-point, where inexpensive measuring instruments could be placed at a number of locations on a water storage surface to provide a continuous assessment with much reduced resolution in the spatial domain.

A broad range of methods for film detection have been trialled by the team at UNE, including visible-near infrared spectrometry, fluoroscopy, polarisation, horizontal surface tension monitoring, laser ripple reflection, lipid dyes and temperature differential measurement. Although many of these methods show a difference between the monolayer surface and water surface while in the laboratory, conditions in the field are not so stable. For this reason the temperature differential methods show the most promise, as there are no moving parts apart from a fan, well above the water, Figure A.24. It is worth noting that the temperature differential method is a single-point measurement system.

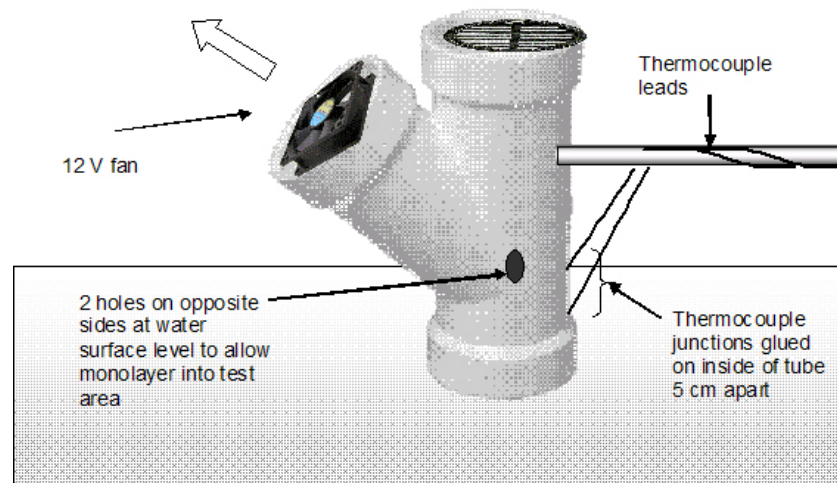


Figure A.24: Prototype temperature differential detection unit (Coop et al. 2008)

As Coop suggests in his 2008 CRC-IF Technical Report,

”On water storages the surface is in constant motion and it is difficult to place a thermocouple in the top 1mm accurately enough to obtain repeatable results. Therefore the favoured method is the accumulation of cold water in a tube. It doesn’t need much accuracy in position in the water and unlike the hot air method, only uses a small amount of power. Further work will be carried out on optimising this model, with field trials planned” (Coop et al. 2008).

Figure A.25 shows the temperature cooling effect a monolayer has on the water inside the Y-tube compared with the bulk water outside the tube while the fan is running.

“... due to the amount of accumulation of cold water produced by the surface under wind conditions produced by the fan. Cold water can ascend away from the surface outside the tube, however inside the tube it is accumulating” (Coop et al. 2008).

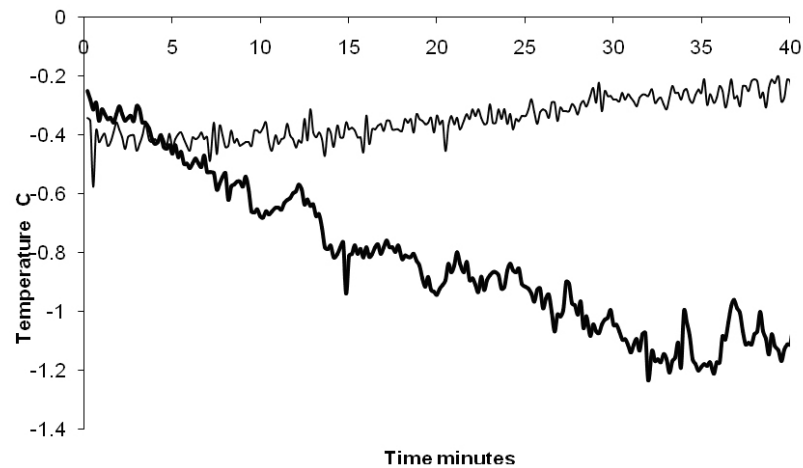


Figure A.25: Comparison of temperature difference between water inside the Y-tube and bulk water outside the tube. Water temperature inside the Y-tube is the thick line. Bulk water temperature outside is the thin line. Humidity at 32% and wind speed at fan is 5.3 m/s. (Coop et al. 2008)

A.6 Water surface management technologies

The deleterious effect of wind on a monolayer film is twofold; firstly wind displaces the film on the downwind shore, and secondly wind creates water waves which can break-up the film. Through both these wind induced effects, monolayer film coverage across the water surface is effectively reduced. It has been hypothesised that the use of wind barriers and/or containment barriers may help to reduce wind speed or film drift across the water surface, and or dissipate wave action. The following is a review of potentially appropriate water surface management technologies.

A.6.1 How wind generates water waves

When a turbulent wind blows across an initially calm water surface, the first waves to appear at a wind speed of about 0.25 to 1 m sec^{-1} are the capillary waves. The restoring force for these waves is the surface tension. The surface capillary waves initially grow in height at a linear rate proportional to the wind speed, as explained by Miles (1957) and Miles (1959).

It has long been observed that a surface film has the effect of damping the capillary waves (Davies & Rose 1965), and it is believed that a portion of the wave energy loss is due to a viscous drag of the associated chains of water molecules which are bonded to the molecules of the adsorbed surface film. The drag occurs when the molecules are forced into movement as a result of the alternating compression and expansions of the surface caused by the passing progressive waves. The circular motions of the water particles laterally compress the surface film on the forward side of the wave, and expand it at the rear. The surface tension forces oppose this, and try to move the surface in the opposite direction to the water motion, which is called the Marangoni effect.

Once these small waves have formed due to the effects of the turbulent wind, they start to interact with the atmosphere through pressure differences and through the increased water surface roughness, which makes the velocity field in the air more complicated and more turbulent. This increases the effective eddy diffusivity of water vapour above the water surface, increasing mixing and increasing the flux of water vapour away from the surface.

If the wind continues to blow, the waves grow in size until they have a length of about 1.7 cm and a speed of about 0.24 m sec^{-1} ; if they grow longer than this they start to become gravity waves for which the restoring force is mainly gravitational. Turbulent eddies in the air cause “cat’s paws” which are groups of capillary-gravity waves of about 40 cm across, which indicate areas of locally high shear stress. At wind speeds above about 2 m sec^{-1} gravity waves are formed, and these waves grow at rates exponentially proportional to the wind speed (as explained by Phillips (1957)), producing larger and larger waves. However the transfer of energy from capillary to longer gravity waves is reduced by the presence of the surface film, as first observed by Cox (1958) and since studied by many authors, for example Alpers & Huhnerfuss (1989)). The nonlinear amplification of gravity waves prior to emergence of breaking and its inhibition by a surface film involves the film damping of parasitic capillary waves riding on the fronts of gravity waves.

At higher wind speeds, there are irregular sharp crests with poorly defined speeds and directions, which further increase the effective eddy diffusivity of the water vapour and its vertical flux rate.

The local rapid motion of the water surface and the variations in wind shear on different parts of the wave can also cause the surface film to develop in homogeneities, which decreases its ability to reduce evaporation. When the wind is blowing from land across a water body the waves under the wind blowing from the land are short, of small amplitude and low speed. As the wind persists, the Miles-Phillips Mechanism process can continue until the transfer of energy to the waves is balanced by their energy loss when they reach equilibrium.

The waves further from the upwind shore become longer and higher and more regular until they reach the downwind edge of the water body. The sizes and speeds of the waves depend on the length of the fetch and the depth of the water body, the waves being smaller and slower on shallower water. Also, the waves may be damped by growths of water weed at or near the surface. The wind shear acting in one consistent direction for a long time also causes the surface film to be pushed towards the downwind shore, leaving a gap upwind. If the waves are breaking on a sloping beach at the downwind shore then the surface film may be deposited on the beach by breaking waves, and when the water sinks into the porous beach some of the surface film may adhere to the particles and be temporarily or permanently lost to the water body.

At higher wind speeds the air and water velocity fields interact in a complicated way and there is air flow separation downwind from the wave crests, with reversal of air flow on the downwind sides of the waves. The waves break and form white caps and water drops form as spray at the top of the wave. The evaporation of these small drops greatly increases the overall evaporation rate, and the surface film will have little effect on this.

The surface layer reduces evaporation by forming a physical barrier to the movement of vapour, and also to some extent by reducing the size of the water waves which tend to cause more turbulence and to disrupt the surface layer. Both of these processes are eventually negated by sufficiently high wind acting for a sufficiently long time, but the degree of the reduction depends on the size of the fetch and the depth of the water body.

A.6.2 Basic water wave theory

In a water wave the motion of the water particles is not strictly perpendicular or strictly parallel to the line along which the wave travels. Instead, the motion includes both transverse and longitudinal components, since the water particles at the surface move on nearly circular paths as indicated in Figure A.26.

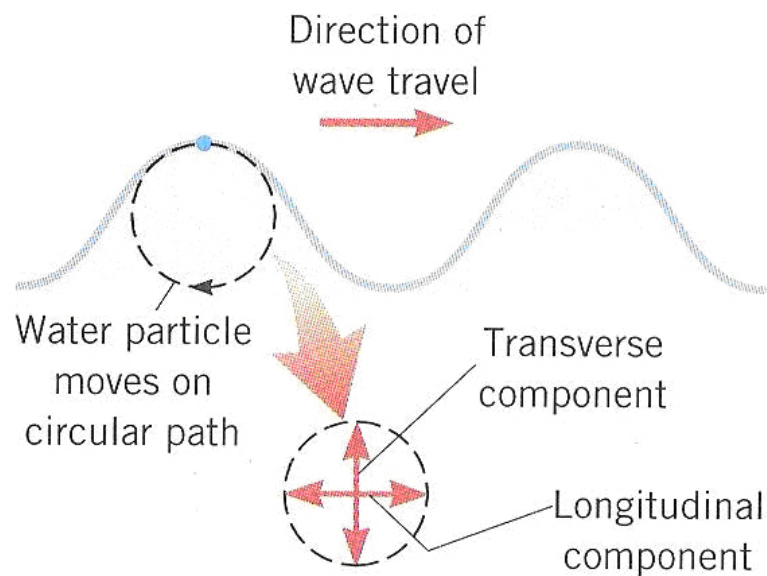


Figure A.26: Water particles at the surface move clockwise on nearly circular paths as the wave moves from left to right (Cutnell & Johnson 2001)

A.6.3 Wind speed reducing technologies

Researchers have identified that wind is probably the single most important determining factor in the application and maintenance of monolayer on open water surfaces. Wind across the water surface can generate water waves which then break up the surface film decreasing its ability to reduce evaporation. Wind waves also increase the effective eddy diffusivity of water vapour above the water surface, which increases mixing and flux of water vapour away from the surface (evaporation). Since monolayers are readily moved or broken up by the wind, the reduction or elimination of this adverse effect should be a logical goal of research.

Wind barriers

Frequently shelterbelts and windbreaks are used to reduce evaporation (Bates, 1911; Van Eimern et al., 1964; Davenport and Hudson, 1967) and to control erosion (Staple, 1961; Chepil and Woodruff, 1963). Evaporation percentages are reduced less than wind speed percentages by shelterbelts and windbreaks (Al'Benskii and Nikitin, 1956; Van Eimern et al., 1964). In fact, evaporation is occasionally increased in sheltered areas. Baltaxe referred to Blenk's observation that evaporation was less in the open wind than in the lee of a solid barrier, which he ascribed to greater turbulence behind the barrier (Baltaxe 1967).

Skidmore & Hagen (1970) demonstrated the relationship between wind speed and evaporation as influenced by barrier porosity. Relative data from five runs with reference wind speeds windward of the barrier were averaged and are plotted in Figure A.27.

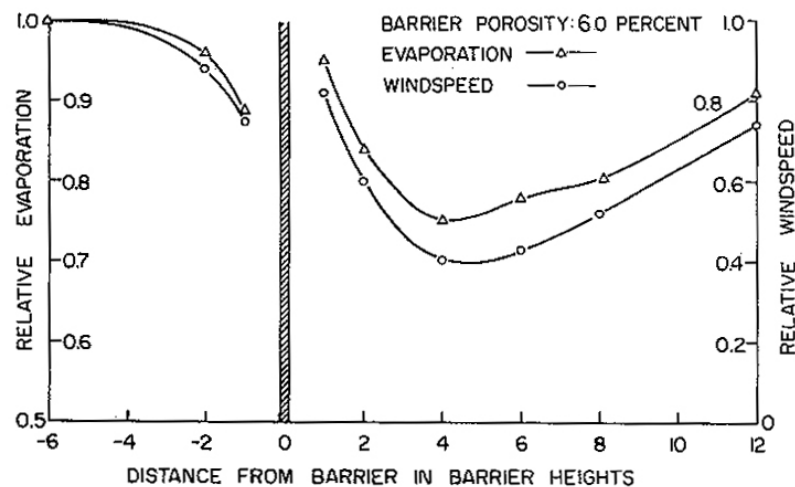


Figure A.27: Relative evaporation and wind speed at various distances from 60% porous slat-fence barrier. Plotted data are averaged from five observation periods with open-field wind speeds from 6.2 to 7.1m/sec at an elevation of 1.42m above soil surface. Reproduced from (Skidmore & Hagen 1970)

Similarly, reference wind speed windward of barriers with porosities of 40% and 0% (i.e. solid) were averaged over five runs and are plotted in Figures A.28 and A.29 respectively.

As can be seen in Figures A.27, A.28 and A.29, evaporation and wind speed varied

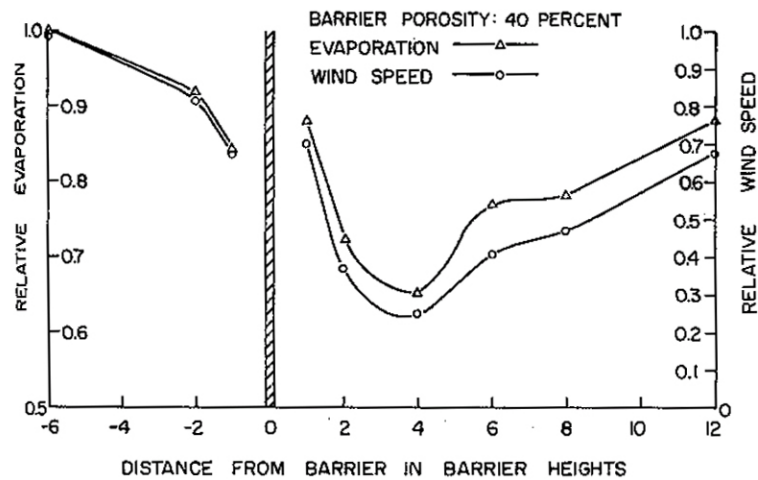


Figure A.28: Relative evaporation and wind speed at indicated distances from 40% porous slat-fence barrier. Plotted data are averaged from five observation periods with open-field wind speeds from 5.6 to 6.2m/sec at an elevation of 1.42m. Reproduced from (Skidmore & Hagen 1970)

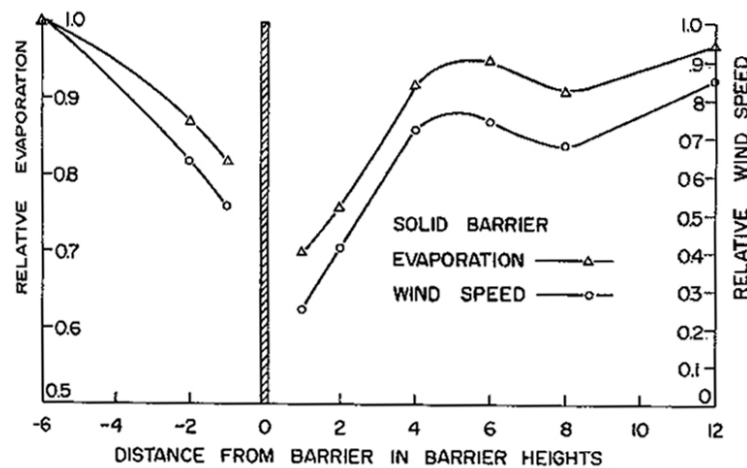


Figure A.29: Relative evaporation and wind speed at various distances from 60% porous slat-fence barrier. Plotted data are averaged from five observation periods with open-field wind speeds from 6.2 to 7.1m/sec at an elevation of 1.42m above soil surface. Reproduced from (Skidmore & Hagen 1970)

widely between the different barrier porosities, however, their two curves are nearly parallel. This suggests that evaporation and wind speed are closely related regardless of barrier porosity, wind speed reduction patterns, or turbulence induced by the barriers.

After wind speed and evaporation reached a minimum leeward of the 60% porous barrier, they gradually increased to open-field conditions as distance from barrier increased (Figure A.27). Whereas, evaporation and wind speed lee of the 40% porous barrier tended to increase quickly after reaching a minimum, then levelled off for two barrier heights before gradually increasing to open-field conditions (Figure A.28). Differently again, when wind speed and evaporation reached a minimum next to the leeward side of the solid barrier, they increased rapidly with distance from the barrier to about 5H then decreased to about 8H before starting to increase again (Figure A.29).

As was observed by Skidmore and Hagen, when barrier porosity is decreased, leeward airflow becomes increasingly chaotic, which is consistent with prior research by (Blenk, 1953; Baltaxe, 1967). Other investigators (Woodruff, 1954; Read, 1964) have also observed greater evaporation reduction with dense barriers.

‘Grided’ wind barriers

Experiments by Crow (1963) and Nicholaichuk (1978) have been conducted to determine the potential for wind barriers to be used in conjunction with a monolayer to help in maintaining an established film. Nicholaichuk notes that transport to the lee-shore by the wind, suspension, and biological degradation are some ways in which the film can be lost. The most important factor is the loss of film due to wind action. Crow suggests that the adverse effects of wind can be reduced by placing windbreaks along the shoreline and confining the film’s movement within a network of floating compartments.

Crow experimented with two types of wind and film barrier systems, type A was an open type wind baffle constructed from 1.5 inch wooden pickets spaced 2 inches apart and fixed to floats arranged in a grid network on the water surface. Type b was a true film barrier formed by securing plastic sheet to the pickets of the type A barrier, still fixed to the floats arranged in the grid network, Figure A.30.



Figure A.30: Crow's experimental pond showing 'Type B' closed wind/film barriers for reducing wind speed and confining monolayer within each bay. Reproduced from (Crow 1963)

However, due to the poor performance of the open type A wind baffles, Crow decided to only continue testing with two different heights (0.25 ft and 0.90 ft) of the type B barriers. During evaporation tests of the 0.9ft high type B closed barriers without monolayer a significant decrease in evaporation (9.1%) was obtained, with no reduction for the 0.25 ft high barriers. The results and conditions of these tests are shown in Figure A.31.

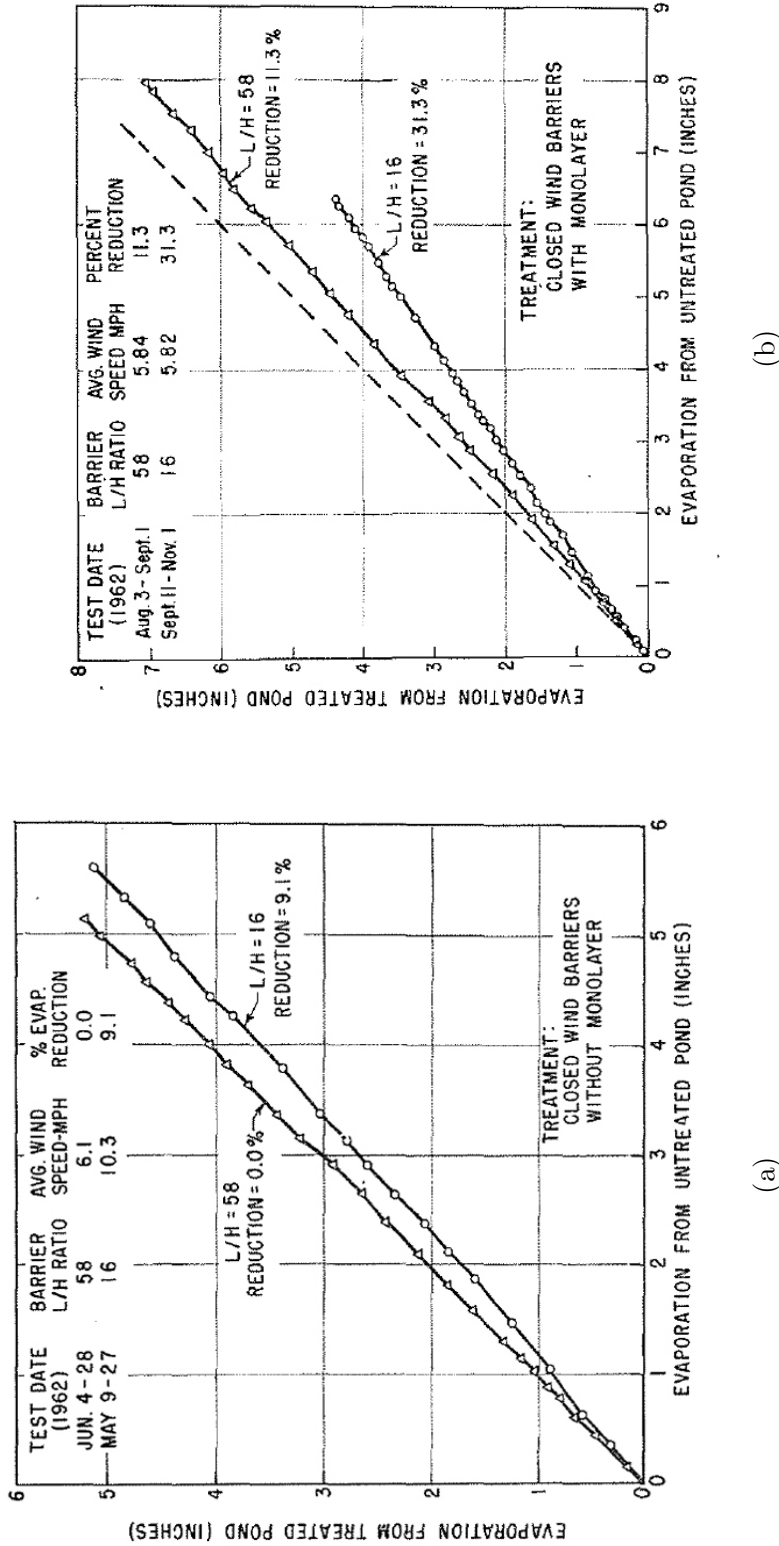


Figure A.31: Crow's evaporation reduction tests of wind barriers and baffles with and without monolayer. (a) The effectiveness of closed wind barriers of different spacing/height (L/H) ratios for reducing evaporation. These tests were made without monolayer. (b) Relative evaporation reduction resulting from confinement of C16OH and C18OH fatty alcohol monolayer confined within closed wind/film barriers of different L/H ratios. Reproduced from (Crow 1963)

Crow notes that one of the expected benefits of the barriers was preventing film losses by wind action. Therefore, evaporation tests of the barriers in combination with monolayer were conducted to determine their combined effect at closed barrier spacing/height (L/H) ratios of 16 and 58. Crow observed that the monolayer in combination with the L/H=16 barriers yielded three times greater evaporation reduction than the L/H=58 setting, Figure A.31. Evaporation was reduced 31.3% when the chemical was confined within the L/H=16 barriers. Crow goes on to suggest that,

”This is probably as much reduction as can be expected, since previous tests Crow (1961) with continuous chemical application resulted in reductions of this magnitude. However, with the barrier system, smaller amounts of chemicals were required, and there was no need for expensive application and control apparatus” (Crow 1963).

Nicholaichuk later experimented with a combination of different options to suppress evaporation, they included (a) application of C16OH from a wind operated automatic dispenser, (b) a snow-fence 2.4 m high, (c) floating wooden grids of 12 m x 12 m. Nicholaichuk reported that the snow-fence reduced the wind speed at the 500 mm level above the water surface by 20%. This reduction improved the efficiency of the monolayer film. The average reduction in evaporation with the monolayer film and snow-fence combination was 20%. The cumulative reduction at the end of the 150 day test period was 30%, Figure A.32.

Furthermore, Nicholaichuk reported that the floating grids also improved the efficiency of the monolayer film, Figure A.33. The average evaporation reduction was 37%, while the cumulative reduction at the end of the 188 day test period was 59%. The combination floating grid and snow-fence thus proved to be most effective.

Shelterbelts

Shelterbelts refers to a belt of trees and/or shrubs arranged as a protection against strong winds. Shelterbelts, similar to windbreaks, alter the airflow primarily according to strength, direction and degree of turbulence. Although most of the effects of

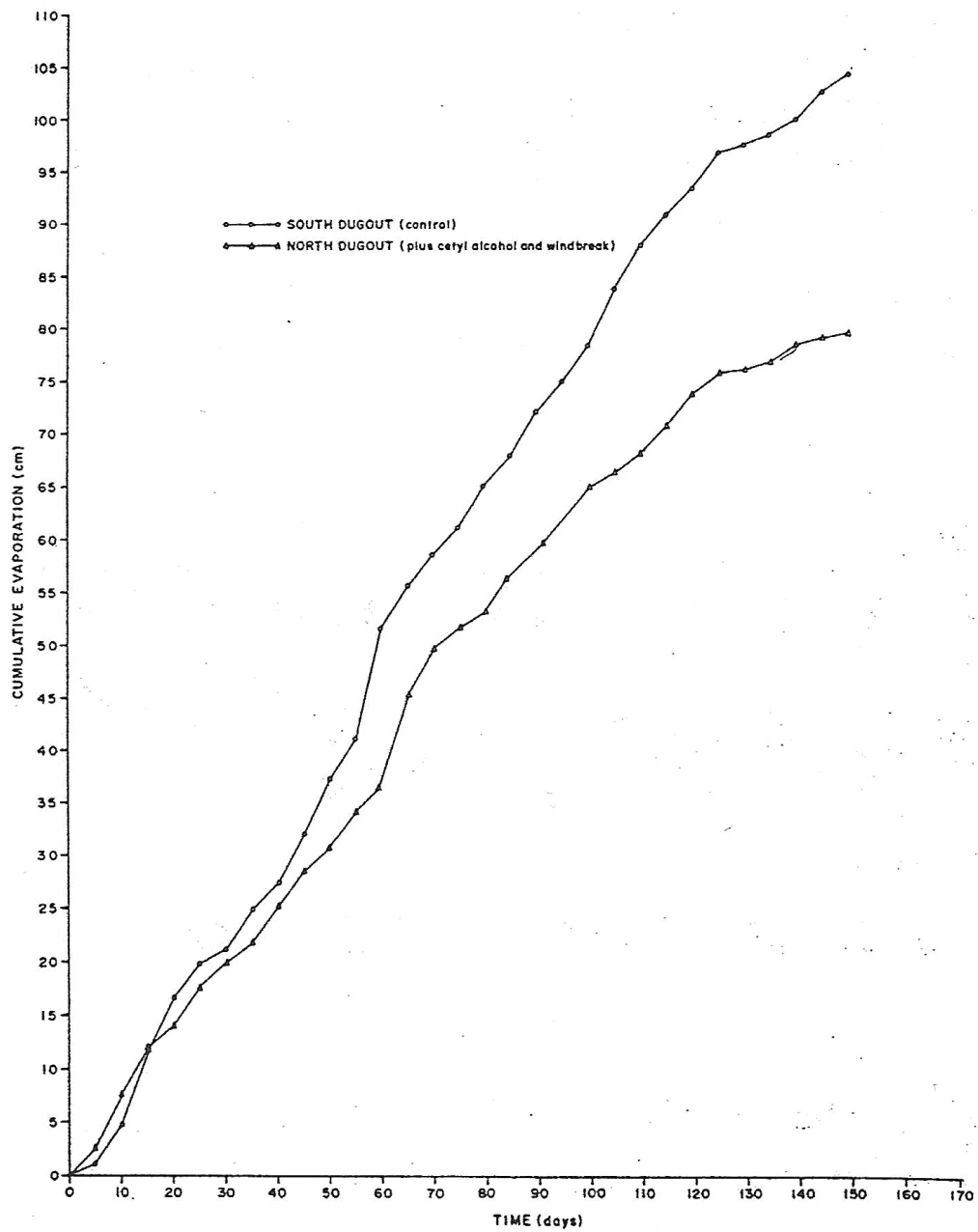


Figure A.32: The effect of a snow-fence windbreak and a monolayer film on cumulative evaporation. The vertical axis is cumulative evaporation ranging from 0 to 110 cm and the horizontal axis is time ranging from 0 to 170 days. Reproduced from Nicholaichuk (1978).

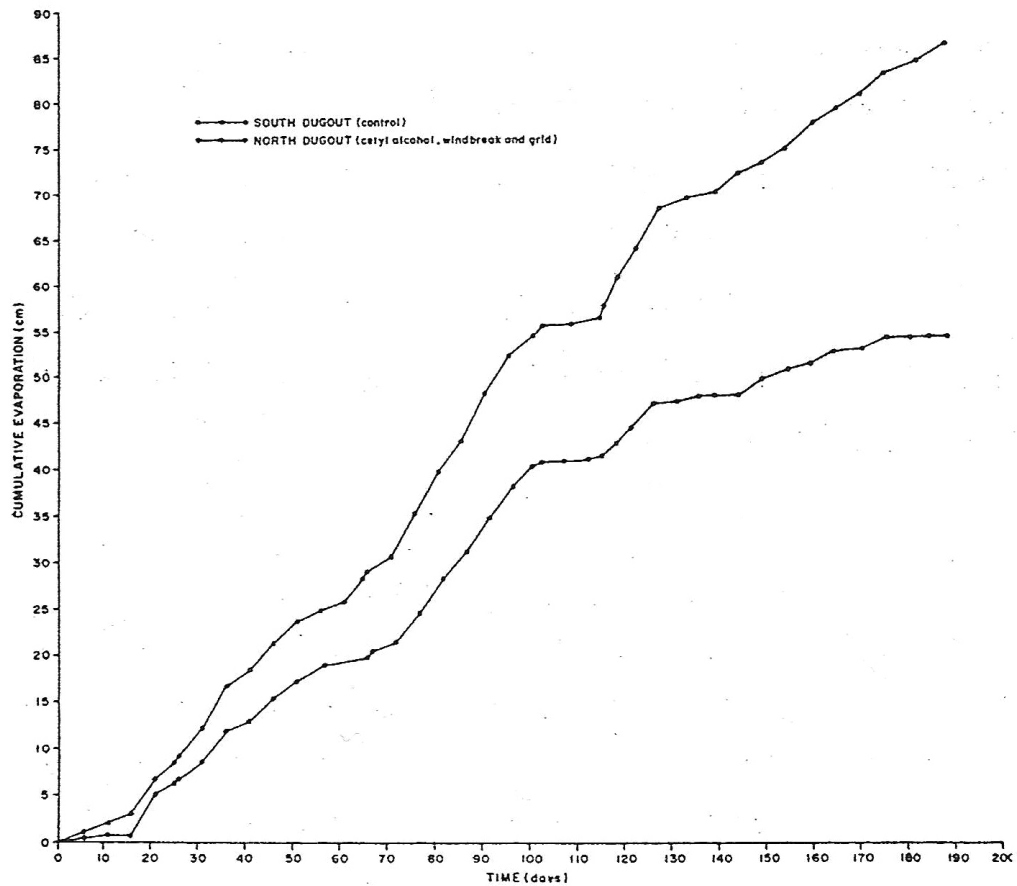


Figure A.33: The effect of a snow-fence windbreak, monolayer film and floating grids on cumulative evaporation. The vertical axis is cumulative evaporation ranging from 0 to 110 cm and the horizontal axis is time ranging from 0 to 170 days. Reproduced from Nicholaichuk (1978).

shelterbelts and windbreaks are the same or similar, shelterbelts also change the whole composition of the biological and abiotic characteristics of the landscape. Shelterbelts are not only a means to improve soil-climate and microclimate, they are also used to recover a landscape and improve its whole natural economy.

Shelterbelt length usually greatly exceeds their width and height, according to Naegeli (1953), the ratio of the length to height of the belt must be at least 11.5, if the wind conditions of an infinitely long belt are to be achieved for a line perpendicular to its centre. The protective effect decreases by about half if a belt is only twice as long as it is high (Blenk and Trienes, 1955). However, the deciding factor for wind reduction with shelter belts is the belt's density or permeability. The degree of permeability is determined by the percentage ratio of the perforated area of the belt, taken perpendicular to its line, to the total vertical area of the belt (Eimern et al. 1964).

Although density or permeability is a deciding factor, it is a difficult parameter to measure for natural obstacles and has not yet been satisfactorily achieved according to Eimern et al. (1964). Despite this according to measurements by Naegeli, Figure A.34, he concluded that when wind reduction extending far behind the belts is required, more than sharp reduction, high belts of medium density are best (Naegeli 1953); (van der Linde 1958).

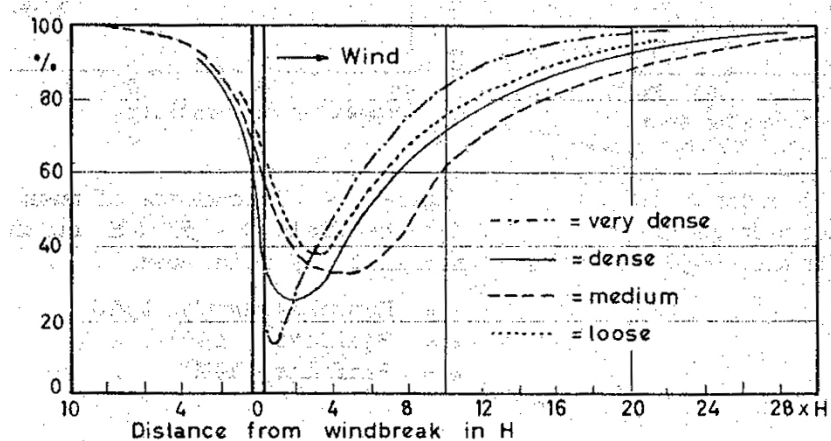


Figure A.34: The wind speed reduction by different shelterbelts. Reproduced from (Naegeli 1953)

The smaller extent of wind reduction with dense belts is a consequence of the stronger displacement flow and the greater power of recovery that this gives the surface wind.

Table A.7: Mean wind speed reduction in the lee of four different density shelterbelts over distances of 10H, 20H and 30H. H is the distance (down wind) from the shelterbelt where the wind speed measurement was taken. Reproduced from (Naegeli 1953)

	0-10H	0-20H	0-30H
A: loose	54%	70%	80%
B: medium	44%	61%	72%
C: dense	44%	65%	76%
D: very dense	52%	71%	80%

The wind recovers speed behind denser belts more quickly than it was reduced, Table A.7 (Naegeli 1953).

van der Linde (1958) presents some classes of natural shelter belts according to their degree of permeability, he classes well cared for leafy *blackthorn* or *yew* hedges as dense, and belts of *Lombardy* popular among those of medium density. *Eucalyptus* makes equally good belts of medium density in warm, semi-arid areas, but according to Duncan (1950) belts of "thin cottonwood" 20m high belong to the very loose and least effective (Eimern et al. 1964). In addition, a list of the kinds of tree and bush suitable for different purposes and different belts are given in Australia by the NSW Forest Nursery Station (1957).

As every situation is different, suitable tree or bush choice to create a shelterbelt will vary greatly according to the soil conditions and topography. E.g. the macro and microclimate suitability of different kinds of trees to one another, the composition of the farm-land and the time available for care of the belts. These are all aspects that need to be considered. For this reason it is even difficult to form rules for small areas, let alone large climate zones (Eimern et al. 1964).

A.6.4 Wave suppression technologies

A number of devices have been designed and patented for inhibiting the propagation of natural and man made waves. Two distinct styles of wave suppression devices have been reviewed; they include floating breakwaters and pool lane dividers. Floating breakwaters have been used for many hundreds of years in harbours and open ocean to protect valuable shorelines, boats, docks and moorings from excessive damage. Whereas pool lane dividers are used in confined water bodies to suppress the propagation of waves generated by a swimmer from one lane into another.

Floating breakwaters - published designs

Floating breakwaters can generally be classed into three different group by the way in which they convert wave energy. Floating breakwaters reduce incident wave heights through the conversion of wave energy via reflection, transformation and/or dissipation. Reflective breakwaters utilise large vertical or inclined surfaces to reflect incoming wave energy back out to sea. Their efficiency is most sensitive to wave height and period, depth and angle of the reflecting surface and the overall structure stability (Morey, Cammaert & Frampton 1995). Transformation systems absorb incident wave energy, and through induced motion responses they transform the energy into secondary wave trains of various heights and periods. Highest efficiencies occur when these transmitted wave trains are out of phase with incident waves (Morey et al. 1995). Dissipative breakwaters convert wave energy into heat, sound, turbulence or friction by breaking waves on sloping surfaces or against structural members. The amount of energy absorbed is governed primarily through geometry and mooring restraints (Morey et al. 1995).

To date a considerable amount of floating breakwater designs have been published, such as Magill (1953), Mito (1974), Olsen (1975), Kodairo & Kunitachi (1976), Tokyo & Matsudo (1976), Bowley (1974), Angioletti (1980) and Kann (1998). These patents are still being reviewed and classified, however, a brief overview of these systems is provided below.

Magill's device consist of a series of horizontally aligned upstanding baffles plates which

diminish wave energy by reflecting incoming waves and creating turbulence between the baffle plates to diminish any subsequent wave action, Figure A.35.

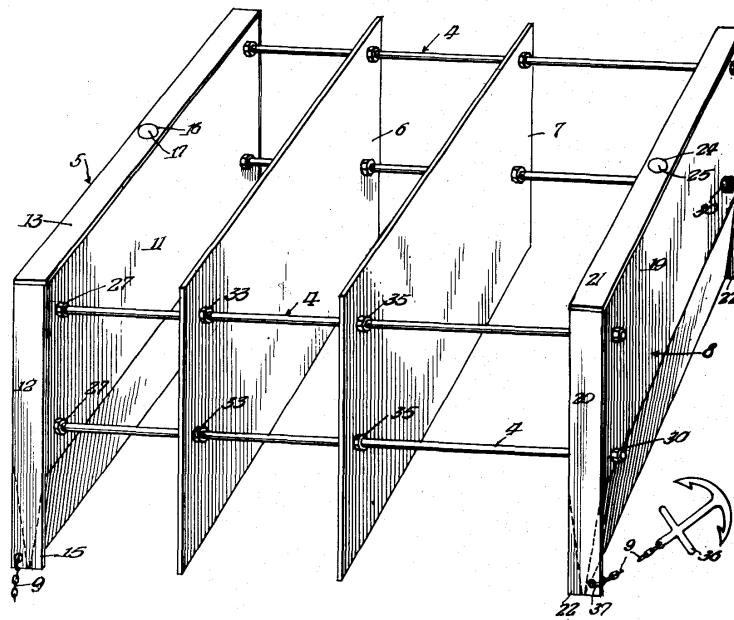


Figure A.35: Perspective view of Magill's preferred embodiment of his baffle plate break-water (Magill 1953)

Mito's device consists of a multiple of elongated floating bodies arranged in parallel to one another, with an upper section foam filled and the lower section water filled. Waves are weakened by the physical resistance provided by the elongated floating bodies, Figure A.36.

Olsen's device consists of a large number of plastic modules arranged together in a grid pattern of walls and openings to form a floating pontoon, Figure A.37. This is done to interrupt the horizontal orbital motion of the wave under the wave crest and create turbulence to dissipate wave action.

Kodairo's device is described as a sealed and hollow floating body with a series of three stepped protrusions on the upper side, Figure A.38. This provides resistance and friction to incoming waves. Also the specific gravity of the floating body is calibrated to increase the wave breaking efficiency due to phase difference.

Tokyo's device functions substantially in accordance with Magill's device by reflecting

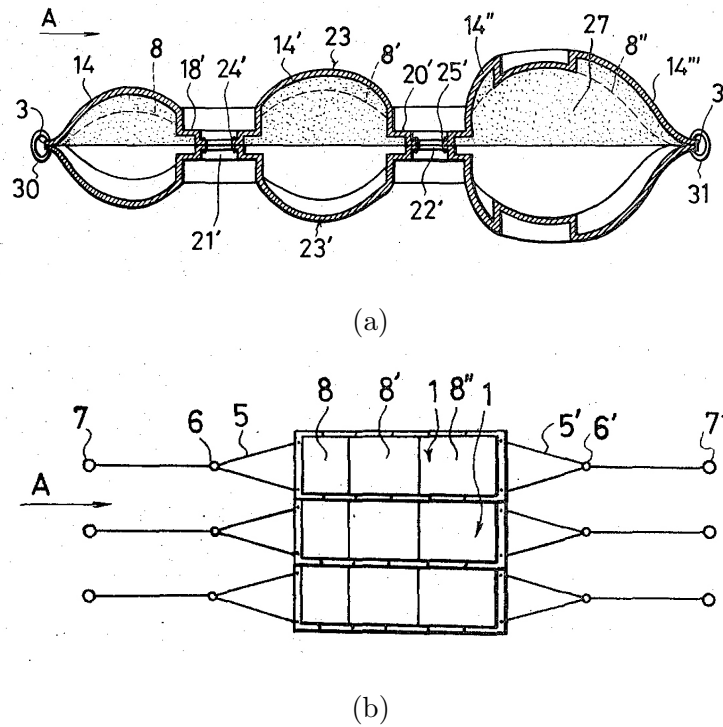


Figure A.36: Mito's floating breakwater design. (a) Longitudinal side sectional view of the elongated floating housing bodies. (b) A plurality of elongated floating housing bodies arranged in parallel to each other. (Mito 1974)

incoming waves and creating turbulence to diminish any subsequent wave action.

Bowley's device consists of a series of sealed hollow vessels with protruding disc shaped plate members, Figure A.39. The vessels float just below the water surface in the top part of the wave. Therefore, vertical movement of the vessels and plate members are out of phase with the one another, which generates a reflected wave out to sea other incoming incident waves to reduce their energy.

Angioletti's device consists of two sealed cylinders spaced laterally apart and connected together in parallel by flexible rubber strips, Figure A.40. This breakwater functions by abating incoming waves which then creates a zone of turbulence between the two cylinders to dissipate subsequent wave action.

Kann's device consists of hollow barrels with a floatation members attached to the top and a stabilising member connected to the bottom, Figure A.41. The majority of

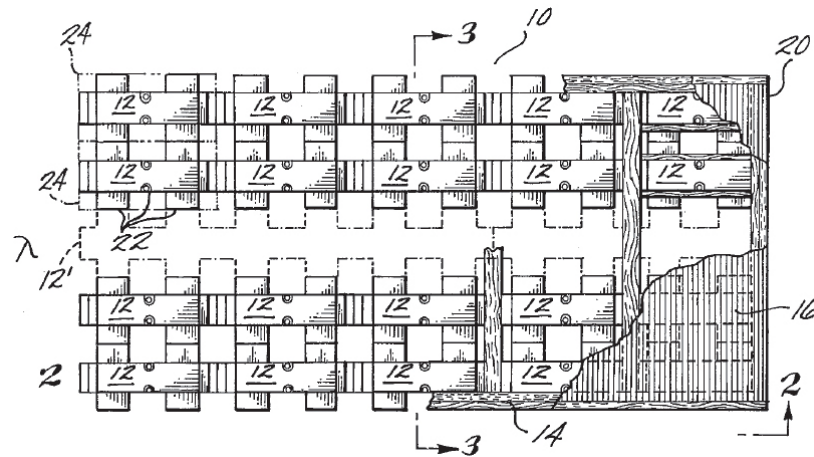


Figure A.37: John O. Olsen's floating breakwater consisting of a large number of plastic interlocking pontoon modules arrangement (Olsen 1975)

the device is submerged which provides significant mass and increases the moment of inertia to resist wave action.

Pool lane dividers

A pioneer device of the general type is described in a patent granted to Adolph G. Kiefer in 1967. Kiefer's device consists of a plurality of hollow cylindrical elongated bodies having perforated surfaces defined by a series of integrally moulded plastic strips arranged in a criss-cross pattern or lattice-work fashion. These bodies are confined in axial alignment by means of a cable, attached to opposite ends of the swimming pool and maintained under tension for the purpose of holding the individual bodies on-half submerged. As the lattice-like bodies and cable has a slightly negative buoyancy, floats are attached to the cable (or to the bodies) to assist in maintaining the bodies at a desired level in the pool, Figure A.42 (Kiefer 1967).

The perforated bodies are designed so that side wash enters the perforations directly, and in this manner the waves and surges are broken up into fragmentary waves which reduce the overall driving force of the wave. Furthermore, kinetic energy in the wake is absorbed by efforts expended in rotating the turbulence reducing bodies which are freely rotatable about the restraining cable.

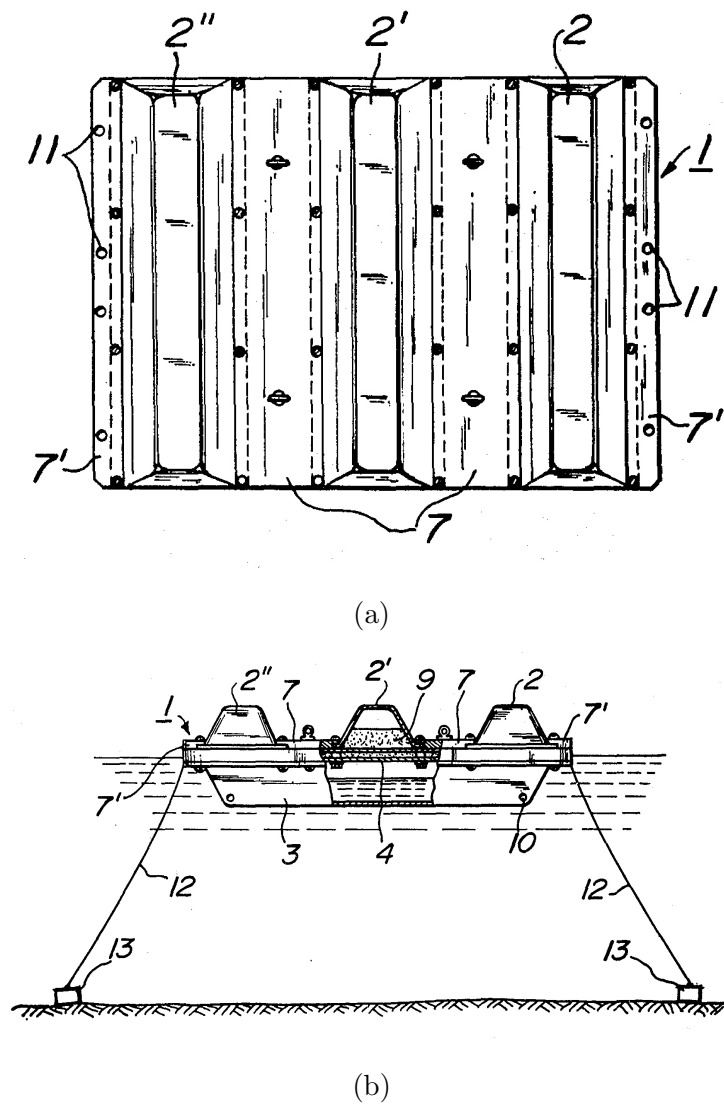


Figure A.38: Kodairo and Kunitachi's floating breakwater design. (a) Plan view of the floating breakwater. (b) Side view showing a partial cross-section of the floating breakwater (Kodairo & Kunitachi 1976)

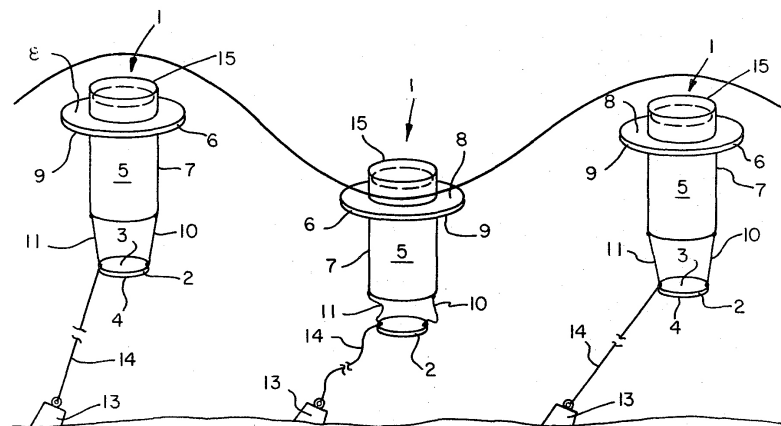


Figure A.39: Wallace W. Bowley's floating wave barrier arrangement comprising a plurality of submerged vessels (Magill 1953)

Another device of this type, which operates substantially in accordance with the principles disclosed in Kiefer's device, is described in a patent by David A. Stanwood. Stanwood's device comprises a plurality of radially disposed ribs supported by a cylindrical housing. A plurality of rings is mounted to the ribs in spaced relation, the area of the space between adjacent rings being smaller than the area of the rings. Additional buoyancy is provided within the cylindrical housing and a cable is passed through each float so as to create a string of freely rotatable floats, figure A.43 (Stanwood 1970).

Mercer D. Walket later patented a wave-suppression assembly which comprises a continuous series of open-faced discs, resembling spoked wheels, strung together in axial alignment on a cable, so that each element is independently freely rotatable about its central axis, figure A.44. On advantage of this device is that it is more restrictive to irregular wake patterns, or eddy currents, than the previous two devices detailed above. In the prior two devices any force acting, for example on one side of an elongated turbulence reducing body and sufficient to effect movement of the body, created a slight counter turbulence back into the area from which the force acting was generated (Walket 1973).

In addition, the shorter length and larger diameter of the disc-shaped bodies of Stanwood's invention have greatly reduced mass, effectively reducing the inertia of each body and makes possible a more localised control of small disturbances in the water (Walket 1973).

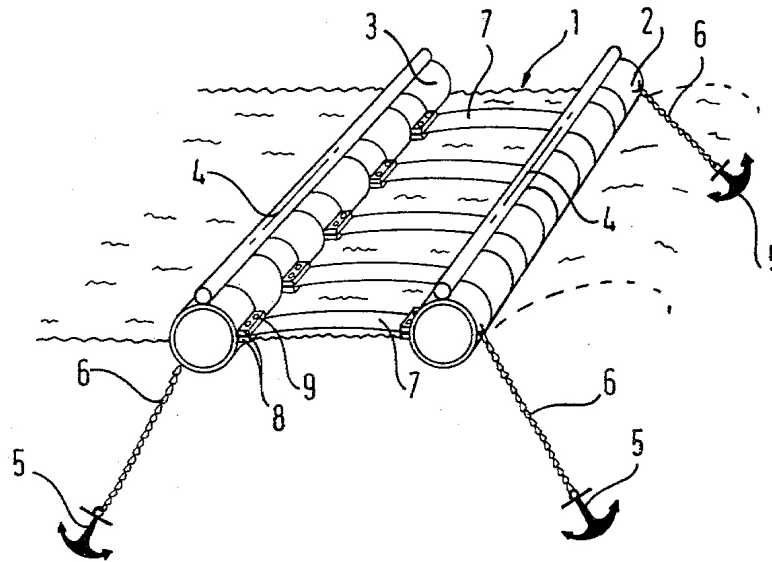


Figure A.40: Perspective view of Angioletti's floating breakwater and the association of the device with water waves (Angioletti 1980)

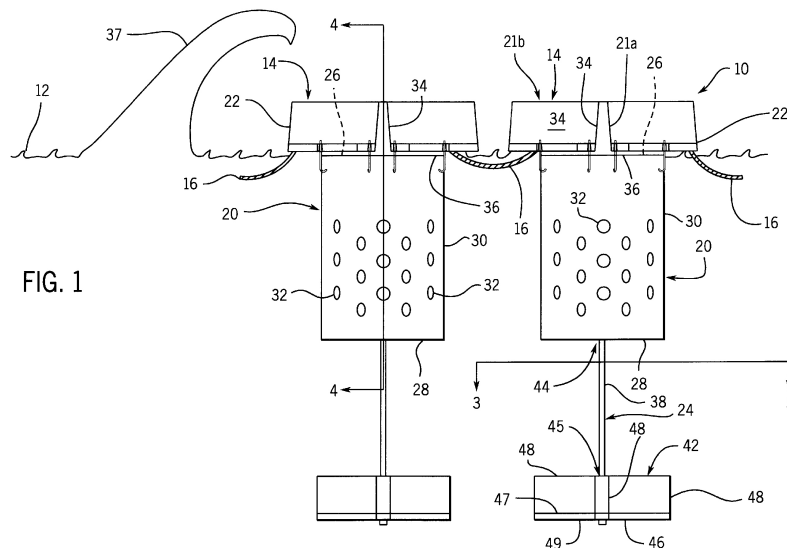


Figure A.41: Side view of Kann's wave suppression system including a plurality of wave suppression members coupled together along a water surface (Kann 1998)

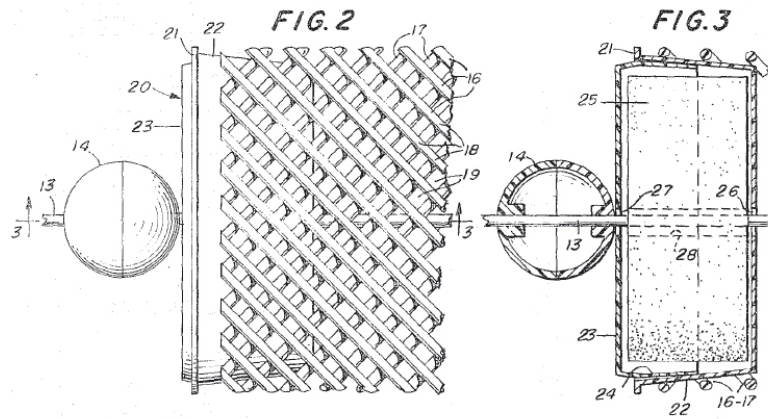


Figure A.42: Side view, on a greatly enlarged scale, of one end of the devices and a cross-section of the device showing the internal construction. (Kiefer 1967)

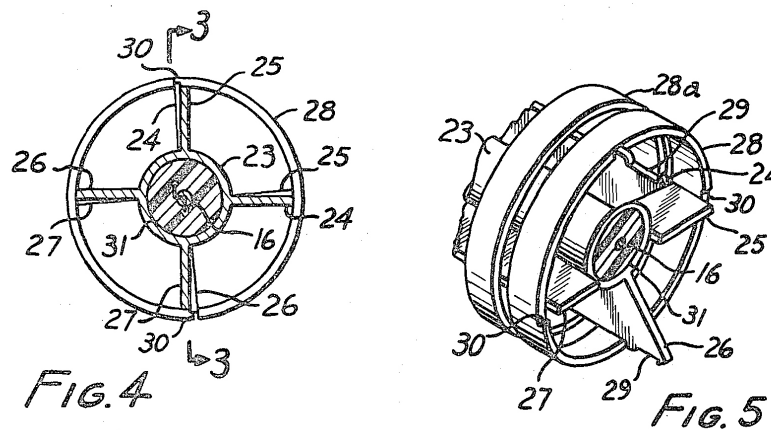


Figure A.43: End view in cutaway cross-section of Stanwood's pool lane float (Stanwood 1970)

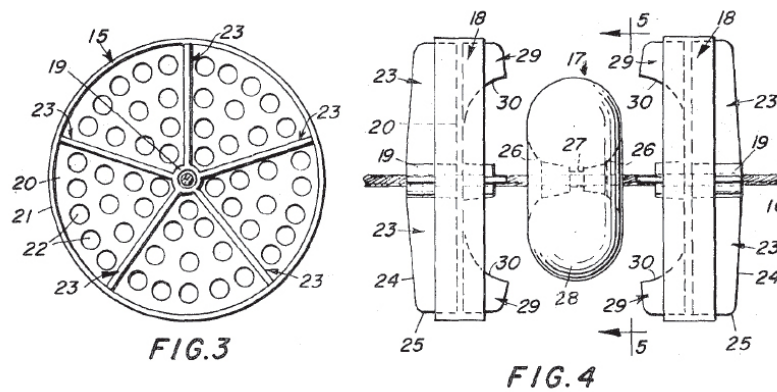


Figure A.44: Side view of a section of one of the racing lane markers and a side view of the racing lane markers arranged with the float means (Walket 1973)

Walket later patented a further wave-suppressing device which was a slight variation of the original device. The prior art devices reviewed so far all depend for their effectiveness upon the generation of resultant opposite forces resisting the rotation of the damping elements for suppression of wave patterns creating turbulence. In the case of Walket's later device (Figure A.45), the individual baffle elements are unbalanced, with respect to their centres of rotation about the restraining cable, both as regards to their physical configuration and/or as to their distribution of mass. This means that the baffle elements ordinarily will only swing about an angle of considerably less than 90, due to the greater rotational resistance provided by the inverted teardrop shape. Walket also states that by increased by increasing the weight of the lower portion of the baffle element can further improve wave suppression (Walket 1974).

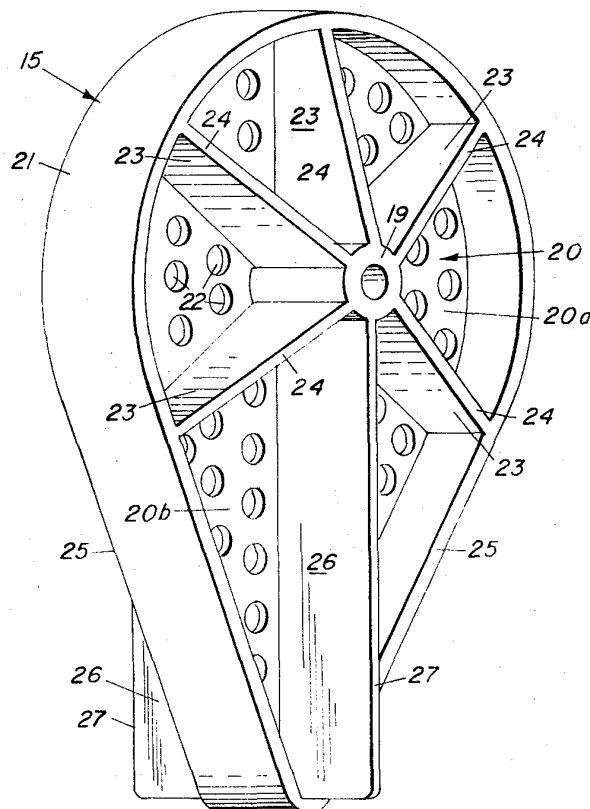


Figure A.45: Perspective view of one of the baffle elements and side view of a portion of the assembly, on an enlarged scale (Walket 1974)

A slightly different wave suppression device patented by Edward G. Lowe that does not appear to be designed to be linked together along a racing line, but instead is intended

to quell waves at the sides of a swimming pool. Essentially, the device comprises a continuous ballast member that serves as a stabilising element, and a continuous floatable member surrounding the ballast member. The floatable member has a volume greater than the ballast member and a density less than the pool water, figure A.46. The continuous ballast member preferably is flexible tubing filled with water, while the continuous floatable member is flexible tubing filled with gas (Lowe 1974).

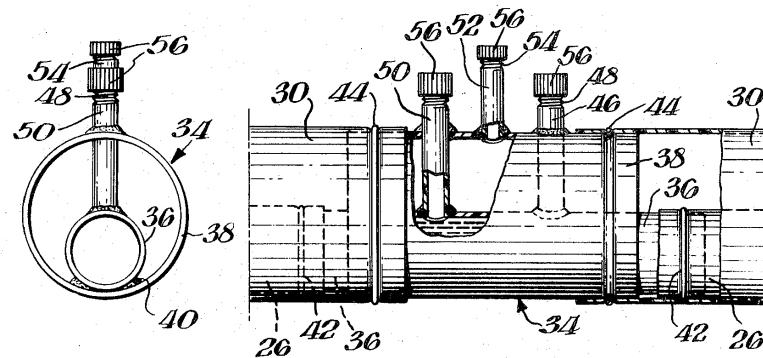


Figure A.46: Side view of a cross-section of Lowe's wave suppression device and a partial side view of a length of the wave suppression device with portions thereof broken away to show detail (Lowe 1974)

A further invention by William H. Baker that comprises a supporting body of lightweight plastic with a hub in the centre and a plurality of buoyant members arranged radially about the hub, figure A.47. The float members are disposed at regular intervals about the hub to float at least one half of the body above the water with the float balanced for free rotation in the water. The plastic body consists of a plurality of wave quelling vanes which are spaced and shaped to receive surges of waves on the body of water and absorb the impact thereof as rotation of the float (Baker 1977).

Anton J. Kajlich later developed a device which is described as being one of a multiple of identical units adapted to be strung on a lane-separating cable for swimming pools, and being formed with deflecting and turbulence-inhibiting baffles or vanes, enclosed within an annular band or shell, figure A.48.

Another device patented by Thomas P. Rademacher for use in a body of water as one of a plurality of such devices, again assembled in axial alignment with one another along a tensioned cable. The individual wave suppressing devices consist of a hub with

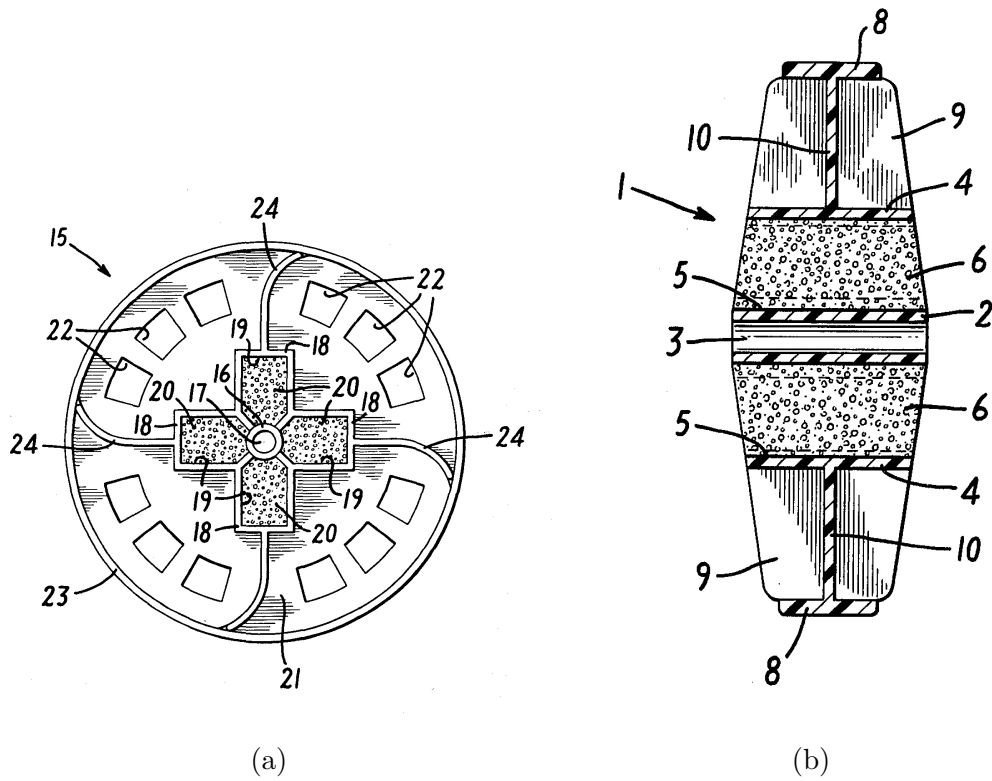


Figure A.47: Baker's wave suppression float member. (a) Cross-sectional view through the float member. (b) Logitudinal section and a cross-section through a float member (Baker 1977)

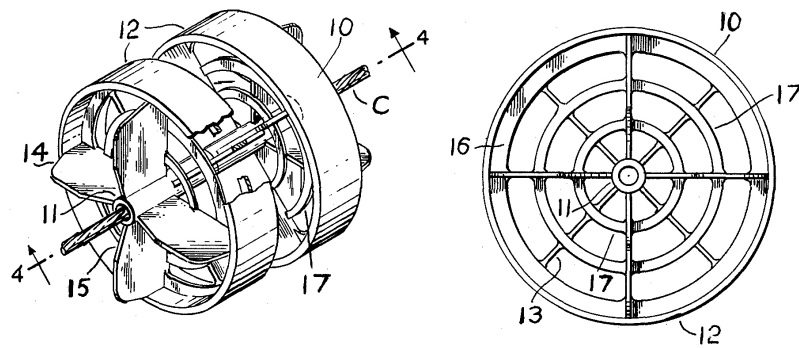


Figure A.48: Perspective view of a pair of the devices in place on a section of cable and a typical end elevation of one of the units (Kajlich 1977)

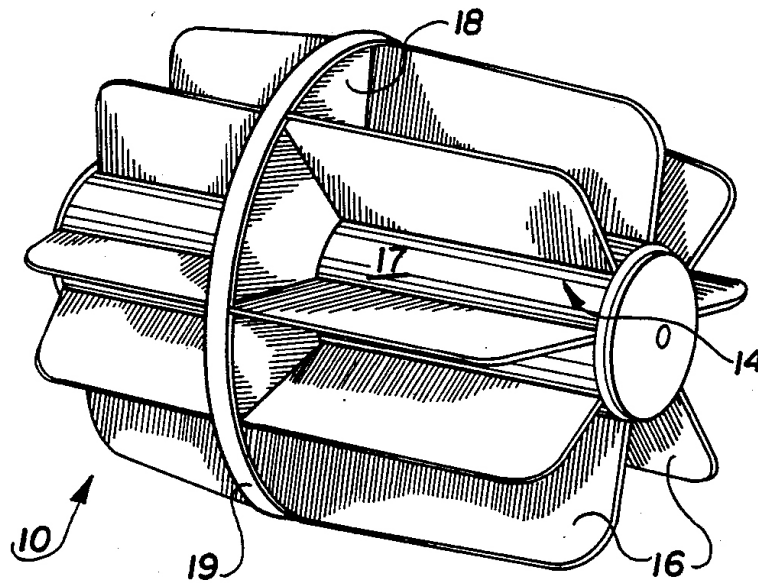


Figure A.50: Perspective view of the Kiefer wave suppression element (Kiefer 1990)

larger diameter wave suppressing devices. However, in tests the present invention has been found to dissipate up to 70% of the longer wavelength waves, Figure A.51.

Another variation of the Kiefer's design was patented by Roger C. Eddy, which consists of two cylindrical cores having a plurality of fins radiating between them. An integral floatation means is then compression fit within the smaller diameter core, figure A.52. The floatation means also has a central opening to permit the wave suppressor to be mounted to a cable. The present device utilises the same wave suppression theory as described by Kiefer's most recent device, however this device improves upon Kiefer's by allowing the floatation means to be more easily inserted into the wave suppressor. In addition, the device is designed to be wound around a storage wheel without the requirements of additional cable that exists with current designs, Figure A.52 (Eddy 1996).

Kajlich presents a further wave inhibiting device for a pool lane divider, the device having an inner region, a plurality of fins extending from the inner region and for blocking at least a portion of any wave incident acting on the surface thereof, Figure A.53. Beyond this, there is no additional information about the functioning of this device is not provided in the patent. However, it is believed that this device would operate

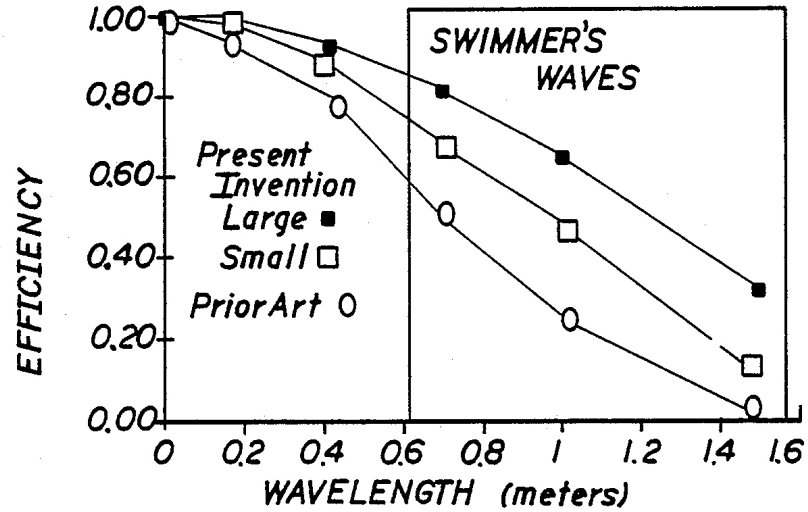


Figure A.51: Graphical representation of the energy dissipation efficiency of the present invention compared to a prior art wave suppression means (Kiefer 1990)

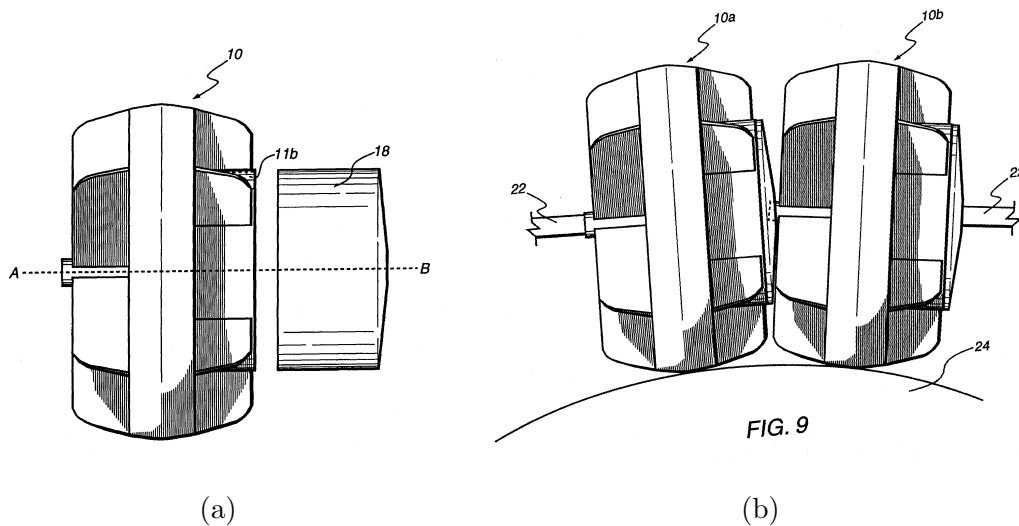


Figure A.52: Eddy's wave suppressor design. (a) Side view of a pair of wave suppressors shown as wound around a storage reel. (b) Side view of the wave suppressor and floatation means prior to insertion. (Eddy 1996)

substantially in accordance with many of the prior art devices already reviewed in this section.

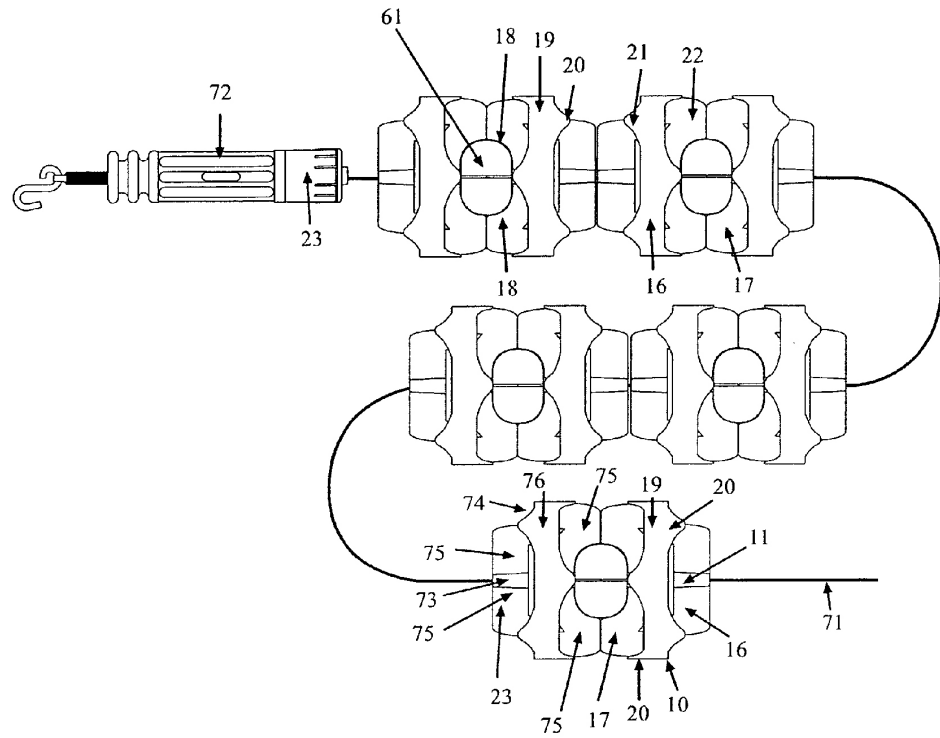


Figure A.53: A plurality of flexible wave inhibiting devices for a pool lane divider arranged on a cable (Kajlich 2006)

A.6.5 Film containment technologies

Various technologies, such as floating oil booms, boom fending devices, floating rings for liquid film maintenance and floating containment grids, are potentially an option for containing and or restricting the movement of a liquid or surface film on the water surface. It is hypothesised that these containment technologies may help to improve the evaporative suppression ability of a monolayer product by increasing effective surface film coverage of the water. In addition, a containment style system may also help to increase the economy of a monolayer product by reducing the need for re-application to make up for monolayer film lost to beaching. The following section is a review of these technologies that may be appropriate for containment of a monolayer surface film.

Conventionally oil booms comprise a shielding screen member, a multiple of reinforced strips placed in a parallel relationship on the screen member, one float secured to each of the reinforcing strips, one sinker attached to one end of each strip and a length of reinforcing rope extending throughout the length of the screen member to cross the reinforcing strips (Kinase et al. 1976). Many variations of this conventional oil fence style boom design have been patented by Ruhlman (1972), Thurman (1973), Cerasari (1974), Kinase et al. (1976), Casey (1976), Geist (1977), Jaffrennou & Cessou (1984) and Smith (1998).

Ruhlman (1972), Figure A.54, provides a water barrier floatation curtain for use in a water body comprising a barrier having a sandwich-like construction, which is substantially vertical having an upper edge and lower edge, a floatation means positioned within the barrier and adapted to float beneath the surface of the water. An anchor is attached to the lower edge of the barrier wherein the lower edge of the barrier substantially follows the contour of the floor of the body of water.

Thurman (1973), Figure A.55, presents a floating oil containment boom which comprises a plurality of interconnected, floating units each supporting a rigid vertical barrier with a part above water and a part submerged. The barriers are interconnected by panels of flexible waterproof material of substantially the same vertical extent as the barriers and both the barriers and the interconnecting panels have flexible, waterproof skirt portions depending below the barriers. Each of the barriers is secured to a tow line

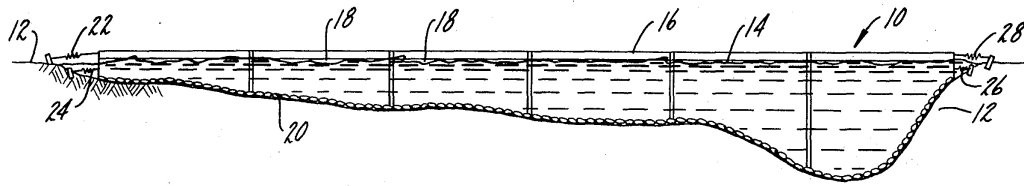


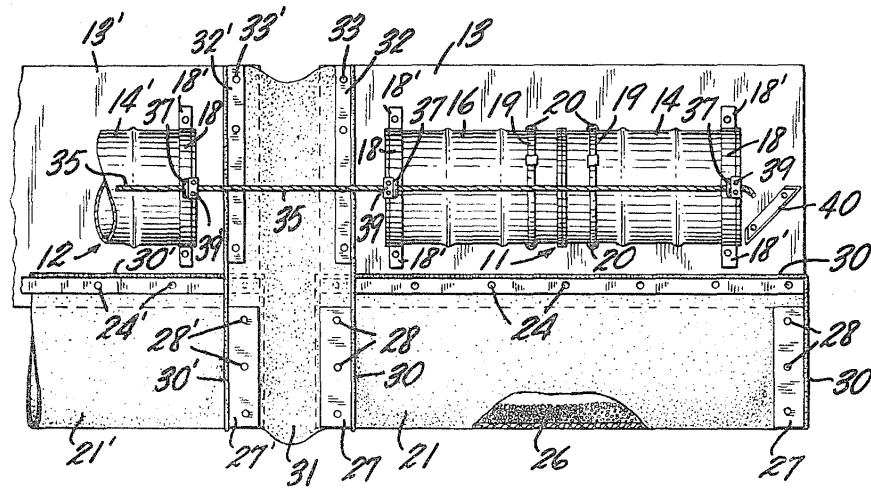
Figure A.54: Diagrammatic view of Ruhlman's water barrier curtain installed in a body of water. Reproduced from: (Ruhlman 1972)

by means of which the boom may be towed to a desired location and there anchored in place.

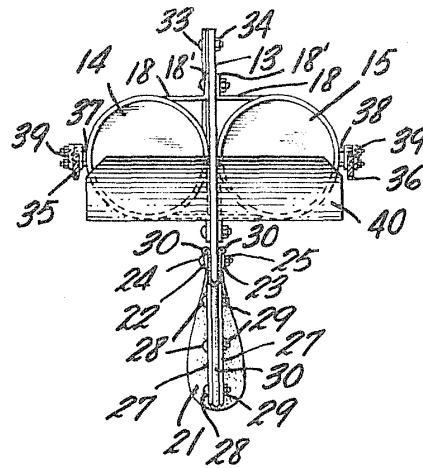
Cerasari (1974) describes a floating boom for collecting and containing oil and floating debris in the open sea or in rough water composed of a plurality of upright support members with the lower end weighted and an inwardly curved upper end. The upright support members are attached to both a barricade wall material and a buoyant support tube to form the boom. The floating boom can be towed by a vessel around an oil spill and floating debris to collect and contain them. The curved upper ends of the support member decreases the loss of collected oil and debris due to action of waves in rough or open sea, Figure A.56.

A slightly more traditional fence style boom is described in a patent by Kinase et al. (1976), which basically consists of an array of semi-cylindrical floats attached on the surface of both sides of a longitudinally elongated screen. A chain-shaped sinker is also disposed along one longitudinal edge of the screen, Figure A.57.

Casey (1976) further presents a collapsible, quickly deployable floating boom barrier comprising an elongated curtain-like partition of strong, flexible, impervious material supported in a substantially vertical position in the water by a plurality of outrigger-style floats spaced along the partition. The outrigger-float also comprises a frame which is in-turn connected to the side of the partition. The float is able to be rotated about a horizontal axis on the frame and the frame is also able to rotate around a vertical axis near the partition, Figure A.58. The articulation of the frame and float provide a self-stabilising action for the outrigger-float, which also allows the float and the frame to be folded back flat against the side of the partition. This allows the barrier to be deployed



(a)



(b)

Figure A.55: Thurman's floating oil containment boom. (a) Side view of a portion of the floating oil containment boom. (b) Front sectional view through the floating oil containment boom. Reproduced from: Thurman (1973)

through narrow passageways while also permitting compact storage and transport of the barrier (Casey 1976).

Geist (1977) also provides a barrier for containing oil spills or other debris on the surface of a body of water which simply comprises buoyant sections connected by a sliding seal for allowing relative vertical motion of each section. This is done to accommodate extreme and abrupt variations in water surface and turbulence resulting from wave

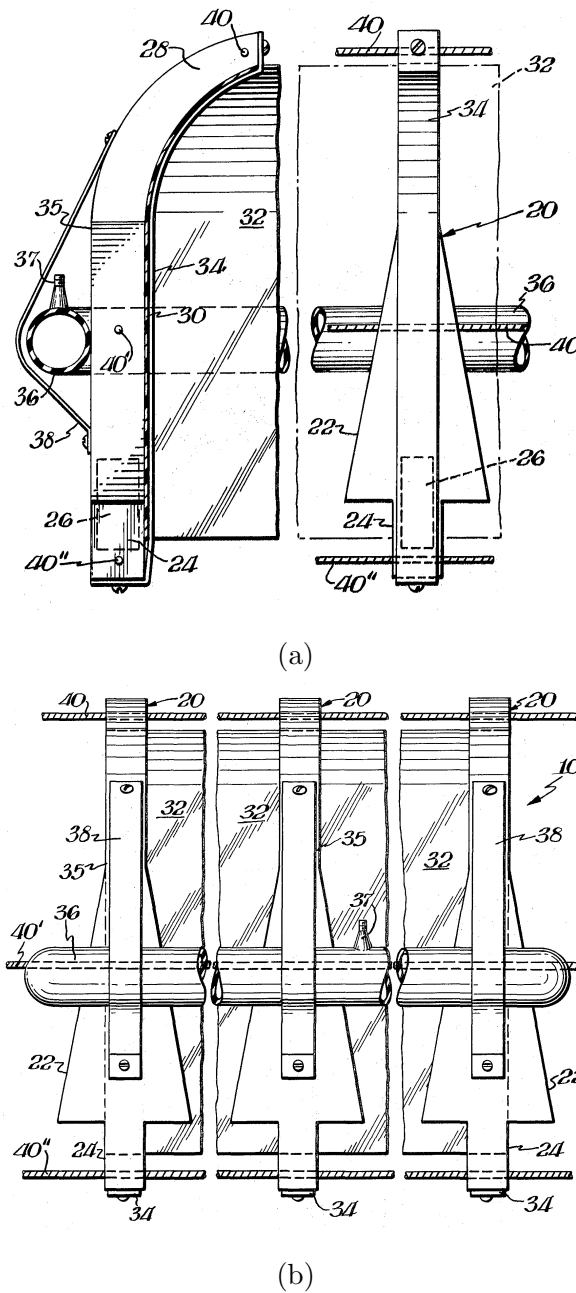


Figure A.56: Cerasari's floating oil containment boom. (a) Side elevational view illustrating the buoyant support member. (b) Front elevational view of several buoyant support members. Reproduced from: (Cerasari 1974)

action. The seal connection is made up of a vertical inner cylindrical rod attached to one end of a section and a mating outer open-ended cylindrical tube attached to the other end of a section, Figure A.59. The outer open-ended tube is preferably wide enough to permit limited relative angular movement between the two joined sections

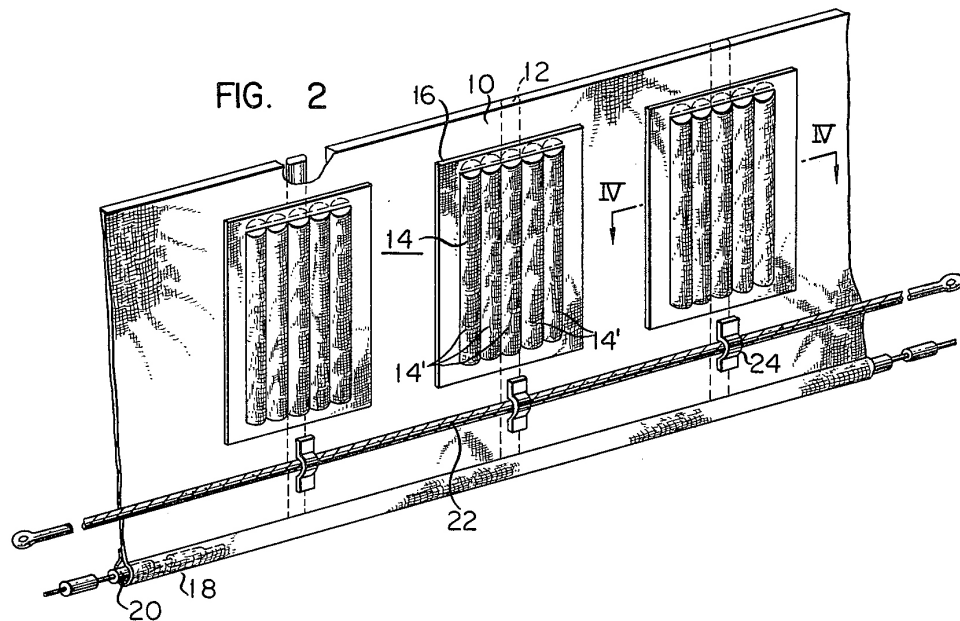


Figure A.57: Fragmental perspective view of the oil fence in a patent by Kinase et al. (1976)

so that the connection serves as a combination sliding seal and hinge (Geist 1977).

Jaffrennou & Cessou (1984) provides a further variation which comprises a flexible structure forming a barrier provided with traverse stiffeners to which floats are secured for support the structure in a substantially vertical position in the water, Figure A.60.

In a patent by Smith (1992) is described an oil containment system for mounting on oil tankers which is easily and rapidly deployable in the event of an oil spill. The system basically comprises a series of connectable floatation members stored around the perimeter of a tanker. A membrane is folded and packed into a recess in each floatation member, one edge of the membrane is held between the member and the tanker, while the opposite edge of the membrane is free. The members are held against the sides of the tanker by a releasable stay, Figure A.61, which can be released sequentially by a trigger-mechanism to allow the members to drop off the tanker into the water in the event of a spill. The free edge of the membrane falls from the canister so that the membrane forms a curtain in the water, Figure A.61. Each floatation member is connected to adjacent members by a flexible jacket, in this manner a continuous curtain surrounds the tanker (Smith 1992).

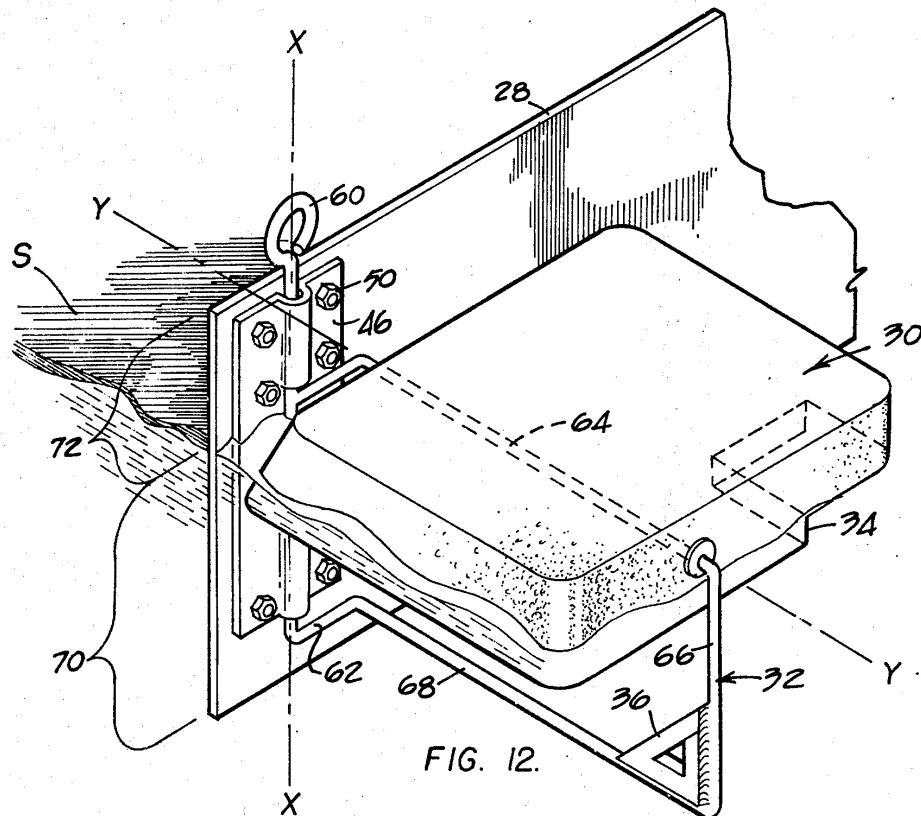


Figure A.58: Isometric view of one individual outrigger-float and frame of the floating barrier. Reproduced from: (Casey 1976)

Slightly different from the traditional floating style booms for oil containment is an apparatus designed by Steven P. Vidal in 1967 for liquid film maintenance on a water surface. The apparatus, Figure A.62, basically consist of a circular floating body which is assembled from sections 18 which are interconnected by interlocking elements 20 having oppositely extending projections 22 received within end slots 24 in each section 18. This allows each member to be easily disassembled for transport purposes (Vidal 1967).

The circular floating bodies are arranged in groups to enclose a substantial portion of water surface area to confine within that a prescribed amount of liquid film. Each floating member is also provided with vanes causing rotation thereof in response to wind in any direction so that the liquid film confined within the floating members may be redistributed by rotation of the floating members (Figure A.63). This prevents the liquid film from being concentrated at any location within the floating member

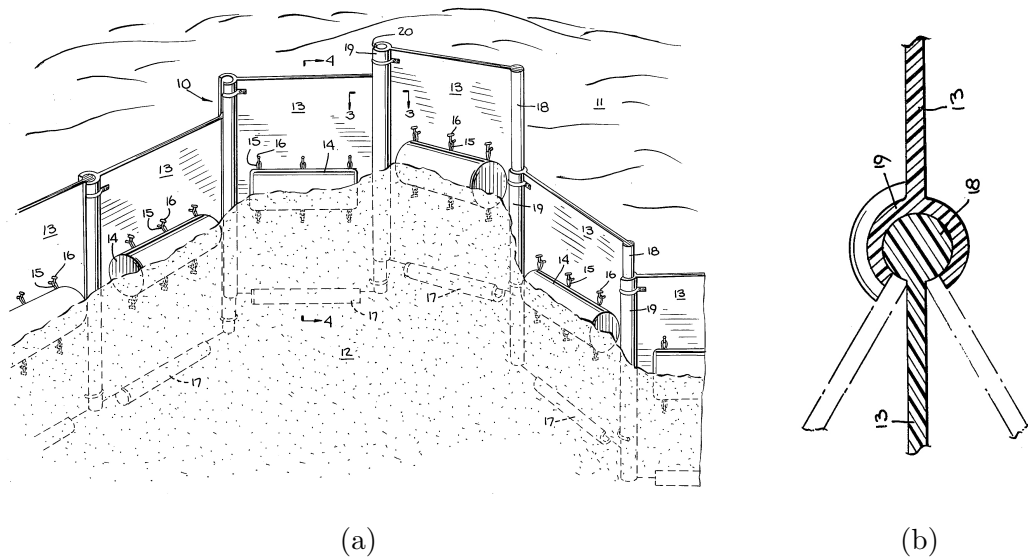


Figure A.59: Geist's articulated floating oil barrier. (a) Perspective view of an assembled preferred embodiment of the barrier. (b) Plan view in section of a portion of two assembled sections of the barrier. Reproduced from: Geist (1977)

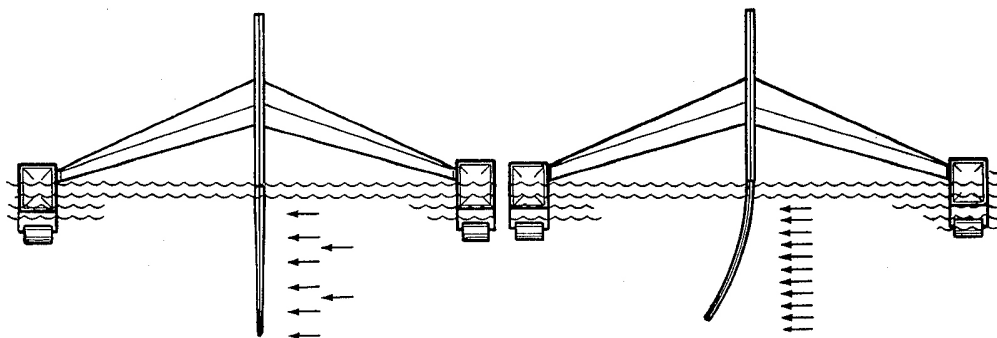


Figure A.60: Illustration of a transverse cross-section of this boom at the location of a stiffener. Reproduced from: Jaffrennou & Cessou (1984)

(Vidal 1967).

Although not for the specific purpose of containing a liquid or surface film within, oil boom fending devices are of particular interest as they may be adapted for containment of a surface film within. One such example, by Erik C. Nielsen, provides a circular floating ring made up of individual segments so that the device can be quickly assembled on site and if necessary readily disassembled for storage, Figure A.64. The main objective of this device is to provide a means for spacing an oil boom a prescribed distance from

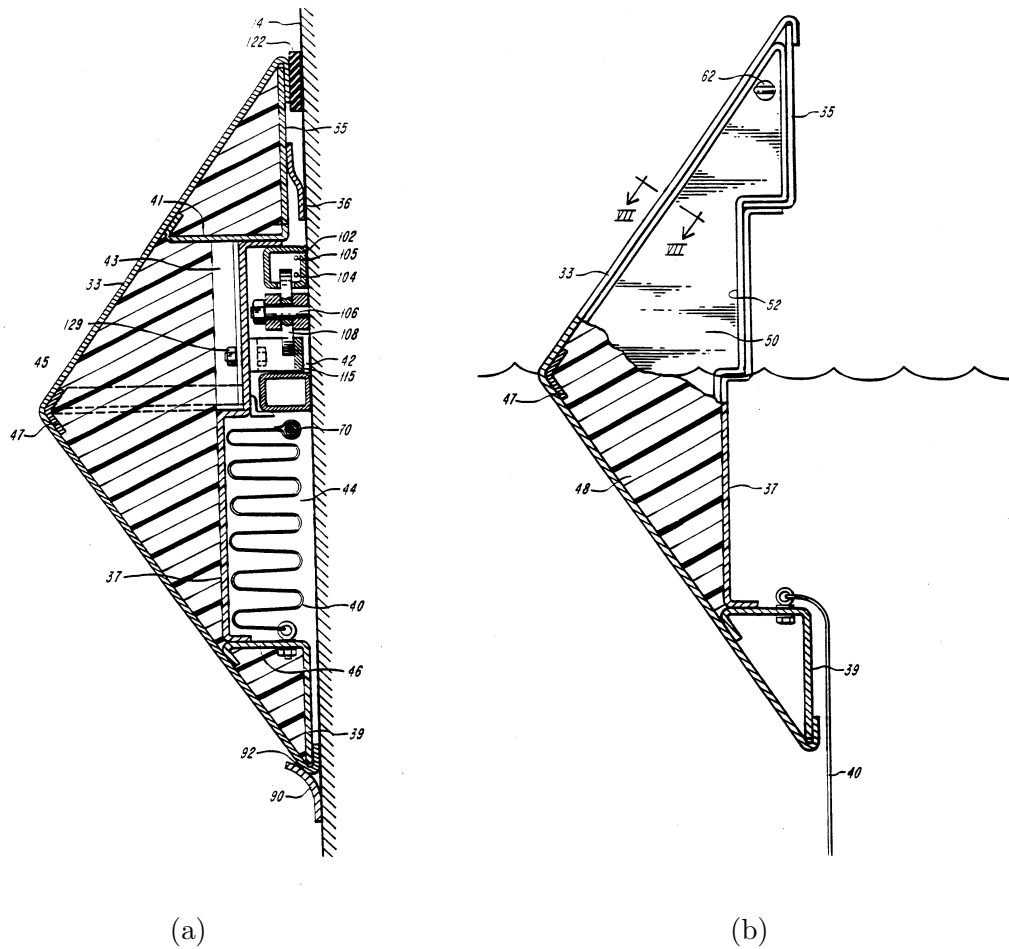


Figure A.61: Smith's oil containment system for emergency use. (a) Partial cross-sectional view of the oil containment system in its stored position. (b) Side elevational view of the containment system in the deployed position. Reproduced from: Smith (1992)

the hull and propeller of a ship during loading or offloading of petroleum, Figure A.65.

It is a further objective of this device to achieve the simplest structural configuration with the highest strength/weight ratio. If the device is in the form of a ring as shown or a distorted ring, forces tending to deform the ring will be resisted by a force proportional to the strength of the ring material in bending (Nielsen 1977). In addition, a very effective way of maintaining a high finess ratio without reducing the strength/weight ratios by adding substantial weighting to the device is achieved by utilising tension elements to effectively reduce the span of the ring material which must resist bending and therefore reduce the bending moment (Nielsen 1977).

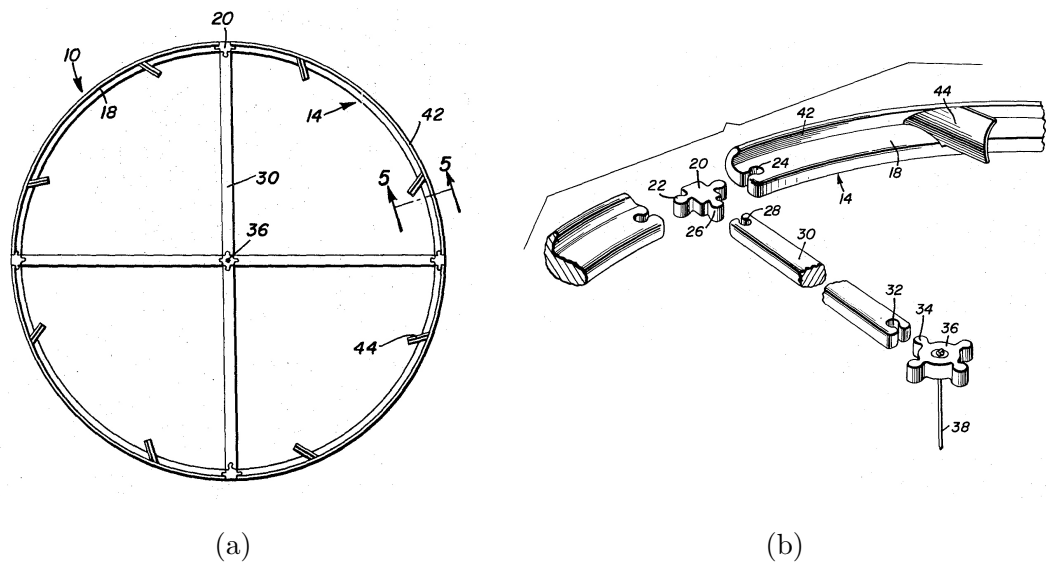


Figure A.62: Vidal's liquid film maintenance apparatus: (a) Enlarged plan view of an assembled float member. (b) Perspective view of the various disassembled parts of one of the float members. Reproduced from: Vidal (1967)

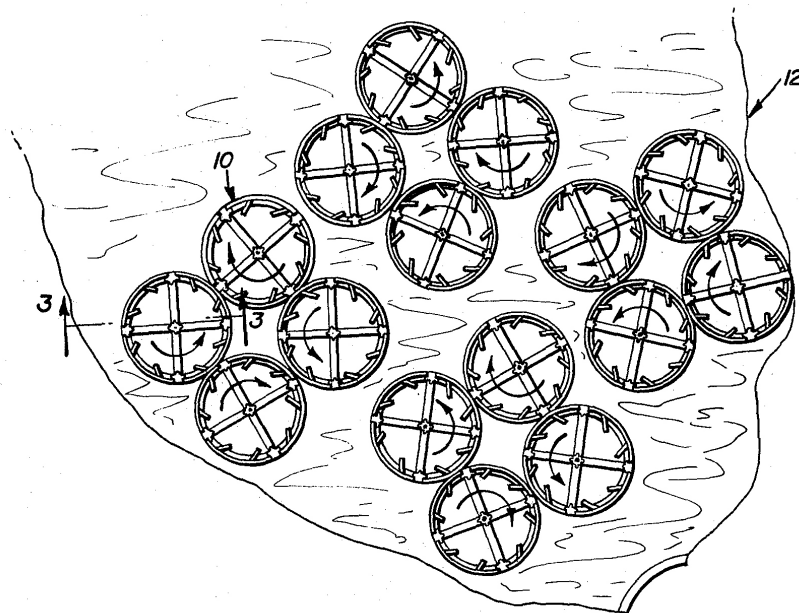


Figure A.63: Plan view of a typical installation for Vidal's apparatus. Reproduced from: Vidal (1967)

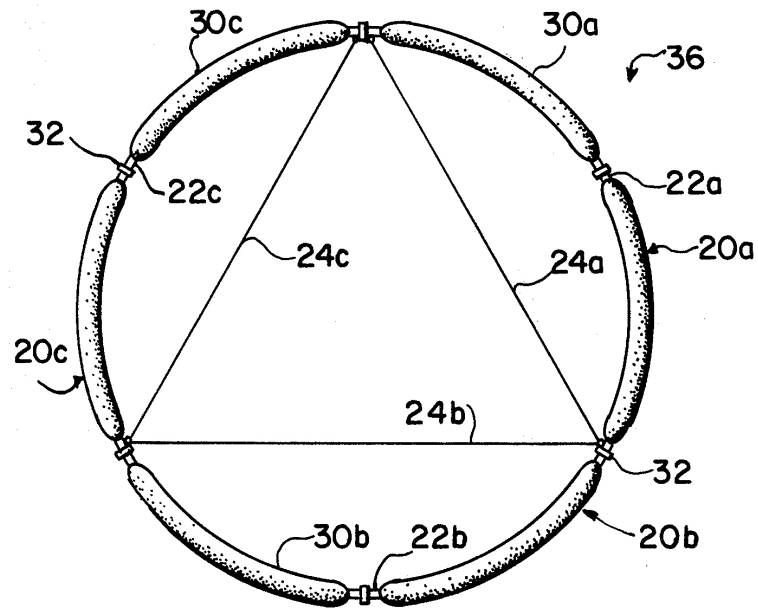


Figure A.64: Plan view of Neilsen's oil boom fending device. Reproduced from: Nielsen (1977)

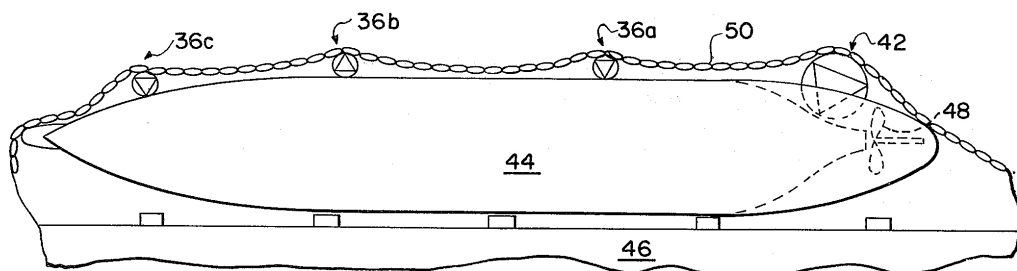


Figure A.65: Plan view illustrating a mode of use of the fending devices. Reproduced from: Nielsen (1977)

Appendix B

Simulation Platform Source Code

B.1 The latest_mono.m main program

```
1 % Inputs:
2 % Size of storage = length (l) and, or width (w) (metres)
3 % Grid spacing = proportional to size of storage (dx, dy) (metres)
4 % Wind speed (u) (km/h converted to m/s)
5 % Wind direction in degrees (Measured counterclockwise from East ...
   = 0 degrees) (degrees converted to radians)
6 % Threshold minimum wind speed (umin) (km/h converted to m/s)
7 % Applicator locations = apploc = [x1, y1; x2, y2; x3, y3; x4, ...
   y4] (metres)
8 % Shore length = shorelength = [L1; L2; L3; L4] (metres): shore ...
   covered by each applicator
9 % Application rate apprate = [r1; r2; r3; r4] (mg/min converted to ...
   kg/second)
10 % Application volume (appvol = mg/m2 converted to kg/m2)
11 % Time-step size (dt) (s)
12 % Total duration of simulation (tfinal) (hours converted to secs)
13 % Number of time-steps between storing values (savefreq)
14 % Time between display of contour lines (displaytime) (min)
15 % apponcent = the point at which the straight line perpendicular ...
   to the
16 % wind will run through to define the start and end points for the
17 % parabola.
18 % apponcurv = curvature of the parabola.
19 % dt_wind = time between updating wind information: this is set to
20 % tfinal
21 % tttotal = total time of simulation
22
23 clear all
24 close all
25 warning off all
26 clc
27 tic
28 % [1,0; 0,0; 0,1; 1,1; 0.5,0.5; 0.5,0; 0,0.5; 1,0.5; 0.5,1];
29 % [1,0.33; 1,0.66; 0,0.33; 0,0.66; 0.33,1; 0.66,1; 0.33,0; 0.66,0];
30
31
32 % Define variables
33 l = 5000;
34 w = 5000;
35 dx = 25;
36 dy = 25;
37 %nx = 100;
38 %ny = 100;
39 %dx = l / (nx-1);
40 %dy = w / (ny-1);
41 u = 15 * 1000 / 3600;
42 utheta = (270) * pi / 180;
43 umin = 3.2 * 1000 / 3600;
44 xapps = 3;
45 yapps = 3;
```

```

46 apploc = [0,0; 1,0; 0,1 ; 1,1 ; 0.5,0.5];
47 apploc = apploc .* repmat([1,w], size(apploc,1),1);
48 shorelength = 10 * ones(size(apploc,1),1);
49 apponcent = [1/2 w/2];
50 apponcurv = 0.07;
51 appvol = 13.8/ 1e6;
52 dt = 3600;
53 tfinal = 20 * 3600;
54 savefreq = 10;
55 dt.wind = tfinal;
56 tttotal = tfinal;
57
58 displaytime = 2 * 60;
59
60 % Programming tasks:
61 % Number of nodes = proportional to the number of grid lines
62 % Applicator indices = variables with applicator positions
63 % Create arrays containing coordinates of each node
64 % Number of applicator indicies
65 % Calculate distribution of monolayer from applicators
66 % Output contour plot of distribution and % of monolayer coverage ...
    versus time
67
68 % Calculate number of nodes:
69 nx = round(l / dx + 1);
70 ny = round(w / dy + 1);
71
72 % Create arrays containing coordinates of each node
73 x = 0 : dx : l;
74 y = 0 : dy : w;
75
76
77 % Create list of coordinates for nodes that are located on boundary
78 boun_nodes = [x', zeros(nx,1);
79              x', w*ones(nx,1);
80              zeros(ny,1), y';
81              l*ones(ny,1), y'];
82
83 % Calculate number of applicator indicies:
84 appind = round(apploc(:,1) / dx + 1);
85 appind(:,2) = round(apploc(:,2) / dy + 1);
86
87 % Initialise old value of application rate
88 apprateold = zeros(size(appind,1),1);
89 Atot = l*w;
90 apprateold(:) = Atot*appvol / (length(apprateold)*tfinal);
91
92 monothick = zeros(nx,ny);
93
94 % Flag to determine whether need to apply product
95 dumpproduct = 1;
96
97 % Determine applicator rates
98
99 % If wind speed is greater than threshold value, then applicators are ...
    to be
100 % turned on if they are on the windward side
101 % NOTE: This section of code has become obsolete:
102
103 % We have commented this section of code out because we don't know ...
    what to
104 % do with it yet:
105 % if 0
106 % if u ≤ umin
107 % apprate = 5 * ones(size(apploc,1),1) / 1e6 / 60;
108 % else
109 % Calculate apprate below
110 % apprate = zeros(size(apploc,1),1);
111 %
112 % This is the new code to define which applicators turn on and ...
    which do
113 % not. Again, this is done according to wind direction:
114 % ubeta = utheta + pi/2;
115 % Lmax = sqrt(l^2 + w^2);
116 % for i = 1:size(apploc,1)
117 % xd(:,i) = [cos(ubeta) sin(ubeta); -sin(ubeta) cos(ubeta)] * ...
    (apploc(i,:) - apponcent)';
118 % end
119 % xd = xd';
120 % f = find(xd(:,2) > apponcurv * (xd(:,1).^2 - (Lmax/2)^2) - ...
    10*eps );
121 % apprate(f) = apprate.u(u) * shorelength(f);
122 % end
123 % end
124
125 save monoinput
126
127 % Load excel data here (call it).
128
129 % Iterate in time, by adjusting the wind conditions
130
131 countu = 0;

```

```

|132 for t = dt_wind : dt_wind : ttotal
|133     countu = countu + 1;
|134     % Assign new values of wind conditions
|135     u = u;
|136     utheta = utheta;
|137
|138     % Calculate distribution of monolayer from applicator/s:
|139     [appttotal,monothick, apprateold,dumpproduct] = calcdistrib(l, w, ...
|140         dx, dy, boun_nodes, u, ...
|141         utheta, umin, apploc, appvol, apprateold, dumpproduct, ...
|142         monothick, nx, ny, ...
|143         appind, dt, dt_wind, savefreq);
|144 end
|145 % Outputs:
|146 % Spacing between applicators
|147 % Amount applied from each applicator
|148 % Total applied amount
|149 % Placement of applicators
|150 % Number of applicator types required (i.e. shore and floating)
|151 % Percentage of surface coverage
|152 % Start plotting
|153 output
|154
|155 % Total amount of monolayer applied for each applicator:
|156 disp('Total amount of monolayer applied for each applicator (in kg):')
|157 disp([apploc,appttotal])
|158
|159 toc

```

B.2 The calcdistrib.m function

```

1 function [appttotal,monothick, apprate,dumpproduct] = calcdistrib(l, ...
2     w, dx, dy, boun_nodes, u, utheta, umin, ...
3     apploc, appvol, apprateold, dumpproduct, monothick, nx, ny, ...
4     appind, dt, tfinal, savefreq)
5
6 load monoinput
7
8 % Number of applicators
9 napploc = size(apploc, 1);
10
11 % Reset application rates
12 apprate = zeros(napploc, 1);
13 area = apprate;
14 area_wedge = apprate;
15 area_loss = apprate;
16 fetch = apprate;
17
18 % Initialise monolayer thickness
19 monopre = zeros(nx,ny);
20 %monothickstore = zeros(nx,ny, round(tfinal/dt / savefreq));
21 %monothickstore(:, :, 1) = monothick;
22 savecounter = 0;
23 save(['monodata', num2str(savecounter)], 'monothick')
24
25 % Create arrays containing coordinates of each node
26 x = 0 : dx : l;
27 y = 0 : dy : w;
28 nodex = repmat(x', 1, ny);
29 nodey = repmat(y, nx, 1);
30 % Array containing the distance of each node from each applicator
31 noder = zeros(nx, ny, napploc);
32 nodetheta = noder;
33 % Array containing whether applicator supplies product to a node
34 nodes_app = zeros(nx*ny, napploc);
35 for i = 1 : napploc
36     noder(:, :, i) = sqrt( (nodex - apploc(i,1)).^2 ...
37         + (nodey - apploc(i,2)).^2 );
38     nodetheta(:, :, i) = atan( (nodey - apploc(i,2)) ...
39         ./ (nodex - apploc(i,1)) );
40     nodetheta(:, :, i) = nodetheta(:, :, i) + pi*(nodex < apploc(i,1));
41     nodetheta(:, :, i) = nodetheta(:, :, i) + 2*pi*(nodetheta(:, :, i)<0);
42     %contour(nodetheta(:, :, i)'/pi*180, 20);colorbar;pause
43
44     % Calculate the location of beaching in the direction of wind
45     % First find all boundary nodes that are not adjacent to applicator
46     fl = find( (boun_nodes(:,1) - apploc(i,1)).^2 ...
47         + (boun_nodes(:,2) - apploc(i,2)).^2 > (dx+dy) );
48     % Now find the node that lies in the direction of wind

```

```

49     if abs(tan(utheta)) > 100
50         % If angle is close to +/- 90 degrees, then x-value is the same
51         [dummy,f] = min(abs(boun_nodes(f1,1) - apploc(i,1)));
52     else
53         % Otherwise use trigonometry to find location
54         [dummy,f] = min(abs((boun_nodes(f1,2) - apploc(i,2)) ...
55             ./ (boun_nodes(f1,1) - apploc(i,1)) - tan(utheta)) );
56     end
57     %
58     % if utheta ≥ 1.5*pi || utheta ≤ 0.5*pi
59     [dummy,f] = min(abs(boun_nodes(f1,2) - apploc(i,2)) ...
60         - (boun_nodes(f1,1) - apploc(i,1)) * tan(utheta)) );
61     else
62         [dummy,f] = min(abs((boun_nodes(f1,2) - apploc(i,2)) ...
63             ./ (boun_nodes(f1,1) - apploc(i,1)) - tan(utheta)) );
64     end
65     % This is the identifier for the node where line of fetch reaches the
66     % dam boundary
67     beach_node(i) = f1(f);
68     % Calculate the fetch
69     fetch(i) = sqrt( (boun_nodes(beach_node(i),1) - apploc(i,1)).^2 ...
70         + (boun_nodes(beach_node(i),2) - apploc(i,2)).^2 );
71
72     % Distribute product from each applicator
73     % Check wind speed to determine shape of distribution
74     if abs(u) < umin
75         % Only need to do this if wind speed just dropped below threshold
76         % value
77         if dumpproduct
78             f = find(monothick == 0);
79             Atot = length(f) * dx*dy;
80             appamt = Atot * appvol;
81             apprate(i) = appamt * (apprateold(i)/sum(apprateold)) / ...
82                 tfinal;
83         end
84     else
85         % Need to apply product
86         dumpproduct = 1;
87
88         % Calculate angle of wedge
89         monotheta = spreadangle(u, umin);
90         % Calculate radius extended
91         disp('need to redo this')
92         r = sqrt( (2*pi)/monotheta * A/pi);
93
94         % Find which nodes are within this wedge
95         % Need to account for the cyclic nature of angles past 360 ...
96         % degrees
97         if utheta - 0.5*monotheta ≥ 0 && utheta + 0.5*monotheta < 2*pi
98             nodes_covered{i} = find( noder(:, :, i) ≤ fetch(i) ...
99                 & nodetheta(:, :, i) ≥ utheta-0.5*monotheta ...
100                 & nodetheta(:, :, i) ≤ utheta+0.5*monotheta );
101         elseif utheta - 0.5*monotheta < 0
102             nodes_covered{i} = find( noder(:, :, i) ≤ fetch(i) ...
103                 & ( nodetheta(:, :, i) ≥ utheta-0.5*monotheta + 2*pi ...
104                 | nodetheta(:, :, i) ≤ utheta+0.5*monotheta ) );
105         elseif utheta + 0.5*monotheta ≥ 2*pi
106             nodes_covered{i} = find( noder(:, :, i) ≤ fetch(i) ...
107                 & ( nodetheta(:, :, i) ≥ utheta-0.5*monotheta ...
108                 | nodetheta(:, :, i) ≤ utheta+0.5*monotheta - 2*pi ) );
109         end
110
111         % These nodes have product coming from this applicator
112         monopre(nodes_covered{i}) = monopre(nodes_covered{i}) + 1;
113         contour(monopre'); colorbar; pause(0.01)
114
115         % This provides a list of which applicator applies to which nodes
116         nodes_app(nodes_covered{i}, i) = 1;
117
118         % Calculate area covered
119         area(i) = length(nodes_covered{i}) * dx*dy;
120         % Calculate theoretical area covered
121         area_wedge(i) = pi*fetch(i)^2 * (monotheta/(2*pi));
122
123         % Compare area of coverage on water and off water
124         area_loss(i) = area_wedge(i) - area(i);
125         % If area on the water surface is greater than or equal to ...
126         % the area
127         % off the surface then compute application rate for these
128         % applicators only:
129         if area_loss(i) ≤ 0.5 * area_wedge(i)
130             % Calculate application rate for this applicator
131             apprate(i) = appvol * area(i) * (drift_speed(u) / ...
132                 fetch(i)) ;
133         else
134             area(i) = 0;
135             nodes_app(:, i) = 0;
136             nodes_covered{i} = [];

```

```

133     end
134
135     end
136
137 end
138
139
140 % List of nodes that have multiple applicators providing overlap
141 mult_cover = find(monopre > 1);
142 % Loop through all nodes to reduce application amount of each overlapping
143 % applicator
144 for j = 1 : length(mult_cover)
145     f = find(nodes_app(mult_cover(j),:));
146     area(f) = area(f) - dx*dy ...
147     * (monopre(mult_cover(j))-1) / monopre(mult_cover(j));
148 %     disp(num2str([j,area(4),dx*dy*(monopre(mult_cover(j))-1) / ...
149     monopre(mult_cover(j))]))
149 end
150 % Calculate application rate for all applicators
151 if u < umin
152     if dumpproduct
153         dumpproduct = 0;
154     else
155         apprate = zeros(napploc,1);
156     end
157 else
158     % Initialise this array
159     monothick = zeros(nx,ny);
160     % Calculate actual application rates for each applicator
161     apprate = appvol * area .* (drift_speed(u) ./ fetch) ;
162 end
163
164 % Iterate in time
165 counter = 0;
166 apptotal = zeros(napploc,1);
167 disp('Steps Total Time Finaltime')
168 for t = dt : dt : tfinal
169     if mod(counter, 1000) == 0
170         disp(num2str([counter, round(tfinal/dt), t, tfinal]))
171     end
172
173     % Distribute product from each applicator
174     for i = 1 : napploc
175         % Calculate area covered
176         %A = apprate(i) * t / appvol;
177         if abs(apprate(i)) > 10*eps
178             A = (0 * t^2 * (apprate(i) * 1e6)^2 + 2.7293e-006 * t^2 * ...
179                 (apprate(i) * 1e6) + 0.002847 * t^2 + 6.8829e-008 * t ...
180                 * (apprate(i) * 1e6)^2 + 3.2603e-005 * t * ...
181                 (apprate(i) * 1e6) + 0.20636 * t + 1.0998e-006 * ...
182                 (apprate(i) * 1e6)^2 + -0.00062192 * (apprate(i) * ...
183                 1e6) + 0.58905) / (appvol * 1e6);
184         else
185             A = 0;
186         end
187
188         % Check wind speed to determine shape of distribution
189         if abs(u) < umin
190             % Radius is calculated for a semi-circle from the area
191             % calculated above:
192             r = sqrt(2 * A / pi);
193
194             % Find which nodes are within this radius
195             f = find(noder(:, :, i) ≤ r);
196             monothick(f) = 1;
197         elseif A > 10*eps
198             % Calculate angle of wedge
199             monotheta = spreadangle(u, umin);
200             % Calculate radius extended
201             r = sqrt((2*pi)/monotheta * A/pi);
202
203             % Find which nodes are within this wedge
204             % Need to account for the cyclic nature of angles past ...
205             % 360 degrees
206             if utheta - 0.5*monotheta ≥ 0 && utheta + 0.5*monotheta ...
207                 < 2*pi
208                 f = find(noder(:, :, i) ≤ r ...
209                     & nodetheta(:, :, i) ≥ utheta-0.5*monotheta ...
210                     & nodetheta(:, :, i) ≤ utheta+0.5*monotheta);
211             elseif utheta - 0.5*monotheta < 0
212                 f = find(noder(:, :, i) ≤ r ...
213                     & (nodetheta(:, :, i) ≥ utheta-0.5*monotheta + ...
214                     2*pi ...
215                     | nodetheta(:, :, i) ≤ utheta+0.5*monotheta));
216             elseif utheta + 0.5*monotheta ≥ 2*pi
217                 f = find(noder(:, :, i) ≤ r ...
218                     & (nodetheta(:, :, i) ≥ utheta-0.5*monotheta ...
219                     | nodetheta(:, :, i) ≤ utheta+0.5*monotheta - 2*pi ...
220                     ));
221             end
222         end
223     end

```

```

213         monothick(f) = 1;
214     end
215 end
216
217 % Cumulative amount of product applied
218 apptotal = apptotal + apprate * dt;
219
220 % Store this time-step's distribution
221 counter = counter + 1;
222 if mod(counter, savefreq) == 0
223     savecounter = savecounter + 1;
224     % disp(num2str([counter, savecounter]))
225     % monothickstore(:, :, savecounter) = monothick;
226     save(['monodata', num2str(savecounter)], 'monothick', ...
227         'apptotal', 't')
227 end
228 end

```

B.3 The spreadangle.m function

```

1 function monotheta = spreadangle(u, umin)
2
3 if abs(u) ≤ umin
4     monotheta = 360 / 180 * pi;
5 else
6     % Maximum angle of monolayer wedge at minimum wind speed:
7     %monotheta = 1/abs(u) + (90/180*pi) - 1/umin;
8     %monotheta = 2 * asin(3.276 * u^(-1.337));
9     monotheta = (446.29 * u^(-1.419))/180*pi;
10 end

```

B.4 The drift_speed.m function

```

1 function v = drift_speed(u)
2 % Drift speed of monolayer if u > umin:
3 v = 0.0459*u - 0.0661;

```

B.5 The output.m function

```

1 load monoinput
2
3 % Plot the average coverage for the domain versus time
4 figure
5 lastfile = round(tfinal/dt / savefreq);
6 meanthick = zeros(1,lastfile+1);
7 for i = 0:lastfile
8     load(['monodata', num2str(i)])
9     meanthick(i+1) = mean(mean(monothick));
10 end
11
12 plot((0:dt*savefreq:tfinal) / 60, ...
13     meanthick * 100)
14 grid on;
15 axis ([0 tfinal/60 0 100 ]);
16 set(gca,'yTick',0:5:100);
17 title('Percentage coverage of the dam')
18 xlabel('time (min)')
19 ylabel('Percentage of coverage')
20
21 toc
22 tic
23 % Plot the distribution of product for particular time-steps
24 figure
25 clf
26 timeused = 0;
27 nplots = round(tfinal / displaytime) + 1;
28 counter = 0;
29 while timeused < tfinal
30     i = round(timeused / dt / savefreq);
31     load(['monodata', num2str(i)])
32     [ccc, hhh] = contour(x,y, monothick', [1 1]);
33     set(hhh, 'color', [0 0 counter / nplots])
34     axis equal;
35     axis([0 1 0 w])
36     hold on
37
38     timeused = timeused + displaytime;
39     counter = counter + 1;
40 end
41 xlabel('x (m)')
42 ylabel('y (m)')
43 title(['Distribution of monolayer every ', num2str(displaytime/60), ...
44     ' minutes'])
45 hold off
46
47 figure
48 plot (apploc(:,1),apploc(:,2),'r.','MarkerSize',20)
49
50 toc

```

Appendix C

Wind Frequency Data Used For Modelling

C.1 Wind frequency data for Amberley, QLD

Wind frequency data was purchased from the Bureau of Meteorology (BOM) for Amberley Airport (BOM station number: 040004), and provides monthly averages for 9am and 3pm wind speed and direction observations from 15 June, 1952 to 30 September, 2010. The wind frequency data as received from the BOM is shown below.

Frequency Analysis of Wind direction versus Wind speed in km/h (15 Jun 1952 to 30 Sep 2010)

Custom times selected, refer to attached note for details

AMBERLEY AMO

Site Number 040004 • Opened Jan 1941 • Still Open • Latitude: -27.6297° • Longitude: 152.7111° • Elevation 24.m

Values are percentage frequency. A "*" indicates the event has occurred but with a frequency less than 0.5%. Other important info about this analysis is available in the accompanying notes.

9 am Jan 1753 Total Observations

Wind speed in km/h	Wind direction								Calm	ALL
	N	NE	E	SE	S	SW	W	NW		
Calm									25	25
> 0 and < 5	1	1	2	1	2	1	1	2		10
>= 5 and < 10	2	3	6	5	4	1	2	4		26
>= 10 and < 15	1	2	5	5	2	*	1	3		19
>= 15 and < 20	*	1	3	3	2	*	*	1		10
>= 20 and < 25	*	*	2	3	2	0	*	*		7
>= 25 and < 30	*	0	1	1	1	*	*	*		3
>= 30 and < 35	0	*	*	*	0	0	0	0		*
>= 35 and < 40	0	0	*	*	*	0	0	0		*
>= 40	0	0	0	0	0	0	0	0		0
All	4	7	18	18	13	2	4	10	25	100

3 pm Feb 1600 Total Observations

Wind speed in km/h	Wind direction								Calm	ALL
	N	NE	E	SE	S	SW	W	NW		
Calm									8	8
> 0 and < 5	1	1	1	*	*	*	*	*		5
>= 5 and < 10	2	4	5	3	1	1	1	1		17
>= 10 and < 15	1	6	8	3	2	*	1	1		22
>= 15 and < 20	1	5	7	2	1	*	*	*		16
>= 20 and < 25	*	5	9	3	1	*	*	*		19
>= 25 and < 30	*	3	5	2	1	*	*	*		12
>= 30 and < 35	0	*	*	*	*	0	0	0		1
>= 35 and < 40	0	*	*	0	*	0	0	0		1
>= 40	0	*	*	*	*	0	0	0		*
All	5	24	36	14	7	1	3	3	8	100

3 pm Jan 1751 Total Observations

Wind speed in km/h	Wind direction								Calm	ALL
	N	NE	E	SE	S	SW	W	NW		
Calm									7	7
> 0 and < 5	*	1	1	*	*	*	*	1		4
>= 5 and < 10	2	3	4	1	1	*	*	1		12
>= 10 and < 15	1	6	8	2	1	*	1	1		20
>= 15 and < 20	1	7	7	2	1	*	*	*		18
>= 20 and < 25	*	9	8	2	1	*	*	*		21
>= 25 and < 30	*	4	7	2	*	0	*	*		13
>= 30 and < 35	*	1	1	*	*	0	*	*		3
>= 35 and < 40	0	*	*	*	*	0	*	*		1
>= 40	0	*	*	*	*	0	0	0		*
All	5	31	36	11	4	1	2	3	7	100

9 am Mar 1780 Total Observations

Wind speed in km/h	Wind direction								Calm	ALL
	N	NE	E	SE	S	SW	W	NW		
Calm									29	29
> 0 and < 5	1	*	1	2	3	1	2	1		11
>= 5 and < 10	1	1	3	6	9	3	1	3		27
>= 10 and < 15	*	*	2	5	6	*	1	1		17
>= 15 and < 20	*	*	1	3	3	*	*	*		7
>= 20 and < 25	0	*	1	3	2	*	*	0		6
>= 25 and < 30	0	0	*	1	1	*	0	0		2
>= 30 and < 35	0	0	*	*	*	0	0	*		*
>= 35 and < 40	0	0	0	0	*	0	0	0		*
>= 40	0	0	*	0	0	0	0	0		*
All	2	2	8	19	25	5	4	6	29	100

9 am Feb 1626 Total Observations

Wind speed in km/h	Wind direction								Calm	ALL
	N	NE	E	SE	S	SW	W	NW		
Calm									27	27
> 0 and < 5	1	1	2	3	2	1	1	1		12
>= 5 and < 10	1	1	4	6	5	2	1	3		24
>= 10 and < 15	1	1	4	5	5	*	1	2		19
>= 15 and < 20	*	*	2	4	2	*	*	*		9
>= 20 and < 25	*	*	1	3	1	*	*	*		6
>= 25 and < 30	0	0	*	1	1	*	*	*		2
>= 30 and < 35	0	*	*	*	*	0	0	0		*
>= 35 and < 40	0	0	0	*	0	0	0	0		*
>= 40	*	0	0	0	0	0	0	0		*
All	3	4	13	22	17	4	3	7	27	100

3 pm Mar 1774 Total Observations

Wind speed in km/h	Wind direction								Calm	ALL
	N	NE	E	SE	S	SW	W	NW		
Calm									11	11
> 0 and < 5	1	1	1	1	*	*	1	*		5
>= 5 and < 10	1	4	5	3	1	1	1	1		18
>= 10 and < 15	1	5	7	4	2	1	1	1		22
>= 15 and < 20	*	4	6	3	1	*	*	*		15
>= 20 and < 25	*	4	8	3	1	*	*	*		17
>= 25 and < 30	*	2	4	2	1	*	*	*		9
>= 30 and < 35	0	*	1	*	*	*	0	0		1
>= 35 and < 40	0	0	*	*	*	0	0	0		*
>= 40	0	0	*	*	*	0	0	0		*
All	4	20	33	16	8	3	3	3	11	100



Copyright © Commonwealth of Australia 2010. Prepared on 14 Dec 2010
 Prepared by National Climate Centre of the Bureau of Meteorology.
 Contact us by phone on (03) 9669 4092, by fax on (03) 9669 4515, or by email on webclim@bom.gov.au
 We have taken all due care but cannot provide any warranty nor accept any liability for this information.

Frequency Analysis of Wind direction versus Wind speed in km/h (15 Jun 1952 to 30 Sep 2010)

Custom times selected, refer to attached note for details

AMBERLEY AMO

Site Number 040004 • Opened Jan 1941 • Still Open • Latitude: -27.6297° • Longitude: 152.7111° • Elevation 24.m

Values are percentage frequency. A "*" indicates the event has occurred but with a frequency less than 0.5%. Other important info about this analysis is available in the accompanying notes.

9 am Apr 1730 Total Observations

Wind speed in km/h	Wind direction								Calm	ALL
	N	NE	E	SE	S	SW	W	NW		
Calm									41	41
> 0 and < 5	1	*	*	1	4	2	1	1		11
>= 5 and < 10	1	*	1	3	9	4	2	4		24
>= 10 and < 15	*	0	*	2	7	1	1	2		13
>= 15 and < 20	*	*	*	2	3	*	*	*		6
>= 20 and < 25	*	*	*	1	2	*	*	*		4
>= 25 and < 30	0	0	*	1	1	0	*	*		2
>= 30 and < 35	0	0	0	0	*	0	0	0		*
>= 35 and < 40	0	0	0	0	*	0	0	0		*
>= 40	0	0	0	0	0	0	0	0		0
All	2	1	2	10	25	7	4	8	41	100

3 pm May 1777 Total Observations

Wind speed in km/h	Wind direction									
	N	NE	E	SE	S	SW	W	NW	Calm	ALL
Calm									18	18
> 0 and < 5	1	2	2	1	1	*	1	1		9
>= 5 and < 10	3	3	4	3	2	2	2	3		22
>= 10 and < 15	2	2	6	4	3	1	3	2		22
>= 15 and < 20	*	1	4	2	2	1	3	1		13
>= 20 and < 25	*	1	2	2	1	1	2	1		9
>= 25 and < 30	0	*	1	1	1	1	2	*		5
>= 30 and < 35	0	0	*	*	*	*	1	*		1
>= 35 and < 40	0	0	0	0	*	0	*	0		*
>= 40	0	0	0	0	0	0	*	0		*
All	6	9	18	12	10	6	15	7	18	100

3 pm Apr 1705 Total Observations

Wind speed in km/h	Wind direction								Calm	ALL
	N	NE	E	SE	S	SW	W	NW		
Calm									13	13
> 0 and < 5	1	2	1	1	*	*	*	*		8
>= 5 and < 10	2	5	5	3	2	1	2	2		22
>= 10 and < 15	1	5	8	4	2	1	2	1		25
>= 15 and < 20	*	3	5	3	2	*	1	1		15
>= 20 and < 25	*	2	4	2	1	*	1	*		11
>= 25 and < 30	0	1	2	1	1	*	1	*		6
>= 30 and < 35	0	*	*	*	*	0	*	*		1
>= 35 and < 40	0	0	*	*	*	0	*	0		*
>= 40	0	0	0	0	0	0	0	0		0
All	5	17	26	15	9	3	7	5	13	100

9 am Jun 1738 Total Observations

Wind speed in km/h	Wind direction									
	N	NE	E	SE	S	SW	W	NW	Calm	ALL
Calm									47	47
> 0 and < 5	1	*	*	1	3	2	2	4		13
>= 5 and < 10	1	*	*	1	5	3	2	5		18
>= 10 and < 15	*	*	*	*	4	1	2	3		10
>= 15 and < 20	*	0	*	*	1	*	1	2		5
>= 20 and < 25	0	0	*	*	1	*	1	1		3
>= 25 and < 30	*	0	*	*	*	*	1	*		2
>= 30 and < 35	0	0	0	0	0	0	*	*		*
>= 35 and < 40	0	0	0	0	0	0	*	*		*
>= 40	0	0	0	0	0	0	*	0		*
All	3	*	1	2	14	6	11	16	47	100

9 am May 1790 Total Observations

Wind speed in km/h	Wind direction								Calm	ALL
	N	NE	E	SE	S	SW	W	NW		
Calm									46	46
> 0 and < 5	1	*	*	*	4	3	2	3		13
>= 5 and < 10	1	*	*	1	7	4	2	6		22
>= 10 and < 15	*	*	*	1	4	1	1	2		10
>= 15 and < 20	*	0	*	1	1	*	1	1		4
>= 20 and < 25	*	0	*	*	1	*	1	1		3
>= 25 and < 30	0	0	*	*	*	0	1	*		1
>= 30 and < 35	0	0	0	*	*	*	*	*		*
>= 35 and < 40	0	0	0	0	0	0	*	0		*
>= 40	0	0	0	0	0	0	0	0		0
All	2	1	1	4	17	8	9	13	46	100

3 pm Jun 1730 Total Observations

Wind speed in km/h	Wind direction									
	N	NE	E	SE	S	SW	W	NW	Calm	ALL
Calm									16	16
> 0 and < 5	2	1	1	1	1	1	1	1		9
>= 5 and < 10	3	3	3	2	2	1	3	3		20
>= 10 and < 15	2	2	3	3	3	1	4	3		22
>= 15 and < 20	*	1	2	2	2	1	3	1		12
>= 20 and < 25	0	*	2	2	2	1	3	1		10
>= 25 and < 30	*	0	*	1	1	1	4	*		7
>= 30 and < 35	0	0	*	*	*	*	1	*		2
>= 35 and < 40	0	0	0	0	0	*	1	*		1
>= 40	0	0	0	0	0	*	*	0		*
All	7	7	10	11	11	7	21	10	16	100



Copyright © Commonwealth of Australia 2010. Prepared on 14 Dec 2010
 Prepared by National Climate Centre of the Bureau of Meteorology.
 Contact us by phone on (03) 9669 4092, by fax on (03) 9669 4515, or by email on webclim@bom.gov.au
 We have taken all due care but cannot provide any warranty nor accept any liability for this information.

Frequency Analysis of Wind direction versus Wind speed in km/h (15 Jun 1952 to 30 Sep 2010)

Custom times selected, refer to attached note for details

AMBERLEY AMO

Site Number 040004 • Opened Jan 1941 • Still Open • Latitude: -27.6297° • Longitude: 152.7111° • Elevation 24.m

Values are percentage frequency. A "*" indicates the event has occurred but with a frequency less than 0.5%. Other important info about this analysis is available in the accompanying notes.

9 am Jul 1818 Total Observations

Wind speed in km/h	Wind direction								Calm	ALL
	N	NE	E	SE	S	SW	W	NW		
Calm									48	48
> 0 and < 5	1	*	*	*	3	3	2	4		14
>= 5 and < 10	2	*	*	*	3	3	3	6		18
>= 10 and < 15	*	*	*	*	2	1	2	3		9
>= 15 and < 20	*	0	*	*	1	*	1	2		5
>= 20 and < 25	*	*	*	*	*	*	1	1		3
>= 25 and < 30	0	0	*	*	*	*	1	*		2
>= 30 and < 35	0	0	*	0	0	*	*	*		*
>= 35 and < 40	0	0	0	0	0	*	*	0		*
>= 40	0	0	*	0	0	*	0	*		*
All	4	1	1	1	2	9	8	11	17	48

3 pm Aug 1795 Total Observations

Wind speed in km/h	Wind direction										
	N	NE	E	SE	S	SW	W	NW	Calm	ALL	
Calm										11	11
> 0 and < 5	1	1	1	1	1	*	1	1		7	
>= 5 and < 10	4	4	3	2	2	2	2	3		21	
>= 10 and < 15	2	3	4	2	1	1	4	4		22	
>= 15 and < 20	1	2	2	1	1	1	3	2		12	
>= 20 and < 25	*	2	2	1	1	1	4	1		13	
>= 25 and < 30	*	1	*	1	*	1	5	1		9	
>= 30 and < 35	*	0	*	*	*	*	2	*		3	
>= 35 and < 40	0	0	*	*	*	*	1	*		2	
>= 40	0	0	*	*	0	*	1	*		1	
All	8	12	13	7	6	8	22	12	11	100	

3 pm Jul 1809 Total Observations

Wind speed in km/h	Wind direction								Calm	ALL
	N	NE	E	SE	S	SW	W	NW		
Calm									14	14
> 0 and < 5	1	1	2	1	1	1	1	1		10
>= 5 and < 10	4	3	2	2	2	2	3	4		22
>= 10 and < 15	2	2	3	2	3	2	4	3		21
>= 15 and < 20	*	1	2	1	1	1	4	1		11
>= 20 and < 25	*	*	1	1	1	1	5	1		11
>= 25 and < 30	0	*	*	1	1	1	4	*		7
>= 30 and < 35	0	0	0	*	*	*	2	*		2
>= 35 and < 40	0	0	*	*	*	*	1	*		1
>= 40	0	0	*	0	0	*	0	*		1
All	8	7	10	8	9	8	24	12	14	100

9 am Sep 1745 Total Observations

Wind speed in km/h	Wind direction										
	N	NE	E	SE	S	SW	W	NW	Calm	ALL	
Calm										33	33
> 0 and < 5	1	1	1	1	2	3	2	2		14	
>= 5 and < 10	2	1	2	2	4	3	4	5		24	
>= 10 and < 15	1	1	1	1	3	1	2	4		14	
>= 15 and < 20	1	*	*	1	1	*	1	2		7	
>= 20 and < 25	*	0	*	*	1	*	1	1		5	
>= 25 and < 30	*	0	0	*	*	*	1	1		3	
>= 30 and < 35	0	0	0	0	0	*	*	*		1	
>= 35 and < 40	0	0	0	0	*	*	*	0		*	
>= 40	0	0	0	0	0	0	*	0		*	
All	6	3	5	6	12	9	11	16	33	100	

9 am Aug 1818 Total Observations

Wind speed in km/h	Wind direction								Calm	ALL
	N	NE	E	SE	S	SW	W	NW		
Calm									44	44
> 0 and < 5	1	*	*	*	3	2	2	3		13
>= 5 and < 10	2	*	*	*	1	4	4	7		22
>= 10 and < 15	*	*	*	*	2	1	2	3		9
>= 15 and < 20	*	*	*	1	1	*	1	1		4
>= 20 and < 25	*	0	0	*	1	*	2	1		4
>= 25 and < 30	0	0	*	*	*	*	1	1		2
>= 30 and < 35	0	0	0	0	*	*	*	*		1
>= 35 and < 40	0	0	0	*	*	*	*	*		*
>= 40	0	0	0	0	0	*	*	0		*
All	3	1	1	3	11	9	12	16	44	100

3 pm Sep 1731 Total Observations

Wind speed in km/h	Wind direction										
	N	NE	E	SE	S	SW	W	NW	Calm	ALL	
Calm										7	7
> 0 and < 5	1	1	1	*	*	*	1	1		5	
>= 5 and < 10	3	3	2	1	1	1	2	3		16	
>= 10 and < 15	4	5	4	2	1	1	2	3		21	
>= 15 and < 20	1	4	4	1	1	1	3	1		16	
>= 20 and < 25	1	5	4	1	1	1	4	1		17	
>= 25 and < 30	*	2	3	*	1	1	4	1		12	
>= 30 and < 35	*	*	*	*	*	*	2	*		3	
>= 35 and < 40	*	*	*	0	*	*	1	*		2	
>= 40	0	0	0	0	0	*	*	*		1	
All	10	21	18	6	5	6	18	10	7	100	



Copyright © Commonwealth of Australia 2010. Prepared on 14 Dec 2010
 Prepared by National Climate Centre of the Bureau of Meteorology.
 Contact us by phone on (03) 9669 4092, by fax on (03) 9669 4515, or by email on webclim@bom.gov.au
 We have taken all due care but cannot provide any warranty nor accept any liability for this information.

Frequency Analysis of Wind direction versus Wind speed in km/h (15 Jun 1952 to 30 Sep 2010)

Custom times selected, refer to attached note for details

AMBERLEY AMO

Site Number 040004 • Opened Jan 1941 • Still Open • Latitude: -27.6297° • Longitude: 152.7111° • Elevation 24.m

Values are percentage frequency. A "*" indicates the event has occurred but with a frequency less than 0.5%. Other important info about this analysis is available in the accompanying notes.

9 am Oct 1782 Total Observations

Wind speed in km/h	Wind direction								Calm	ALL
	N	NE	E	SE	S	SW	W	NW		
Calm									25	25
> 0 and < 5	1	1	2	1	2	1	1	2		12
>= 5 and < 10	3	2	4	3	3	3	3	5		26
>= 10 and < 15	2	2	3	2	2	1	2	6		20
>= 15 and < 20	1	*	1	1	1	*	1	2		8
>= 20 and < 25	*	*	1	1	1	*	1	1		6
>= 25 and < 30	*	*	*	*	*	*	1	*		2
>= 30 and < 35	*	0	0	0	0	*	*	*		1
>= 35 and < 40	0	0	0	0	0	0	*	0		*
>= 40	0	0	0	0	0	0	*	0		*
All	8	6	11	8	10	6	9	17	25	100

3 pm Nov 1717 Total Observations

Wind speed in km/h	Wind direction								Calm	ALL
	N	NE	E	SE	S	SW	W	NW		
Calm									5	5
> 0 and < 5	1	1	1	*	*	*	*	1		4
>= 5 and < 10	2	3	3	1	1	1	1	2		13
>= 10 and < 15	2	6	5	2	1	1	1	1		19
>= 15 and < 20	1	6	5	1	*	1	2	1		16
>= 20 and < 25	1	9	7	1	*	*	1	*		20
>= 25 and < 30	*	7	7	*	*	*	2	*		17
>= 30 and < 35	*	1	1	*	*	*	1	*		3
>= 35 and < 40	*	1	*	*	*	*	*	*		2
>= 40	*	*	*	*	*	*	*	*		1
All	6	33	30	6	3	4	8	5	5	100

3 pm Oct 1764 Total Observations

Wind speed in km/h	Wind direction								Calm	ALL
	N	NE	E	SE	S	SW	W	NW		
Calm									6	6
> 0 and < 5	1	1	1	*	1	*	*	*		4
>= 5 and < 10	2	3	3	1	1	*	1	1		13
>= 10 and < 15	2	4	5	1	1	1	2	2		18
>= 15 and < 20	1	6	5	1	*	1	2	1		17
>= 20 and < 25	1	8	6	1	*	1	2	1		19
>= 25 and < 30	*	7	5	*	*	1	3	1		17
>= 30 and < 35	*	1	2	0	*	*	1	*		5
>= 35 and < 40	0	*	*	0	0	*	1	*		2
>= 40	0	*	*	0	*	*	*	*		1
All	6	29	27	5	3	4	13	8	6	100

9 am Dec 1766 Total Observations

Wind speed in km/h	Wind direction								Calm	ALL
	N	NE	E	SE	S	SW	W	NW		
Calm									22	22
> 0 and < 5	2	1	2	1	1	1	1	2		11
>= 5 and < 10	4	3	5	3	3	1	2	5		27
>= 10 and < 15	2	2	6	3	3	*	2	5		23
>= 15 and < 20	1	1	3	2	1	*	2	1		10
>= 20 and < 25	*	*	1	2	1	*	*	1		5
>= 25 and < 30	*	0	*	*	*	*	*	*		2
>= 30 and < 35	0	0	0	*	*	0	*	0		*
>= 35 and < 40	0	0	0	0	0	0	0	0		*
>= 40	0	0	0	0	0	0	0	0		0
All	10	8	17	10	9	3	6	15	22	100

9 am Nov 1721 Total Observations

Wind speed in km/h	Wind direction								Calm	ALL
	N	NE	E	SE	S	SW	W	NW		
Calm									19	19
> 0 and < 5	1	1	2	1	1	1	1	2		11
>= 5 and < 10	4	3	5	4	4	2	3	5		29
>= 10 and < 15	2	3	5	3	2	1	2	5		23
>= 15 and < 20	1	1	2	2	1	*	1	2		10
>= 20 and < 25	*	*	1	1	1	*	1	1		5
>= 25 and < 30	*	*	*	1	*	*	*	*		2
>= 30 and < 35	0	0	0	*	*	*	*	*		1
>= 35 and < 40	0	0	0	0	*	*	*	0		*
>= 40	0	0	0	0	0	0	0	0		0
All	8	8	15	11	9	5	8	16	19	100

3 pm Dec 1761 Total Observations

Wind speed in km/h	Wind direction								Calm	ALL
	N	NE	E	SE	S	SW	W	NW		
Calm									6	6
> 0 and < 5	1	1	1	*	*	*	*	*		4
>= 5 and < 10	2	3	2	1	1	1	1	2		13
>= 10 and < 15	2	5	5	2	1	*	1	1		18
>= 15 and < 20	1	6	5	1	1	1	1	*		15
>= 20 and < 25	1	9	9	1	*	*	1	1		22
>= 25 and < 30	*	7	7	1	*	*	1	*		17
>= 30 and < 35	*	1	2	*	*	*	*	*		4
>= 35 and < 40	*	1	*	*	*	*	*	*		2
>= 40	0	*	*	*	*	0	*	0		1
All	6	33	31	7	4	2	6	5	6	100



Copyright © Commonwealth of Australia 2010. Prepared on 14 Dec 2010
 Prepared by National Climate Centre of the Bureau of Meteorology.
 Contact us by phone on (03) 9669 4092, by fax on (03) 9669 4515, or by email on webclim@bom.gov.au
 We have taken all due care but cannot provide any warranty nor accept any liability for this information.

The 9am and 3pm wind speed and direction observation for each month were summed and averaged. This data was then used to produce wind frequency tables C.1 and C.2, which were subsequently used for post-processing of simulation outputs.

Table C.1: Amberley average annual (9am and 3pm) wind frequency table used in modelling (Part 1).

Wind Speed (km/h):	Wind Direction (°):	Frequency:
0	0	0.250416667
5	0	0.032916667
15	0	0.0175
25	0	0.001666667
30	0	0.0
5	45	0.03125
15	45	0.04625
25	45	0.036666667
30	45	0.0025
5	90	0.040416667
15	90	0.065833333
25	90	0.04625
30	90	0.0025
5	135	0.032083333
15	135	0.040833333
25	135	0.02125
30	135	0.0
Continued on Table C.2		

Table C.2: Amberley average annual (9am and 3pm) wind frequency table used in modelling, continued (Part 2).

Wind Speed (km/h):	Wind Direction (°):	Frequency:
Continued from Table C.1		
5	180	0.046666667
15	180	0.039166667
25	180	0.014583333
30	180	0.0
5	225	0.02875
15	225	0.010833333
25	225	0.005
30	225	0.0
5	270	0.03
15	270	0.030833333
25	270	0.025833333
30	270	0.006666667
5	315	0.049166667
15	315	0.035833333
25	315	0.008333333
30	315	0.0

C.2 Wind frequency data for Moree, NSW

Wind frequency data was purchased from the Bureau of Meteorology (BOM) for Moree Airport (BOM station number: 053115), and provides monthly averages for 9am and 3pm wind speed and direction observations from 18 May, 1995 to 30 September, 2010. The wind frequency data as received from the BOM is shown below.

Frequency Analysis of Wind direction versus Wind speed in km/h (18 May 1995 to 30 Sep 2010)

Custom times selected, refer to attached note for details

MOREE AERO

Site Number 053115 • Opened Apr 1995 • Still Open • Latitude: -29.4898° • Longitude: 149.8471° • Elevation 213m

Values are percentage frequency. A "*" indicates the event has occurred but with a frequency less than 0.5%. Other important info about this analysis is available in the accompanying notes.

9 am Jan 462 Total Observations

Wind speed in km/h	Wind direction									
	N	NE	E	SE	S	SW	W	NW	Calm	ALL
Calm										*
> 0 and < 5	0	*	*	0	0	0	0	0		1
>= 5 and < 10	1	1	1	1	*	1	0	*		5
>= 10 and < 15	2	4	6	1	2	0	*	*		16
>= 15 and < 20	4	6	6	1	1	*	*	0		19
>= 20 and < 25	8	14	8	1	1	0	*	*		33
>= 25 and < 30	6	11	1	*	0	0	0	0		18
>= 30 and < 35	1	3	*	*	1	0	0	0		6
>= 35 and < 40	*	2	0	0	0	0	0	0		2
>= 40	0	0	0	0	0	0	0	0		0
All	23	41	24	4	4	1	1	1		100

3 pm Feb 423 Total Observations

Wind speed in km/h	Wind direction									
	N	NE	E	SE	S	SW	W	NW	Calm	ALL
Calm										0
> 0 and < 5	*	0	*	0	0	0	*	0		1
>= 5 and < 10	4	3	4	2	2	1	2	3		19
>= 10 and < 15	9	6	6	4	6	3	2	6		43
>= 15 and < 20	5	1	1	2	1	1	2	1		14
>= 20 and < 25	2	2	2	*	*	3	2	*		13
>= 25 and < 30	1	1	0	1	0	1	*	*		5
>= 30 and < 35	*	0	1	0	0	1	*	0		2
>= 35 and < 40	0	0	1	*	*	*	0	0		2
>= 40	0	0	0	0	0	*	*	0		1
All	21	13	16	9	10	11	9	11		100

3 pm Jan 462 Total Observations

Wind speed in km/h	Wind direction									
	N	NE	E	SE	S	SW	W	NW	Calm	ALL
Calm										*
> 0 and < 5	*	0	0	0	0	0	0	0		*
>= 5 and < 10	5	3	1	3	2	1	2	3		20
>= 10 and < 15	13	6	4	5	4	2	3	4		41
>= 15 and < 20	5	3	2	*	2	1	1	1		14
>= 20 and < 25	4	2	2	1	1	3	2	2		17
>= 25 and < 30	1	*	1	*	0	1	*	1		5
>= 30 and < 35	*	*	0	0	0	0	1	0		2
>= 35 and < 40	0	*	0	0	*	*	*	*		2
>= 40	0	0	0	0	0	0	*	0		*
All	29	15	10	10	8	9	10	10		100

9 am Mar 464 Total Observations

Wind speed in km/h	Wind direction									
	N	NE	E	SE	S	SW	W	NW	Calm	ALL
Calm										1
> 0 and < 5	0	0	0	*	*	0	1	0		1
>= 5 and < 10	1	2	5	2	1	1	*	0		11
>= 10 and < 15	2	9	9	3	1	1	*	0		25
>= 15 and < 20	3	9	8	2	2	1	0	0		24
>= 20 and < 25	4	10	7	2	1	1	0	0		25
>= 25 and < 30	3	6	1	*	*	0	0	0		11
>= 30 and < 35	*	1	*	*	*	0	*	0		2
>= 35 and < 40	0	0	*	0	*	0	0	0		1
>= 40	0	0	0	0	0	0	0	0		0
All	12	36	30	10	6	4	1	0		100

9 am Feb 423 Total Observations

Wind speed in km/h	Wind direction									
	N	NE	E	SE	S	SW	W	NW	Calm	ALL
Calm										*
> 0 and < 5	0	0	*	*	*	0	*	0		1
>= 5 and < 10	1	2	1	*	1	*	0	0		5
>= 10 and < 15	2	7	8	2	2	1	*	0		22
>= 15 and < 20	3	8	8	2	*	1	*	*		22
>= 20 and < 25	5	13	9	1	*	*	0	0		29
>= 25 and < 30	4	9	3	*	0	1	0	0		16
>= 30 and < 35	1	1	0	0	0	0	0	0		2
>= 35 and < 40	*	*	0	0	0	*	0	0		1
>= 40	0	*	*	0	0	0	0	0		*
All	16	39	30	6	4	3	1	*		100

3 pm Mar 465 Total Observations

Wind speed in km/h	Wind direction									
	N	NE	E	SE	S	SW	W	NW	Calm	ALL
Calm										0
> 0 and < 5	*	0	0	0	*	*	*	*		1
>= 5 and < 10	5	2	2	1	3	2	3	3		21
>= 10 and < 15	9	6	5	5	5	4	4	3		41
>= 15 and < 20	2	2	1	2	1	2	1	2		14
>= 20 and < 25	2	2	1	2	1	4	2	1		15
>= 25 and < 30	0	*	*	*	1	3	0	0		5
>= 30 and < 35	*	0	0	*	1	*	0	0		3
>= 35 and < 40	0	0	*	*	*	*	0	0		1
>= 40	0	0	0	0	0	*	0	*		*
All	19	12	10	12	11	16	10	10		100



Copyright © Commonwealth of Australia 2010. Prepared on 14 Dec 2010
 Prepared by National Climate Centre of the Bureau of Meteorology.
 Contact us by phone on (03) 9669 4092, by fax on (03) 9669 4515, or by email on webclim@bom.gov.au
 We have taken all due care but cannot provide any warranty nor accept any liability for this information.

Frequency Analysis of Wind direction versus Wind speed in km/h (18 May 1995 to 30 Sep 2010)

Custom times selected, refer to attached note for details

MOREE AERO

Site Number 053115 • Opened Apr 1995 • Still Open • Latitude: -29.4898° • Longitude: 149.8471° • Elevation 213m

Values are percentage frequency. A "*" indicates the event has occurred but with a frequency less than 0.5%. Other important info about this analysis is available in the accompanying notes.

9 am Apr 450 Total Observations

Wind speed in km/h	Wind direction								Calm	ALL
	N	NE	E	SE	S	SW	W	NW		
Calm									1	1
> 0 and < 5	*	0	*	*	*	*	*	0	*	2
>= 5 and < 10	2	2	2	2	1	1	1	*		12
>= 10 and < 15	3	8	11	3	2	2	1	1		30
>= 15 and < 20	4	6	8	3	1	1	1	*		23
>= 20 and < 25	4	6	8	2	1	*	*	0		21
>= 25 and < 30	2	2	2	*	1	*	*	0		8
>= 30 and < 35	*	*	0	*	1	*	*	0		2
>= 35 and < 40	0	0	0	0	0	0	0	0		*
>= 40	0	0	0	0	0	0	0	0		0
All	15	25	30	10	7	6	3	2	1	100

3 pm May 477 Total Observations

Wind speed in km/h	Wind direction								Calm	ALL
	N	NE	E	SE	S	SW	W	NW		
Calm									0	0
> 0 and < 5	0	0	*	*	1	*	*	1		3
>= 5 and < 10	4	3	2	2	4	4	3	3		25
>= 10 and < 15	5	2	4	3	3	7	3	3		30
>= 15 and < 20	1	1	2	1	3	5	1	*		13
>= 20 and < 25	1	1	*	2	1	7	3	*		15
>= 25 and < 30	*	*	*	*	*	6	2	*		10
>= 30 and < 35	0	0	0	0	0	2	*	*		3
>= 35 and < 40	0	0	*	0	1	*	*	*		1
>= 40	0	0	0	0	0	0	*	0		*
All	10	7	9	8	13	31	13	8	0	100

3 pm Apr 450 Total Observations

Wind speed in km/h	Wind direction								Calm	ALL
	N	NE	E	SE	S	SW	W	NW		
Calm									*	*
> 0 and < 5	0	0	0	0	0	0	0	0		0
>= 5 and < 10	3	4	3	4	4	4	2	2		26
>= 10 and < 15	4	3	3	5	6	5	2	2		32
>= 15 and < 20	2	1	2	2	3	5	2	*		16
>= 20 and < 25	1	1	1	1	1	7	2	2		16
>= 25 and < 30	0	0	*	0	*	2	1	*		4
>= 30 and < 35	0	0	0	*	1	2	1	0		4
>= 35 and < 40	0	0	0	*	0	*	0	0		1
>= 40	0	0	0	*	0	*	*	*		1
All	11	8	10	13	15	25	11	7	*	100

9 am Jun 479 Total Observations

Wind speed in km/h	Wind direction								Calm	ALL
	N	NE	E	SE	S	SW	W	NW		
Calm										3
> 0 and < 5	*	*	1	*	*	1	*	*		4
>= 5 and < 10	1	4	7	2	5	3	1	1		24
>= 10 and < 15	3	6	17	2	2	6	1	1		38
>= 15 and < 20	1	3	6	*	*	2	1	1		14
>= 20 and < 25	1	2	3	*	1	3	1	1		11
>= 25 and < 30	1	1	0	0	0	2	1	*		5
>= 30 and < 35	0	0	0	0	*	0	*	*		1
>= 35 and < 40	0	0	0	0	0	0	0	0		0
>= 40	0	0	0	0	0	0	0	0		0
All	8	17	34	4	8	15	6	4	3	100

9 am May 478 Total Observations

Wind speed in km/h	Wind direction								Calm	ALL
	N	NE	E	SE	S	SW	W	NW		
Calm									4	4
> 0 and < 5	*	*	1	1	*	*	*	0		3
>= 5 and < 10	1	4	8	3	2	2	1	1		22
>= 10 and < 15	1	8	14	3	4	2	*	*		33
>= 15 and < 20	1	5	9	2	1	2	1	1		21
>= 20 and < 25	1	3	4	1	*	3	1	*		13
>= 25 and < 30	*	1	1	0	0	1	0	0		3
>= 30 and < 35	0	0	0	*	*	0	*	0		1
>= 35 and < 40	0	0	0	0	0	0	0	0		0
>= 40	0	0	0	0	*	0	0	0		*
All	5	21	36	10	8	10	3	2	4	100

3 pm Jun 480 Total Observations

Wind speed in km/h	Wind direction								Calm	ALL
	N	NE	E	SE	S	SW	W	NW		
Calm									*	*
> 0 and < 5	1	*	1	*	1	*	0	1		3
>= 5 and < 10	4	3	4	2	4	2	3	2		23
>= 10 and < 15	8	2	4	2	2	8	3	1		30
>= 15 and < 20	3	1	*	1	1	5	3	1		15
>= 20 and < 25	0	1	*	*	2	6	4	2		15
>= 25 and < 30	1	0	*	*	*	4	2	*		8
>= 30 and < 35	0	0	0	0	*	2	2	0		4
>= 35 and < 40	0	0	0	0	*	1	0	1		1
>= 40	0	0	0	0	*	0	0	*		*
All	16	8	9	6	11	27	16	7	*	100



Copyright © Commonwealth of Australia 2010. Prepared on 14 Dec 2010
 Prepared by National Climate Centre of the Bureau of Meteorology.
 Contact us by phone on (03) 9669 4092, by fax on (03) 9669 4515, or by email on webclim@bom.gov.au
 We have taken all due care but cannot provide any warranty nor accept any liability for this information.

Frequency Analysis of Wind direction versus Wind speed in km/h (18 May 1995 to 30 Sep 2010)

Custom times selected, refer to attached note for details

MOREE AERO

Site Number 053115 • Opened Apr 1995 • Still Open • Latitude: -29.4898° • Longitude: 149.8471° • Elevation 213m

Values are percentage frequency. A "*" indicates the event has occurred but with a frequency less than 0.5%. Other important info about this analysis is available in the accompanying notes.

9 am Jul 495 Total Observations

Wind speed in km/h	Wind direction								Calm	ALL
	N	NE	E	SE	S	SW	W	NW		
Calm									5	5
> 0 and < 5	*	0	1	0	1	*	*	1		4
>= 5 and < 10	1	2	7	2	4	3	2	1		23
>= 10 and < 15	2	7	14	1	3	4	3	1		34
>= 15 and < 20	1	4	8	1	1	2	1	*		18
>= 20 and < 25	2	2	3	0	*	3	1	*		12
>= 25 and < 30	*	1	0	0	*	1	1	*		4
>= 30 and < 35	0	0	0	0	0	*	0	0		*
>= 35 and < 40	0	0	0	0	0	0	0	*		*
>= 40	0	*	0	0	0	0	0	0		*
All	7	17	33	4	9	13	8	4	5	100

3 pm Aug 496 Total Observations

Wind speed in km/h	Wind direction								Calm	ALL
	N	NE	E	SE	S	SW	W	NW		
Calm									0	0
> 0 and < 5	0	1	0	0	0	*	1	*		2
>= 5 and < 10	2	2	2	1	3	4	3	2		20
>= 10 and < 15	5	3	2	1	2	4	4	2		22
>= 15 and < 20	3	2	1	1	*	7	3	1		18
>= 20 and < 25	4	1	*	*	1	7	5	1		19
>= 25 and < 30	1	*	*	*	1	5	2	1		12
>= 30 and < 35	*	0	*	*	1	2	*		5	
>= 35 and < 40	0	0	0	0	0	*	1	*		1
>= 40	*	0	0	0	0	*	1	*		2
All	15	9	5	3	8	29	21	9	0	100

3 pm Jul 495 Total Observations

Wind speed in km/h	Wind direction								Calm	ALL
	N	NE	E	SE	S	SW	W	NW		
Calm									1	1
> 0 and < 5	1	*	1	*	*	*	*	*		4
>= 5 and < 10	2	1	3	1	3	3	2			17
>= 10 and < 15	7	2	1	2	2	8	5	3		30
>= 15 and < 20	3	1	*	1	1	4	3	1		15
>= 20 and < 25	2	1	*	*	1	8	3	1		16
>= 25 and < 30	*	*	0	0	*	6	4	*		12
>= 30 and < 35	0	*	0	0	0	1	1	*		3
>= 35 and < 40	1	0	0	0	0	0	1	0		2
>= 40	0	0	0	0	0	*	0	0		*
All	16	5	6	4	7	32	21	8	1	100

9 am Sep 481 Total Observations

Wind speed in km/h	Wind direction								Calm	ALL
	N	NE	E	SE	S	SW	W	NW		
Calm									1	1
> 0 and < 5	1	*	*	0	1	1	*	0		3
>= 5 and < 10	1	3	3	1	2	*	3	1		14
>= 10 and < 15	5	6	6	1	1	2	1	1		24
>= 15 and < 20	2	6	4	1	1	1	*	0		14
>= 20 and < 25	5	10	2	1	1	3	1	1		24
>= 25 and < 30	6	4	*	*	1	1	1	*		13
>= 30 and < 35	2	1	0	*	0	1	*	0		5
>= 35 and < 40	1	*	0	0	0	*	*	0		1
>= 40	0	0	0	0	0	0	0	0		0
All	22	30	15	4	6	10	6	4	1	100

9 am Aug 495 Total Observations

Wind speed in km/h	Wind direction								Calm	ALL
	N	NE	E	SE	S	SW	W	NW		
Calm									2	2
> 0 and < 5	0	*	*	*	1	*	*	*		3
>= 5 and < 10	2	2	5	2	4	2	1	*		18
>= 10 and < 15	2	8	9	2	2	4	1	1		28
>= 15 and < 20	3	6	4	1	1	2	1	*		18
>= 20 and < 25	4	5	3	*	1	3	1	1		18
>= 25 and < 30	3	3	*	*	1	2	1	*		9
>= 30 and < 35	1	*	0	*	0	*	0	0		2
>= 35 and < 40	1	*	0	0	0	*	0	0		1
>= 40	0	0	0	0	0	0	0	0		0
All	15	26	21	6	8	14	6	3	2	100

3 pm Sep 480 Total Observations

Wind speed in km/h	Wind direction								Calm	ALL
	N	NE	E	SE	S	SW	W	NW		
Calm									1	1
> 0 and < 5	0	0	*	0	0	0	1	0		1
>= 5 and < 10	4	1	3	1	3	2	3	2		20
>= 10 and < 15	6	3	1	1	1	6	5	3		26
>= 15 and < 20	3	2	1	0	2	4	5	1		17
>= 20 and < 25	3	1	1	*	1	7	5	2		21
>= 25 and < 30	2	*	0	0	*	4	3	1		10
>= 30 and < 35	*	0	0	0	0	1	2	0		3
>= 35 and < 40	*	*	0	0	0	*	1	*		2
>= 40	0	0	0	0	0	0	0	0		0
All	19	8	6	3	7	24	24	10	1	100



Copyright © Commonwealth of Australia 2010. Prepared on 14 Dec 2010
 Prepared by National Climate Centre of the Bureau of Meteorology.
 Contact us by phone on (03) 9669 4092, by fax on (03) 9669 4515, or by email on webclim@bom.gov.au
 We have taken all due care but cannot provide any warranty nor accept any liability for this information.

Frequency Analysis of Wind direction versus Wind speed in km/h (18 May 1995 to 30 Sep 2010)

Custom times selected, refer to attached note for details

MOREE AERO

Site Number 053115 • Opened Apr 1995 • Still Open • Latitude: -29.4898° • Longitude: 149.8471° • Elevation 213m

Values are percentage frequency. A "*" indicates the event has occurred but with a frequency less than 0.5%. Other important info about this analysis is available in the accompanying notes.

9 am Oct 465 Total Observations

Wind speed in km/h	Wind direction									
	N	NE	E	SE	S	SW	W	NW	Calm	ALL
Calm									1	1
> 0 and < 5	*	*	0	0	0	*	*	*		1
>= 5 and < 10	3	2	1	1	1	2	1	1		12
>= 10 and < 15	5	4	3	2	2	3	1	*		19
>= 15 and < 20	4	4	2	0	2	1	*	0		13
>= 20 and < 25	10	8	3	*	1	3	1	1		28
>= 25 and < 30	9	6	*	*	0	1	*	0		17
>= 30 and < 35	3	1	*	0	*	1	0	*		6
>= 35 and < 40	1	3	0	0	*	0	*	0		4
>= 40	0	*	0	0	0	0	0	0		*
All	36	28	9	3	6	11	4	3	1	100

3 pm Nov 449 Total Observations

Wind speed in km/h	Wind direction									
	N	NE	E	SE	S	SW	W	NW	Calm	ALL
Calm									0	0
> 0 and < 5	*	*	0	0	0	0	0	0		*
>= 5 and < 10	2	2	2	1	1	2	2	1		13
>= 10 and < 15	7	4	4	3	5	4	3	2		33
>= 15 and < 20	4	1	1	*	1	3	1	1		13
>= 20 and < 25	7	3	1	1	2	4	3	2		23
>= 25 and < 30	2	*	*	*	*	2	2	2		10
>= 30 and < 35	*	0	*	0	*	2	*	*		3
>= 35 and < 40	*	0	0	0	*	1	1	0		3
>= 40	0	0	0	0	0	1	*	0		1
All	24	12	8	6	9	19	12	9	0	100

3 pm Oct 465 Total Observations

Wind speed in km/h	Wind direction									
	N	NE	E	SE	S	SW	W	NW	Calm	ALL
Calm									1	1
> 0 and < 5	*	*	*	0	0	*	0	0		1
>= 5 and < 10	4	3	3	1	1	2	2	3		19
>= 10 and < 15	7	5	2	2	3	4	3	4		30
>= 15 and < 20	4	1	1	1	1	4	2	1		15
>= 20 and < 25	3	2	*	*	1	5	4	1		17
>= 25 and < 30	2	1	1	0	1	5	2	1		12
>= 30 and < 35	*	*	0	0	0	2	1	*		4
>= 35 and < 40	0	0	0	0	0	*	1	0		2
>= 40	0	0	0	0	0	*	*	*		1
All	21	11	7	4	7	22	17	10	*	100

9 am Dec 465 Total Observations

Wind speed in km/h	Wind direction									
	N	NE	E	SE	S	SW	W	NW	Calm	ALL
Calm									1	1
> 0 and < 5	*	*	0	0	*	0	0	0		1
>= 5 and < 10	2	1	2	1	1	1	1	*		8
>= 10 and < 15	3	6	4	1	2	*	1	1		17
>= 15 and < 20	3	6	3	0	1	1	0	*		14
>= 20 and < 25	9	12	3	*	*	1	0	0		27
>= 25 and < 30	9	10	1	*	*	1	*	0		22
>= 30 and < 35	3	5	*	0	*	0	0	0		8
>= 35 and < 40	1	1	0	*	*	*	0	0		3
>= 40	0	0	0	0	0	0	0	0		0
All	31	40	13	2	5	5	2	1	1	100

9 am Nov 450 Total Observations

Wind speed in km/h	Wind direction									
	N	NE	E	SE	S	SW	W	NW	Calm	ALL
Calm									0	0
> 0 and < 5	*	0	*	0	*	*	0	0		1
>= 5 and < 10	3	1	2	1	1	1	*	*		10
>= 10 and < 15	4	4	4	1	1	2	0	1		15
>= 15 and < 20	5	5	4	1	1	1	*	0		17
>= 20 and < 25	6	11	4	1	1	2	*	*		25
>= 25 and < 30	8	9	1	*	1	1	0	*		20
>= 30 and < 35	4	2	0	0	1	*	*	0		7
>= 35 and < 40	1	1	0	0	0	*	0	0		3
>= 40	*	0	0	0	0	0	0	0		*
All	31	33	14	5	6	7	1	1	*	100

3 pm Dec 465 Total Observations

Wind speed in km/h	Wind direction									
	N	NE	E	SE	S	SW	W	NW	Calm	ALL
Calm									0	0
> 0 and < 5	0	*	0	0	*	0	0	*		1
>= 5 and < 10	6	2	2	1	2	2	2	2		17
>= 10 and < 15	10	5	3	2	2	4	2	3		32
>= 15 and < 20	5	2	1	1	1	2	2	1		15
>= 20 and < 25	5	2	1	0	*	4	3	2		17
>= 25 and < 30	2	1	1	*	1	3	2	1		11
>= 30 and < 35	1	*	0	0	*	2	*	*		3
>= 35 and < 40	*	0	0	0	0	1	1	*		3
>= 40	0	0	0	0	*	0	*	0		1
All	28	13	8	4	8	17	11	11	0	100



Copyright © Commonwealth of Australia 2010. Prepared on 14 Dec 2010
 Prepared by National Climate Centre of the Bureau of Meteorology.
 Contact us by phone on (03) 9669 4092, by fax on (03) 9669 4515, or by email on webclim@bom.gov.au
 We have taken all due care but cannot provide any warranty nor accept any liability for this information.

The 9am and 3pm wind speed and direction observation for each month were summed and averaged. This data was then used to produce wind frequency tables C.3 and C.4, which were subsequently used for post-processing of simulation outputs.

Table C.3: Moree average annual (9am and 3pm) wind frequency table used in modelling (Part 1).

Wind Speed (km/h):	Wind Direction (°):	Frequency:
0	0	0.008964542
5	0	0.02878476
15	0	0.085227702
25	0	0.067039136
30	0	0.009411368
5	45	0.02406671
15	45	0.090121845
25	45	0.077734636
30	45	0.009009207
5	90	0.034268549
15	90	0.0974513
25	90	0.033993521
30	90	0.000877193
5	135	0.016749031
15	135	0.034925757
25	135	0.007349735
30	135	0.0
Continued on Table C.4		

Table C.4: Moree average annual (9am and 3pm) wind frequency table used in modelling, continued (Part 2).

Wind Speed (km/h):	Wind Direction (°):	Frequency:
Continued from Table C.3		
5	180	0.025731731
15	180	0.040561015
25	180	0.012054291
30	180	0.002174896
5	225	0.020660161
15	225	0.06192619
25	225	0.060223327
30	225	0.009517397
5	270	0.018915812
15	270	0.034013696
25	270	0.029247436
30	270	0.007722002
5	315	0.01548631
15	315	0.024169421
25	315	0.011621323
30	315	0.0

Appendix D

Illustrative UDF Decision Tables

Due to the cumbersome size and repetitive nature of the data in decision Tables A and B, only the application strategies (i.e. the applicators used for dosing and the application rate for each) for the first 37, of the total 841, wind conditions are shown. To produce Tables A and B, an application duration of 1 hour was specified, which also represents the time-step to be implemented on-site (i.e. which applicators to dose with and the application rate for each according to on-site wind conditions, is re-determined every hour).

D.1 ‘Table A’

These tables detail the application strategies to be used after a high wind speed or rainfall event to re-establish steady-state conditions. To reduce the time taken to re-establish steady-state conditions, all applicators may be used for dosing (depending on the prevailing wind conditions on-site).

Table D.1: Decision table A (Part 1).

Wind Speed (km/h):	Wind Direction (°):	Applicator Coordinates		Application
		x:	y:	Rate ($\times 10^{-4}$ kg/s):
0	0	0	115	0.3112
		0	230	0.3112
		0	345	0.3112
		0	460	0.3112
		150	92	0.3112
		150	184	0.3112
		150	276	0.3112
		150	368	0.3112
		100	0	0.3112
		200	0	0.3112
		300	0	0.3112
		300	92	0.3112
		300	184	0.3112
		300	276	0.3112
		300	368	0.3112
		300	460	0.3112
4	0	150	460	0.3112
		0	115	0.0173
		0	230	0.0359
		0	345	0
		0	460	0
		150	92	0.0245
		150	184	0.0485
		150	276	0.0476
		150	368	0
		100	0	0
		200	0	0
		300	0	0
		300	92	0
		300	184	0
		300	276	0
		300	368	0
300	460	0		
150	460	0		

Continued on Table D.2

Table D.2: Decision table A (Part 2).

Wind Speed (km/h):	Wind Direction (°):	Applicator Coordinates		Application
		x:	y:	Rate ($\times 10^{-4}$ kg/s):
Continued from Table D.1				
4	10	0	115	0.0172
		0	230	0.0354
		0	345	0
		0	460	0
		150	92	0.0243
		150	184	0.0484
		150	276	0.0487
		150	368	0
		100	0	0
		200	0	0
		300	0	0
		300	92	0
		300	184	0
		300	276	0
		300	368	0
		300	460	0
150	460	0		
4	20	0	115	0
		0	230	0
		0	345	0
		0	460	0
		150	92	0.0247
		150	184	0.0515
		150	276	0.0528
		150	368	0
		100	0	0
		200	0	0
		300	0	0
		300	92	0.0132
		300	184	0.027
		300	276	0
		300	368	0
		300	460	0
150	460	0		
Continued on Table D.3				

Table D.3: Decision table A (Part 3).

Wind Speed (km/h):	Wind Direction (°):	Applicator Coordinates		Application
		x:	y:	Rate ($\times 10^{-4}$ kg/s):
Continued from Table D.2				
4	30	0	115	0
		0	230	0
		0	345	0
		0	460	0
		150	92	0.0249
		150	184	0.0513
		150	276	0.0511
		150	368	0
		100	0	0
		200	0	0
		300	0	0
		300	92	0.0133
		300	184	0.0276
		300	276	0
		300	368	0
300	460	0		
150	460	0		
4	40	0	115	0
		0	230	0
		0	345	0
		0	460	0
		150	92	0.0273
		150	184	0.0525
		150	276	0
		150	368	0
		100	0	0
		200	0	0
		300	0	0
		300	92	0.0149
		300	184	0.0299
		300	276	0
		300	368	0
300	460	0		
150	460	0		
Continued on Table D.4				

Table D.4: Decision table A (Part 4).

Wind Speed (km/h):	Wind Direction (°):	Applicator Coordinates		Application
		x:	y:	Rate ($\times 10^{-4}$ kg/s):
Continued from Table D.3				
4	50	0	115	0
		0	230	0
		0	345	0
		0	460	0
		150	92	0.0312
		150	184	0.0537
		150	276	0.0534
		150	368	0
		100	0	0
		200	0	0
		300	0	0
		300	92	0
		300	184	0
		300	276	0
		300	368	0
		300	460	0
150	460	0		
4	60	0	115	0
		0	230	0
		0	345	0
		0	460	0
		150	92	0.0373
		150	184	0.0556
		150	276	0.0572
		150	368	0.0455
		100	0	0
		200	0	0
		300	0	0
		300	92	0
		300	184	0
		300	276	0
		300	368	0
		300	460	0
150	460	0		
Continued on Table D.5				

Table D.5: Decision table A (Part 5).

Wind Speed (km/h):	Wind Direction (°):	Applicator Coordinates		Application
		x:	y:	Rate ($\times 10^{-4}$ kg/s):
Continued from Table D.4				
4	70	0	115	0
		0	230	0
		0	345	0
		0	460	0
		150	92	0.0452
		150	184	0.0545
		150	276	0.0557
		150	368	0.0474
		100	0	0
		200	0	0
		300	0	0
		300	92	0
		300	184	0
		300	276	0
		300	368	0
		300	460	0
150	460	0		
4	80	0	115	0
		0	230	0
		0	345	0
		0	460	0
		150	92	0.0474
		150	184	0.0529
		150	276	0.0538
		150	368	0.0494
		100	0	0
		200	0	0
		300	0	0
		300	92	0
		300	184	0
		300	276	0
		300	368	0
		300	460	0
150	460	0		
Continued on Table D.6				

Table D.6: Decision table A (Part 6).

Wind Speed (km/h):	Wind Direction (°):	Applicator Coordinates		Application
		x:	y:	Rate ($\times 10^{-4}$ kg/s):
Continued from Table D.5				
4	90	0	115	0
		0	230	0
		0	345	0
		0	460	0
		150	92	0.047
		150	184	0.0505
		150	276	0.0514
		150	368	0.0493
		100	0	0
		200	0	0
		300	0	0
		300	92	0
		300	184	0
		300	276	0
		300	368	0
		300	460	0
150	460	0.0313		
4	100	0	115	0
		0	230	0
		0	345	0
		0	460	0
		150	92	0.0472
		150	184	0.0502
		150	276	0.0511
		150	368	0.0498
		100	0	0
		200	0	0
		300	0	0
		300	92	0
		300	184	0
		300	276	0
		300	368	0
		300	460	0
150	460	0.0314		
Continued on Table D.7				

Table D.7: Decision table A (Part 7).

Wind Speed (km/h):	Wind Direction (°):	Applicator Coordinates		Application
		x:	y:	Rate ($\times 10^{-4}$ kg/s):
Continued from Table D.6				
4	110	0	115	0
		0	230	0
		0	345	0
		0	460	0
		150	92	0.0472
		150	184	0.0502
		150	276	0.0512
		150	368	0.0498
		100	0	0.0198
		200	0	0
		300	0	0
		300	92	0
		300	184	0
		300	276	0
		300	368	0
		300	460	0
150	460	0		
4	120	0	115	0
		0	230	0
		0	345	0
		0	460	0
		150	92	0.0464
		150	184	0.0504
		150	276	0.0515
		150	368	0.0493
		100	0	0.0198
		200	0	0
		300	0	0
		300	92	0
		300	184	0
		300	276	0
		300	368	0
		300	460	0
150	460	0		
Continued on Table D.8				

Table D.8: Decision table A (Part 8).

Wind Speed (km/h):	Wind Direction (°):	Applicator Coordinates		Application
		x:	y:	Rate ($\times 10^{-4}$ kg/s):
Continued from Table D.7				
4	130	0	115	0
		0	230	0
		0	345	0
		0	460	0
		150	92	0.0465
		150	184	0.0528
		150	276	0.0541
		150	368	0.0495
		100	0	0.0197
		200	0	0
		300	0	0
		300	92	0
		300	184	0
		300	276	0
		300	368	0
		300	460	0
150	460	0		
4	140	0	115	0
		0	230	0
		0	345	0
		0	460	0
		150	92	0.0446
		150	184	0.0547
		150	276	0.0555
		150	368	0.0464
		100	0	0
		200	0	0
		300	0	0
		300	92	0
		300	184	0
		300	276	0
		300	368	0
		300	460	0
150	460	0		
Continued on Table D.9				

Table D.9: Decision table A (Part 9).

Wind Speed (km/h):	Wind Direction (°):	Applicator Coordinates		Application
		x:	y:	Rate ($\times 10^{-4}$ kg/s):
Continued from Table D.8				
4	150	0	115	0
		0	230	0
		0	345	0
		0	460	0
		150	92	0.0426
		150	184	0.0549
		150	276	0.0554
		150	368	0.0375
		100	0	0
		200	0	0
		300	0	0
		300	92	0
		300	184	0
		300	276	0
		300	368	0
		300	460	0
150	460	0		
4	160	0	115	0
		0	230	0
		0	345	0
		0	460	0
		150	92	0
		150	184	0.0507
		150	276	0.0528
		150	368	0.0311
		100	0	0
		200	0	0
		300	0	0
		300	92	0
		300	184	0
		300	276	0
		300	368	0
		300	460	0
150	460	0		
Continued on Table D.10				

Table D.10: Decision table A (Part 10).

Wind Speed (km/h):	Wind Direction (°):	Applicator Coordinates		Application
		x:	y:	Rate ($\times 10^{-4}$ kg/s):
Continued from Table D.9				
4	170	0	115	0
		0	230	0
		0	345	0
		0	460	0
		150	92	0
		150	184	0
		150	276	0.0502
		150	368	0.0265
		100	0	0
		200	0	0
		300	0	0
		300	92	0
		300	184	0
		300	276	0.0283
		300	368	0.0142
		300	460	0
150	460	0		
4	180	0	115	0
		0	230	0
		0	345	0
		0	460	0
		150	92	0
		150	184	0.0481
		150	276	0.0487
		150	368	0.0247
		100	0	0
		200	0	0
		300	0	0
		300	92	0
		300	184	0
		300	276	0.0261
		300	368	0.0132
		300	460	0
150	460	0		
Continued on Table D.11				

Table D.11: Decision table A (Part 11).

Wind Speed (km/h):	Wind Direction (°):	Applicator Coordinates		Application
		x:	y:	Rate ($\times 10^{-4}$ kg/s):
Continued from Table D.10				
4	190	0	115	0
		0	230	0
		0	345	0
		0	460	0
		150	92	0
		150	184	0.0488
		150	276	0.0482
		150	368	0.024
		100	0	0
		200	0	0
		300	0	0
		300	92	0
		300	184	0
		300	276	0.0253
		300	368	0.0127
		300	460	0
150	460	0		
4	200	0	115	0
		0	230	0.0362
		0	345	0.018
		0	460	0
		150	92	0
		150	184	0.0491
		150	276	0.0492
		150	368	0.0251
		100	0	0
		200	0	0
		300	0	0
		300	92	0
		300	184	0
		300	276	0
		300	368	0
		300	460	0
150	460	0		
Continued on Table D.12				

Table D.12: Decision table A (Part 12).

Wind Speed (km/h):	Wind Direction (°):	Applicator Coordinates		Application
		x:	y:	Rate ($\times 10^{-4}$ kg/s):
Continued from Table D.11				
4	210	0	115	0
		0	230	0.0373
		0	345	0.019
		0	460	0
		150	92	0
		150	184	0.0487
		150	276	0.0507
		150	368	0.027
		100	0	0
		200	0	0
		300	0	0
		300	92	0
		300	184	0
		300	276	0
		300	368	0
		300	460	0
150	460	0		
4	220	0	115	0
		0	230	0
		0	345	0.0207
		0	460	0
		150	92	0
		150	184	0
		150	276	0.0529
		150	368	0.0292
		100	0	0
		200	0	0
		300	0	0
		300	92	0
		300	184	0
		300	276	0
		300	368	0
		300	460	0
150	460	0		
Continued on Table D.13				

Table D.13: Decision table A (Part 13).

Wind Speed (km/h):	Wind Direction (°):	Applicator Coordinates		Application
		x:	y:	Rate ($\times 10^{-4}$ kg/s):
Continued from Table D.12				
4	230	0	115	0
		0	230	0
		0	345	0
		0	460	0
		150	92	0
		150	184	0.0532
		150	276	0.0558
		150	368	0.0349
		100	0	0
		200	0	0
		300	0	0
		300	92	0
		300	184	0
		300	276	0
		300	368	0
		300	460	0
150	460	0		
4	240	0	115	0
		0	230	0
		0	345	0
		0	460	0
		150	92	0.0434
		150	184	0.0565
		150	276	0.0575
		150	368	0.0405
		100	0	0
		200	0	0
		300	0	0
		300	92	0
		300	184	0
		300	276	0
		300	368	0
		300	460	0
150	460	0		
Continued on Table D.14				

Table D.14: Decision table A (Part 14).

Wind Speed (km/h):	Wind Direction (°):	Applicator Coordinates		Application
		x:	y:	Rate ($\times 10^{-4}$ kg/s):
Continued from Table D.13				
4	250	0	115	0
		0	230	0
		0	345	0
		0	460	0
		150	92	0.0458
		150	184	0.0555
		150	276	0.0563
		150	368	0.048
		100	0	0
		200	0	0
		300	0	0
		300	92	0
		300	184	0
		300	276	0
		300	368	0
		300	460	0
150	460	0		
4	260	0	115	0
		0	230	0
		0	345	0
		0	460	0
		150	92	0.0468
		150	184	0.0524
		150	276	0.0534
		150	368	0.0493
		100	0	0
		200	0	0.0198
		300	0	0
		300	92	0
		300	184	0
		300	276	0
		300	368	0
		300	460	0
150	460	0		
Continued on Table D.15				

Table D.15: Decision table A (Part 15).

Wind Speed (km/h):	Wind Direction (°):	Applicator Coordinates		Application
		x:	y:	Rate ($\times 10^{-4}$ kg/s):
Continued from Table D.14				
4	270	0	115	0
		0	230	0
		0	345	0
		0	460	0
		150	92	0.0469
		150	184	0.0507
		150	276	0.0519
		150	368	0.0499
		100	0	0
		200	0	0.0195
		300	0	0
		300	92	0
		300	184	0
		300	276	0
		300	368	0
		300	460	0
150	460	0		
4	280	0	115	0
		0	230	0
		0	345	0
		0	460	0
		150	92	0.0472
		150	184	0.0502
		150	276	0.0511
		150	368	0.0498
		100	0	0
		200	0	0
		300	0	0
		300	92	0
		300	184	0
		300	276	0
		300	368	0
		300	460	0
150	460	0.0314		
Continued on Table D.16				

Table D.16: Decision table A (Part 16).

Wind Speed (km/h):	Wind Direction (°):	Applicator Coordinates		Application
		x:	y:	Rate ($\times 10^{-4}$ kg/s):
Continued from Table D.15				
4	290	0	115	0
		0	230	0
		0	345	0
		0	460	0
		150	92	0.0468
		150	184	0.0484
		150	276	0.0476
		150	368	0.045
		100	0	0
		200	0	0
		300	0	0
		300	92	0
		300	184	0
		300	276	0
		300	368	0
		300	460	0
150	460	0.0279		
4	300	0	115	0
		0	230	0
		0	345	0
		0	460	0
		150	92	0.0466
		150	184	0.0491
		150	276	0.0483
		150	368	0.0446
		100	0	0
		200	0	0
		300	0	0
		300	92	0
		300	184	0
		300	276	0
		300	368	0
		300	460	0
150	460	0.0279		
Continued on Table D.17				

Table D.17: Decision table A (Part 17).

Wind Speed (km/h):	Wind Direction (°):	Applicator Coordinates		Application
		x:	y:	Rate ($\times 10^{-4}$ kg/s):
Continued from Table D.16				
4	310	0	115	0
		0	230	0
		0	345	0
		0	460	0
		150	92	0.0459
		150	184	0.0507
		150	276	0.0503
		150	368	0.0446
		100	0	0
		200	0	0
		300	0	0
		300	92	0
		300	184	0
		300	276	0
		300	368	0
		300	460	0
150	460	0		
4	320	0	115	0
		0	230	0
		0	345	0
		0	460	0
		150	92	0.0437
		150	184	0.053
		150	276	0.0529
		150	368	0.0432
		100	0	0
		200	0	0
		300	0	0
		300	92	0
		300	184	0
		300	276	0
		300	368	0
		300	460	0
150	460	0		
Continued on Table D.18				

Table D.18: Decision table A (Part 18).

Wind Speed (km/h):	Wind Direction (°):	Applicator Coordinates		Application
		x:	y:	Rate ($\times 10^{-4}$ kg/s):
Continued from Table D.17				
4	330	0	115	0
		0	230	0
		0	345	0
		0	460	0
		150	92	0.0356
		150	184	0.0529
		150	276	0.0526
		150	368	0.0408
		100	0	0
		200	0	0
		300	0	0
		300	92	0
		300	184	0
		300	276	0
		300	368	0
		300	460	0
150	460	0		
4	340	0	115	0
		0	230	0
		0	345	0
		0	460	0
		150	92	0.0302
		150	184	0.051
		150	276	0.049
		150	368	0
		100	0	0
		200	0	0
		300	0	0
		300	92	0
		300	184	0
		300	276	0
		300	368	0
		300	460	0
150	460	0		
Continued on Table D.19				

Table D.19: Decision table A (Part 19).

Wind Speed (km/h):	Wind Direction (°):	Applicator Coordinates		Application
		x:	y:	Rate ($\times 10^{-4}$ kg/s):
Continued from Table D.18				
4	350	0	115	0.0186
		0	230	0
		0	345	0
		0	460	0
		150	92	0.0263
		150	184	0.0493
		150	276	0
		150	368	0
		100	0	0
		200	0	0
		300	0	0
		300	92	0
		300	184	0
		300	276	0
		300	368	0
		300	460	0
150	460	0		

D.2 'Table B'

These tables detail the application strategies to be used once steady-state conditions have been achieved. During steady-state conditions only shore-based applicators are used for dosing as applicators floating within the storage provide no additional benefit.

Table D.20: Decision table B (Part 1).

Wind Speed (km/h):	Wind Direction (°):	Applicator Coordinates		Application
		x:	y:	Rate ($\times 10^{-4}$ kg/s):
0	0	0	115	0.4069
		0	230	0.4069
		0	345	0.4069
		0	460	0.4069
		100	0	0.4069
		200	0	0.4069
		300	0	0.4069
		300	92	0.4069
		300	184	0.4069
		300	276	0.4069
		300	368	0.4069
		300	460	0.4069
		150	460	0.4069
4	0	0	115	0.0234
		0	230	0.0484
		0	345	0
		0	460	0
		100	0	0
		200	0	0
		300	0	0
		300	92	0
		300	184	0
		300	276	0
		300	368	0
		300	460	0
		150	460	0

Continued on Table D.21

Table D.21: Decision table B (Part 2).

Wind Speed (km/h):	Wind Direction (°):	Applicator Coordinates		Application
		x:	y:	Rate ($\times 10^{-4}$ kg/s):
Continued from Table D.20				
4	10	0	115	0.0231
		0	230	0.0476
		0	345	0
		0	460	0
		100	0	0
		200	0	0
		300	0	0
		300	92	0
		300	184	0
		300	276	0
		300	368	0
		300	460	0
		150	460	0
4	20	0	115	0
		0	230	0
		0	345	0
		0	460	0
		100	0	0
		200	0	0
		300	0	0
		300	92	0.017
		300	184	0.0364
		300	276	0
		300	368	0
		300	460	0
		150	460	0
Continued on Table D.22				

Table D.22: Decision table B (Part 3).

Wind Speed (km/h):	Wind Direction (°):	Applicator Coordinates		Application
		x:	y:	Rate ($\times 10^{-4}$ kg/s):
Continued from Table D.21				
4	30	0	115	0
		0	230	0
		0	345	0
		0	460	0
		100	0	0
		200	0	0
		300	0	0
		300	92	0.0174
		300	184	0.0375
		300	276	0
		300	368	0
300	460	0		
150	460	0		
4	40	0	115	0
		0	230	0
		0	345	0
		0	460	0
		100	0	0
		200	0	0
		300	0	0
		300	92	0.0199
		300	184	0.0409
		300	276	0
		300	368	0
300	460	0		
150	460	0		
Continued on Table D.23				

Table D.23: Decision table B (Part 4).

Wind Speed (km/h):	Wind Direction (°):	Applicator Coordinates		Application
		x:	y:	Rate ($\times 10^{-4}$ kg/s):
Continued from Table D.22				
4	50	0	115	0
		0	230	0
		0	345	0
		0	460	0
		100	0	0
		200	0	0
		300	0	0
		300	92	0.0199
		300	184	0.0409
		300	276	0
		300	368	0
300	460	0		
150	460	0		
4	60	0	115	0
		0	230	0
		0	345	0
		0	460	0
		100	0	0
		200	0	0
		300	0	0
		300	92	0.0199
		300	184	0.0409
		300	276	0
		300	368	0
300	460	0		
150	460	0		
Continued on Table D.24				

Table D.24: Decision table B (Part 5).

Wind Speed (km/h):	Wind Direction (°):	Applicator Coordinates		Application
		x:	y:	Rate ($\times 10^{-4}$ kg/s):
Continued from Table D.23				
4	70	0	115	0
		0	230	0
		0	345	0
		0	460	0
		100	0	0
		200	0	0
		300	0	0
		300	92	0.0199
		300	184	0.0409
		300	276	0
		300	368	0
		300	460	0
		150	460	0
4	80	0	115	0
		0	230	0
		0	345	0
		0	460	0
		100	0	0
		200	0	0
		300	0	0
		300	92	0.0199
		300	184	0.0409
		300	276	0
		300	368	0
		300	460	0
		150	460	0
Continued on Table D.25				

Table D.25: Decision table B (Part 6).

Wind Speed (km/h):	Wind Direction (°):	Applicator Coordinates		Application
		x:	y:	Rate ($\times 10^{-4}$ kg/s):
Continued from Table D.24				
4	90	0	115	0
		0	230	0
		0	345	0
		0	460	0
		100	0	0
		200	0	0
		300	0	0
		300	92	0
		300	184	0.0099
		300	276	0
		300	368	0
		300	460	0
		150	460	0.0378
4	100	0	115	0
		0	230	0
		0	345	0
		0	460	0
		100	0	0
		200	0	0
		300	0	0
		300	92	0
		300	184	0
		300	276	0
		300	368	0
		300	460	0
		150	460	0.0378
Continued on Table D.26				

Table D.26: Decision table B (Part 7).

Wind Speed (km/h):	Wind Direction (°):	Applicator Coordinates		Application
		x:	y:	Rate ($\times 10^{-4}$ kg/s):
Continued from Table D.25				
4	110	0	115	0
		0	230	0
		0	345	0
		0	460	0
		100	0	0.0232
		200	0	0
		300	0	0
		300	92	0
		300	184	0
		300	276	0
		300	368	0
		300	460	0
		150	460	0
4	120	0	115	0
		0	230	0
		0	345	0
		0	460	0
		100	0	0.0233
		200	0	0
		300	0	0
		300	92	0
		300	184	0
		300	276	0
		300	368	0
		300	460	0
		150	460	0
Continued on Table D.27				

Table D.27: Decision table B (Part 8).

Wind Speed (km/h):	Wind Direction (°):	Applicator Coordinates		Application
		x:	y:	Rate ($\times 10^{-4}$ kg/s):
Continued from Table D.26				
4	130	0	115	0
		0	230	0
		0	345	0
		0	460	0
		100	0	0.0236
		200	0	0
		300	0	0
		300	92	0
		300	184	0
		300	276	0
		300	368	0
		300	460	0
		150	460	0
4	140	0	115	0
		0	230	0
		0	345	0
		0	460	0
		100	0	0.0236
		200	0	0
		300	0	0
		300	92	0
		300	184	0
		300	276	0
		300	368	0
		300	460	0
		150	460	0
Continued on Table D.28				

Table D.28: Decision table B (Part 9).

Wind Speed (km/h):	Wind Direction (°):	Applicator Coordinates		Application
		x:	y:	Rate ($\times 10^{-4}$ kg/s):
Continued from Table D.27				
4	150	0	115	0
		0	230	0
		0	345	0
		0	460	0
		100	0	0.0236
		200	0	0
		300	0	0
		300	92	0
		300	184	0
		300	276	0
		300	368	0
		300	460	0
		150	460	0
4	160	0	115	0
		0	230	0
		0	345	0
		0	460	0
		100	0	0.0236
		200	0	0
		300	0	0
		300	92	0
		300	184	0
		300	276	0
		300	368	0
		300	460	0
		150	460	0
Continued on Table D.29				

Table D.29: Decision table B (Part 10).

Wind Speed (km/h):	Wind Direction (°):	Applicator Coordinates		Application
		x:	y:	Rate ($\times 10^{-4}$ kg/s):
Continued from Table D.28				
4	170	0	115	0
		0	230	0
		0	345	0
		0	460	0
		100	0	0
		200	0	0
		300	0	0
		300	92	0
		300	184	0
		300	276	0.0384
		300	368	0.0189
300	460	0		
150	460	0		
4	180	0	115	0
		0	230	0
		0	345	0
		0	460	0
		100	0	0
		200	0	0
		300	0	0
		300	92	0
		300	184	0
		300	276	0.0346
		300	368	0.0171
300	460	0		
150	460	0		
Continued on Table D.30				

Table D.30: Decision table B (Part 11).

Wind Speed (km/h):	Wind Direction (°):	Applicator Coordinates		Application
		x:	y:	Rate ($\times 10^{-4}$ kg/s):
Continued from Table D.29				
4	190	0	115	0
		0	230	0
		0	345	0
		0	460	0
		100	0	0
		200	0	0
		300	0	0
		300	92	0
		300	184	0
		300	276	0.0333
		300	368	0.0162
		300	460	0
		150	460	0
4	200	0	115	0
		0	230	0.0488
		0	345	0.0243
		0	460	0
		100	0	0
		200	0	0
		300	0	0
		300	92	0
		300	184	0
		300	276	0
		300	368	0
		300	460	0
		150	460	0
Continued on Table D.31				

Table D.31: Decision table B (Part 12).

Wind Speed (km/h):	Wind Direction (°):	Applicator Coordinates		Application
		x:	y:	Rate ($\times 10^{-4}$ kg/s):
Continued from Table D.30				
4	210	0	115	0
		0	230	0.051
		0	345	0.0266
		0	460	0
		100	0	0
		200	0	0
		300	0	0
		300	92	0
		300	184	0
		300	276	0
		300	368	0
		300	460	0
		150	460	0
4	220	0	115	0
		0	230	0
		0	345	0.0294
		0	460	0
		100	0	0
		200	0	0
		300	0	0
		300	92	0
		300	184	0
		300	276	0
		300	368	0
		300	460	0
		150	460	0
Continued on Table D.32				

Table D.32: Decision table B (Part 13).

Wind Speed (km/h):	Wind Direction (°):	Applicator Coordinates		Application
		x:	y:	Rate ($\times 10^{-4}$ kg/s):
Continued from Table D.31				
4	230	0	115	0
		0	230	0
		0	345	0.0294
		0	460	0
		100	0	0
		200	0	0
		300	0	0
		300	92	0
		300	184	0
		300	276	0
		300	368	0
		300	460	0
		150	460	0
4	240	0	115	0
		0	230	0
		0	345	0.0294
		0	460	0
		100	0	0
		200	0	0
		300	0	0
		300	92	0
		300	184	0
		300	276	0
		300	368	0
		300	460	0
		150	460	0
Continued on Table D.33				

Table D.33: Decision table B (Part 14).

Wind Speed (km/h):	Wind Direction (°):	Applicator Coordinates		Application
		x:	y:	Rate ($\times 10^{-4}$ kg/s):
Continued from Table D.32				
4	250	0	115	0
		0	230	0
		0	345	0.0294
		0	460	0
		100	0	0
		200	0	0
		300	0	0
		300	92	0
		300	184	0
		300	276	0
		300	368	0
		300	460	0
		150	460	0
4	260	0	115	0
		0	230	0
		0	345	0
		0	460	0
		100	0	0
		200	0	0.0236
		300	0	0
		300	92	0
		300	184	0
		300	276	0
		300	368	0
		300	460	0
		150	460	0
Continued on Table D.34				

Table D.34: Decision table B (Part 15).

Wind Speed (km/h):	Wind Direction (°):	Applicator Coordinates		Application
		x:	y:	Rate ($\times 10^{-4}$ kg/s):
Continued from Table D.33				
4	270	0	115	0
		0	230	0
		0	345	0
		0	460	0
		100	0	0
		200	0	0.0229
		300	0	0
		300	92	0
		300	184	0
		300	276	0
		300	368	0
		300	460	0
		150	460	0
4	280	0	115	0
		0	230	0
		0	345	0
		0	460	0
		100	0	0
		200	0	0
		300	0	0
		300	92	0
		300	184	0
		300	276	0
		300	368	0
		300	460	0
		150	460	0.0378
Continued on Table D.35				

Table D.35: Decision table B (Part 16).

Wind Speed (km/h):	Wind Direction (°):	Applicator Coordinates		Application
		x:	y:	Rate ($\times 10^{-4}$ kg/s):
Continued from Table D.34				
4	290	0	115	0
		0	230	0
		0	345	0
		0	460	0
		100	0	0
		200	0	0
		300	0	0
		300	92	0
		300	184	0
		300	276	0
		300	368	0
		300	460	0
		150	460	0.0329
4	300	0	115	0
		0	230	0
		0	345	0
		0	460	0
		100	0	0
		200	0	0
		300	0	0
		300	92	0
		300	184	0
		300	276	0
		300	368	0
		300	460	0
		150	460	0.0331
Continued on Table D.36				

Table D.36: Decision table B (Part 17).

Wind Speed (km/h):	Wind Direction (°):	Applicator Coordinates		Application
		x:	y:	Rate ($\times 10^{-4}$ kg/s):
Continued from Table D.35				
4	310	0	115	0
		0	230	0
		0	345	0
		0	460	0
		100	0	0
		200	0	0
		300	0	0
		300	92	0
		300	184	0
		300	276	0
		300	368	0
		300	460	0
		150	460	0.0331
4	320	0	115	0
		0	230	0
		0	345	0
		0	460	0
		100	0	0
		200	0	0
		300	0	0
		300	92	0
		300	184	0
		300	276	0
		300	368	0
		300	460	0
		150	460	0.0331
Continued on Table D.37				

Table D.37: Decision table B (Part 18).

Wind Speed (km/h):	Wind Direction (°):	Applicator Coordinates		Application
		x:	y:	Rate ($\times 10^{-4}$ kg/s):
Continued from Table D.36				
4	330	0	115	0
		0	230	0
		0	345	0
		0	460	0
		100	0	0
		200	0	0
		300	0	0
		300	92	0
		300	184	0
		300	276	0
		300	368	0
		300	460	0
		150	460	0.0331
4	340	0	115	0
		0	230	0
		0	345	0
		0	460	0
		100	0	0
		200	0	0
		300	0	0
		300	92	0
		300	184	0
		300	276	0
		300	368	0
		300	460	0
		150	460	0.0331
Continued on Table D.38				

Table D.38: Decision table B (Part 19).

Wind Speed (km/h):	Wind Direction (°):	Applicator Coordinates		Application
		x:	y:	Rate ($\times 10^{-4}$ kg/s):
Continued from Table D.37				
4	350	0	115	0.0257
		0	230	0
		0	345	0
		0	460	0
		100	0	0
		200	0	0
		300	0	0
		300	92	0
		300	184	0
		300	276	0
		300	368	0
		300	460	0
		150	460	0

Appendix E

Monolayer Application System Design

This appendix details some of the monolayer application system options, including some conceptual designs for different methods of monolayer application. Most of the concepts presented are purely conceptual and have not yet been prototyped or produced in any physical form, except for the prototype floating applicator detailed in Section E.3.3.

The conceptual designs herein serve as an example for the potential options available for the application of monolayer to a farm dam.

E.1 Application system options

Application systems for monolayer can typically be classed as either centralised, de-centralised or a hybrid of both systems. Centralised distribution systems may include a single reservoir of monolayer and distribution mechanism (i.e. pump) that would distributed monolayer to a series of application outlets via a network of pipes (Section E.1.1). In contrast, a de-centralised distribution system would require multiple self-contained applicator units, with their own reservoir and distribution mechanism, that are employed as the evaporation mitigation system as a whole (Section E.1.2). A

hybrid system combining both centralised and de-centralised methods of application could also be employed as another alternative (Section E.1.3).

Although monolayer in either a liquid or powder form could be applied by centralised, decentralised or hybrid systems, the mechanism/s used for distribution for each will most likely be completely different for each.

E.1.1 Centralised system

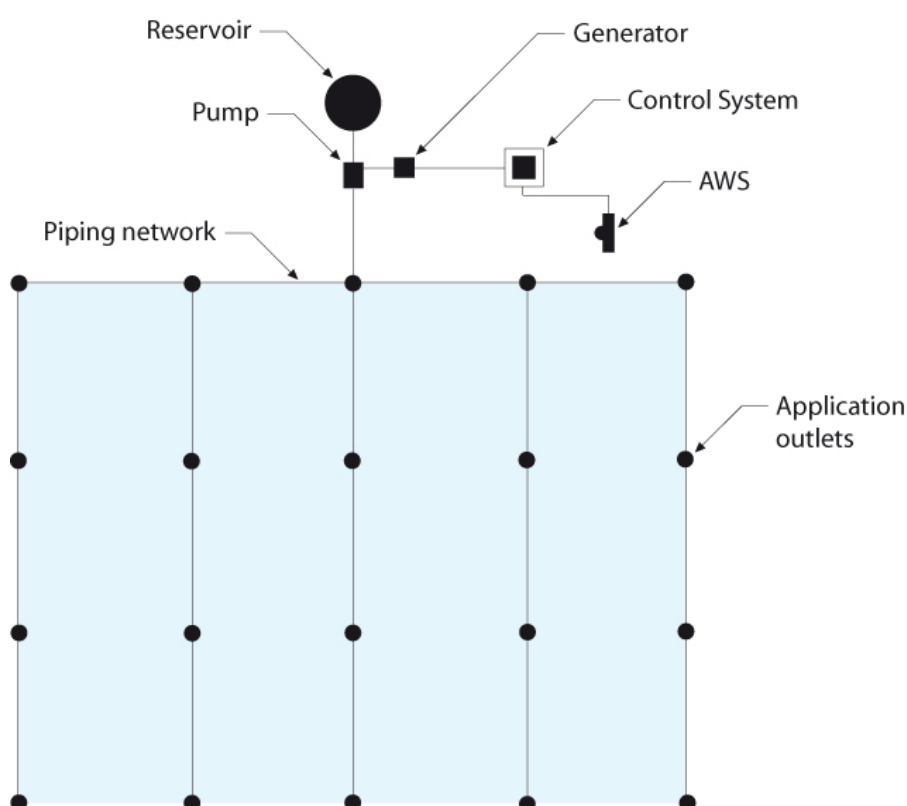


Figure E.1: The design for a centralised monolayer application system.

One of the most important considerations for a centralised application system (Figure E.1) would be the distribution mechanism, like a pump for example. The pump type and size would need to be carefully selected for each installation dependant on the size of the distribution network and requirements for flow rate and head pressure, product viscosity, and required mechanical efficiency. Note the selected power source will also impact on pump selection.

As only one distribution mechanism is used in centralised systems, the power requirements are usually quite high. Therefore, main power is required directly or via a generator, the latter option will also require diesel. With a single reservoir of product located by the side of the dam, the reservoir could be made quite large thereby reducing the filling demand. Refilling would also be relatively easy as it is on land compared to de-centralised applicators which may need to be filled from a boat.

A suitable cost-effective piping material would also need to be selected. The desired material would be durable, UV resistant, light weight and strong enough to be tethered to anchors. A form of communication would also be required between the control system and the latching solenoid valves, to control the release of monolayer at each application outlet.

E.1.2 De-centralised system

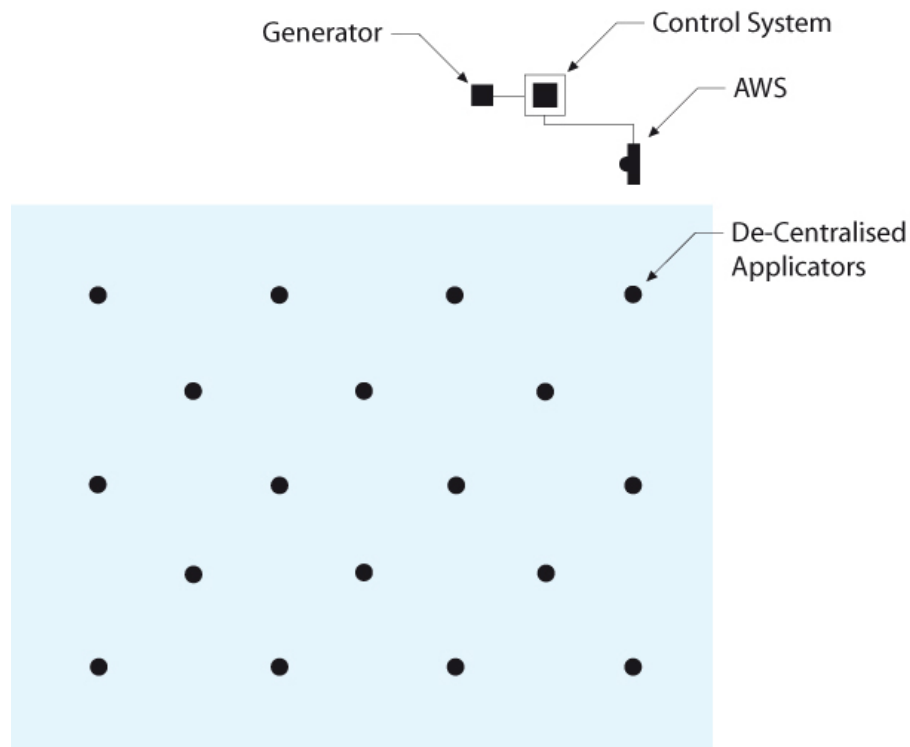


Figure E.2: The design for a de-centralised monolayer application system.

A de-centralised application system (Figure E.2) would need to incorporate a floating

support platform to mount necessary components to keep them out of the water and safe from moisture. A floating platform would also require a semi-permanent anchor/-mooring to maintain a prescribed position within a water body. Power would typically be supplied from a 12/24V DC battery, charged by a solar panel.

Savings would be gained by removing the requirement to distribute product through a large network of pipes, while eliminating any added maintenance issues. Although, added costs would be incurred from refilling the reservoirs of each applicator and the duplication of pumping equipment required. However, much smaller and potentially much cheaper pumps could be used in the de-centralised applicators.

E.1.3 Hybrid (centralised and de-centralised) system

Both of the centralised and de-centralised application systems could be combined to make a hybrid of the two (Figure E.3). With reference to Figure E.3, centralised style applicators could be installed around the edges of a storage while a number of de-centralised style applicators used to cover the bulk of the surface area in the middle. Another alternative may be to employ hybrid clusters of two or more floating applicators that are serviced by a single product reservoir. This reduces the number of refilling points.

E.2 Design of methods for monolayer application

The design of the method for monolayer application is primarily influenced by the form that the monolayer is in, be it solid, powder, liquid, molten, or other. The following concepts for methods of monolayer application are therefore based around a specific monolayer form. These include concepts for application of monolayer from a solid-cast, tape, molten and effervescent tablet.

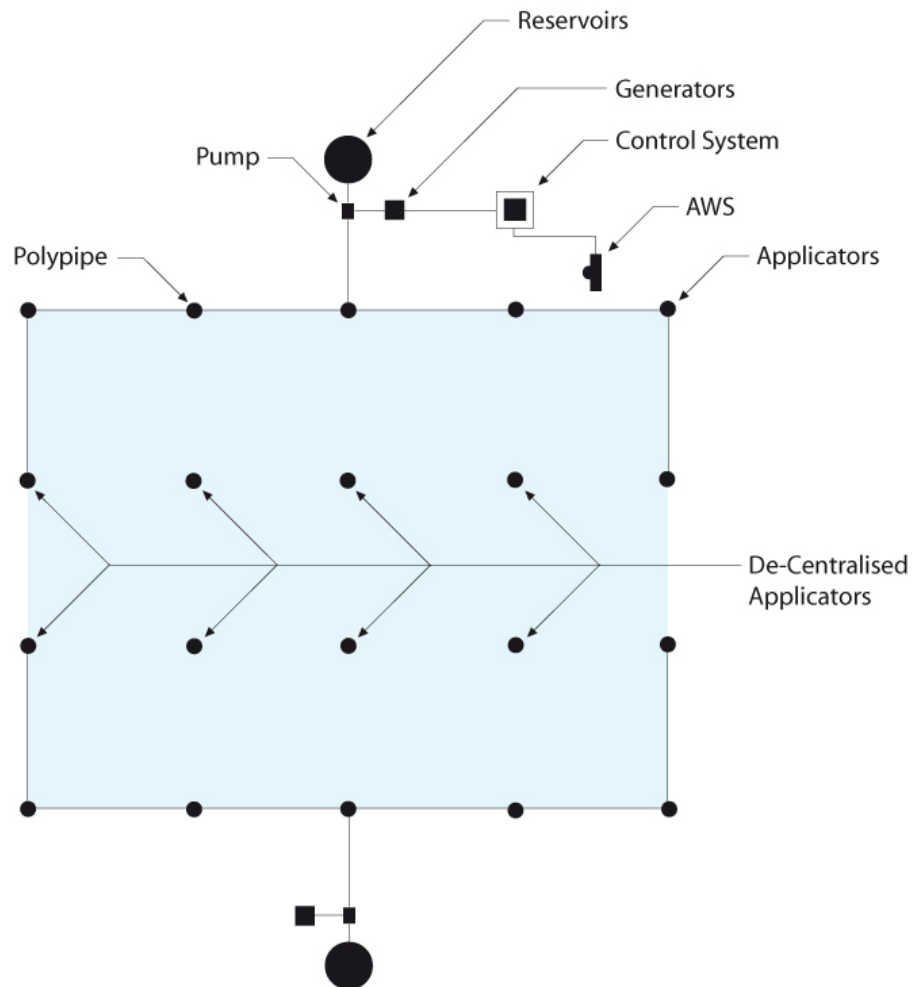


Figure E.3: The design for a hybrid application system, which is a combination of the centralised and de-centralised systems.

E.2.1 Solid-cast application

If monolayer was cast into a solid rod it could be packaged, transported and stored with relative ease. The solid-cast could then be applied by grinding it into a fine powder when required and applied to the water surface (Figures E.4 and E.5). This method of application would give very good control over the application of varying dosage quantities with wind speed. As can be seen in Figure E.4 this concept employs a wire-brush wheel driven by a motor to grind the solid-cast monolayer onto the water surface with. The motor could be driven at different speeds to achieve variable dosing and the coarseness of the wire-brush wheel could be altered to produce different powdered particle sizes.

Due to the lack of mains power at most farms dams, the motor driving the grinding wheel would need to be powered by a 12 or 24v battery. The battery could be replenished by a suitably sized solar panel fixed to the top of the electronics housing. This would make it completely power autonomous. Although this wire-brush grinding wheel style method of application was prototyped back in the 60s by Robertson (1966), his grinding apparatus was used in a boat. In this design, the grinding apparatus is adapted for use within an applicator with a fixed position.

Some other methods for grinding solid-cast monolayer onto the water surface are detailed in Figure E.5. These include, clockwise from the top right, a metal grinding wheel, rotating razor shearing plates, rotating metal grinding plates, a belt style sander and a mechanically driven cheese-grater style grinder. Probably the greatest drawback of these solid-cast monolayer grinding methods is that they will be rather inefficient and therefore may be quite power intensive. However, a working prototype of one of the most suitable grinding method presented herein would need to be bench tested to confirm this hypothesis.

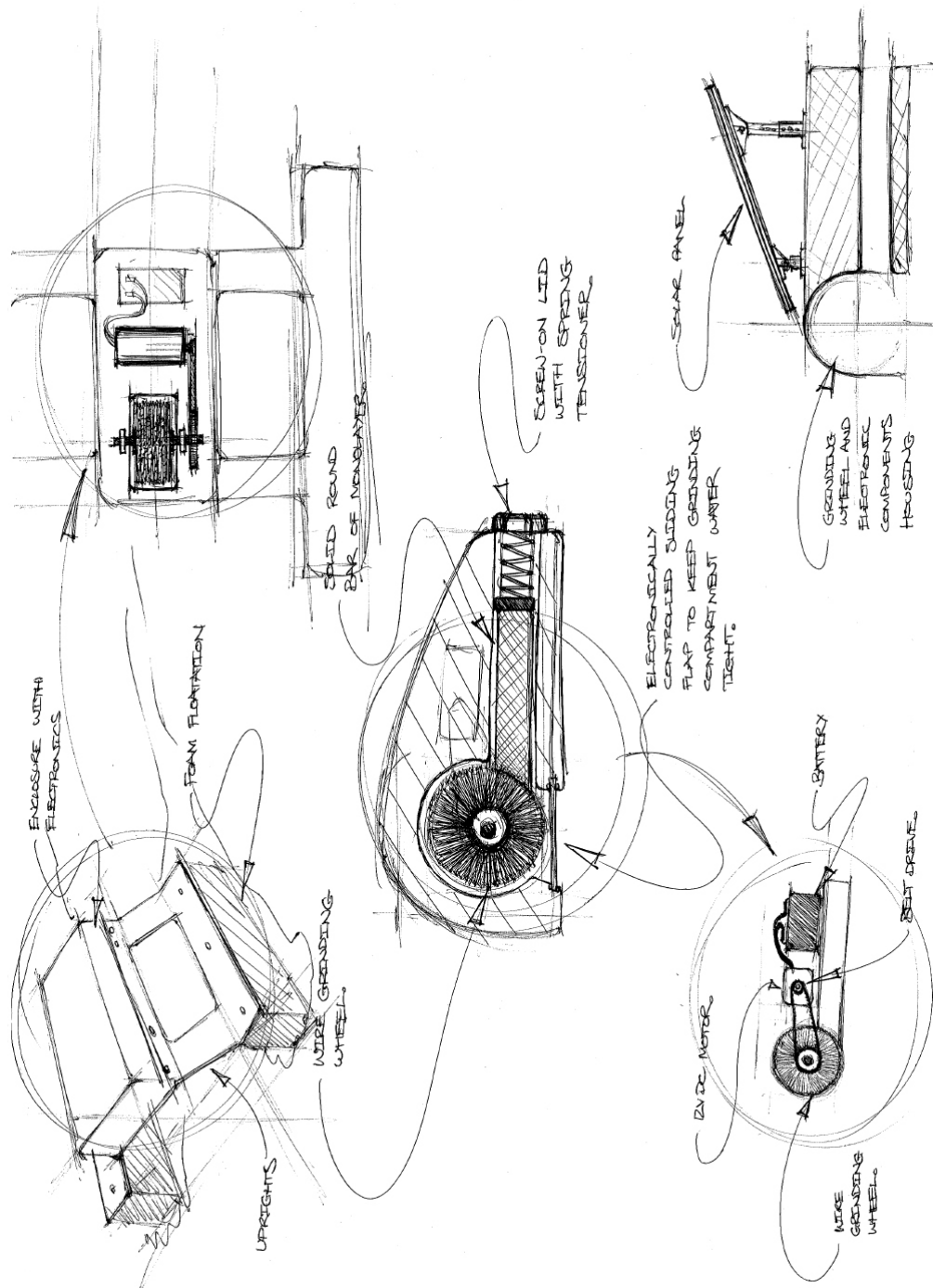


Figure E.4: A concept of a method for applying monolayer as a fine powder ground from a solid-rod using a wire-brush.

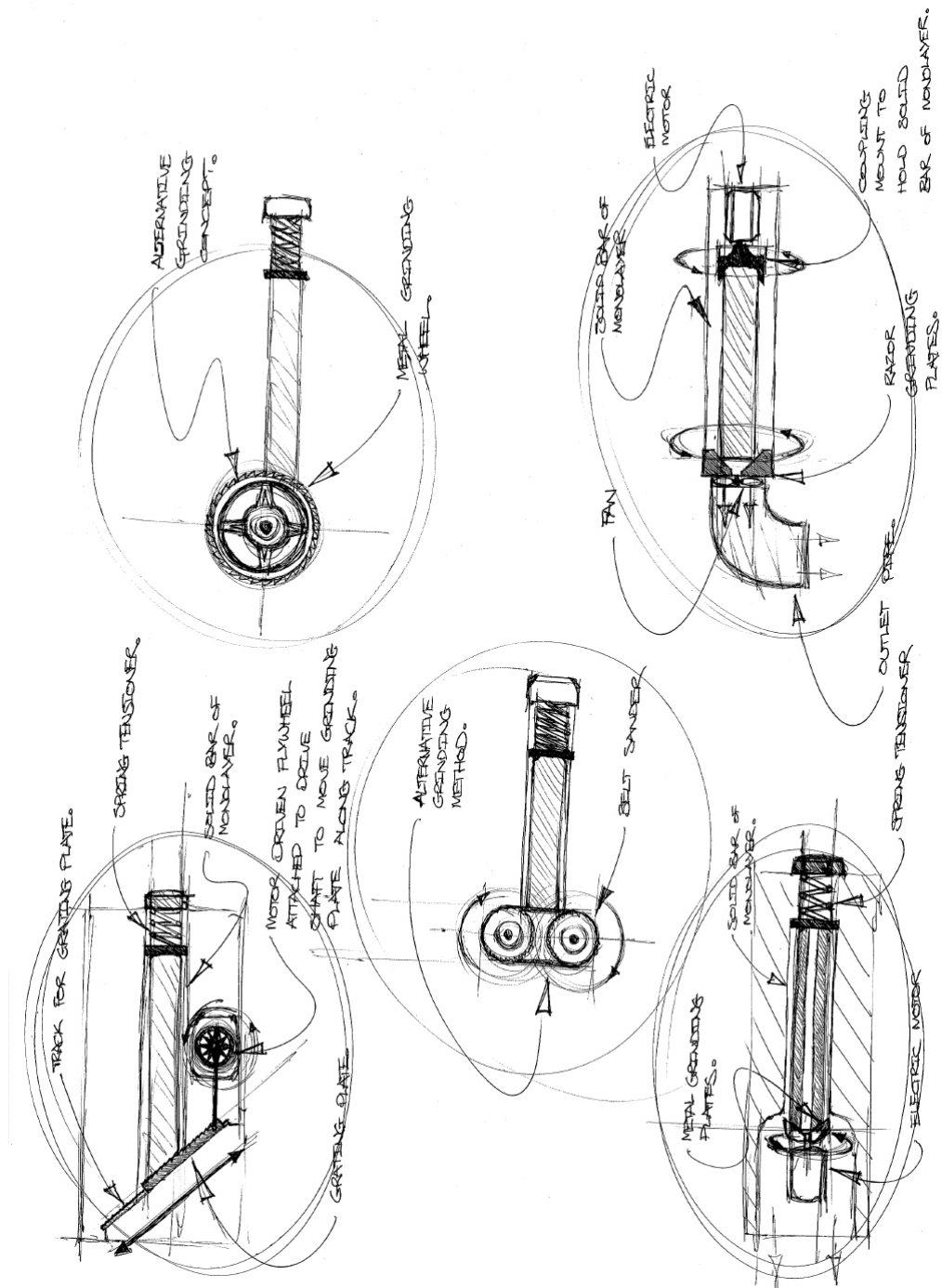


Figure E.5: A variety of other concepts for grinding solid-cast monolayer into a fine powder for application.

E.2.2 Tape application

This concept suggests that monolayer is sprayed onto or applied to one side of a very long length of wax paper, or other suitable water-proof non-stick material, then rolled onto a spool. This paper could then be fed through a series of guides where the monolayer side of the tape just contacts the water surface before being rolled onto a second spool (Figure E.6). The theory is that when the wax paper contacts the water surface the monolayer will attach to the water molecules leaving the wax paper behind. It is proposed that the spool that rolls up the used wax paper, with no monolayer on it, is driven by an electronic motor whose speed can be altered to achieve varying dosage rates. Also the width of the wax paper could be altered to achieve different dosage rates.

If monolayer could be spray-dried onto wax paper and rolled onto a spool, this would make packaging, transport and storage relatively easy. Also, the used wax paper could be reused to spray-dry monolayer onto again.

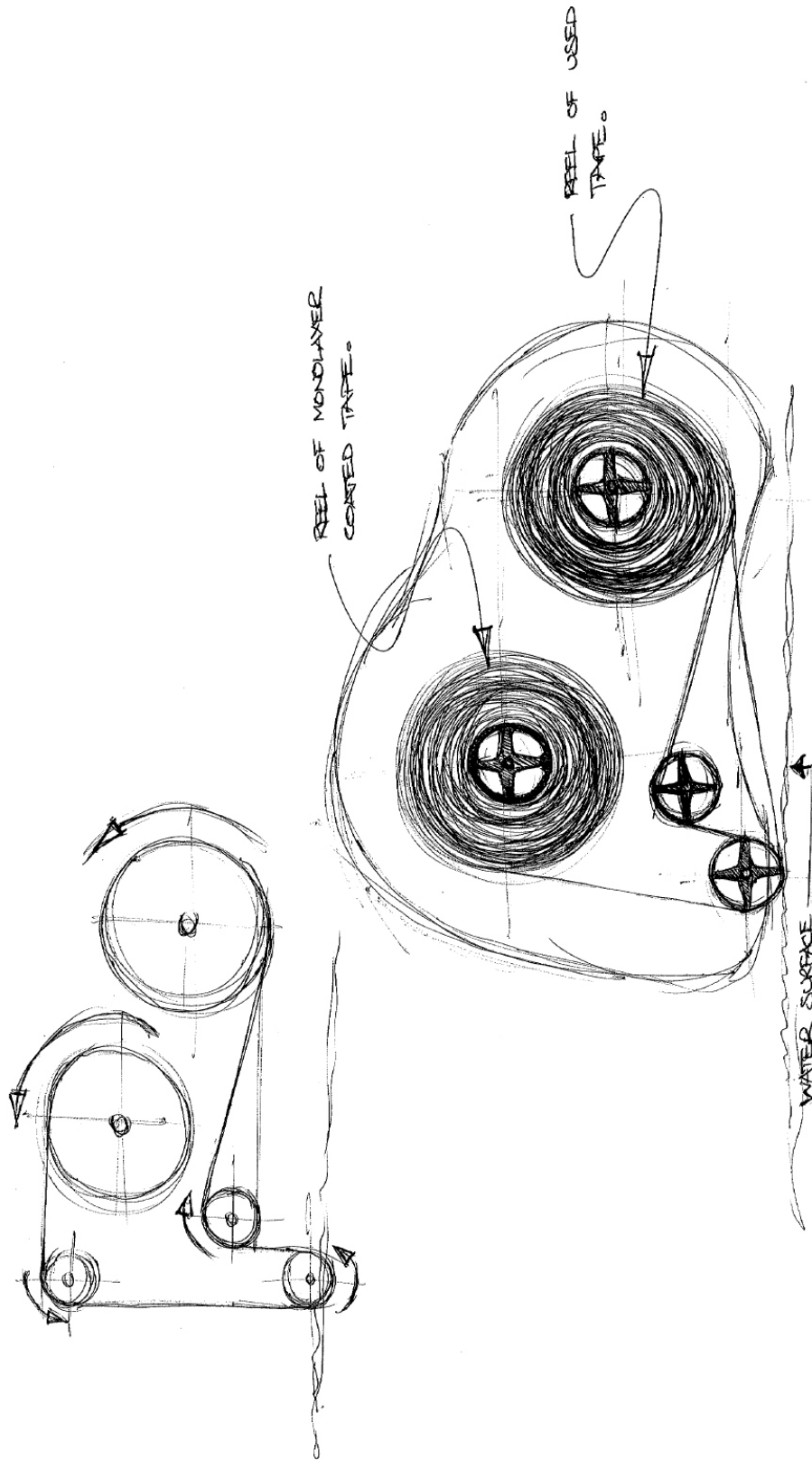


Figure E.6: This is a concept for the application of monolayer from a wax tape. The general idea is that monolayer would be applied to one side of a long length of wax tape and then the wax tape would be rolled onto a spool ready for application.

E.2.3 Molten application

As monolayer has a fairly low melting point (in the range of 60-70°C depending on the monolayer compound), therefore it could be kept at a temperature just greater than its melting temperature and applied in molten form (i.e. liquid). Figure E.7 details a design comprising a reservoir in which monolayer is kept in a molten state by a heated element. The molten monolayer is then pumped up from the reservoir into the outlet tube by venturi effect, using compressed air, and sprayed into the air just above the water surface. The molten particles of monolayer will then solidify in the air and fall onto the water surface, which would promote rapid spreading.

However, the power required for the heater element and the air compressor, for this method of application, may be far too power intensive as to be practical for use on farm dams. Although, this would need to be evaluated with a prototype bench-test unit. A similar style application system to apply molten monolayer was prototyped and tested by Florey (1965) with little success.

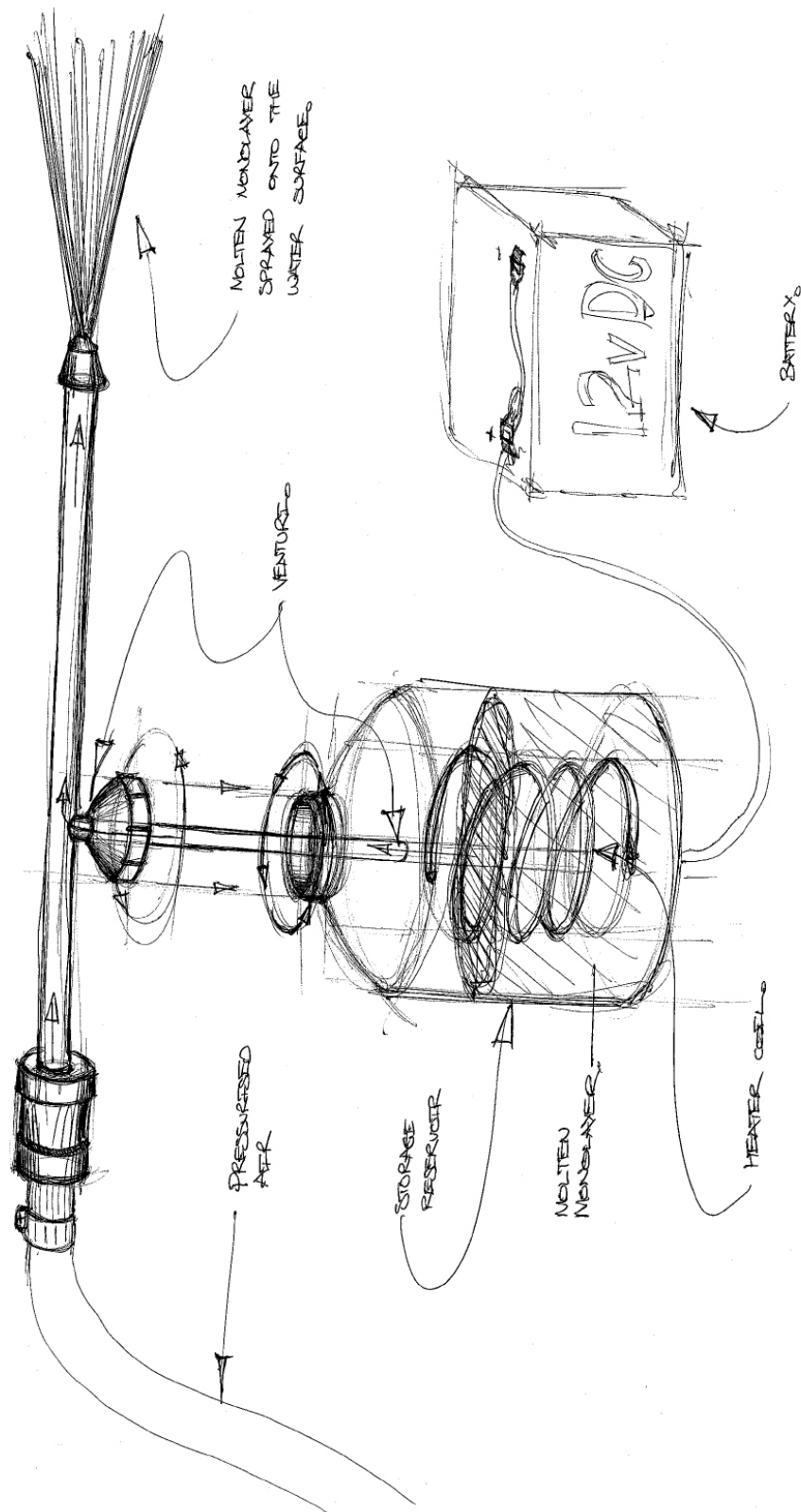


Figure E.7: Concept for the spray application of molten monolayer. When the molten monolayer is sprayed into the air just above the water surface it would solidify into fine particles, which would fall onto the water surface. It is believed that this form of application would improve the spreading properties of the monolayer.

E.2.4 Effervescent application

If the monolayer material was mixed with bicarbonate soda and citric acid, as a dry powder for example, this would create a powdered mixture that would effervesce when coming in to contact with water. The powder could then be produced in any desired form, i.e. a disk shaped tablet or a solid sphere, and when placed on the water surface the tablet or sphere would effervesce therefore promoting the spread and formation of a monolayer film to suppress evaporation. Having a monolayer material in an effervescent form such as this would also allow the development of a number of alternative methods of application (for example those shown in Figures E.8 and E.9).

An effervescent tablet or sphere could be packaged, transported and applied in a number of interesting ways, while also solving many of the handling and application issues associated with monolayer in a dry powder form (Frenkiel 1965).

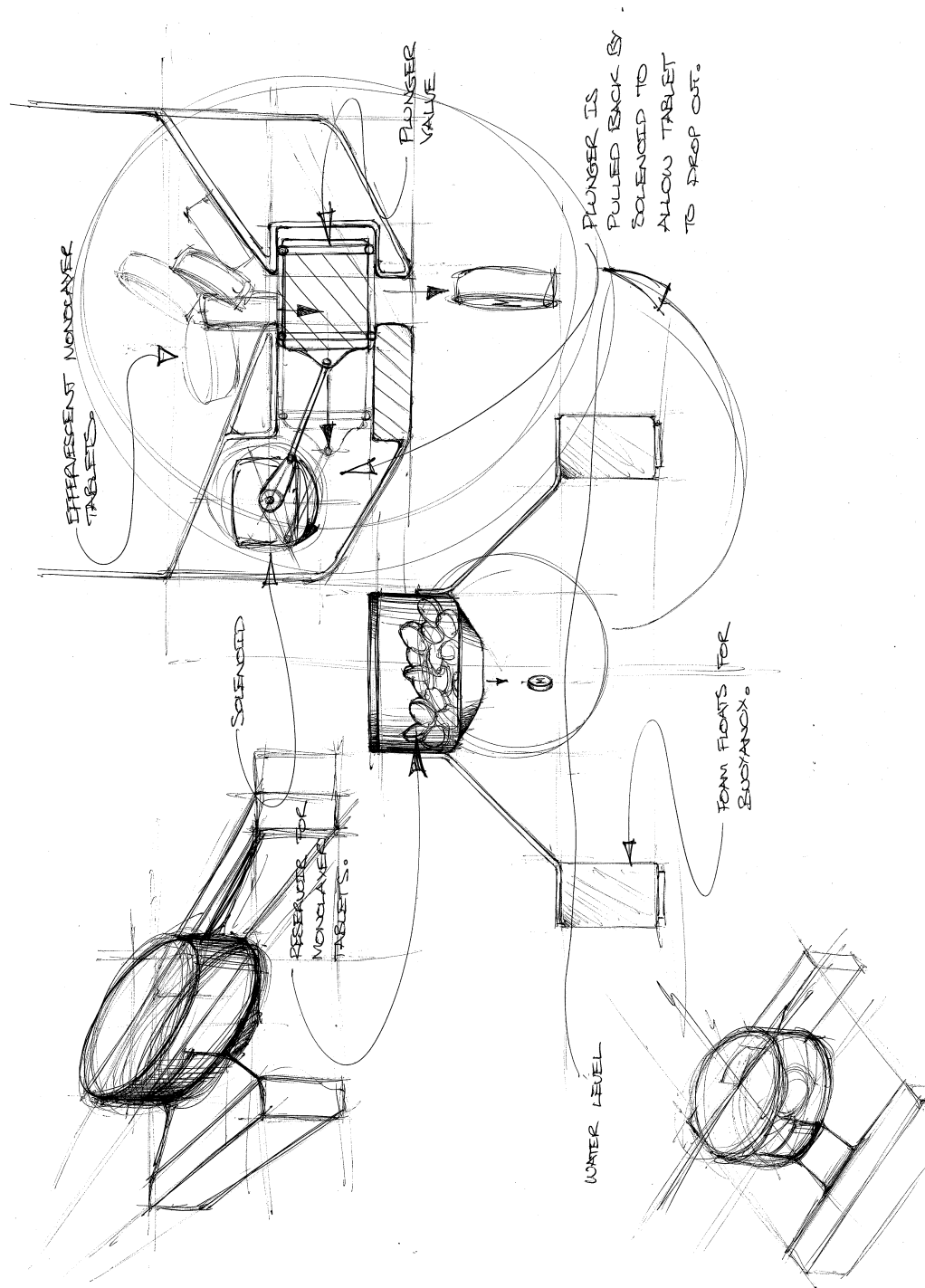


Figure E.8: Concept for the application of monolayer as an effervescent tablet.

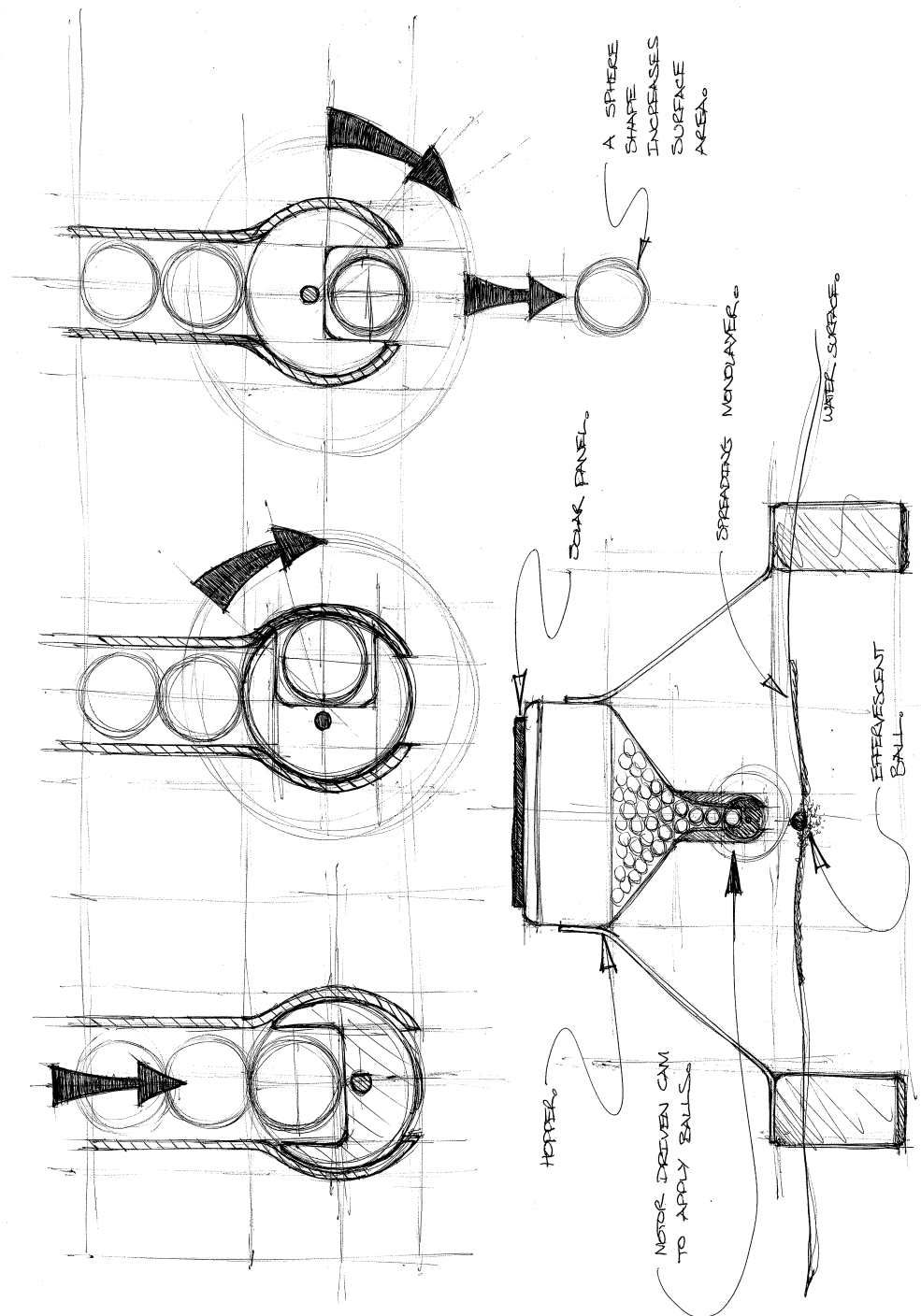


Figure E.9: Concept for the application of monolayer as an effervescent ball/sphere. A sphere shaped tablet would increase surface area over the traditional disk shaped tablet, thereby enhancing the effervescent reaction upon contact with water.

E.3 De-centralised applicator design

E.3.1 Floating applicator conceptual design

A concept for a floating monolayer applicator is presented in Figure E.10. This is a catamaran style design employing closed cell foam floatation and a two-tier reservoir and electronics support system connected at the floatation devices. The electronics components sit above the reservoir and contain the control and communications electronics including the batteries and pump. The solar panel would sit atop the electronics enclosure. This style of design would allow the storage of much larger volumes of product than the present Cooperative Research Centre for Irrigation Futures (CRC-IF) prototype floating applicator (Section E.3.3), which only provides a 20L reservoir.

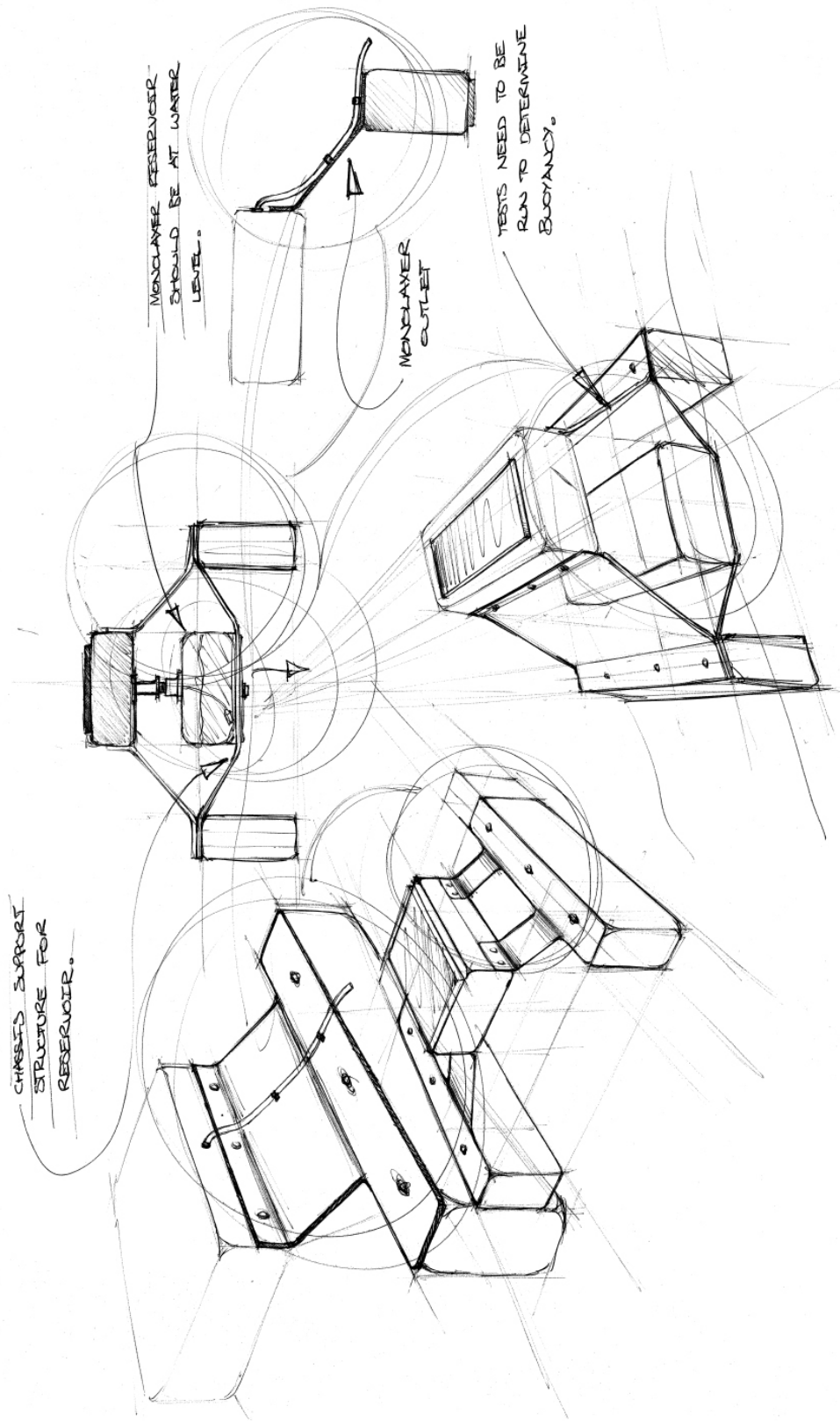


Figure E.10: Concept floating monolayer applicator design.

E.3.2 Shore-based applicator conceptual design

The following concept shown in Figure E.11 presents a design for a shore-based applicator, which would be anchored by a deadweight to the batter of the dam via a rotating cantilever arm. This design also utilises a shore based delivery system, which would allow for easy refilling and also provide capacity for a much greater volume of product to be stored; thus increasing the time between refills. The delivery of monolayer product from the shore reservoir would typically be by gravity feed. The applicator pump and small pressure from gravity should be enough to transfer low to mid viscosity product through the supply line and to the water surface.

Figure E.12 presents the cantilever anchoring system of the shore based application node in a pseudo-sectional view. The simple design of the hinged support system allows the applicator to rise and fall with the changes in dam water levels without the need for a complicated mooring line that automatically self-adjusts. This prototype design suggests a concrete cinder block as the fixed anchoring point. Modifications to this design may see a similar heavy weight or plate in place of the cinder block. Similarly, the PVC tethering arm may require strengthening, or even a different material all together, to support the floating applicator during high wind or wave events.

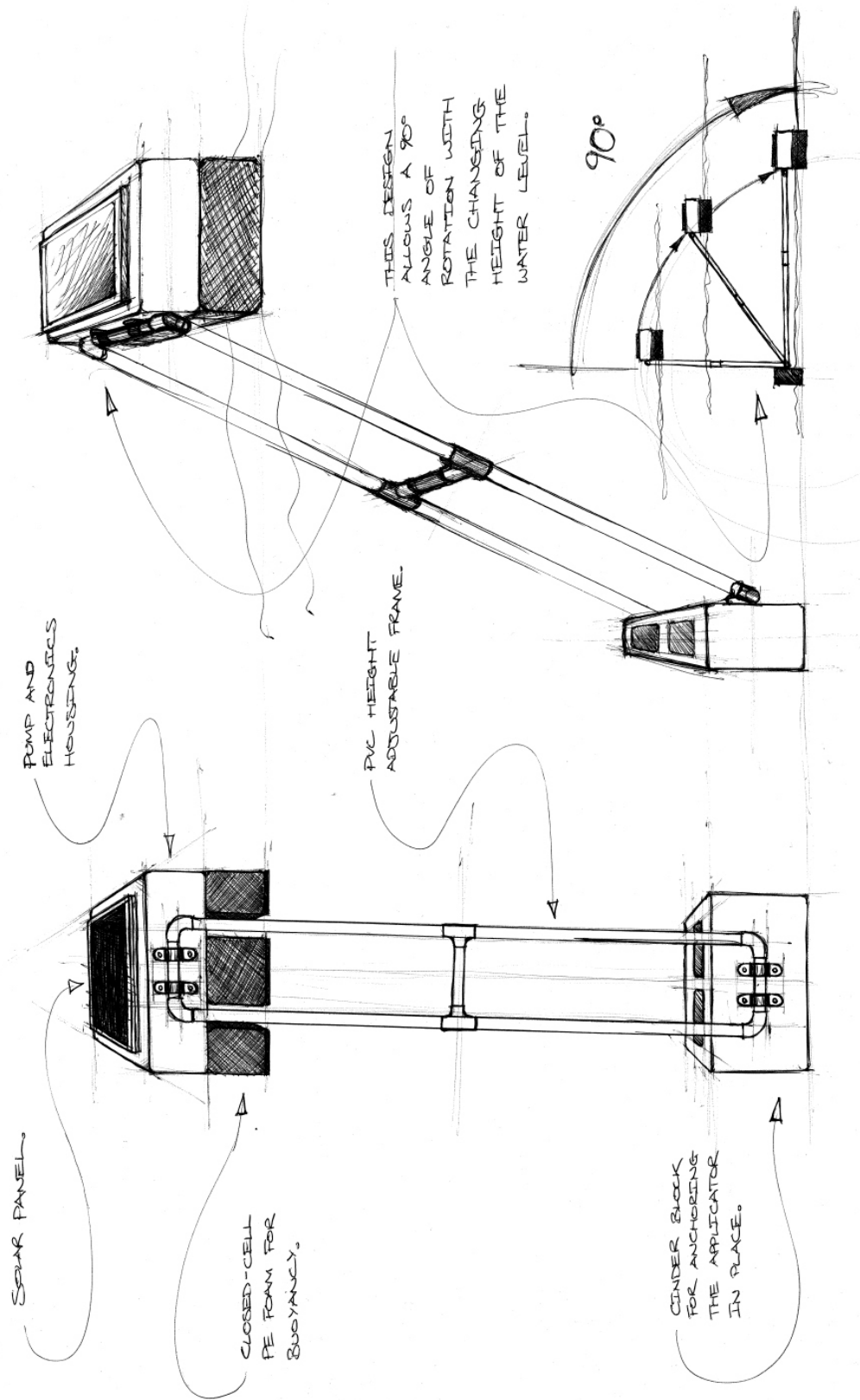


Figure E.11: Concept design for a low cost adaptation of the current (or similar) CRCJF Floating Applicator for shore-based delivery of monolayer product.

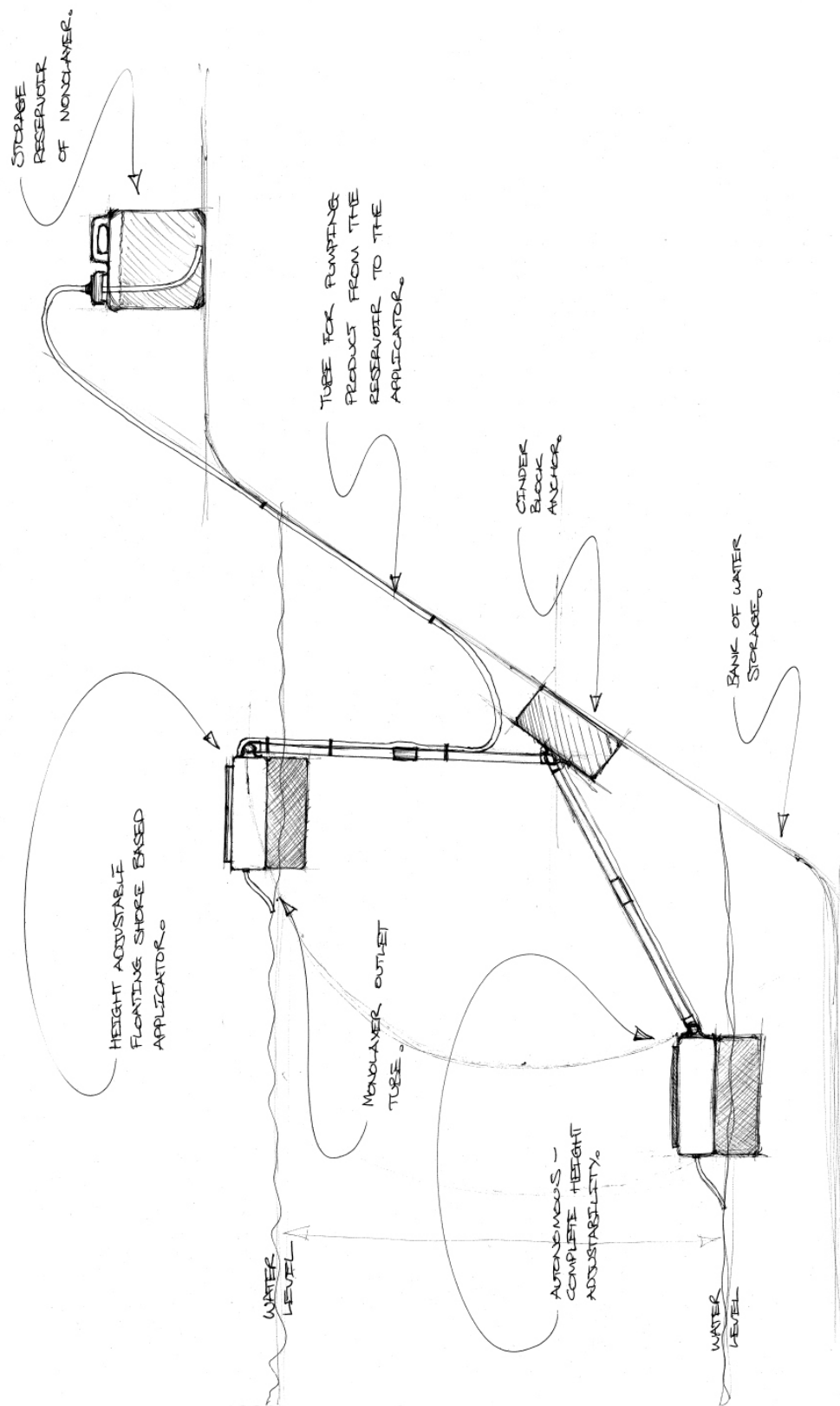


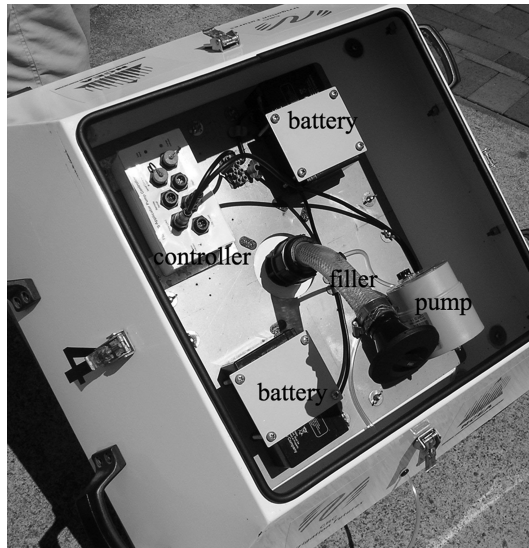
Figure E.12: A pseudo-sectional view of the simple cantilever anchoring system for the shore-based monolayer applicator.

E.3.3 Prototype floating applicator

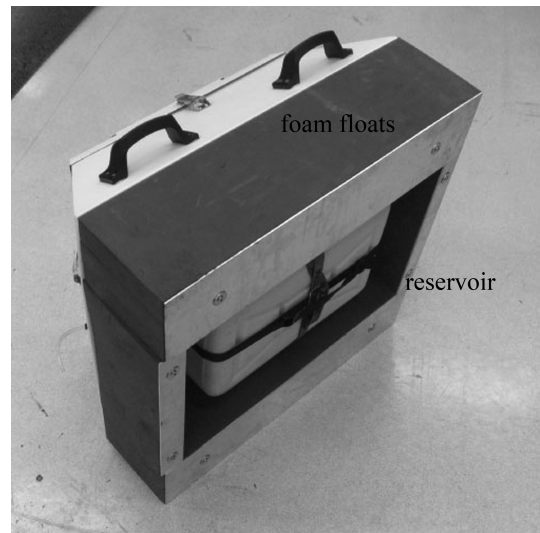
A prototype de-centralised floating applicator (Figure E.13), for monolayer in a liquid form, was constructed for in-field testing. The applicator utilises a 12V DC peristaltic pump, powered by a sealed lead-acid (SLA) battery which is recharged by a 10W polycrystalline solar panel. Therefore, the applicator is fully self-powered and portable for remote applications where alternative power sources may be limited, unavailable and/or unviable.

The application system hardware is housed in a custom-built metal housing that has four closed-cell polyethylene foam floats for buoyancy (Figure 3(a)). A 20L polypropylene reservoir for monolayer is attached to the bottom of the metal housing surrounded by the foam floats (Figure 3(b)). Although the capacity of the monolayer reservoir is only 20L for testing purposes, this would need to be increased for commercial applications, depending on the concentration of the liquid monolayer formulation. The reservoir also has a refill line inside the metal housing, which is accessed by removing the housing lid. The removable lid also allows easy access to application hardware for servicing, replacement, repair or modification (Figure 3(c)). The applicator is anchored in location via a 20 kg concrete deadweight. The mooring line attached to the applicator passes through an eye on the anchor and is tensioned by a float consisting of a sealed 20L container as illustrated in Figure 3(d).

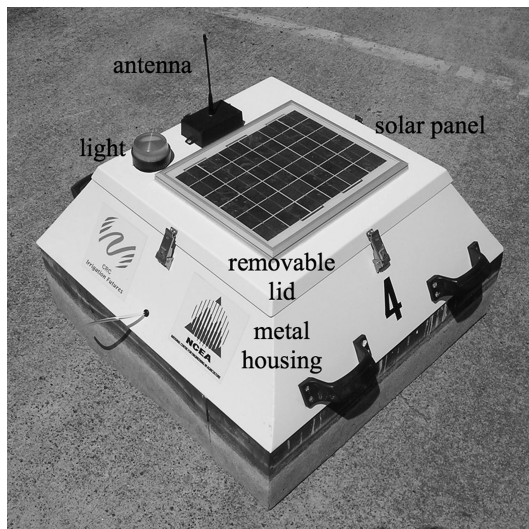
For more detailed information with regard to the prototype monolayer application system shown, the reader is referred to Brink et al. (2011).



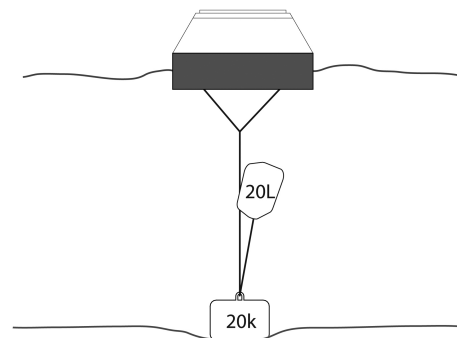
(a)



(b)



(c)



(d)

Figure E.13: Pre-prototype floating applicator; (a) three-quarter view of the applicator; (b) view underneath the applicator; (c) view inside the metal housing; and (d) schematic of the anchor and self-adjusting mooring set-up for the applicator on a farm dam (the rope is free to slip through the eye in the anchor). Reproduced from Brink et al. (2011).